PNL-3300
UC-48

Pacific Northwest Laboratory Annual Report for 1979 to the DOE Assistant Secretary for Environment

Part 4 Physical Sciences February 1980

Prepared for the U.S. Department of Energy
under Contract EY-76-C-06-1830

Pacific Northwest Laboratory
Operated for the U.S. Department of Energy
by Battelle Memorial Institute

Battelle

NOTICE

PACIFIC NORTHWEST LABORATORY
operated by
BATTELLE
for the
UNITED STATES DEPARTMENT OF ENERGY
Under Contract EY-76-C-06-1830

Printed in the United States of America
Available from
National Technical Information Service
United States Department of Commerce
5285 Port Royal Road
Springfield, Virginia 22151

Price: Printed Copy $____*; Microfiche $3.00

*Pages	NTIS Selling Price
001-025	$4.00
026-050	$4.50
051-075	$5.25
076-100	$6.00
101-125	$6.50
126-150	$7.25
151-175	$8.00
176-200	$9.00
201-225	$9.25
226-250	$9.50
251-275	$10.75
276-300	$11.00

PNL-3300 PT4
UC-48

Pacific Northwest Laboratory Annual Report for 1979 to the DOE Assistant Secretary for Environment

Part 4 Physical Sciences

J. M. Nielsen and Staff Members
of Pacific Northwest Laboratory

February 1980

Prepared for
the U.S. Department of Energy
under Contract EY-76-C-06-1830

Pacific Northwest Laboratory
Richland, Washington 99352

PREFACE

Pacific Northwest Laboratory's (PNL) 1979 Annual Report to the Department of Energy (DOE) Assistant Secretary for Environment describes research in environment, health, and safety conducted during fiscal year 1979. The report again consists of five parts, each in a separate volume.

The five parts of the report are oriented to particular segments of our program. Parts 1-4 report on research performed for the DOE Office of Health and Environmental Research. Part 5 reports progress on all other research performed for the Assistant Secretary for Environment, including the Office of Technology Impacts and the Office of Environmental Compliance and Overview. Each part consists of project reports authored by scientists from several PNL research departments, reflecting the interdisciplinary nature of the research effort. Parts 1-4 are organized primarily by energy technology.

The parts of the 1979 Annual Report are:

Part 1:	Biomedical Sciences	
	Program Manager - H. Drucker	D. L. Felton, Editor
Part 2:	Ecological Sciences	
	Program Manager - B. E. Vaughan	B. E. Vaughan, Report Coordinator
		C. H. Connally, Editor
Part 3:	Atmospheric Sciences	
	Program Manager - C. E. Elderkin	R. L. Drake, Report Coordinator
		G. B. Long, Editor
Part 4:	Physical Sciences	
	Program Manager - J. M. Nielsen	J. M. Nielsen, Report Coordinator
		J. L. Hooper, Editor
Part 5:	Environmental Assessment, Control, Health and Safety.	
	Program Managers - D. L. Hessel	
	S. Marks	W. J. Bair, Report Coordinator
	C. M. Unruh	R. W. Baalman, C. W. Dotson, Editors

Activities of the scientists whose work is described in this annual report are broader in scope than the articles indicate. PNL staff have responded to numerous requests from DOE during the year for planning, for service on various task groups, and for special assistance.

Credit for this annual report goes to many scientists who performed the research and wrote the individual project reports, to the program managers who directed the research and coordinated the technical progress reports, to the editors who edited the individual project reports and assembled the five parts, and to Dr. Ray Baalman, editor in chief, who directed the total effort.

W. J. Bair, Manager
S. Marks, Associate Manager
Environment, Health, and Safety Research Program

Previous Reports in this series:

Annual-Report for	
1951	W-25021, HW-25709
1952	HW-27814, HW-28636
1953	HW-30437, HW-30464
1954	HW-30306, HW-33128, HW-35905, HW-35917
1955	HW-39558, HW-41315, HW-41500
1956	HW-47500
1957	HW-53500
1958	HW-59500
1959	HW-63824, HW-65500
1960	HW-69500, HW-70050
1961	HW-72500, HW-73337
1962	HW-76000, HW-77609
1963	HW-80500, HW-81746
1964	BNWL-122
1965	BNWL-280, BNWL-235, Vol. 1-4, BNWL-361
1966	BNWL-480, Vol. 1, BNWL-481, Vol. 2, Pt. 1-4
1967	BNWL-714, Vol. 1, BNWL-715, Vol 2, Pt. 1-4
1968	BNWL-1050, Vol. 1, Pt. 1-2, BNWL-1051, Vol. 2, Pt. 1-3
1969	BNWL-1306, Vol. 1, Pt. 1-2, BNWL-1307, Vol. 2, Pt. 1-3
1970	BNWL-1550, Vol. 1, Pt. 1-2, BNWL-1551, Vol. 2, Pt. 1-2
1971	BNWL-1650, Vol. 1, Pt. 1-2, BNWL-1651, Vol. 2, Pt. 1-2
1972	BNWL-1750, Vol. 1, Pt. 1-2, BNWL-1751, Vol. 2, Pt. 1-2
1973	BNWL-1850, Pt. 1-4
1974	BNWL-1950, Pt. 1-4
1975	BNWL-2000, Pt. 1-4
1976	BNWL-2100, Pt. 1-5
1977	PNL-2500, Pt. 1-5
1978	PNL-2850, Pt. 1-5

FOREWORD

Part 4 of the Pacific Northwest Laboratory Annual Report for 1979 to the Assistant Secretary for Environment, DOE, includes those programs funded under the title "Physical and Technological Programs." The Field Task program studies reports are grouped under the most directly applicable energy technology heading. Each energy technology section is introduced by a divider page which indicates the Field Task Agreement reported in that section. These reports only briefly indicate progress made during 1979. The reader should contact the principal investigators named or examine the publications cited for more details.

CONTENTS

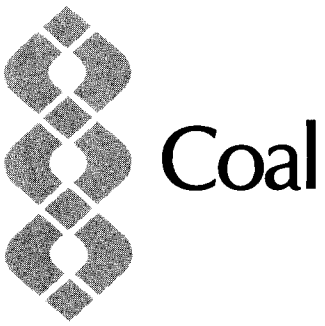
Coal

• Reaction Kinetics of Combustion Products

The goal of the Reaction Kinetics of Combustion Products program is to determine the conditions, mechanism, and chemical reactions that control the identity and concentrations of emissions from coal combustion processes. The program initially emphasized the characterization of fly ash and the development of a model for its formation that successfully rationalized the large enrichments observed for many trace elements in fly ash emitted from coal-fired steam plants. The direction of the program presently includes an increasing emphasis on the mechanism of formation of organic pollutants during combustion. Mass spectrometric techniques have been developed for the study of the high-temperature kinetics relevant to coal combustion, with specific emphasis on techniques that will allow investigation of the mechanism and rates of formation for toxic and carcinogenic organic compounds.

Formation of Fly Ash During Coal Combustion

R. D. Smith

It has been established that the smaller fly-ash particles formed during coal combustion show significant enrichments of several volatile trace elements. The accepted mechanism for trace element enrichment during fly-ash formation involves the volatilization of these elements during combustion, followed by condensation or adsorption over the available matrix material, which is composed primarily of the nonvolatile oxides of aluminum, manganese, and silicon. The larger surface-to-volume ratio of the smaller particle should then lead to a trace element concentration inversely related to the particle diameter (Campbell et al. 1979). Our work, in which we found that fly-ash surfaces were enriched in several trace elements, supports this mechanism for the larger particles. This work has resulted in the improvement of a model for fly-ash formation and the enrichment processes (Smith, Campbell and Nielson 1979a; Smith, Campbell and Nielson 1979b).

To predict the enrichment of trace elements in fly ash during combustion, one must first be able to predict the volatility of the various species during combustion. Earlier we had postulated that the organic association of trace elements in coal may be related to their relative volatilities during combustion. To examine the effect of organic association upon enrichments, the organic affinities of 30 elements in a coal were determined using several methods (flotation, oil agglomeration, and coal solvolysis). The method found to produce the most precise organic affinity measurements was coal flotation. The results were compared to enrichment data for elements in fly ash, as determined from the concentration dependence upon particle size. The results are consistent with two trace element source components: actual organically bound elements that are efficiently volatilized during combustion, and a disperse mineral phase that is not volatilized. Further experiments to determine the nature of organically associated elements in coal and their fate during combustion are planned. This information will be used as input for the model for fly-ash formation and trace element enrichment, which was developed previously.

High-Temperature Reactions Related to Coal Combustion

R. D. Smith

Mutagenic and/or carcinogenic organic compounds emitted from combustion facilities can be generated from two sources: 1) breakdown products of complex fuels such as coal, and 2) formation from reactions of smaller organic molecules. A more complete understanding of the temperature dependence of the major reaction pathways (formation, decomposition by pyrolysis, and oxidation) could lead to the prediction of the nature and concentration of the organic pollutants from combustion processes. The construction of a model for these chemical processes may

also suggest combustion parameters designed to minimize the emission of the organic pollutants.

The studies to date have employed the high-temperature, mass spectrometer system described in the last report for the study of gas-phase and gas-solid reactions. A new instrument has also been constructed to allow the study of higher pressure reactions (up to atmospheric pressure) and the quantitative evaluation of rate constants for second and higher order kinetic processes. Figure 1 gives a schematic illustration of the prototype high-temperature, fast-flow, reactor-modulated, molecular beam mass spectrometer. The combination of the high-temperature capability (up to 2200°C) and modulated molecular beam mass spectrometric analysis is unique and highly valuable since product identification can be obtained in addition to the rate constant data for important combustion-related reactions. Modulated molecular beam mass spectrometry eliminates all background and allows one to analyze only species sampled from the high-temperature region.

During the last year, the mass spectrometers have been interfaced to a minicomputer for complete control of data acquisition and processing. Computer control has greatly speeded data acquisition and handling, while also increasing the quality of the analytical data. Figure 2 gives part of the raw data for the pyrolysis of benzene at approximately 10^{-3} torr and a residence time of a few milliseconds. For the low-energy electron impact used for ionization in these studies, the ions observed in the mass spectra correspond to the neutral species in the high-temperature vapors. The transition to computer control allows an entire series of measurements of this type to be made in less than 1 hr. These advances are allowing a rapid extension of such experiments to a variety of compounds.

The initial studies on the pyrolysis of toluene showed that both complex radical and molecular studies are readily produced during high-temperature pyrolysis. Table 1 gives the concentrations (excluding hydrogen) of species observed in the vapors of toluene pyrolyzed at 1210°C at a pressure of approximately 10 N/m^2 ($\sim 10^{-1}$ torr). Species corresponding to anthracene, pyrene, and benzopyrene are observed. Such species are known to be products of nearly all combustion processes.

An important aspect of pollutant formation during combustion is the nature of the transformations for high-temperature species to the final pollutants emitted. By quenching the molecular beam of high-temperature products on a surface of well-defined composition and temperature, it is possible to investigate the fate of the high-temperature species since the composition can be readily determined. Table 2 gives the composition of products from the pyrolysis of toluene at 1400°C and 10^{-1} torr pressure as determined by gas chromatography-mass spectrometry after quenching on an aluminum surface at -50°C.

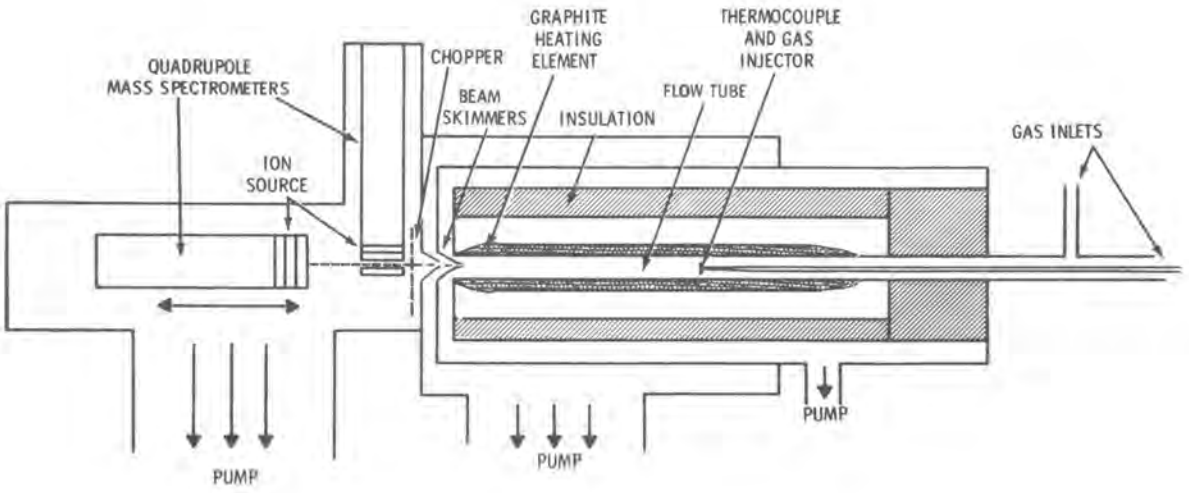

FIGURE 1. Prototype High-Temperature, Fast-Flow, Reactor-Modulated, Molecular Beam Mass Spectrometer

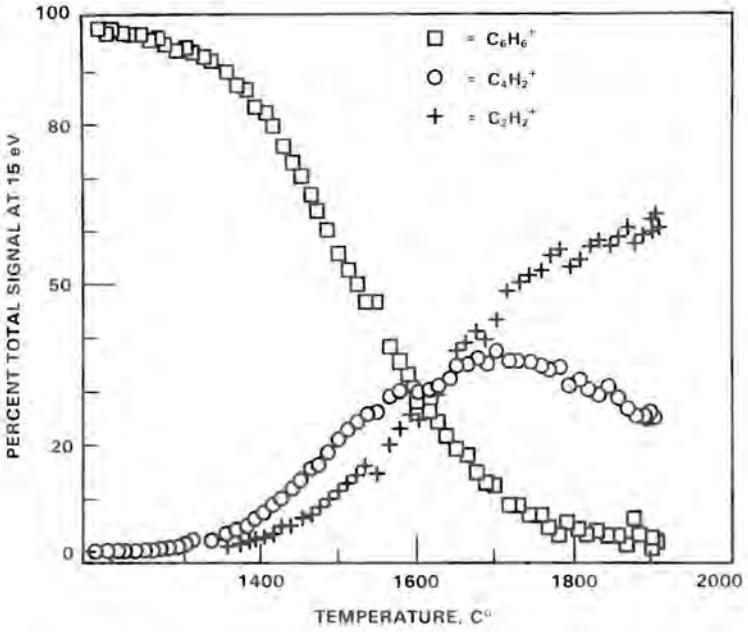

FIGURE 2. Raw Data for the Pyrolysis of Benzene at Approximately 10^{-3} Torr and a Residence Time of a Few Milliseconds

TABLE 1. Concentration of Toluene Pyrolysis Products in a Small Orifice Knudsen Cell

Species	Concn, Mol %	Species	Concn, Mol %
CH_3	12	C_9H_7	1.5
CH_4	<0.3	C_9H_8	0.5
C_2H_2	9	$C_{10}H_6$	0.2
C_2H_4	5	$C_{10}H_8$	2.0
C_3H_3	2.4	$C_{11}H_7$	0.2
C_3H_4	0.9	$C_{11}H_8$	0.1
C_3H_5	0.3	$C_{11}H_9$	0.1
C_4H_2	3.0	$C_{11}H_{10}$	0.1
C_4H_3	0.08	$C_{12}H_8$	1.0
C_4H_4	0.8	$C_{12}H_9$	0.2
C_5H_3	0.2	$C_{12}H_{10}$	0.3
C_5H_4	0.2	$C_{13}H_9$	1.4
C_5H_5	2.0	$C_{13}H_{10}$	0.3
C_5H_6	0.4	$C_{13}H_{11}$	0.1
C_6H_2	0.2	$C_{14}H_8$	0.1
C_6H_4	0.2	$C_{14}H_{10}$	0.8
C_6H_5	0.4	$C_{15}H_9$	0.2
C_6H_6	23	$C_{16}H_{10}$	0.3
C_7H_5	0.5	$C_{17}H_{11}$	0.1
C_7H_6	0.6	$C_{17}H_{12}$	0.03
C_7H_7	14	$C_{18}H_{10}$	0.08
C_7H_8	13	$C_{18}H_{12}$	0.04
C_8H_6	1.9	$C_{19}H_{11}$	0.07
C_8H_7	0.3	$C_{20}H_{12}$	0.05
C_8H_8			

TABLE 2. GC/MS Analysis of Quenched Toluene Pyrolysis Products (1400°C)

Molecular Weight	Compound	Mole Percent
116	Indene	2.9
154	Biphenyl	0.8
166	Phenalene	4.5
166	Fluorene	30
168	Methyl Biphenyl	0.5
178	Anthracene	59
192	$C_{15}H_{12}$	0.5
202	$C_{16}H_{10}$	∿0.7
228	$C_{18}H_{12}$	∿0.3
252	$C_{20}H_{12}$	∿0.5

Further experiments are in progress to determine the precise nature of the reactions occurring at the gas-solid interface. Such experiments may be of direct importance in understanding the role of gas-particle reactions during combustion.

• Solvent Refined Coal Effluent/Product Characterization

Samples of products and effluents from two coal liquefaction processes (SRC-I and SRC-II) have been collected, cataloged, and stored for future analytical work. Some samples of these research materials have been chemically fractionated and subjected to microbial mutagenicity and animal carcinogenicity testing programs. New techniques have been developed for the identification of constituents possessing microbial mutagenicity by gas chromatography/mass spectrometry and by high resolution mass spectrometry. Samples of solid waste materials from other emerging technologies have been subjected to a comparative evaluation of RCRA and ASTM leaching procedures.

Sample Collection, Storage, and Inventorying

W. C. Weimer, M. R. Petersen, B. A. Vieux, and W. D. Felix

We have continued our collection, chemical characterization, and storage of samples of products, effluent streams, and waste materials from the Solvent Refined Coal (SRC) Pilot Plant. We have obtained approximately 400 kg of SRC-I solid product and 225 ℓ of SRC-II fuel oil to meet PNL's research material needs for the chemical characterization, biological testing, and long-term ecological testing.

Additionally, we have implemented a computerized inventory control and information retrieval system utilizing an in-house PDP 11/70 computer. This data management system tracks the history of all SRC research material that we have stored and/or that we have distributed to authorized investigators. This system provides a current record for each material in stock consisting of the quantity of material initially received, the quantity remaining, the investigators to whom the material has been issued, the testing program for which each of the investigators is using the material, and general descriptive information regarding the results of the testing program. This system can be searched by requesting that all information for a given research material, a specific investigator, or a specific chemical, biological, or ecological testing program be provided.

Fractionation of Samples for Biological Testing

W. C. Weimer, D. S. Sklarew, J. E. Burger, M. R. Petersen, and B. A. Vieux

The extremely complex chemical nature of most of the SRC research materials requires some preliminary chemical fractionation prior to microbial mutagenicity or carcinogenicity testing. This separation involves the division of the constituents into rather broadly defined chemical compound classes which can then be tested independently. Three types of chemical fractionation procedures are being evaluated for the ability to (1) yield fractions containing distinct chemical classes with little overlap from one fraction to another and (2) result in fractions amenable to biological analyses. This research requires very careful coordination between personnel of the Physical Sciences and the Biology Departments at PNL.

Earlier work employed an acid-base extraction method (described by Petersen et al. 1977 Annual Report). The fractions produced by this method include polynuclear aromatic (PNA), neutral, isooctane insoluble tar, acid-induced, acid-induced tar, base-induced, and base-induced tar. (The last five fractions in the above list have previously been termed neutral tar, basic, basic tar, acidic, and acidic tar, respectively.

A second method now in use involves partition chromatography on Sephadex LH-20 and is a modification of the technique described by Klimisch and Stadler (1972) and further developed by Jones, Guerin and Clark (1977). The Sephadex LH-20 is first swelled in methanol:water (85:15); the sample is then eluted with hexane, toluene:hexane (95:5), and finally with methanol. This elution sequence provides a separation of constituents according to their polarity. For example, corresponding work with standard compounds has indicated that aliphatic hydrocarbons and polycyclic aromatic hydrocarbons elute in the hexane phase; aromatic amines and phenolics elute in the methanol phase. The hexane fraction can be subdivided into an aliphatic fraction and an aromatic fraction by an adsorption technique in which Sephadex LH-20 is swelled in isopropanol and the sample subsequently eluted with isopropanol, followed by elution with tetrahydrofuran.

A third method of chemical fractionation now being evaluated utilizes high performance liquid chromatography and is based on the method described by Wise et al. (1977). With this technique, the undiluted sample or the sample in a hexane or hexane:methylene chloride solvent is loaded onto a normal-phase NH_2 column. Classes of compounds are then eluted by gradient chromatography in which the eluting solvent is changed from the initial 100% hexane to 100% methylene chloride and subsequently to 100% isopropanol. Treatment of solvent-refined coal research materials with this procedure results in three distinct fractions. Comparative analyses with standard compounds have shown that the first fraction contains neutral aliphatic and aromatic constituents; the second fraction, nitrogenous bases and amines; and the third fraction, phenolic constituents. These three fractions are then available for biological testing or for further confirmatory chemical analyses. Alternatively, each of these fractions can be rechromatographed and separated on a reverse-phase C-18 column for either compound identification or isolating more discrete fractions for biological testing.

Each fraction has been analyzed for microbial mutagenicity in the Ames assay using Salmonella typhimurium TA98 as target cells. The results of these assays for acid-base and Sephadex LH-20 fractionations on three SRC-II fuel-oil samples are shown in Figures 3 and 4. For the untreated fuel oil sample, the Sephadex fractionation yields a separation of bioactive materials superior to that achieved by the acid-base-neutral fractionation; essentially all of the activity is concentrated in the methanol

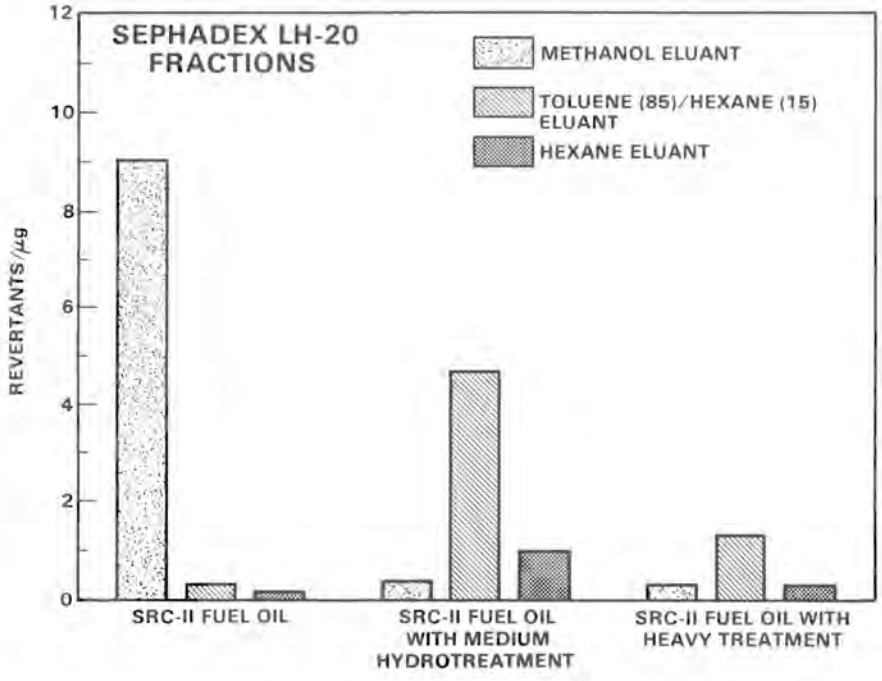

FIGURE 3. Microbial Mutagenicities of Sephadex LH-20 Column Fractions of Three SRC-II Fuel Oil Samples

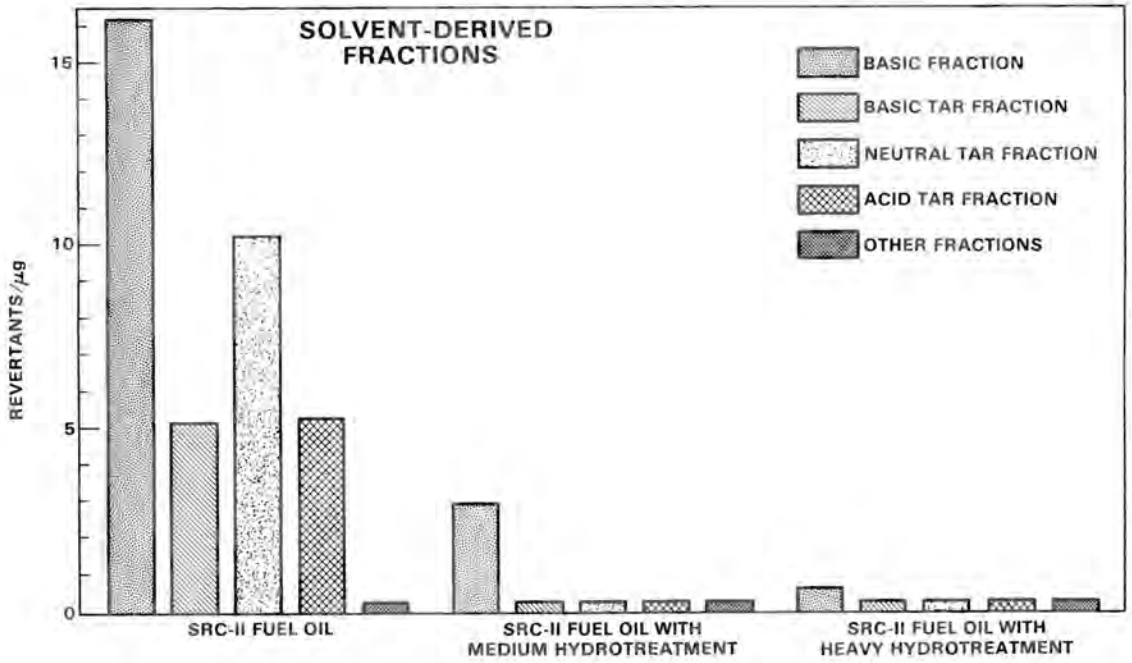

FIGURE 4. Microbial Mutagenicities of Acid-Base-Neutral, Solvent-Derived Fractions of Three SRC-II Fuel Oil Samples

fraction. The two products from the hydrogenation of the fuel oil appear to be fractionated more discretely by the acid-base-neutral technique than by the Sephadex procedure. However, the total activity is quite low for these samples and quantitative comparisons are difficult. Comparative data for the microbial mutagenicity testing of the fractions from the liquid chromatographic separations are not yet available.

Identification of Mutagenic Constituents

B. W. Wilson, R. A. Pelroy,
D. M. Schoengold, M. R. Petersen,
B. A. Vieux, and J. T. Cresto

Chemical constituents, in several coal liquefaction products, capable of affecting microbial mutagenicity have been identified based upon coupled Ames assay and mass spectral analyses of isolated chemical fractions. This identification may be of considerable value in developing process modification and/or control technologies capable of ameliorating potential biological effects.

Subfractions of SRC research materials have been analyzed for microbial mutagenicity by the Ames assay. Chemical fractions identified as having high biological activity have been further fractionated by thin layer chromatographic techniques. Regions from the thin layer chromatography (TLC) separations have been re-evaluated by additional Ames assay procedures and have been analyzed by both packed and capillary column gas chromatography/mass spectrometry (GC/MS) and high resolution mass spectrometry. Low resolution GC/MS has been operated in both the electron impact (EI) and chemical ionization (CI) mode. Selected reagent gas CI methodology (the subject of a separate section in this report) has proved to be a valuable tool in the analysis of these subfractions.

The results of this initial work have suggested that the principal compound types responsible for microbial mutagenic activity in SRC-II heavy distillate fraction are primary aromatic amines. These constituents have not previously been reported as present in coal liquefaction products, probably due to both their extremely low concentrations (up to 50 ppm) and the fact that they are identical in elemental composition to a number of alkyl aza compounds. The primary aromatic amines that have been identified include compounds based upon two-, three-, and four-ring aromatic nuclei and are listed in Figure 5. This figure also indicates the TLC regions in which these amines are

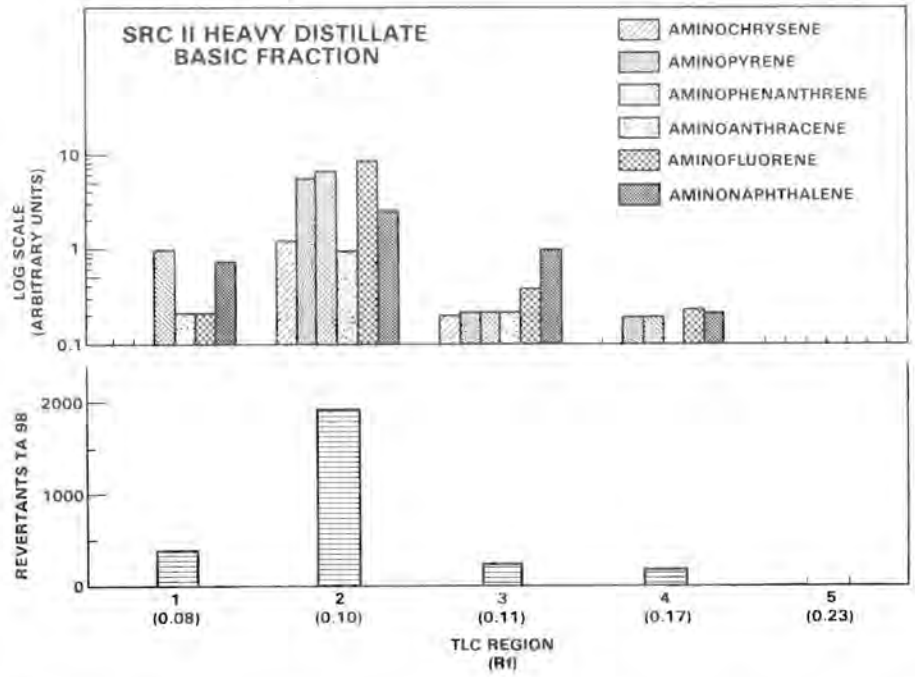

FIGURE 5. Identification and Relative Concentrations of Primary Aromatic Amines in Thin Layer Chromatography Regions from SRC-II Heavy Distillate Cut, Basic Fraction

concentrated. Results thus far have shown excellent correlation between the concentration of the primary aromatic amines and the amount of microbial mutagenic activity evidenced by the Ames test.

Selective Chemical Ionization Reagent Gases for GC/MS Analysis of Carcinogenic Aromatic Hydrocarbons and Aromatic Amines

D. M. Schoengold

We have previously reported the use of argon charge transfer mass spectrometry as a highly selective procedure for analysis of polynuclear aromatic hydrocarbons (PAHs) allowing determination of benzo[a]pyrene (BAP) in crude biological samples (Ryan and Petersen 1977). Ames test data have shown that certain trace constituents in some SRC materials are microbially mutagenic; sensitive and selective procedures are required for the analysis of these active agents in complex mixtures. Of particular interest are improved analytical capabilities for aromatic amines, as well as PAHs, in the complex samples. The use of selective reagent gases in the chemical ionization (CI) mode results in the enhancement of the mass spectra signal obtained from certain compound classes relative to the remaining constituents in the mixture.

We have studied argon charge transfer response to a number of carcinogenic nitrogen bases. We have also evaluated ammonia as a selective CI reagent gas for these compounds. The relative response shown by each technique is summarized in Table 3. Argon CI is demonstrated to discriminate against aliphatic and small-ring aromatic constituents. More importantly, however, the use of ammonia CI techniques provides even better discrimination against these interfering compounds for the analysis of both PAHs and aromatic amines. Ammonia CI gives no response for alkanes, aromatics, and for PAHs having molecular weight less than that of BAP and benzo[e]pyrene (BEP). Ammonia also is a more selective reagent gas for the higher molecular weight carcinogenic aromatic amines than is argon.

The relative response for carcinogenic BAP is greater than for noncarcinogenic BEP. This sensitivity difference when using ammonia CI is most likely due to the higher proton affinity of BAP over BEP. Using appropriate alkyl-amines as reagent gases, it should be possible to determine BAP selectively in the presence of BEP. This would eliminate the difficult problem of resolving these compounds chromatographically.

TABLE 3. Relative Response of Selected Compounds to Three Ionization Modes

	Relative Response		
	Electron Impact	Argon	Ammonia
C19 alkane	5	—	—
Triethylbenzene	60	10	—
Dimethylnaphthalene	180	90	—
Chrysene	387	150	—
Benzo[e]pyrene	215	135	25
Benzo[a]pyrene[a]	320	135	53
Trimethylphenol	65	27	15
Trimethylpyridine	100	100	100
2-aminonaphthalene[a]	45	35	15
Diphenylamine	40	21	13
2-aminobiphenyl	180	125	75
Benzoquinoline	335	315	265
1-aminoanthracene	85	45	85
1-aminopyrene[a]	60	17	25
6-aminochrysene[a]	65	22	64

[a] Animal carcinogen or microbial mutagen

High-Resolution Mass Spectral Analysis of Coal Liquefaction Products

B. W. Wilson and M. R. Petersen

High-resolution mass spectrometry has been evaluated as an analytical tool for constituent identification of complex coal liquefaction products and of chemical fractions of these materials. Several classes of compounds previously undetected and unidentified in SRC products have been found during these investigations.

Through arrangement with the Department of Chemistry at the Massachusetts Institute of Technology, high resolution mass spectral analyses have been performed on a number of SRC research materials and the fractions produced by acid-base-neutral separation of these materials. An extensive amount of elemental compositional information has been generated by these analyses, and such information has served as a valuable reference data base for these complex samples. Through careful interpretation of the mass spectral results, we have identified the following classes of compounds which have previously been undetected in SRC material:

- alkyl polynuclear aromatic hydrocarbons (PAHs),
- PAHs with nitrogen in the ring (aza PAHs)
- $C_8H_8N_2$ (amino indole),
- $C_{12}H_{10}N_2$ (amino carbazole),
- $C_{14}H_9N$[4 H-benzo(def)carbazole],
- $C_{15}H_9NS$[phenanthro(2,1-d)thiazole],
- $C_{14}H_8S$[benzo(def)dibenzothiophene],
- benzo naphthothiophene,
- bisphenols,
- binaphthols,
- $C_{14}H_{10}O$ (anthrane), and
- $C_{14}H_{20}O$[4 H-benzo(def)dibenzofuran].

The information obtained from these high-resolution mass spectral studies has proved to be a valuable confirmatory tool when used in conjunction with gas chromatography/low resolution mass spectrometry and Ames assay testing. These data have assisted in the identification of constituents active in microbial mutagenesis in some of the SRC research materials.

RCRA and ASTM Leaching Analysis Testing Program

W. C. Weimer, J. C. Kutt, and B. A. Vieux

Resource Conservation Recovery Act (RCRA) and American Society for Testing and Materials (ASTM) solid-waste leaching methodologies were evaluated and compared as part of a program managed by the ASTM. PNL was one of 17 laboratories participating in this program to evaluate the reproducibility of each of three leaching procedures on the same solid waste materials at different institutions. The three leaching techniques evaluated included (a) ASTM Method A, a distilled water leaching technique; (b) ASTM Method B, an acetic acid leaching technique; and (c) the EPA-designed RCRA method, also an acetic acid leaching technique. The three waste materials on which these leaching methodologies were evaluated included a fly ash, a fluidized bed combustion waste, and a fixed fluidized bed combustion waste. The leachates were analyzed for their final pH values and for the following metal concentrations: calcium, barium, chromium, cadmium, lead, arsenic, selenium, mercury, and silver. The final results of this program are currently being compiled and evaluated by Engineering-Science, McLean, Virginia.

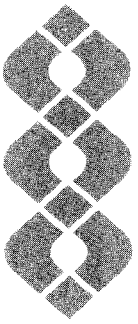

Fission

• Radiation Physics

A fundamental knowledge of the mechanisms by which radiation interacts with matter is essential for understanding dose-response relationships in terms of quantifiable chemical and physical processes. The Radiation Physics Program is directed toward investigation of the fundamental processes of energy deposition by fast charged particles and the subsequent transport and degradation of that energy as it leads to the formation of chemically active molecular species. The initial deposition of energy is studied through the measurements of differential ionization cross sections for fast charged particles which, when coupled with theoretical calculations, provide insight into the mechanisms of energy deposition in biologically significant matter. These measurements also provide the necessary data base for energy transport studies. Our effort in energy transport and degradation combines the use of Monte Carlo calculations and theoretical investigation of condensed-phase chemical kinetics. Monte Carlo calculations provide detailed information on the initial structure of the particle track, and the theoretical investigation of energy transport provides the link between initial energy deposition and the final observation of chemically active molecular species. Time-resolved measurements of fluorescence from liquid systems excited by irradiation with pulsed beams of fast charged particles and ultraviolet light provide definitive tests of the theoretical results. This integrated program of experimental and theoretical investigation results in a unified approach to understanding the mechanisms by which chemically active species are formed as a result of energy deposition via exposure in a radiation field.

• Initial Interaction Processes

The study of initial interaction processes has concentrated on differential ionization cross sections in collisions of protons, alpha particles, and carbon ions with atomic and molecular gas targets. These cross sections provide the data required as source terms in the study of charged-particle track structure and energy transport. During the past year, we have extended our proton measurements from 2 to 4.2 MeV for a variety of low-Z molecular targets and for atomic targets of argon and krypton. A comparison of the krypton data to calculations using the Born approximation has revealed unexpected discrepancies. Analysis of our results for helium ion impact illustrate the importance of projectile structure on interaction cross sections. Further evidence of projectile structure, as well as effects of target structure, is observed in ionization of helium, neon, argon, and methane by 1.2 MeV carbon ions. In addition to the study of continuum electrons, preliminary analysis of autoionization electrons observed in heavy-ion collisions with helium appears to show evidence of quasi-molecular effects in intermediate velocity ion-atom collisions.

Ionization of Molecules by Fast Protons

L. H. Toburen and W. E. Wilson

The spatial distributions and correlation of stochastic energy deposition events produced in macromolecular volumes by a radiation field are of increasing importance in understanding radiation effects in biological materials. Mathematical models of energy transport and degradation that follow initial energy deposition events require detailed knowledge of the relevant interaction cross sections. Because of the wide range of collision data required and the complexity of the absorbing material, mathematical models of energy transport and degradation in biologically significant media can be greatly simplified if the relevant interaction cross sections can be described in analytic forms.

The development of a parameterized analytic form for cross sections appropriate to biological systems relies on a broad base of cross sections for molecules of low-Z atomic constituents. Until recently, our data base has been limited primarily to the proton energy range of 0.3 to 2.0 MeV. During the past year, we have initiated measurements to extend our previous work to higher proton energies. Double differential cross sections were measured for molecular targets of H_2O, CH_4, $(CH_3)_2NH$, C_6H_6, NH_3, and CO at proton energies of 3.0 and 4.2 MeV. These results will provide additional information on scaling of molecular cross sections and enable extension of our phenomenological model (Wilson and Toburen 1977) to higher proton energies. This extension to higher proton energies is particularly important in providing an accurate source term for Monte Carlo calculations of charged-particle track structure at energies relevant to the dosimetry of fission and fusion neutrons.

During the past 8 to 10 years, a considerable amount of work has been published (much of it from this project) regarding differential ionization cross sections for proton impact. We have recently begun a comprehensive review of these data in our study of cross section systematics. The emphasis of this work is on the effects of molecular structure on differential ionization cross sections. Preliminary results were presented as an invited paper at the Sixth International Congress of Radiation Research held in Tokyo in May 1979 (Toburen and Wilson 1979, "Secondary Electron Emission in Ion-Atom Collisions"). The discussion involved an assessment of cross-section scaling and a description of the spectral features observed in the spectra of electron emission for ion-atom collisions. Further discussion of cross-section systematics will be found in the Track Structure segment of this report.

Ionization of Atoms by Fast Protons

L. H. Toburen and S. T. Manson*

Detailed analysis of double differential cross sections for ionization of noble gas atoms by fast protons and comparison to appropriate theoretical results provide information on mechanisms of ionization, as well as an assessment of the reliability of theoretical techniques. In our study of ionization of helium by protons (Manson et al. 1975), excellent agreement was obtained between measured cross sections and those calculated using the Born approximation with Hartree-Slater wave functions to describe initial bound and final continuum states. The primary differences between theory and experiment were for ejected electrons with small emission angles and velocities near those of the incident proton. These differences were attributed to continuum-charge-transfer, which is not incorporated into the theoretical description, and were found to disappear in the case of protons on helium at proton energies above a few MeV.

We have recently extended this analysis to ionization of krypton by fast protons. Results at proton energies to 1.5 MeV showed relatively large discrepancies between Born calculations and measured cross sections for electron energies of 100 to 500 eV and small emission angles (Manson and Toburen 1977). It was anticipated that these disparities were due to continuum-charge-transfer and would disappear as the proton energy increased further. With the addition of our tandem accelerator, it was possible to extend our measurements to higher energies. During the past year, we obtained preliminary data for proton energies to 4.2 MeV. Calculated contributions from inner shells of the target atom have also been tabulated to provide an indication of the relative importance of the various subshell contributions.

A comparison of measured and calculated cross sections for ejection of 136 eV electrons at 30° is shown in Figure 1 as a function of proton energy. Note that the disparity between theory and experiment does not decrease with increasing proton energy as was expected. Partial cross sections for the various subshells calculated within the Born approximation are also shown to illustrate the relative contributions of the differential cross sections. From this

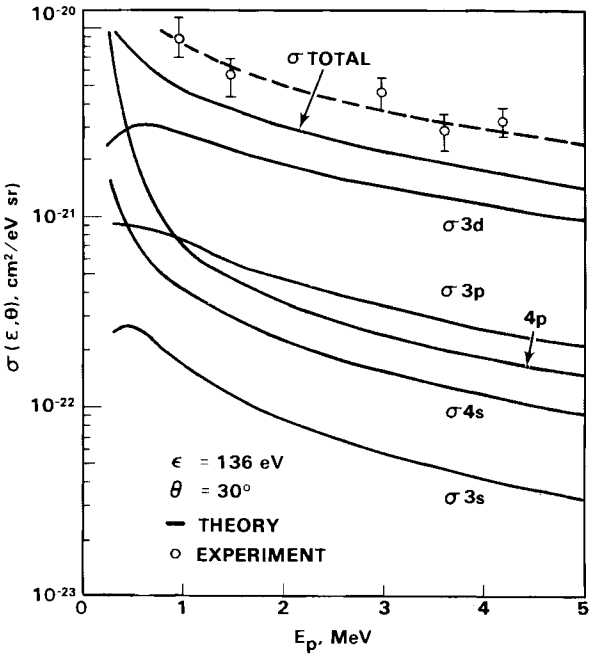

FIGURE 1. Ionization of Krypton by Fast Protons. The theoretical subshell and total cross sections are from Born calculations of the type described in Manson et al. (1975).

comparison, it is evident that the major contribution to the cross sections in this energy and angular range is for electrons ejected from the 3d shell. One may speculate that the observed differences occur because theory underestimates the contribution from the 3d subshell; however, if the angular distribution is examined (Figure 2), it is apparent that increasing the 3d contribution by a constant fraction to obtain better agreement at one angle will tend to increase differences at other angles. From a comparison of both energy and angular distributions, it appears that a simple underestimation of the 3d subshell contribution is unlikely to be the origin of the observed discrepancies. We are presently attempting to improve the precision of these data to provide a more definitive measure of the differences between theory and experiment and are exploring possible explanations for these discrepancies.

In addition to our investigation of krypton, we have also extended the energy range of our measurements of differential cross sections for ionization of argon by protons.

*Consultant, Dept. of Physics, Georgia State University, Atlanta, GA.

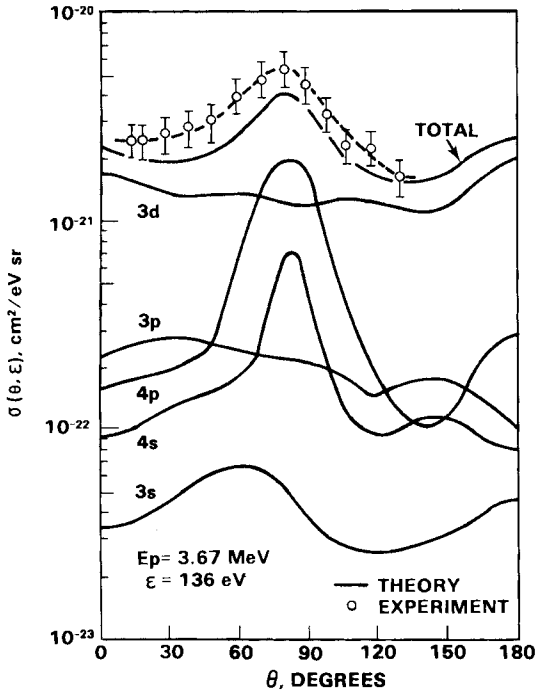

FIGURE 2. Angular Distribution of 136 eV Electrons Ejected from Krypton by 3.67 MeV Proton Impact. The theoretical results are from a Born calculation of the type described in Manson et al. (1975).

Cross sections were measured for proton energies of 2, 3, 3.67, and 4.2 MeV. These data will be included in a compilation of proton impact ionization cross sections initiated by Prof. M. E. Rudd of the University of Nebraska which are being published by Atomic Data and Nuclear Data Tables (Rudd et al., "Differential Cross Sections for Ejection of Electrons from Argon by Protons"). This compilation, to which our laboratory, Hahn-Meitner Institute (Berlin), and the University of Nebraska contributed, provides tabulated cross sections for incident proton energies from 5 keV to 5 MeV. Results of our recent high-energy measurements are included along with our previous results for lower-energy protons (Criswell et al. 1977; Toburen et al. 1978).

Differential Cross Sections for Helium-Ion Impact

L. H. Toburen, W. E. Wilson, S. T. Manson,* and R. J. Popowich**

An understanding of the effects of projectile structure on differential ionization cross sections is particularly important in the study of energy loss by alpha particles as they slow to energies less than a few MeV. As the alpha particle slows, the capture and loss of electrons have a strong influence on the energy loss process. Electrons bound to the projectile provide screening of the nuclear charge of the incident ion and contribute to the spectra of ejected electrons when they are stripped from the projectile.

During the past two years, we have studied the double differential ionization cross sections for helium ions. Our results of a measurement of electron emission from argon for ionization by 0.3 to 2.0 MeV He^+ and He^{2+} impact have recently been published (Toburen and Wilson 1979, "Differential Cross Sections for Ionization of Argon by 0.3-2.0 MeV He^+ and He^{2+} Ions"), and similar measurements for water vapor have been accepted for publication (Toburen et al. 1979, "Secondary Electron Emission from Ionization of Water Vapor by 0.3-2.0 MeV He^+ and He^{2+} Ions"). These publications address the reliability of Z^2 scaling of cross sections in this energy range and the effect of screening of the nuclear charge of the He^+ ion by the bound electron on the ionization cross sections.

Screening is particularly important in double differential cross sections since the degree of screening depends on the impact parameter and thus on the momentum transfer during the collision. To provide a better understanding of the effects of screening, we have initiated a theoretical investigation of ionization by structure projectiles within the framework of the Born approximation. Comparison of calculated and measured differential ionization cross sections for the He^+-He collision system is expected to provide insight into the effects of screening on heavy-ion collisions.

---

* Consultant, Dept. of Physics, Georgia State University, Atlanta, GA.
** Current address: Dept. of Energy, 1333 Broadway, Oakland, CA 94612.

Differential Cross Sections for Heavy-Ion Impact

L. H. Toburen

The interaction of low-Z heavy ions, such as carbon, oxygen and nitrogen, is important in radiological physics as a consequence of the recoil ions produced in the stopping of fission or fusion neutrons in tissue and in the use of heavy-ion beams for radiation therapy. Assessment of the interaction cross sections for heavy ions is particularly difficult because of the electronic structure of the ion itself. Ionic electrons provide partial screening of the nuclear charge, and excited states of the projectile can have sizable influence on the interaction probabilities. In addition, for ion energies relevant to neutron-produced recoils, the ion velocities are low and the interaction cross sections may be dominated by the quasi-molecular aspects of the slow collision. The contrast between electron spectra arising from bare and structured projectiles was described in an invited paper presented at the Small Accelerator Conference (Toburen 1979, "Differential Cross Sections for Electron Emission in Heavy-Ion Collisions"). In particular, one notes that cross sections for ejection of low-energy electrons are greatly reduced from estimated "Z^2" scaling due to the screening effect of the projectile electrons. Ejection of high-energy electrons, on the other hand, occurs at small impact parameters, and screening of the nuclear charge of the projectile is much less important. A significant result of this energy-transfer dependent screening is a shift in the mean energy of ejected electrons to much higher energies than for comparable velocity bare projectiles.

In the study of relatively low-energy, heavy-ion collisions, the structures of both projectile and target are important. By the study of double differential ionization cross sections for electron ejection for several target elements at a constant ion velocity and charge state, we have explored the effect of atomic and molecular structure on the collision process. The results in Figure 3 illustrate the differences in ejected electron energy spectra observed at 20° and 130° for ionization of helium, neon,

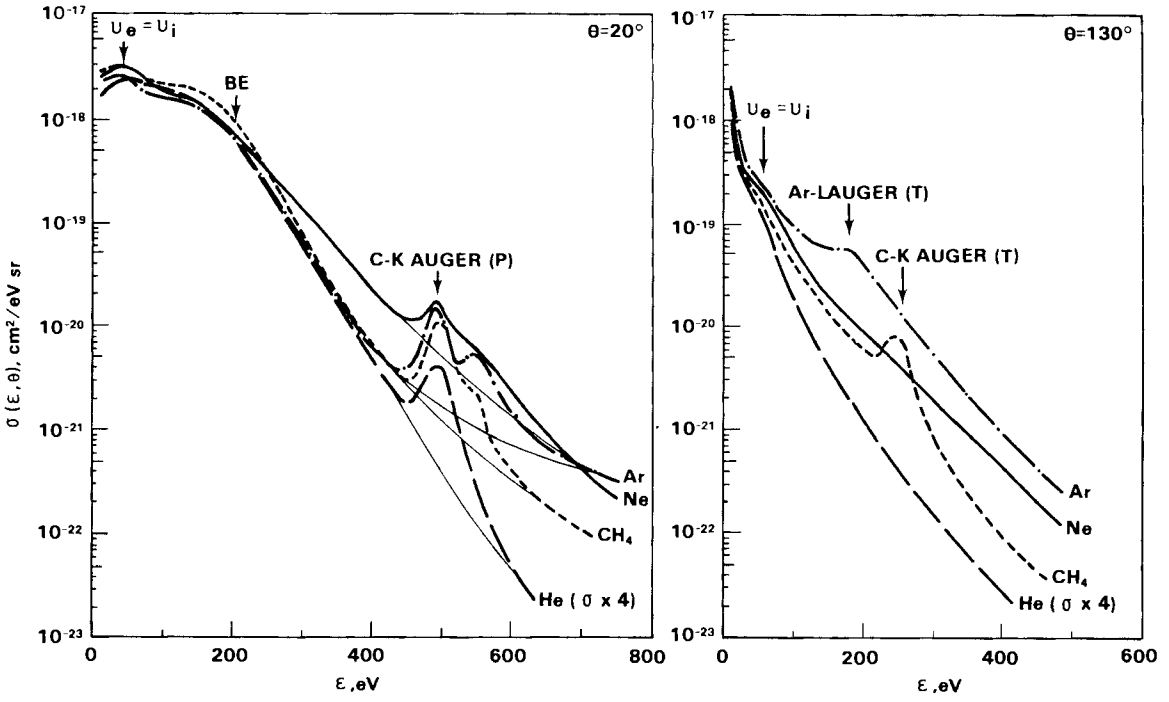

FIGURE 3. Differential Cross Sections for Electron Emission at 20° and 130° by 1.2 MeV C^+ Ionization of He, Ne, Ar, and CH_4

argon, and methane by 1.2 MeV carbon ion impact. The low-energy portion of the spectra exhibits features expected for ejection of outer shell electrons by the screened nuclear charge of the projectile. The higher-energy portion of the spectra appear to depend in more detail on the inner shell structure of the target atom or molecule. The shape of the high-energy portion of the spectra can be approximated by an exponential of the form

$$\sigma(\varepsilon,\theta)\alpha e^{-\frac{\varepsilon}{(IT)^{1/2}}}$$

where ε is the ejected electron energy, I is the binding energy of the ejected electron, and T is proportional to the ion energy ($T = \frac{1}{2}m_e v_i^2$; m_e = mass of the electron, v_i = velocity of the ion). This exponential dependence has been observed previously in proton and heavy-ion impact and is attributed to radial coupling of bound and continuum states during the collisions (Rudd and Macek 1979; Woerlee et al. 1979).

These results lead one to consider analysis of the spectra of electrons ejected in these intermediate velocity heavy-ion collisions as resulting from a combination of coulomb and molecular promotion processes. The systematics of the low-energy electron cross sections resemble those of the screened nuclear charge observed in our He^+ studies, whereas the ejection of high-energy electrons has the ejected electron energy dependence expected for promotion of inner shell electrons via molecular couplings. A more thorough investigation of these effects for different ion charge states and velocities is in progress in order to provide additional insight into these ionization mechanisms.

Autoionization in Heavy-Ion Collisions

L. H. Toburen, S. T. Manson,* and
D. Schneider**

The study of autoionizing transitions following excitation in heavy-ion collisions provides additional information on the collision dynamics. In particular, information is obtained regarding the excitation of target states, the mixing of these states in the coulomb field of the projectile, and the interaction of electronic states of the target with final states of the projectile. For collisions in which the ion velocity is comparable to the bound electrons of the target atom or molecule, excitation via electron promotion is expected to play a dominant role. In addition, perturbation due to the decay of excited states in the presence of the coulomb field of the passing ion can influence both the identity of the final states populated and the angular distributions of the ejected electrons (Stolterfoht 1978; Stolterfoht 1979; Brandt et al. 1979).

To provide further insight into the ionization process, we have measured the energy and angular distribution of autoionization electrons from helium excited by copper and iodine ions. These ions provide an excellent opportunity to study the influence of the projectile on final states of the target since they can be produced with multiple charges and with velocities near those of the target electrons.

The energy and angular distributions of autoionization electrons ejected from helium by incident Cu^{3+} and I^{3+} ions with velocities from 0.96 to 2.0 atomic units (6.3 MeV Cu^{3+}, 3.17, 4.5, and 6.4 MeV I^{3+}) were measured at emission angles of 50^o, 90^o, and 130^o. The energy distributions of electrons emitted at 90^o from autoionizing states in helium are shown in Figure 4 for several ion velocities. Strong variations in line intensities and energies are observed. Similar variations in line intensities and energies are observed as a function of ejected electron angle and, in particular, the angular distributions are not symmetric to 90^o. These results are similar to recently reported measurements for slow Li^+ collisions (Brandt et al. 1979). These results indicate that the autoionizing states of helium are perturbed by the coulomb field of the slow-moving projectile. This perturbation may cause the intensity and energy variation as well as interference between closely lying autoionizing states. Note in particular the strong enhancement in the spectra near 37 eV as the ion velocity decreases. It is particularly interesting that the autoionizing lines have intensity variations that do not appear to be symmetric with respect to 90^o. If we assume that excitation and decay of these states is a two-step process, the angular distributions should be symmetric to 90^o. The observed asymmetry is indicative of the influence of the projectile on the decay process, e.g., Stark mixing of target states by the coulomb

* Consultant, Dept. of Physics, Georgia State University, Atlanta, GA.
** Consultant, Hahn-Meitner Institute, Berlin, Germany.

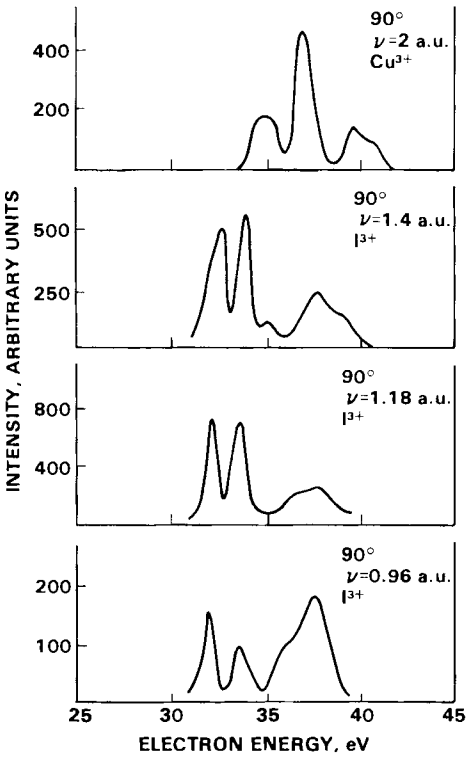

FIGURE 4. Helium Autoionization Lines Excited by Heavy Ion Impact at Different Velocities

field of the projectile (Brandt et al. 1979). Further measurements are in progress to provide a more definitive test of the interaction mechanisms.

In addition to excitation of autoionizing transitions in the target atom, the electron emission spectra from copper ion impact exhibit structure attributed to excitation of autoionizing states in the projectile. Structure in the electron spectra at ejected electron energies from about 60 to 140 eV in Cu^{n+} collisions with helium shown in Figure 5 are attributed to Doppler-shifted autoionization spectra from the copper ion. The corresponding autoionization energies in the projectile rest frame would be from about 8 to 30 eV. These structures were also observed for Cu^{n+}, n = 2, 3, 4, in collisions with neon and argon. The spectra shown in Figure 5 illustrate the interesting result that the contribution from projectile autoionization appears to increase in increasing charge state of the ion. Preliminary interpretation of this trend is that the number of energetically possible autoionizing states of Cu^{n+} increases as the charge state increases, thus resulting in a higher probability for autoionization. The alternative explanation is that the production of higher charge-state projectile ions is accompanied by a higher probability of producing ions in metastable states. These metastable states would then lead to autoionization upon excitation in collisions with the target atom.

It is expected that investigation of autoionization for heavy ions will provide additional information on the dynamics of the interaction processes for slow ion-atom collisions. This information, when coupled with emission cross sections for production of direct ionization electrons, will enable a more complete description of the interaction process. Through our study of differential ionization cross sections for protons, alpha particles, carbon ions, and heavier ions, all with comparable velocities, we expect to provide detailed knowledge on the systematics of ionization cross sections of importance in understanding the stopping of heavy ions typical of neutron recoils in biologically important matter.

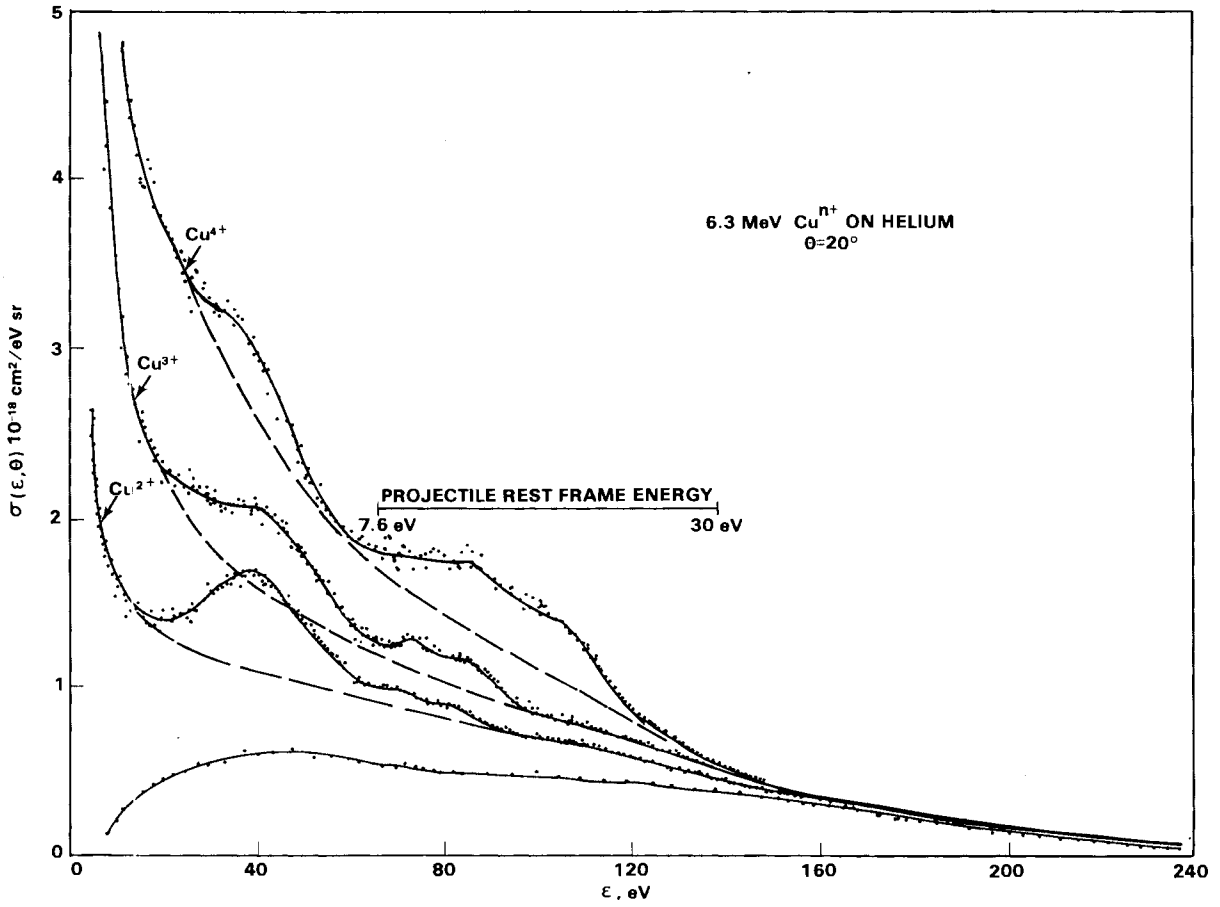

FIGURE 5. Ejected Electron Spectra for Ionization of Helium by 0.1 MeV/amu Cu^{n+} and C^+ ions.

• Track Structure

Experimental determination of radiation interactions in small absorber sites is limited to volumes greater than about 0.1 μm. This restriction has encouraged the development of computational methods to obtain the desired information in sites of arbitrary size. We are developing a Monte Carlo code, MOCA13, to calculate ionization and energy imparted in submicron sites by MeV positive ions. This code draws on extensive data for electron production in ion-molecule collisions as the source term for energy degradation calculations. The systematics of molecular cross sections are analyzed to provide information regarding the implications of molecular structure on energy deposition calculations. Optimization of the calculational technique is addressed through the use of conditional probabilities. The reliability of calculations using gas-phase cross sections for energy transport in condensed phase is indicated by comparison of calculated multicollision electron spectra with measurements of the corresponding electron spectra emitted from foil targets by proton impact.

Survey of Electron Ejection Cross Sections for Low-Z Molecules by Fast Protons

W. E. Wilson and L. H. Toburen

A fundamental difficulty in performing calculations of track structure in biologically significant material is the complexity of the absorbing media. Calculational techniques, such as Monte Carlo, can be greatly simplified if interaction cross sections for various molecular constituents can be shown to vary in a systematic manner. During the past several years, we have measured differential ionization cross sections for a wide variety of molecular targets and we are now involved in a critical evaluation of these data. The primary goal of this study is to obtain some measure of the amount of variation in the ejected electron yields and energies from molecules containing low-Z atoms in a range of chemical forms. The presumption is made that ejected electrons in tissue will exhibit a similar variation. The achievement of this goal will guide us in perfecting our positive ion model for track structure calculations. A secondary goal of this study is to discover where gaps and shortcomings exist in the data set in order to optimumly guide future experimental effort.

The existing data set is large and there are many types of intercomparisons to be made in order to reveal variations in the systematics among the target molecules. Therefore, to facilitate the intercomparison, we have assembled the experimental data as a preliminary data base on the central computer facility (operated for the Department of Energy by Boeing Computer Services Richland). An interactive computer terminal with graphics capability is used for plotting and comparing the double differential cross sections (DDCS) and single differential cross sections (SDCS) for the many target molecules.

A comparison is shown in Figure 6 of the SDCS for 1 MeV proton ejection of electrons from CH_4, NH_3, H_2O, and O_2, which illustrates systematic effects of the progressive hydrogenation of the molecule. The quantity on the ordinate is the ratio (Y) of SDCS to the Rutherford cross section for n_e electrons, where n_e is the number of weakly bound (valence) electrons in the molecule (equal to the total number of electrons minus the number of K-shell electrons). The abscissa is the $\log_{10}$ of the energy loss in units of the Rydberg (13.6 eV). This representation is especially useful for illustrating the relative contributions to the stopping power that arise from different portions of the delta-ray spectrum. This can be seen from

$$S = \int E\sigma(E)dE \qquad (1)$$

where S is the portion of the stopping power arising from ionizing collisions, and $E = \varepsilon + I_p$ is energy loss. Equation (1) can be expressed

$$S = \int E^2\sigma(E) \quad , \qquad (2)$$

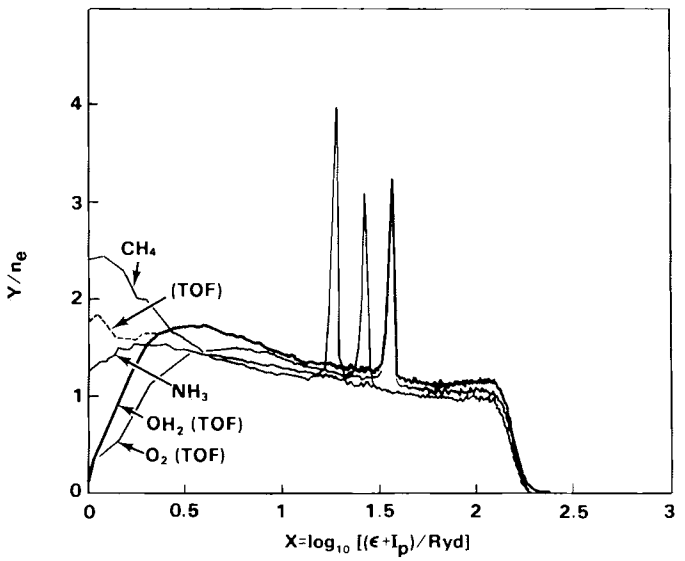

FIGURE 6. Ratio of SDCS to Rutherford Cross Section for n_e Electrons, Y, vs Logarithm (Base 10) of Energy Loss ($\epsilon + I_p$) in Rydbergs for CH_4, NH_3, H_2O, and O_2. The total number of electrons in the molecule minus the number of K-shell electrons is n_e. Equal areas under the curves contribute equally to the stopping power.

which is simply

$$S = \int Y(E)d(\ln E) \qquad (3)$$

This is of the form $\int f(x)dx$ and, therefore, the area under Y(x) vs x, where $x = \ln(\varepsilon+I_p)$, gives the electronic contribution to the stopping power. It should be noted that for fast-charged particles, ionizing collisions account for the major contribution to stopping power (Miller and Green 1973). The narrow peaks occurring at x = 1.5 in Figure 6 arise from Auger electron emission from the respective heavy atom of the molecule.

The preliminary indication from the data in Figure 6 is that molecules having a large fraction of "hydrogenic electrons" have a corresponding large proportion of their total stopping power in the form of low-energy delta rays. Except for O_2, these molecules all have the same number of outer shell electrons, $n_e = 8$. The spectra above an energy loss of about 135 eV (x = 1) do not exhibit any systematic variation and are equivalent within experimental uncertainties. A similar trend is shown in Figure 7 where some of our earliest data on a set of hydrocarbons (methane, ethane, and ethylene) (Wilson and Toburen 1975) are presented in the same type of plot as Figure 6. Again, a correlation can be made with the fraction of "hydrogenic electrons" in the molecule.

One must be cautious in drawing conclusions regarding the shape and intercept of the low-energy portion of the spectra shown in Figures 6 and 7. These data were measured using an electrostatic analyzer which has large uncertainty for transmission of low-energy electrons, i.e., less than 20 eV, $x \sim 0.37$. It is clear that we must study the small energy loss portions of the spectra with time-of-flight techniques that provide more reliable low-energy electron data in order to confirm the observed systematic trends. How important these molecular effects will be for track structure must also be determined. One might suggest, based on these data, that "tissue equivalent" will need to be extended to include chemical equivalence as well as elemental (nuclear) equivalence. If the spatial distributions of energy deposition are significantly affected by the degree of hydrogenation within microscopic sites, then the homogeneous nature of the absorber becomes important and a new stochastic variable comes into play.

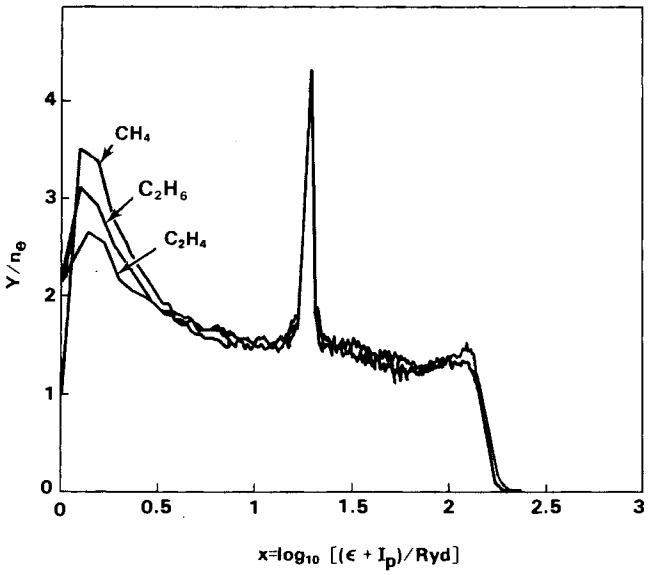

FIGURE 7. Ratio of SDCS to Rutherford Cross Section for n_e Electrons, Y, vs Logarithm (Base 10) of Energy Loss ($\epsilon + I_p$) in Rydbergs for Methane, Ethane, and Ethylene

Ion Tract Model

W. E. Wilson

At the present time, the Monte Carlo method is the only technique for transport calculations that retains the inherent stochastics. A major disadvantage, however, is that the Monte Carlo method is generally a very inefficient numerical procedure; i.e., large amounts of computer time are required to find an approximate answer. We have improved the running speed of our code MOCA13 for calculating certain problems by modifying it to use conditional probabilities.

The conditional probability, $P(\varepsilon/E)$, that a delta ray ejected by a proton will have energy equal to or greater than ε on the condition that it must be equal to or greater than E is defined by

$$P(\varepsilon/E) = \int_{\varepsilon}\sigma(\varepsilon')d\varepsilon' / \int_{E}\sigma(\varepsilon')d\varepsilon' \qquad (4)$$

where $\sigma(\varepsilon')$ is the SDCS for electron ejection with energy ε'. $P(\varepsilon/E)$ is obtained by numerical integration of Equation (4) and using $\sigma(\varepsilon)$ from our phenomenological model of cross-section data (Wilson 1978). In earlier versions of MOCA13, E was fixed at 10 eV; we have modified the code to allow any value for E from zero to the kinematic maximum energy. This is particularly useful where the quantity of energy is not influenced by delta rays with initial energy below the critical energy E.

Equation (4) was evaluated and is shown in Figure 8 for E = 10, 30, and 100 eV for the case of 1 MeV protons. Note that each curve has a magnitude of 1 at ε = E, as required by Equation (4). The respective curve in Figure 7 is inverted to provide a table of delta-ray energies vs probability, which is the form required for Monte Carlo calculations (Figure 9). This inversion is accomplished by straightforward numerical methods and linear interpolation. The advantage to be realized can be seen in Figure 9. The curve for E = 10 reaches a value of 100 eV at about 0.125, i.e., P(100/10) = 1/8, which means that 7/8 of the time the computer would select delta rays with energy between 10 and 100 eV. For E = 30 eV, P(100/30) = 1/3, or about 2/3 of the time the delta-ray energy is between 30 and 100 eV. Finally, of course, P(100/100) = 1 and delta rays of less than 100 eV are never selected.

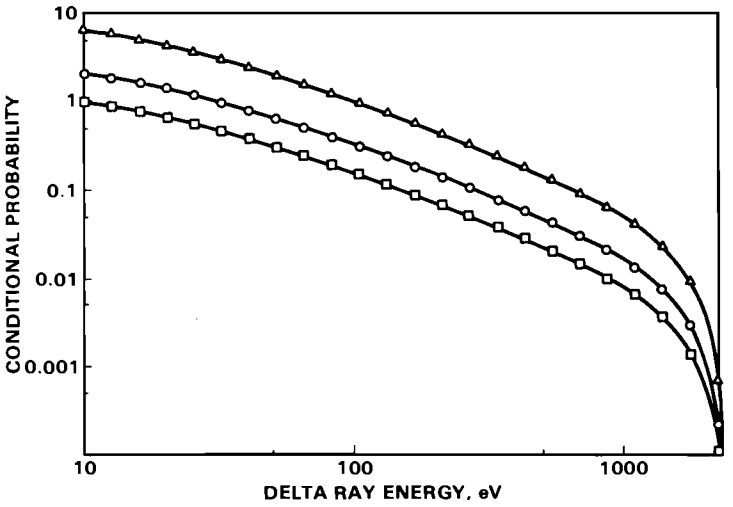

FIGURE 8. Conditional Probabilities for Ejection of Delta Rays of Energy E or Greater, on the Condition that the Energy Be Greater than 10, 30, or 100 eV, Respectively

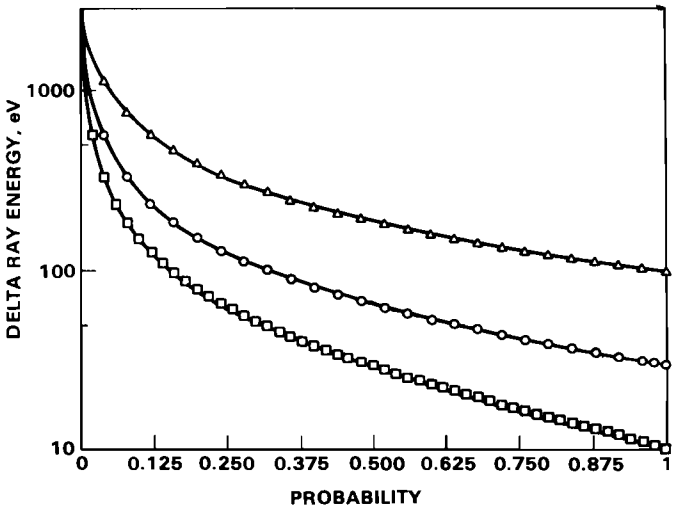

FIGURE 9. Delta-Ray Energies Selected for Random Numbers Between 0 and 1 for the Three Cases in Figure 8

We expect to employ this procedure when calculating energy imparted and ionization in small sites for ion tracks that pass at some distance outside the site. In this case, only delta rays with range greater than the minimum distance from ion path to absorber need be considered. The above example indicates we should realize a factor approaching 8X in computation speed when the ion-path-to-absorber distance is equivalent to the range of 100 eV electrons (~55 Å).

Ionization Distributions in Condensed Phase

W. E. Wilson, L. H. Toburen, and
H. G. Paretzke*

Real radiological problems in dosimetry most often involve radiation interactions in condensed phase. Because MOCA13 is modeled after gaseous phase data, the validity of our calculations must be carefully and continuously verified for utility in condensed phase. Unfortunately, useful experimental measurements of ionization and energy deposition distributions in condensed phase are not readily available. We have devised an alternative check of the reliability of our electron transport calculations by experimental measurement in which the ionization is initially created in condensed phase and detected in vacuum. The experimental measurements are spectra of secondary electron emission from solid foils that are sufficiently thick to cause the secondaries to multi-scatter before exiting from the foil.

The same energy and angular distributions can be calculated from MOCA13. Preliminary results reported last year (Wilson et al. 1978) suffered from low statistical accuracy. We have now obtained results with sufficient statistical significance to be able to draw definitive conclusions. In Figure 10, we compare the MOCA13 calculations (histogram) for 5×10^5 protons passing through a 3 $\mu g/cm^2$ solid foil with experiment (solid line). The overall absolute agreement is within experimental uncertainties (±20%). However, systematic disparities are apparent. There are two major ones: the first is in the shape(s) of the spectra and their angular dependency, and the second is the absence of K-Auger contributions to the calculated spectra. At 50^o, the calculation is lower than experiment between 100 and 1000 eV and higher above 1000 eV. This trend carries over to larger angles with the "too high" region growing and the "too low" region lessening as 90^o is approached. At back angles, as the emission angle moves away from 90^o, the trend reverses and quite good agreement is found at 125^o.

The disagreement in shape of energy spectra suggests a possible error in foil thickness. If we calculate for a foil thicker than 3 $\mu g/cm^2$, the energy spectra increase for energetic electrons relative to intermediate energy ones, i.e., the disparity with experiment, increases. The 3 $\mu g/cm^2$ figure for the thickness is the supplier's specification and we have no easy means of independently verifying it. Calculations for a thinner foil are under consideration, but we feel that the problem regarding a lack of Auger contribution to the spectra must be solved before additional calculations are undertaken. As indicated above and illustrated in Figure 10, we simply do not see sufficient evidence for Auger electrons at any angle. This may arise from a coding error in the dynamics of simulating Auger emission or it may be that we have a poor representation of the relative inner shell ionization cross section. Both possibilities are being investigated.

---

* Consultant, Institüt für Strahlenshutz, Munich, Germany.

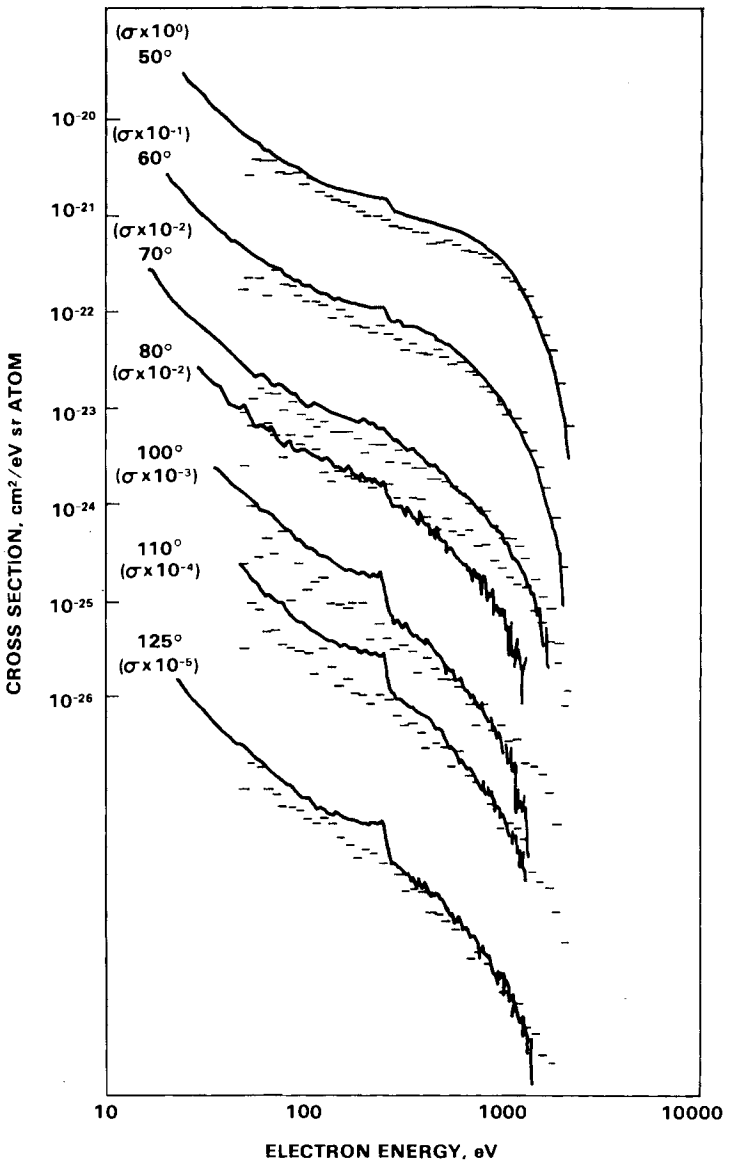

FIGURE 10. Secondary Electron Emission for 1.0 MeV Protons Passing Through a 3 g/cm^2 Foil. Solid curves are experiment; histograms are calculated by MOCA13. Curves are offset for clarity.

• Energy Transport

The study of energy transport following energy deposition in binary liquid systems by both ionizing and nonionizing radiation has led to the development of diffusion kinetic models of radiation chemistry that incorporate track structure phenomena (Miller and West 1978). These models, which maintain the stochastic nature of the interactions, provide a more detailed understanding of the nature of radiation effects on biological systems. Pulsed radioluminescence from binary liquid systems is studied as a probe of the energy transport process. The radioluminescence decay is characterized by a solvent quenching term associated with intramolecular and intermolecular processes that can be observed for ultraviolet excitation and a radiation-induced quenching term associated with the nonhomogeneous deposition of energy in the form of tracks. Our initial measurements of the temperature (West and Miller 1979) and energy dependence (Miller and West 1977) of proton-induced fluorescence support this model of intratrack quenching by radiation products. We have since extended these studies to include the concentration dependence of proton radioluminescence and time-resolved emission from liquids irradiated with pulsed alpha-particle beams. Comparison of luminescence induced by protons and alpha particles of the same stopping power plays a key role in the development of the stochastic model for diffusion kinetics. This model has also been formulated for a multiradical system as a step toward the prediction of track structure effects in pulsed radiolysis of aqueous media.

Fluorescence Decay in Binary Liquid Systems

M. L. West

Concentration Dependence

When dilute solutions of benzene in cyclohexane are irradiated with subnanosecond bursts of protons, the asymptotic slope of the fluorescence decay of benzene increases with increased benzene concentration (West and Miller 1978). This observed change in the time-resolved emission with change in benzene concentration has been interpreted as a concentration dependence of the radiation-induced quenching term. Such an interpretation suggests that the concentration of quenching molecules along the particle track depends on the number of benzene molecules in solution. This implies that either benzene alters the products of radiolysis or that the radiolysis products of benzene are responsible for quenching.

In this interpretation of the results, there has been an implicit assumption that fluorescence decay of the first excited single state of benzene under ultraviolet excitation is exponential and independent of benzene concentration. Gregory and Helman (1972) have reported that the lifetime of this first excited singlet state of benzene in methylcyclohexane at room temperature is independent of concentration for concentrations less than 0.5M. Dillon and Burton (1965) showed that lifetimes were constant up to concentrations of 0.05M benzene in solutions of cyclohexane + p-terphenyl for excitation by 30-kV x-rays. Changes in lifetime at higher concentrations are attributed to the formation of excimers between excited and ground-state benzene molecules. At the lower concentrations, the excimer formation is very improbable and no effects have been reported.

In our previous studies of the energy and temperature dependence of proton-induced quenching, experimental measurements of proton and ultraviolet-induced fluorescence were made at concentrations below 0.05M. Here we present decay measurements for ultraviolet excitation as a function of benzene concentrations to check for consistency with published results and to provide complete decay curves to complement our previous measurements of proton-induced fluorescence (West and Miller 1978). Gregory and Helman (1972) present only extrapolated lifetimes.

A commercially available (ORTEC) nanosecond spectrofluorometer forms the basic apparatus for our lifetime measurements for ultraviolet excitation. However, because of the low light levels, a more intense flash lamp was used. The present excitation source has adequate photon intensity but is limited to 9 nsec full width at half maximum (FWHM) resolution as compared to 2 nsec FWHM for the ORTEC system. During this past year, the system was put into operation and preliminary measurements have been made. Fluorescence decay curves for 0.0125, 0.05, and 0.2M benzene in cyclohexane are shown in Figure 11. For the lower concentrations of 0.0125 and 0.05M, the decay curves appear to be identical and there is no apparent excimer quenching. However, at the higher concentration of 0.2M, excimer effects are readily apparent. These results are consistent with those of Dillon and Burton (1965) and indicate that excimer kinetics must be considered at the higher concentration of benzene for both ultraviolet and proton-induced fluorescence.

In our previous interpretation of the concentration dependence of proton-induced fluorescence, such effects were ignored. This correction still does not explain the observed concentration dependence of proton-induced fluorescence at concentrations of 0.05 and 0.0125M, unless there is perhaps a radiation enhancement effect of the excimer contributions.

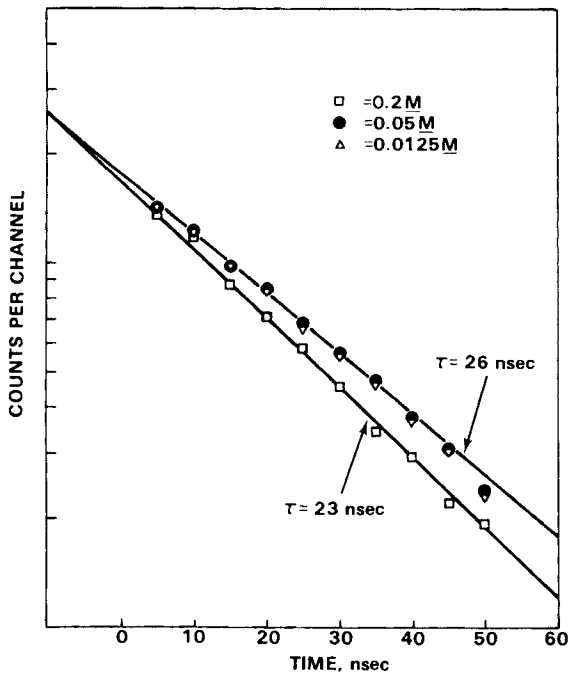

FIGURE 11. Time Dependence of Ultraviolet-Induced Benzene Fluorescence at Several Concentrations of Benzene in Cyclohexane

Radiation Quality Effects

When dilute solutions of benzene in cyclohexane are irradiated with protons, there is an observed decrease in the quenching of benzene fluorescence with increase in incident proton energy. This energy dependence agrees with our diffusion model, which predicts a linear relationship between the proton-induced quenching and the linear energy transfer (LET) of the incident particle.

In the usual LET approximation, particles of the same LET would be expected to have identical fluorescence decay. However, when the details of track structure are considered, i.e., different spatial energy distributions for different particle types, our model predicts a reduced quenching for alpha particles as compared to protons of identical LET.

To test this hypothesis of a radiation quality effect, we have initiated an experimental investigation (West and Miller 1979) of the time-resolved emission induced by high-energy alpha particles with the 20-MV tandem accelerator facility at the University of Washington Nuclear Physics Laboratory. Pulsed alpha beams of about 2 nsec FWHM with energies up to 27 MeV are available from the tandem accelerator using a three-stage klystron buncher (Weitkamp and Schmidt 1974).

Samples of 0.04M benzene in cyclohexane at a constant temperature of 20°C were irradiated with alpha particles of energies 6, 8, 12, 18, and 27 MeV for comparison with the proton data. Typical decay curves are shown in Figure 12. The dashed line represents an exponential decay with a lifetime of 32 nsec, which is the value measured at 20° for ultraviolet excitation. A series of five runs with 8000 counts in the peak were made at each energy to insure adequate statistics for parameter extraction using least squares analysis.

The rate of decay for alpha-particle-induced fluorescence is initially much greater than that for ultraviolet excitation but approaches the ultraviolet rate as time increases. This is similar to the previously reported results for proton excitation (Miller and West 1977). Alpha-particle

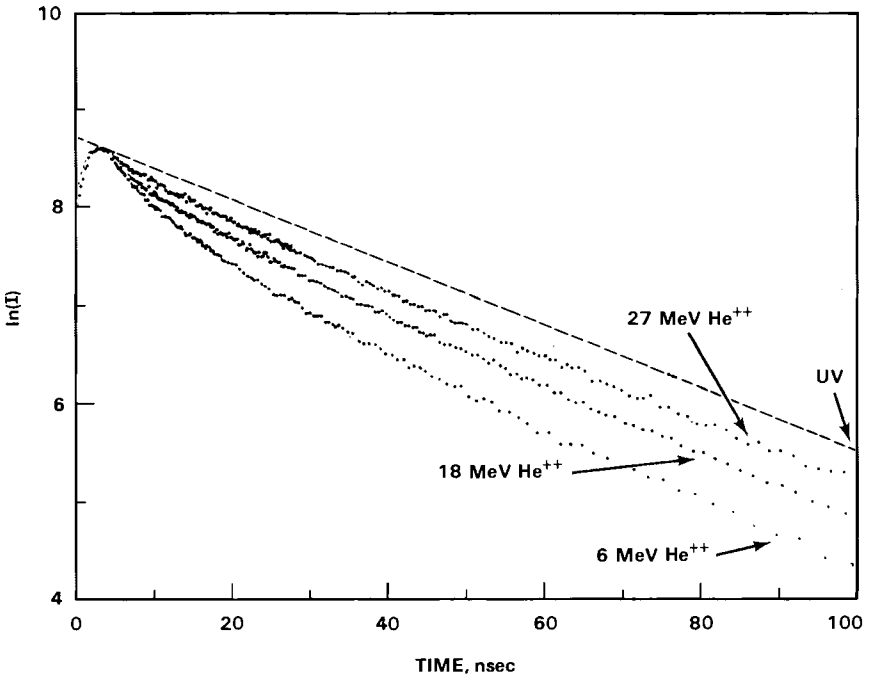

FIGURE 12. Time Dependence of Alpha-Induced Benzene Fluorescence at Several Alpha Particle Energies

excitations at 6, 8, 12, 18, and 27 MeV correspond to mean stopping powers of 13, 11, 9, 7, and 5 eV/Å, respectively. Proton-induced fluorescence measurements over the energy interval 0.75 to 13 MeV correspond to mean stopping powers of approximately 7 to 1 eV/Å, respectively. Figure 13 compares the 0.75 MeV proton data with the 18-MeV alpha particle fluorescence. At these energies, alpha particles and protons have approximately the same LET of 7 eV/Å. The radiation quality effect of reduced quenching for alpha particles is clearly illustrated.

A more detailed analysis of these data will include a test of the predicted linear relationship between alpha particle-induced quenching and LET and a comparison of the quenching rates with model prediction (see J. H. Miller, next discussion).

Quantitative Analysis of Time-Resolved Radioluminescence Data

J. H. Miller

The radioluminescence decay curve of most aromatic scintillators consists of a prompt component similar to the fluorescence of the medium and a slow component from the delayed formation of singlet emission. The effects of radiation quality on the slow component have been extensively investigated (Fuchs and Heisel 1977). Effects of radiation quality on the prompt component were expected to be small since it was assumed that singlet states produced in the early stages of radiation action would decay in the same manner as singlets produced by nonionizing radiation. This assumption ignores the nonspecific and inhomogeneous characteristics of energy deposition by ionizing radiation. Singlet states produced by ionizing radiation decay in a medium that has been strongly perturbed by the radiation. We are investigating the effect of this perturbation on the radioluminescence of benzene in cyclohexane, which does not exhibit delayed luminescence due to the instability of the benzene negative ion (Christophorous 1976).

The perturbation of a medium by radiation with large linear energy transfer (LET) can be modeled to a first approximation by a concentration of reactive species that is cylindrically symmetric with respect to the trajectory of the ion. This approximation was used by Miller and West (1977) to derive the expression

$$\ln(I/I_0) = -t/\tau - \alpha \ln(1 + t/t_D) \qquad (5)$$

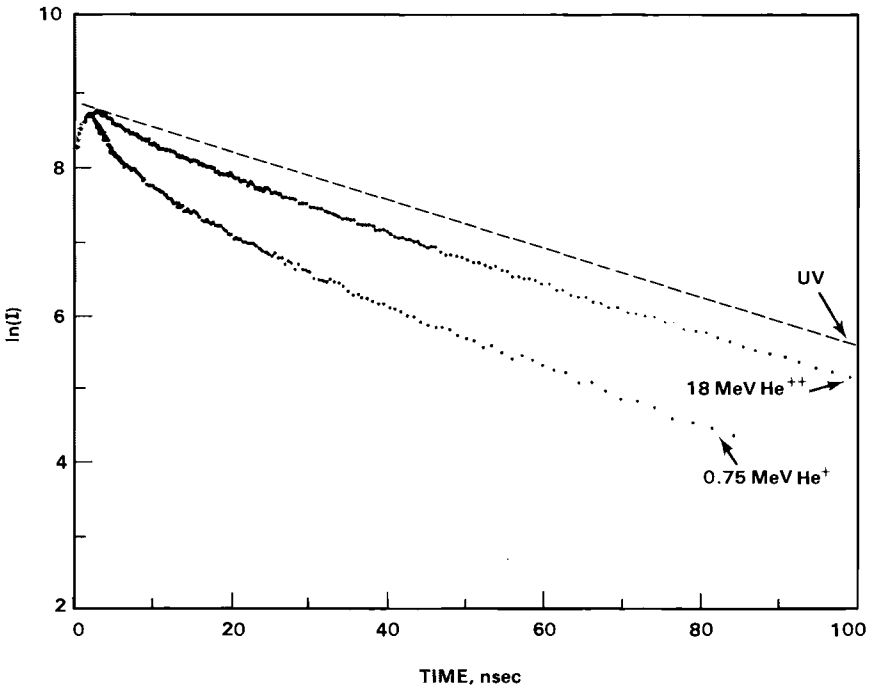

FIGURE 13. Comparison of Alpha- and Proton-Induced Benzene Fluorescence at Nearly Equal Stopping Power

for the time dependence of pulsed proton radioluminescence. In Equation (5), τ denotes the mean lifetime of benzene singlet states in the unperturbed medium, and

$$\alpha = \rho_{Q^*} g_Q \frac{dE}{dX} \qquad (6)$$

is the product of the interaction radius for quenching, ρ_{Q^*}, the yield of radiation induced quenchers, g_Q, and the mean stopping power of the radiation, $\frac{dE}{dX}$. The parameter t_D is the time required to reduce the concentration of quenchers to half its initial value due to diffusion of chemical species away from the trajectory of the primary ion.

When Equation (5) was used to analyze alpha particle luminescence data, the nonlinear least squares program for estimating the parameters τ, α, and t_D, frequently did not converge. The problem was traced to the estimation of t_D which is expected to have a value of the order of one nanosecond. Since the time resolution of the alpha radioluminescence is considerably poorer than the pulsed proton data, the condition $t \gg t_D$ is satisfied for most of the data that are not influenced by convolution with the experimental resolution function. When $t \gg t_D$, Equation (5) reduces to

$$\ln I = \ln I_0 + \alpha \ln t_D - t/\tau - \alpha \ln t \qquad (5')$$

The effect of t_D on the predicted decay curve cannot be distinguished from the overall normalization constant. Hence, it was concluded that a new method of data analysis was needed for the alpha radioluminescence which did not require simultaneous determination of the parameter t_D.

The luminescence decay predicted by Equation (5') is a linear function of the parameters τ^{-1} and α. Hence, by neglecting the early part of the decay curve ($t \leq$ 10 ns) from the fitting, τ^{-1} can be determined by linear regression without information about the parameter t_D. This method has the further advantages that it is readily adaptable to on-line data analysis and is susceptible to rigorous statistical analysis of the uncertainty in parameter estimates.

Figure 14 illustrates the results obtained for the mean lifetime of excited states of benzene in cyclohexane when this method of data reduction is applied to pulsed proton luminescence at various sample temperatures (West and Miller 1979). The error bars denote 99% confidence intervals on the parameter estimates. The agreement between fluorescence decay rates (solid curve) and values of τ^{-1} deduced from proton radioluminescence data lends support to the quenching model and to the method of data reduction.

Values of the parameter α deduced from proton and alpha particle luminescence data at various beam energies are shown in Figure 15 plotted as a function of the mean stopping power of the primary ion in the sample. For each particle type, the quenching parameter α is proportional to the mean stopping power, as predicted by Equation (6). If the interaction radius is 5 Å, then the proton data suggest that the yield of quencher is 1.5 ± 0.2 quenchers per 100 eV of absorbed energy. If the same species are involved in the quenching of alpha particle radioluminescence, then the cylindrical track model predicts that the slope of the α vs $\frac{dE}{dX}$ relationship should be the same for both types of radiation. From Figure 15, it can be seen that this slope is only half as great for alpha particles as for protons.

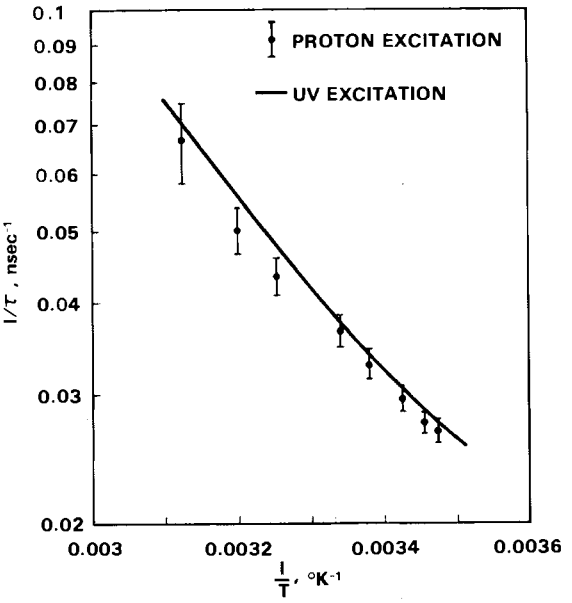

FIGURE 14. Mean Lifetime of Benzene Luminescence Excited by Protons for Various Sample Temperatures

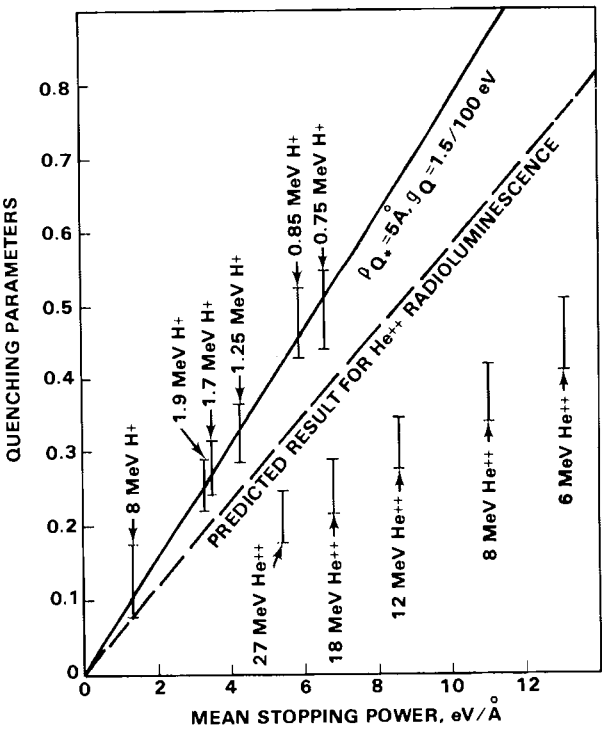

FIGURE 15. Values of the Quenching Parameter α for Proton and Alpha Particle-Induced Luminescence of Benzene as a Function of the Stopping Power of the Incident Ion

A part of the reduction in quenching observed in alpha radioluminescence relative to protons of the same mean stopping power can be attributed to the difference in the spatial distribution of energy deposited by the two types of radiation. The higher velocity ion produces a more energetic spectrum of secondary electrons, which leads to a more diffuse pattern of energy deposition. Hence, for the same quencher yield per unit energy absorbed, the concentration of quenchers would be less for alpha particles than for protons of the same stopping powers. The dashed line in Figure 15 shows the predicted variation of α with mean stopping power when these track structure effects are included in the calculation of quenching for alpha particle radioluminescence (see next section). These results were also presented at the Sixth International Congress of Radiation Research, May 13-19, 1979. The basis of this prediction and possible sources of error will be discussed in the next section.

Diffusion Kinetics of Radioluminescence Quenching

J. H. Miller

Energy deposited by ionizing radiation gives rise to a nonhomogeneous distribution of reactive species. A stochastic model of diffusion kinetics has been proposed (Miller and West 1978) which relates the concentration of reactants to detailed track structure calculations (Wilson and Paretzke 1979) of the initial spatial distribution of absorbed energy. This model has been used to calculate the relative amount of quenching in the decay of radioluminescence induced by protons and alpha particles of the same stopping power (PNL Annual Report 1978). Analysis of pulsed alpha particle radioluminescence data (Miller and West 1979) showed that predictions of the stochastic model underestimated the reduction in quenching of alpha particle luminescence. In this section, the stochastic model will be reviewed briefly and possible sources of this discrepancy will be discussed.

Since the concentration of benzene in the scintillator is small, the quenching reaction should obey pseudo first-order kinetics. Hence, the rate of radiation-induced quenching, K_R, is the product of the bimolecular quenching rate, K_{Q*}, and the mean concentration of quencher near an excited state. Both excited states and quenchers are assumed to be produced in regions where the density of energy transferred from the radiation to medium is high. Following the tradition established by Samuel and Magee (1953), these regions are referred to as "spurs." We have characterized each spur by the amount of energy deposited, ε, the position, $\vec{r}$, and the distribution of reactants produced by the energy deposition. The distribution of reactants is assumed to be Gaussian with a variance, σ, which increases with time due to diffusion.

The rate of radiation-induced quenching is calculated from the expression

$$K_R = K_{Q*} \left\langle \sum_{j=1}^{N} \frac{g_Q \varepsilon_j}{8\pi^{3/2}\sigma^3} \exp\left[\frac{(\vec{r} - \vec{r}_j)^2}{4\sigma^2} \right] \middle| \vec{r} \right\rangle \qquad (7)$$

where g_Q is the quencher yield, the sum extends over all spurs in the medium, and the average is with respect to the position of excited states. The factor $g_Q\varepsilon_j/8\pi^{3/2}\sigma^3$ may be interpreted as the concentration of quenchers in the spur at position $\vec{r}_j$ and the exponential factor is the probability that this spur overlaps the spur at $\vec{r}$, which contains the excited state. Diffusion increases the probability of intraspur quenching; however, it also decreases the concentration of reactants within a spur. The net effect is that radiation-induced quenching decreases with time and the decay rate of singlet states in the unperturbed medium is approached.

It is useful to normalize numerical results obtained from Equation (7) to those obtained when spurs are assumed to be randomly dispersed along the axis of the primary ion (Ganguly and Magee 1956):

$$K_R^{CT} = \frac{k_{Q*} g_Q}{8\pi^{3/2}\sigma^3} \left(\langle \varepsilon \rangle + 2\sqrt{\pi\sigma}\, dE/dX \right) \qquad (8)$$

This result is labeled CT for cylindrical track approximation since it leads to the expression given in Equation (5) for the luminescence decay curve.

The principal area of uncertainty in the stochastic model is the relationship between inelastic electronic collisions, which occur on a time scale of 10^{-16} sec, and the concentration of chemical species at a time of the order of 10^{-12} sec when it becomes appropriate to describe the relaxation of

the irradiated medium in terms of diffusion kinetics (Kupperman 1974). In the absence of a general theory of the formation of chemical species, we have made the assumption that the yield of a reactant at a given point in the medium is proportional to the amount of energy absorbed by the medium near that point. Let ε_C denote the energy at which an electron may be considered to be localized in the medium. If a secondary electron is ejected from a molecule with energy less than ε_C, it is assumed that its kinetic energy will be dissipated near the parent ion and both the ionization potential and the kinetic energy of the electron are included in the energy of the spur at the position of the ionization. We call this type of event a "glancing ionization." Similarly, if the residual energy of an electron after an inelastic collision is less than ε_C, this residual kinetic energy is included in the energy of the spur at the position of last inelastic collision. We call this type of an event a "track end." In addition to these two types of event, we also have "hard ionizations" where the secondary electron has energy greater than ε_C and "excitations" where no secondary electron is generated. For these events, the spur energy is set equal to the ionization potential or the energy level of the excitation, respectively.

Table 1 shows the mean energy for each of the four types of spurs included in the model and the fraction of the total energy absorbed in this type of event when the cut-off energy is 50 eV. Note that the largest fraction of energy is deposited in the form of glancing ionizations; however, the most frequent collision is a simple excitation of the medium. As ε_C is decreased, the average energy of a spur decreases and the fraction of energy absorbed in small energy transfer events increases. Results obtained for the quenching rate were not significantly different when the cut-off energy was changed from 50 to 25 eV. A more dramatic way to alter the relationship between energy absorbed and the initial concentration of reactants would be to assume that quenchers were formed only in certain types of spurs; for example, track ends. The effect of this kind of assumption on the predictions of the model is currently being tested.

The cross-section data used to calculate the position and energy of spurs is another possible area of uncertainty in the model calculations. The Monte Carlo program used for these calculations is essentially the same as that described by H. Paretzke (1973). Two types of cross-section data are required by the program: differential ionization cross sections for the production of secondary electrons by the primary ion and cross sections required for the transport of these electrons. The Thomas approximation (Rudd and Macek 1972) was used for the differential ionization cross section. Table 2 compares the mean energy of secondary electrons calculated in this approximation with that deduced from measured differential ionization cross sections for proton impact on water vapor (Toburen and Wilson 1977). The mean is slightly greater for the measured spectrum and the difference tends to increase as the ion velocity increases. This may be due in part to the uncertainty in the measured spectrum at low electron energy. No data are presently available for alpha particles at the energies used in the radioluminescence studies. Sensitivity of the model predictions to the secondary electron spectrum is being investigated.

The model predictions shown in Figure 15 were based on data for electron impact on water vapor (Oliver et al. 1972). A set of electron transport cross sections based on

TABLE 1. Mean Energy and Frequency of Localized Energy Transfer Events (Spurs)

Spur Type	Mean Energy per Event, eV	Fraction of Total Energy Absorbed, %
Excitation	5	25
Hard Ionization	10	10
Glancing Ionization	25	50
Track Ends	50	15

TABLE 2. Mean Energy of Secondary Electron Spectra from Proton Impact Ionization of Water

Proton Energy, eV	$\bar{\varepsilon}$,eV[a]	$\bar{\varepsilon}$,eV[b]
0.5	31	34
1.0	36	42
1.5	40	48
2.0	42	53

[a] Calculated from Thomas approximation
[b] Calculated from cross-section data

hydrocarbon data, which may be more appropriate for transport of electrons in cyclohexane, has been developed. Figure 16 compares the cross section per valence electron for elastic scattering and ionization by electrons in H_2O and C_6H_{12}. The principal difference between these two sets of cross sections is that elastic scattering predominates at higher electron energy in the H_2O data. Figure 17 shows the difference in the predictions of the model that results from this change in electron transport cross sections. The relative frequency of elastic and inelastic collisions affects the model predictions at early times when the radius of the spurs is small. When the spur radius exceeds about 100 Å, the two sets of cross-section data give essentially the same results.

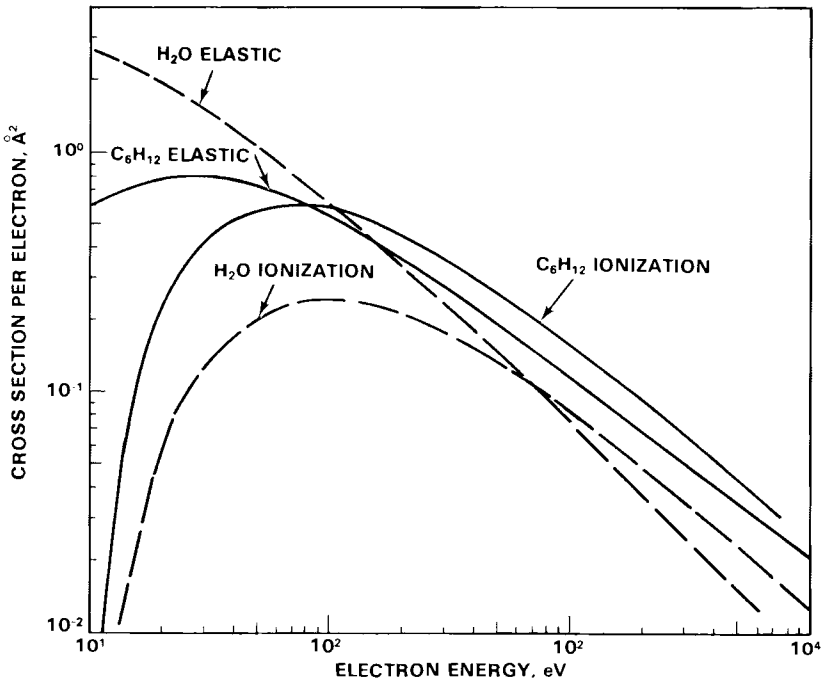

FIGURE 16. Comparison of Cross Sections for Elastic Scattering of and Ionization by Electrons in Water Vapor and Benzene

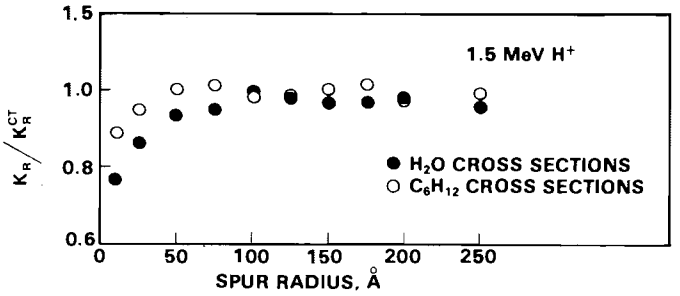

FIGURE 17. Sensitivity of the Model Predictions to Electron Transport, Cross-Section Data. Ratio of quenching rates calculated in stochastic and cylindrical track model (●) using H_2O data and (○) using hydrocarbon data.

A third area in which the model may be deficient is with regard to the chemical kinetics. We have assumed that the radiation-induced quenching species are stable on the time scale of the luminescence measurements (≳100 nsec). These quenchers may be free radical species which would undergo some recombination during the first 100 nsec following the excitation pulse. However, it is difficult to see how this effect would contribute to lower quenching of alpha luminescence relative to protons, since the more diffuse track structure should hinder the recombination reaction.

The principal areas of uncertainty in the predictions of the stochastic model have been examined. More tests of the sensitivity of the results to model assumptions and data input need to be made. However, none of the tests performed thus far modify the predictions of the model sufficiently to explain all of the observed reduction in quenching of alpha radioluminsecence on the basis of track structure effects.

Stochastic Model of Diffusion Kinetics for Multi-Radical Systems

J. H. Miller

The model presented in the previous section for the quenching of prompt radioluminescence was based on the simplifying assumption that the population of quenching species was time independent. This is a reasonable approximation provided the rates of reactions that alter the quencher population are significantly lower than the quenching reaction rate. To incorporate more complex chemical kinetics into the quenching model or to adapt the stochastic model to aqueous systems, it is necessary to develop a mathematical method for treating coupled reactions. A method that is applicable to systems of binary reactions is presented in this section.

Assume that a set of inhomogeneously distributed chemical species are undergoing simultaneous diffuse and chemical reactions of the form A + B → products. Let C_α denote the concentration of the reactant α with diffusion coefficient D_α. Let $A_{\alpha\beta}$ denote the rate of annihilation of α by reaction with β, and $P_{\beta\gamma}$ denote the rate of production of α by the reaction between species β and γ. Then the concentration of each reactant in the system will satisfy an equation of the form:

$$\frac{\partial C_\alpha}{\partial t} = D_\alpha \nabla^2 C_\alpha - \sum_\beta A_{\alpha\beta} C_\alpha C_\beta + \sum_{\beta,\gamma\neq\alpha} P_{\beta\gamma} C_\beta C_\gamma \quad (9)$$

We approximate the concentration of reactants as a linear super-position of Gaussian distribution functions centered at the positions of large local energy transfer between the radiation and the medium:

$$C_\alpha(\vec{r},t) = \sum_{j=1}^{N} \frac{n_{\alpha j}(t)}{\pi^{3/2} b^3_j(t)} \exp\left[-\frac{(\vec{r}-\vec{r}_j)^2}{b^2_{\alpha j}(t)}\right] \quad (10)$$

As in the previous section, we refer to these regions as "spurs." The variance of

the distribution of reactants within a spur is assumed to increase linearly with the time according to

$$b_{\alpha j}^2(t) = 2\rho_{\alpha j}^2 + 4D_\alpha t \qquad (11)$$

where $\rho_{\alpha j}$ is the initial variance of the distribution, which results from processes that intervene between the initial energy deposition and the onset of diffusion and chemical reactions. The factor $n_{\alpha j}$ in Equation (10) is the contribution from the j^{th} spur to the concentration of reactant α. We assume that at all times this contribution is proportional to the initial energy deposited in the spur:

$$n_{\alpha j} = g_\alpha(t)\varepsilon_j \qquad (12)$$

where g_α is the mean yield of reactant α per unit energy absorbed.

Substitution of Equation (10) into Equation (9) and integrating over spatial coordinates gives ordinary differential equations for the time-dependent yield of reactants:

$$\frac{dg_\alpha}{dt} = -\sum_\beta A_{\alpha\beta} g_\alpha g_\beta \bar{d}_{\alpha\beta} + \sum_{\beta,\gamma\neq\alpha} P_{\beta\gamma}\, g_\beta g_\alpha \bar{d}_{\beta\gamma} \qquad (13)$$

where

$$\bar{d}_{AB}(t) = E^{-1}\sum_{i=1}^{N}\varepsilon_i \sum_{j=1}^{N}\varepsilon_j \frac{e^{-(\vec{r}_i-\vec{r}_j)^2/(b_A^2+b_B^2)}}{\pi^{3/2}(b_A^2+b_B^2)^{3/2}} \qquad (14)$$

is a time-dependent mean energy density associated with the reaction A + B → products. The quantity $\bar{d}_{AB}$ may be interpreted as the mean energy per unit volume available for the production of species A in the neighborhood of species B. Given that species B is present in the i^{th} spur, the sum over j gives the contribution to the energy density at $\vec{r}_i$ from all spurs in the medium. The probability of finding B in the i^{th} spur is proportional to the energy deposited in the i^{th} spur; hence, ε_i is present as a weight factor in the average with respect to positions of molecule B. The total energy deposited in the medium, E, normalizes the weighted average. With respect to the interchange of A and B, $\bar{d}_{AB}$ is symmetric.

The stochastic aspects of this model all refer to the random nature of the initial energy deposition. The subsequent diffusion and reaction of chemical species are treated in a deterministic manner. The approximation we have made allows us to separate the stochastic, track structure aspects of the problem from the chemical kinetics aspects. Given the initial spur radius and diffusion coefficient for each reactant, the energy density functions for each reaction are calculated from Monte Carlo simulation of the track structure. Given the time-dependent energy densities, the time-dependent yields are found by solution of coupled ordinary differential equations. This formulation of the problem is similar to that presented by Schwartz (1968); however, his model is based on the simplifying assumption that spurs are randomly distributed along the axis of the primary ion. The present model should offer the opportunity to investigate the effect of more detailed track structure information on the predictions of diffusion kinetic models.

• Radiation Dosimetry and Radiation Biophysics

Radiation dosimetry and radiation biophysics are two closely integrated programs whose joint purpose is to explore the connections between the primary physical events produced by radiation and their biological consequences in cellular systems. The radiation dosimetry program includes the theoretical description of primary events and their connection with the observable biological effects. This program also is concerned with design and measurement of those physical parameters used in the theory or to support biological experiments. The radiation biophysics program tests and uses the theoretical developments for experimental design. Also, this program provides information for further theoretical development through experiments on cellular systems.

Rapid Repair in Mitotic Mammalian Cells

J. M. Nelson, L. A. Braby, and W. C. Roesch

Fast and slow repair processes typically exist and function simultaneously within a single organism. This seriously compromises the ability to investigate either. In addition, observations in mammalian cells even at very short time intervals are seriously impaired by time-dependent changes in cellular radiation sensitivity. As a result, studies become possible only with the development of techniques to establish different sorts of stationary cultures. Cells in mitosis, however, appear to be a unique exception to this.

Mitotic mammalian cells exposed to lethal doses of ionizing radiation usually exhibit simple straight-line survival curves when the logarithm of survival is plotted as a function of dose. The absence of a shoulder on this curve has led investigators to assume that mitotic cells do not repair radiation damage and, therefore, should not exhibit dose rate or dose fractionation effects. Indeed, they do not at conventional dose rates. This lack of "normal" or slow repair leads us to conclude that there should be little or no interference with attempts to investigate fast repair were it to be present in mitotic mammalian cells.

Cells irradiated during mitosis show an increase in relative biological effectiveness (RBE) with increasing linear energy transfer (LET), which suggests that some sublethal damage repair does indeed take place (Roesch 1978a). That it is not seen in dose-rate and split-dose experiments at conventional dose rates could be due to a familiar phenomenon: as the dose rate is lowered, the survival curves of cells that do show protraction and fractionation effects tend to become simple exponential curves. The dose rates at which the curvature becomes inappreciable increase as the repair process becomes faster. We have speculated that a repair process exists in mitotic cells that functions so fast that dose rates heretofore used were so low that curvature was not detectable; but if the dose rate were increased, the curves would develop the expected curvature.

The survival curves of most other cells that exhibit pronounced shoulders for gamma irradiation always become simple exponentials at very low dose rates. Such an argument assumes that the sublethal damage responsible for the LET effect is the same as (or closely related to) that responsible for dose-rate or fractionation effects; an assumption which must be tested, but one which is certainly the simplest hypothesis. In theory then, one would predict that if mitotic mammalian cells do repair sublethal radiation damage, their simple exponential survival curve would give way to the characteristic exponential curve with a shoulder at higher dose rates. The result of this hypothesis is illustrated in Figure 18. Other modeling activities suggest that such rapid processes may contribute to what is currently thought of as the single-event component of cell killing (Roesch 1978a). From these two converging lines of reasoning, we were therefore led to look for protraction or fractionation effects in mitotic mammalian cells using very high dose rates.

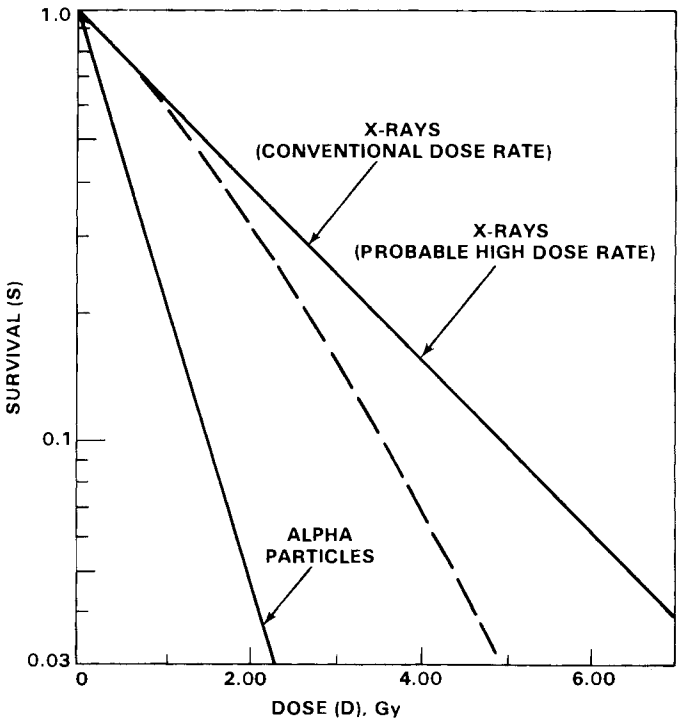

FIGURE 18. Theoretical Survival Curves for Mitotic Mammalian Cells After High LET Irradiation and Low LET Irradiations at Conventional and Extremely High Dose Rates. At conventional dose rates, both curves are simple exponentials, i.e., straight lines, indicating that repair must be very fast; the shoulder would appear only at very high dose rates.

Conventional dose-rate experiments using large numbers of morphologically identical cells selected from synchronous mitotic cell populations derived from exponentially growing cultures of Chinese hamster ovary (CHO) cells were used to investigate these fast repair phenomena. Populations of exponentially growing cells were irradiated with 1.5 MeV electrons at very high dose rates. Immediately after irradiation, mitotic cells were removed from these populations by mechanical methods (mitotic selection) and these selected cells were then counted and replated. Several hundred individual cells on these new plates were observed 2 hr later using a computer-controlled video camera-microscope system. Their images and the necessary digital information identifying the specific image location were recorded on video disks (Braby and Nelson 1979). Six days later, those specific cells morphologically identified earlier were again observed to determine which had produced sufficient progeny to be classified as survivors and which had not. The majority of the cells shaken off (greater than 96%) were single cells at the time of their mechanical removal but had developed into doublets when first observed at 2 hr. These were confirmed to be late metaphase to mid-anaphase cells at the time they were irradiated, which continued their progression through telephase by the time they were first observed. Only the survivors of these selected doublets were scored.

Results of these experiments are shown in Figure 19. For dose rates of less than 1 krad/sec, we observe the familiar straight-line survival curve indistinguishable from the exponential survival curves observed at much lower dose rates. In contrast, at 75 krad/sec, the curve is found to have a shoulder similar to that predicted in Figure 18. This is probably the same phenomenon observed with cells that exhibit slower repair processes, i.e., the shoulder appears as the dose rate is increased.

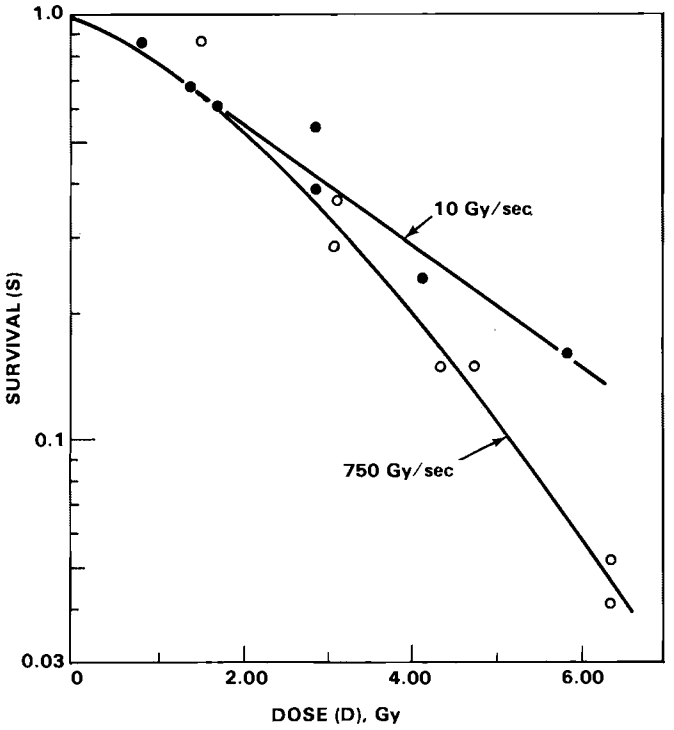

FIGURE 19. Experimental Findings Using Mitotic Mammalian Cells Which Support the Theoretical Predictions Illustrated in Figure 18. Simple exponential survival persists at does rates as high as 10 Gy/sec (1000 rad/sec); however, at 750 Gy/sec (75,000 rad/sec), a shoulder on the survival curve and an increase in radio-sensitivity have both become apparent.

We believe these experiments have conclusively demonstrated some form of repair or recovery process not observable at conventional dose rates. We realize, too, that this may not necessarily represent repair in the classical sense, i.e., enzymatic repair. It nevertheless represents a subcellular process which leads to a reduction of radiation damage, which in turn results in an increased survival as a function of time. As this work is still in progress, we are not yet able to report a characteristic time for the process but can tell from these experiments that it is on the order of 0.1 sec or less. These results are consistent with theoretical predictions, although the nature of the process or processes is not clear at this time.

Induction and Repair of Radiation Injury in Plateau-Phase Mammalian Cells

J. M. Nelson and L. A. Braby

As detailed in last year's annual report (Nelson 1979), a rapid repair process has been identified and extensively studied in the algal eukaryote Chlamydomonas reinhardi. This and the commonly observed slower process function simultaneously and are believed to represent repair of distinctly different kinds of damage; the rapid process is characterized by mean repair times on the order of 2-4 min in contrast to 20-30 min for conventional Elkind-Sutton repair at the same temperature. These experiments were performed to test models and obtain information for further modeling, and all employed C. reinhardi as the test organism. This alga was used for a variety of reasons, including the fact that these cells are easily synchronized and they have an extended period during which radiation sensitivity does not change significantly. This latter feature permitted the long exposures and long interfraction intervals required for both dose-rate and split-dose experiments.

Multiple processes associated with repair of sublethal radiation damage are also believed to exist in mammalian cells. Fast

repair in mammalian cells was first suggested from observations using plateau-phase cultures of various cells, including both a mouse embryo cell line (Little and Williams 1976) and the V-79 Chinese hamster cell line. However, these experiments were not decisive and repair rates could not be quantitated. Multiple processes, however, have never been identified in proliferating mammalian cells.

Ordinarily, the radiosensitivity of mammalian cells changes considerably as they move through their reproductive cycle. This change is too rapid to permit direct application of the same type of experiments as performed with C. reinhardi to proliferating mammalian cells. On the other hand, the cycling activity of certain plateau-phase cultures appears to be deeply suppressed. These cells are effectively blocked somewhere in their cycle; the specific point (or points) of this blockage is still uncertain. Nevertheless, this raises the possibility that such cultures may be stable enough to permit satisfactory application to long interval split-dose and dose-rate experiments. Thus, we have begun to use noncycling stationary populations of Chinese Hamster ovary (CHO) cells in experiments similar to those performed with C. reinhardi in the past.

To this end, we have developed suitable techniques to stop exponential growth and establish parasynchronous-nonproliferating populations of otherwise normal metabolically active mammalian cells. Such stationary cultures may be induced by either nutritional deficiencies or by density-contact inhibition, both of which yield large numbers of viable but reproductively inactive mammalian cells. Culture conditions resulting in this noncycling characteristic of specific plateau-phase populations were detailed last year (Nelson 1979). We are not attempting to determine if a rapid repair process similar to that observed in C. reinhardi exists in mammalian (CHO) cells as well.

We have looked for evidence of rapid repair in noncycling plateau-phase CHO cells by both split-dose and dose-rate methods. Results of these studies are not entirely clear. Split-dose irradiation techniques similar to those described for C. reinhardi have not demonstrated repair of any sort in either density-contact inhibited or nutritionally inhibited plateau-phase cultures of CHO cells.

There are several possible explanations that could account for these negative findings, the most likely of which are differences in the kinetic status of so-called "plateau phase" cultures and the dose rates we have thus far employed. The term "plateau phase" in its normal context implies a nonexpanding population and should not be extended to define the kinetic status of the cells themselves. The existence of such a plateau implies an equilibrium population density and, in itself, is not evidence of noncycling or resting status. This homeostasis reflects both cell production and cell loss and may be dynamic or static. Both the density and nutritionally induced plateau cultures used in these experiments are very nearly static or noncycling populations--populations of viable stationary phase cells in which replicative and reproductive activities have fallen to much less than 1% of that found in exponentially growing cells (Nelson 1979).

Although we have found no evidence for any repair by split-dose methods, simple survival curves have yielded results indicative of considerably more repair in noncycling plateau-phase populations than in exponentially growing ones. Results of these studies may be seen in Figure 20 where survival parameters from both stationary populations may be compared with those from exponentially growing cells. These results are consistent with published data (Hahn and Little 1972) (see Table 3) and indicate that the radiation sensitivity of our plateau-phase cells is not unlike that of other plateau populations, human cells being a possible exception. Consequently, although more difficult to interpret, these experiments have been used to obtain preliminary radiosensitivity data and to look for evidence of repair in both of these stationary cell systems. The fact that no repair process has become apparent from split-dose experiments is not yet clear but remains a subject of continued investigation.

Studies of Chlamydomonas reinhardi: Experimental

L. A. Braby, J. M. Nelson, and W. C. Roesch

The time-dependent features of the production of radiation damage in Chlamydomonas reinhardi are complex but may reveal a great deal about the types of reactions which result in the damage produced by electron and

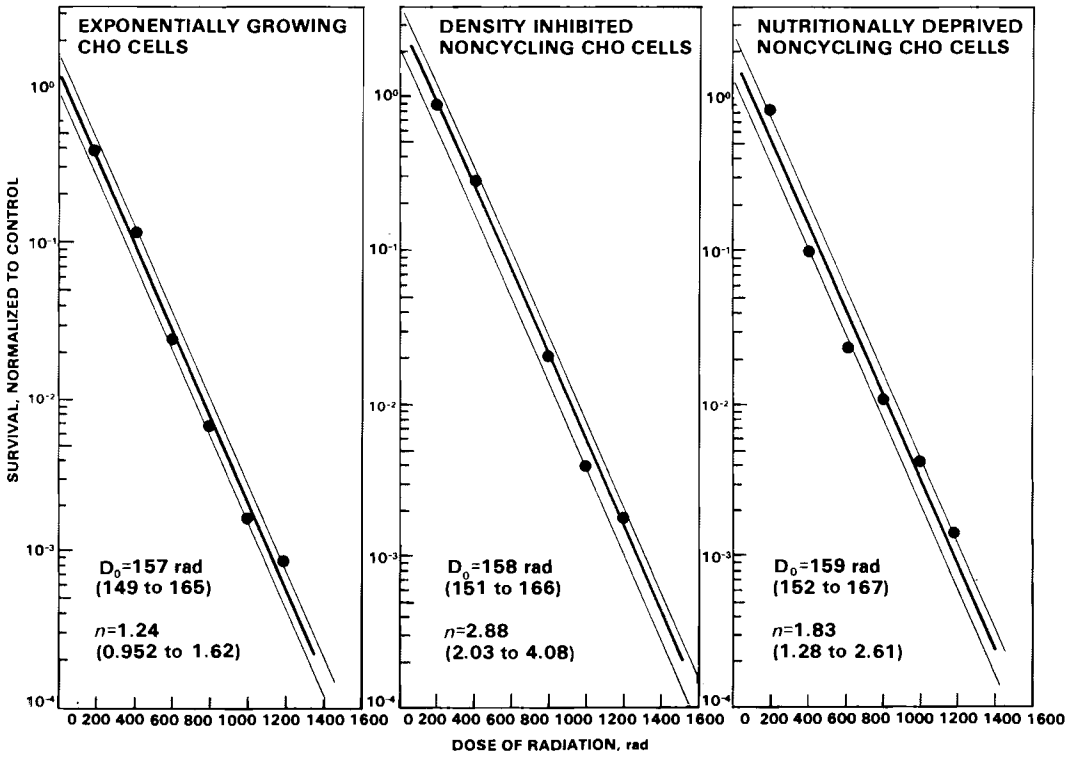

FIGURE 20. Survival Curves for (A) Exponentially Growing, (B) Density-Inhibited, and (C) Nutritionally Deprived CHO Cells Irradiated with 1.5 MeV van de Graaff Electrons. Exponentially growing cultures were irradiated on the fourth day of passage; both stationary-phase cultures were irradiated on the eighteenth day, at which time DNA-synthetic activity had fallen to 0.1% to 0.5% of that observed during exponential growth. Plating efficiencies of stationary-phase cultures were both around 45% in contrast to 95% for the exponentially growing cultures. Data have been fitted by the least squares method; each straight line has been surrounded by its standard error of estimate (Sy·x = Se), a regression statistic analogous to the point standard deviation.

high LET radiation. In addition to a conventional repair process with a characteristic time of about 20 min and a fast repair process with a characteristic time of about 3 min, there is a damage potentiating process with a characteristic time probably less than 0.5 sec. Also, there is evidence that some of the sublesions that accumulate and interact to produce potentially lethal lesions are themselves the product of interaction between things that can be produced by separate radiation events. This results in essentially a three (or more) event type of killing which can be observed only with moderately high dose-rate irradiations.

Our previous work with C. reinhardi established the presence of at least two repair processes (Nelson et al. 1979a; Nelson et al. 1979b) and showed that they probably modify distinctly different types of damage, rather than two types of damage that interact with each other. To further characterize these types of damage and to detect any additional types, further studies at higher dose rates and with shorter interfraction times were undertaken. A complete picture of all of the damage sequences and repair capabilities of cells will require still higher dose rates. However, it has become evident that comparing effects at

TABLE 3. Survival Parameters for Monolayer Cultures of Mammalian Cells Irradiated in Different Phases of Growth[a]

Cell type	Growth Phase	D_o	Y_o	References
Chinese hamster (HA-1)	Exponential	142-150	1.9-4.2	Stewart et al. (1968)
	Plateau fed	135-148	1.0-2.0	Stewart et al. (1968)
	Plateau unfed	127-148	1.8-3.9	Stewart et al. (1968)
Chinese hamster (CHL-F)	Exponential	113-148	3.0-16.7	Berry et al. (1970)
	Plateau fed	123-155	3.9-16.2	Berry et al. (1970)
	Plateau unfed	133-158	5.5-13.6	Berry et al. (1970)
Chinese hamster (V-79)	Exponential	100	5.0	Revesz and Littbrand (1969)
	Plateau unfed	unchanged	2.0	
Human liver (Chang)	Exponential	152+1.3	2.1+0.2	Little (1969b)
	Plateau fed	123+1.8	3.8+0.4	Little (1969b)
	Plateau unfed	122+4.3	3.2+0.5	Little (unpublished)
Hela S-3 (Oxf.)	Exponential	161-249	1.0-6.3	Berry et al. (1970)
	Plateau unfed	123-149	1.4-2.8	Berry et al. (1970)
	Plateau unfed	109-133	1.9-4.7	Berry et al. (1970)
Rat sarcoma	Exponential	144+3.6	12.0+1.3	Madoc-Jones (1964)
	Plateau unfed	95	100	Madoc-Jones (1964)
		(b)	(c)	
Chinese hamster (CHO)	Exponential	149-165	1.0-1.6	Nelson et al. (1979)
	Density inhibited	151-166	2.0-4.1	Nelson et al. (1979)
	Nutritionally Deprived	152-167	1.3-2.6	Nelson et al. (1979)

[a]The upper portion of this table is from Hahn, G.M. and J.B. Little. 1972. Plateau phase cultures of mammalian cells: An *in vitro* model for human cancer. *Current Topicsin Radiat. Res. Q.* 8:39-83.
[b]Values expressed as $D_o \pm 1$ s.d. of slope, i.e., $-1/m \pm 1.0\ (Sm/m^2)$, where m = slope and Sm = std dev. of the slope.
[c]Values expressed as $\hat{Y}_o \pm 1\,\hat{S}e$, where $\hat{Y}_o = \hat{n}$ = Y-intercept and $\hat{S}e$ = std. error of estimate, a regression statistic analogous to the point standard deviation.

conventional and at very high dose rates is not adequate since the effects of many individual processes are lumped together in such a comparison. In some cases, different processes have opposite effects on survival and such lumping may even lead to the conclusion that there are no fast processes altering cell survival. Thus, it is necessary to test for repair and related effects at relatively small intervals along the time scale.

The experiments that we reported previously (Nelson et al. 1979a; Nelson et al. 1979b; Braby and Roesch 1978) relied on the scattered beam of the electron van de Graaff operating at 1.5 MV. This provides dose rates of from approximately 1 rad/sec to 2 x 10^3 rad/sec. To provide higher dose rates, it is necessary to irradiate cells in the primary particle beam. This results in a slightly different radiation quality since the scattered beam has a depth dose curve similar to that for the direct beam after it has penetrated about 200 mg/cm^2 of plastic. However, it also results in dose rates of 10^5 rad/sec with a uniform dose over a 35-mm dish. [This maximum dose rate may be further increased by installation of a beam-flattening electrostatic lens (Johnson 1975), which is being assembled.] In the direct beam, both the intended dose rate and the dose rate from the accelerator dark current are increased. Because the intended exposure times are very short compared to the time to turn the accelerator terminal voltage on and off, the dark current beam can produce a significant fraction of the total dose. To prevent this, an electrostatic deflection system was installed. This system holds the beam off the exit window except when the terminal is being

pulsed. To make DC irradiations, this system is turned off and does not affect the electron optics. Using combined electrostatic deflection and terminal pulsing, we have made preset exposures as short as a millisecond and fixed pulse length exposures of 5 μsec.

When there are many time-dependent processes acting simultaneously, it is difficult to separate them using split-dose experiments. Consequently, we used dose-rate experiments with a fixed dose to investigate the possibility of additional time-dependent phenomena with characteristic times down to a tenth of a second. The results are shown in Figure 21. The decrease in survival with increasing dose rate up to 1000 rad/sec is expected as a result of the conventional and fast repair processes measured previously. However, the increase in survival with increasing dose is the first clear evidence for a reverse dose-rate effect, a phenomenon which has only been suggested by the results of previous experiments. Also, the value of A, the two-event factor, derived from these results is substantially lower than had been obtained for a wide variety of experiments in the scattered beam. This was an unexpected result since 1.5 MeV electrons are near the minimum of the stopping power curve, and scattering was expected to result in only a modest change in the electron energy. However, experiments at a constant dose rate (1 krad/sec) comparing the effect of irradiation in the direct beam, scattered beam, and in the direct beam with a 400 mg/cm^2 plastic filter show that the filtered direct beam and the scattered beam are approximately equally effective and have an RBE of about 1.75 relative to the direct beam for 10% survival of C. reinhardi (Figure 22). Apparently this large RBE is the result of high sensitivity to low-energy electrons which are produced as the beam penetrates matter. Since this effect has not been observed at conventional dose rates, it may be related to the damage that is involved in the reverse dose-rate effect.

In the course of these survival measurements, we also observed that A, the two-event factor, was not independent of dose, even though we had observed that it was independent of dose at lower dose rates. This is most easily observed as a plot of $\ln S/D^2$, as in Figure 23. The accumulation of damage model for two-event damage indicates that data plotted this way will fit a single curve with the ordinate proportional to A and the slope inversely proportional to τ. This has been found repeatedly to be the case for irradiation times greater than a few minutes. When these experiments produce data for various combinations of dose and dose rate that result in the same irradiation time, they have the same value of $\ln S/D^2$. However, at higher dose rates, this no longer holds. As can be seen in Figure 23 for irradiation times between 1 and 100 sec, a higher dose results in a higher value of A compared to a lower dose taking the same amount of time. "A" apparently depends on dose rather than dose rate because, as the dose given at a constant rate decreases, so does the value of A. However, if the rate and exposure times are varied to give a constant dose, A appears to

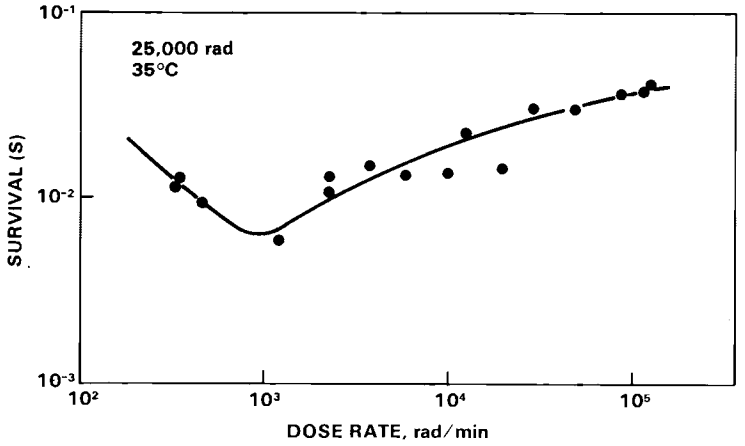

FIGURE 21. Results of a Dose-Rate Experiment with Chlamydomonas reinhardi Showing a Reverse Dose-Rate Effect

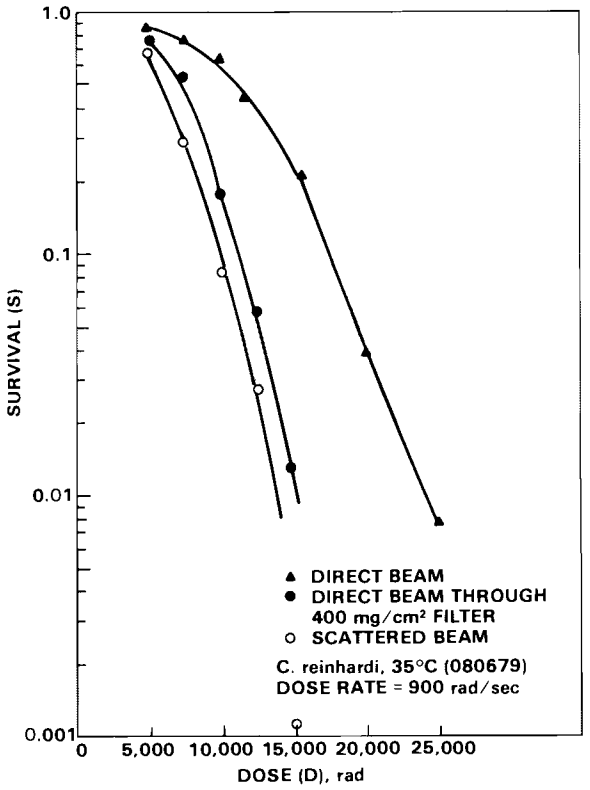

FIGURE 22. An Experiment Showing the High Sensitivity of Chlamydomonas reinhardi to Changes in Beam Quality

be constant. This type of behavior is consistent with some of the sublethal damage itself being the product of the interaction of products of two radiation events. This additional type of damage may also be related to the damage responsible for the reverse dose-rate effect and the unusually large RBE of scattered electrons, since all these effects seem to be related to processes that occur in a few seconds. Experiments to define these relationships are being planned.

Studies of Chlamydomonas reinhardi: Theoretical

W. C. Roesch, L. A. Braby, and J. M. Nelson

As described in the preceding article, our initial work with Chlamydomonas reinhardi agreed well with the accumulation of damage model (Braby and Roesch 1978) for dose-rate and fractionation effects, but results we obtained at higher dose rates in the past year differed from the model. The main differences are that the two-event factor, a parameter of the model, depends on radiation quality instead of being independent of it and that the two-event factor depends on dose, at low doses, instead of being constant. We have known about the quality dependence for many years and introduced a model to justify using the time-dependent features of the accumulation model in spite of it (Roesch 1975). We have returned to the older model and elaborated on it by introducing reaction rates for the different steps in it. Although the work is not complete yet, it is far enough along for us to feel confident that it will describe C. reinhardi's radiation response at all dose rates.

First, however, the preceding article also described our observation of a reverse dose-rate effect in C. reinhardi, an effect we attribute to a third observable rate process in the cells. We compared these data to an accumulation model with three rate processes of the type described last year (Roesch 1978b). Figure 24 shows the model fitted separately to data obtained with the direct and scattered beams of the electron accelerator. The time-dependent behavior is satisfactory, but the two-event factors for the scattered beam are 2.7 times those for the direct beam.

In the older model (Roesch 1975) for C. reinhardi, inactivation resulted from 2 two-event processes. In more detail, a charged particle produces damage that by itself does not inactivate the cell; this damage can repair if not interfered with. A second particle produces complementary damage that combines with the first to produce a new entity that is also nonlethal and repairable--but at a rate different from the first. Two of these second entities have to complement each other to inactivate the cell.

In that earlier work, we considered the repair rate of the second kind of damage but assumed only that repair of the first kind was very fast. Now we have introduced the repair rate of the first kind. (As suggested by Figure 24, a third rate is also necessary; but we are postponing that complication.) The model does not have an analytical solution, so we examined two methods of approximation (Roesch 1978a; Payne and Garrett 1975). The two agree in giving results almost identical to the accumulation model. The difference is that the two-event factor is now a product, and one of the factors in this product is the

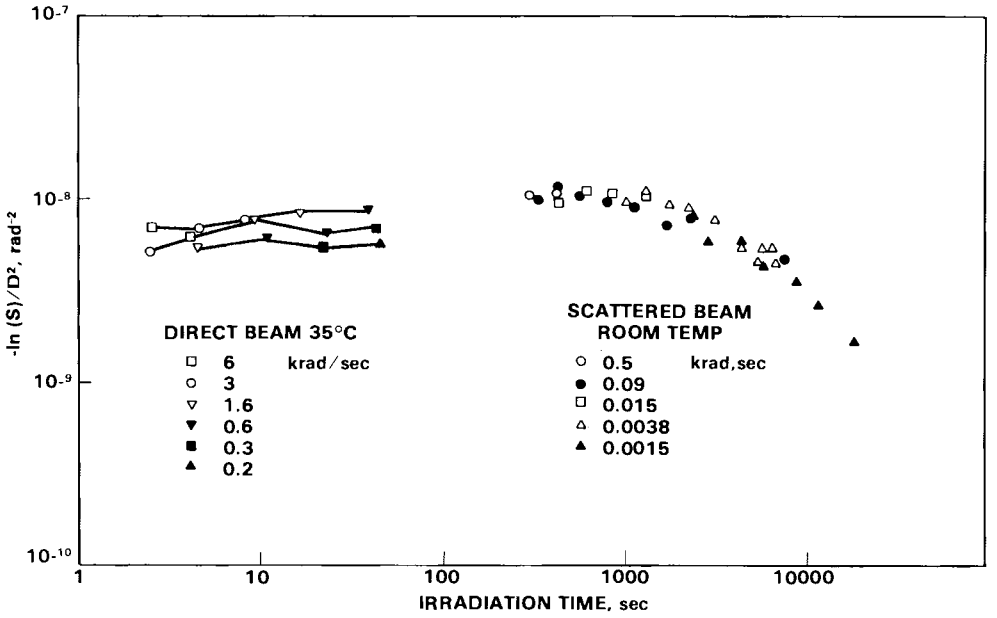

FIGURE 23. An Experiment with Chlamydomonas reinhardi Showing the Dependence of the Two-Event Factor on Dose and Radiation Quality

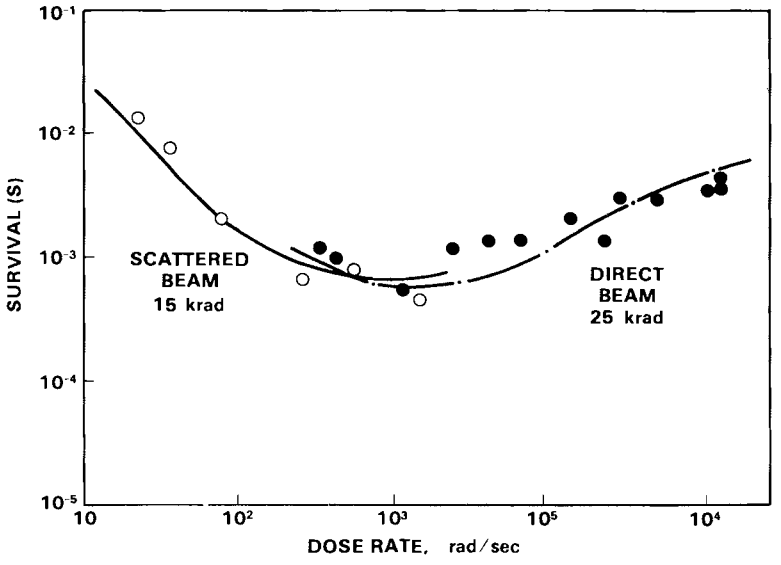

FIGURE 24. Accumulation Model Fit to Dose-Rate Data for Chlamydomonas reinhardi Exposed to Fast Electrons

square of a quantity that is the sum of the quotient of the mean-square specific energy (the microdosimetric quantity) by the mean specific energy [the "dose mean" used so much by Kellerer and Rossi (1972)] and a term that is proportional to the dose at low doses and constant and proportional to the dose rate at high doses.

The dependence of this factor on the dose-mean is what led to the model in the first place (Roesch 1978b). The dose-mean is approximately proportional to the LET until "saturation" sets in. Thus, the two-event factor is proportional to the square of the LET at low dose rates, in accord with the available data for C. reinhardi.

The inclusion with the dose-mean of a term whose maximum value depends on the dose rate explains why our early work (Braby and Roesch 1978) agreed with the simple accumulation model, i.e., why the two-event factor was observed to be independent of dose. At low dose rates, this added term is negligible compared with the dose-mean, and no effect on the two-event factor is observable.

At high dose rates, it is not negligible. It makes the two-event factor increase with dose at low doses and then become constant at a high value at high doses--effects we see in our data.

Effects of Repair on Relative Biological Effectiveness

L. A. Braby, W. C. Roesch, and J. M. Nelson

The choice of quality factors to be assigned to various ionizing radiations is a subject of continuing controversy. Decisions are generally based on scanty human data reinforced by our understandings of the relative biological effectiveness for animal and cellular populations. However, the need to assess quality for very low doses and dose rates (those which are particularly important in health physics applications) makes the problem particularly difficult, because it is impossible to get populations large enough to yield statistically significant results either experimentally or in human experience. Since direct measurements at the desired dose level are impossible, one must extrapolate from the region where measurements can be made, frequently nearly two decades higher. For such an extrapolation to be of any value, it must be based on some mathematical model that relates the observed effect (usually reproductive death of a cell) to the dose. The existence of repair of radiation damage in cells and animals has been known for some time (Elkind and Whitmore 1967) and is known to contribute to the survival of the cells irradiated at low doses and low dose rates (Braby and Roesch 1978).

Typical repair times known for most kinds of cellular systems are on the order of 20-60 min at normal temperatures. However, recent results by Malcolm and Little (1978), Todd (1968), and by ourselves (Nelson et al. 1979b) suggest that there are possibly many additional repair mechanisms, in at least some cells, that repair damage more rapidly. Figure 19 shows typical results for mitotic Chinese hamster ovary (CHO) cells. The survival of mitotic mammalian cells at conventional dose rates is typically exponential and continues to be essentially exponential for dose rates up to 1000 rad/sec (see Figure 19). However, at much higher dose rates, 75,000 rad/sec, survival is less and there is a distinct shoulder on the survival curve. This suggests a very rapid repair process in these mitotic cells. This rapid repair may also be present in cells at other times in the cell cycle but would then be hidden by the survival curve shoulder resulting from the conventional repair process.

If there are two different repair rates in one cell, they must occur as a result of repair of different types of damage. There is definite evidence for two simultaneous repair processes at different rates in experiments with Chlamydomonas reinhardi. In split-dose experiments, when the results are plotted as a log of the log of the maximum survival expected if complete repair occurs, divided by the survival obtained for a given interfraction interval, against that interval, one should obtain (if repair is an exponential function of time) a straight line for a single repair process. The upper portion in Figure 25 clearly shows that, at large intervals, the data are easily fitted by a straight line. However, there is substantially more damage being repaired during the first few minutes than would be indicated by this line. As in the evaluation of the decay rates of radioisotopes, this can be separated by subtracting the long process from the remainder of the data, and the lower portion of Figure 25 shows this fast repair. The characteristic time is about 2 min. If there is one or more repair process of this sort and the survival for a fixed dose as a function of dose rate is measured, the survival will decrease with increasing dose rate because there will be less time during the exposure for repair to

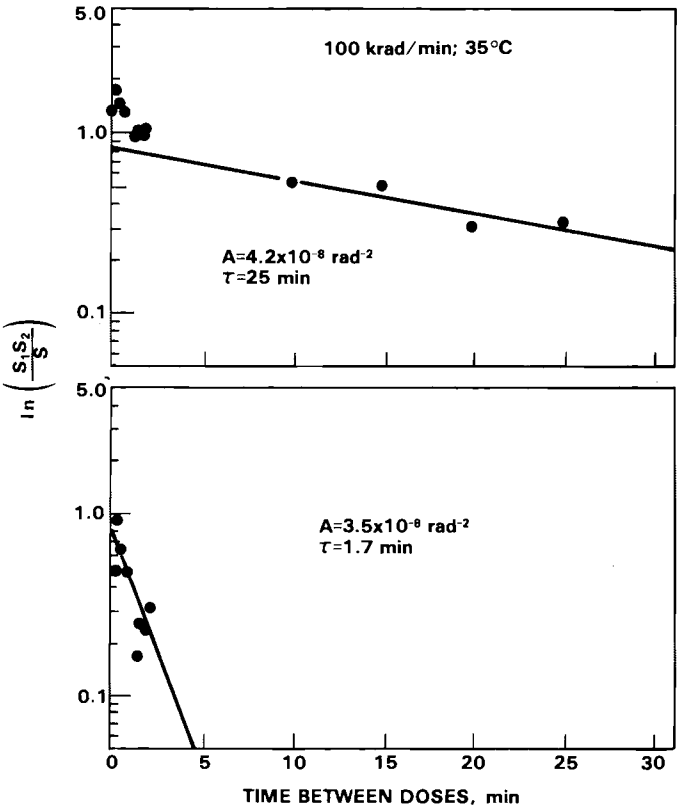

FIGURE 25. A Split-Dose Experiment with Chlamydomonas reinhardi that Shows the Effects of a Fast Repair Process Superimposed on Those of a Slow Process

occur. This, in fact, is observed in the case of C. reinhardi, Figure 21. On the left side, the survival drops as anticipated. However, the survival reaches a minimum and, as the dose rate increases further, there is an increase in survival, as is discussed in the second previous article.

One can determine how these various rapid repair processes affect the estimation of RBE by investigating calculated survival curves. In Figure 26, the points plotted are for a two-event-only model, assuming a rapid as well as a conventional repair process. The two lines fitted to these data, as one would probably attempt to fit experimental data, are based on a one-event-plus-two-event model and on a two-event-only model. Clearly, the one-event-plus-two-event model would be chosen as the best fit to the data in this survival region, and extrapolation to very low doses could then be based on this model. One feature of this figure is that the differences between the two models and the "experimental data" are all quite small. This is observed experimentally; Figure 27 shows data for T_1 kidney cells obtained by Todd (1968), which show only a slight difference in survival; but this difference corresponds to a large difference in the estimated fraction of one-event damage, as indicated by the right-hand panel where the vertical intercept is proportional to the one-event factor (Roesch 1978a). These small differences in survival are very difficult to measure experimentally and often are attributed to experimental variation. However, if the high survival portion of two-event and one-plus-two-event curves are expanded, one finds a very significant difference in the predicted survival to the low LET radiation and, therefore, in the interpretation of the RBE for high LET radiations. Figure 28 is an expansion of the one-event-plus-two-event curve of Figure 27. The "data" from the fast

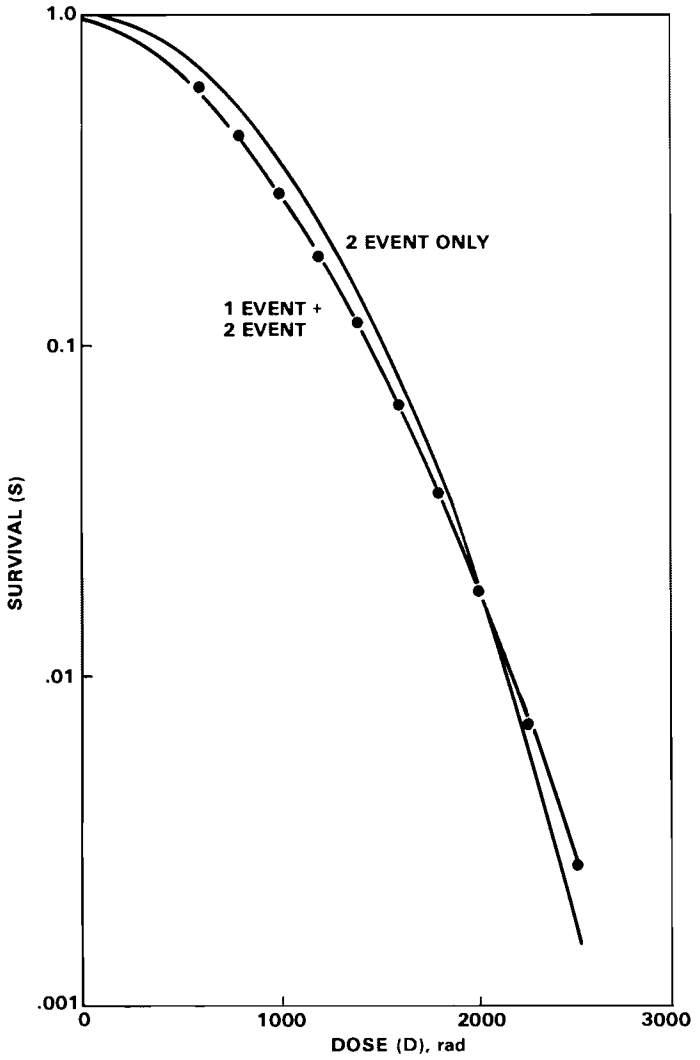

FIGURE 26. An Example of Curve Fitting and Its Effect on Extrapolated Low-Dose Behavior

repair model have much higher survival than given by the one-event and two-event models, which fit the data best in the experimentally measurable regions.

However, the increase in survival with increasing dose rate, which was observed in C. reinhardi, might have the opposite effect. Figure 29 illustrates the consequences of extrapolating experimental data assuming a two-event-only model when, in fact, the data might belong to the type of curve shown with the dashed line. The very high dose rate behavior of C. reinhardi would result in this type of error; since very high survival cannot be measured, a significant amount of single-event damage may go undetected. In this case, if one makes the extrapolation to very low doses based on the two-event-only model, one obtains a higher survival and higher RBE than would occur if there is really a one-event damage.

Multiple repair processes have been observed in some, but not all, cell types that have been investigated in a way to detect them. For example, Malcolm and Little (1978) have not found fast repair in exponentially growing V-79 cells, only in

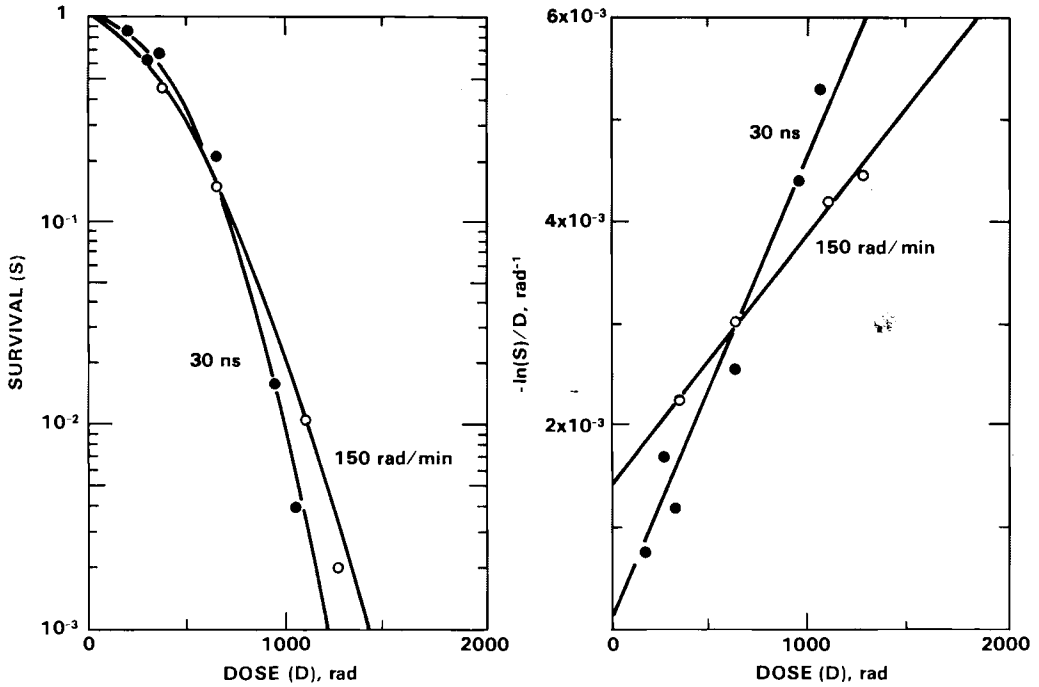

FIGURE 27. An Example of the Small Differences in Experimental Data that Hide Significant Changes in Interpretation

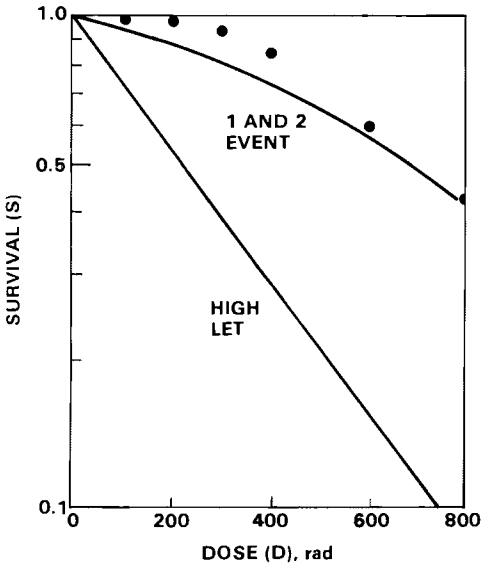

FIGURE 28. The Effect of Erroneous Extrapolation on the Determination of RBE

plateau-phase cells. Although fast repair processes are most easily observed in high dose-rate experiments, they also affect the shape of survival curves at very small doses for moderate to low dose rates. Survival curves involving one-event and two-event damage, with or without fast repair, cannot easily be distinguished in the region of measurable survival. However, at very high survivals, even at low dose rates, these various combinations of types of damage and repair may result in substantially different slopes. Thus, one cannot rely simply on survival measurements, but must also include split-dose and dose-rate measurements to determine which model best fits the data, so that they can be properly extrapolated to determine the effects at very low doses.

Mixed Radiations

W. C. Roesch

In ordinary radiation protection practice, the dose equivalents (product of absorbed dose and quality factor) of different radiations received by the same person are added together. This addition implies the

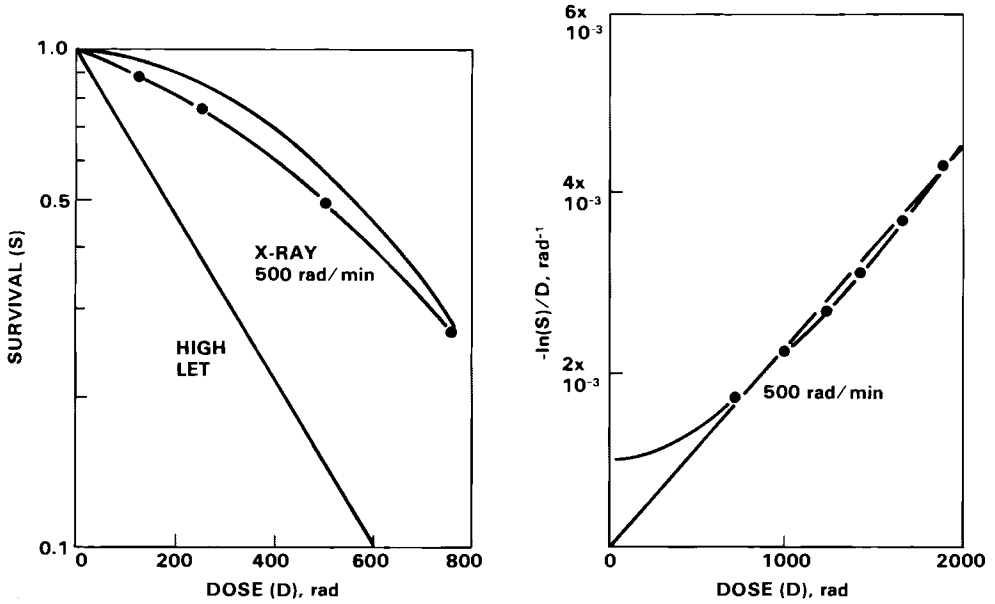

FIGURE 29. Another Example of the Effect of Erroneous Extrapolation on the Determination of RBE

assumption that the effects of the radiations are additive. The quality factors were chosen with the intention of making this a safe assumption, but the effects are seldom truly additive; usually mixtures exhibit synergism. The nature of the synergy is of interest for the light it sheds on fundamental processes and for application in radiation protection and in radiation therapy.

Several current biophysical theories of radiation action contain hypotheses that bear on the behavior of mixtures. To show how these hypotheses can be used, we first calculated the fraction of the cells in a homogeneous population that survive and can reproduce after irradiation with a dose D_1 of one radiation immediately followed by a dose D_2 of another. Let this fraction be S; let $S_1(D)$ and $S_2(D)$ be the fractions, as functions of the absorbed dose, D, for the radiations given alone. After the dose D_1, some of the cells can no longer reproduce, some have been damaged, and some have not been affected by the radiation. The damaged cells will recover, given enough time and freedom from further injury--they are said to have "sublethal damage." But the dose D_2 of the second radiation can convert some of this sublethal damage into damage that prevents reproduction. This conversion is the means by which synergism is assumed to occur in the present model.

The radiation theories apply here because they postulate how much damage is produced. Tobias (1971) and Kellerer and Rossi (1972), for example, assumed that, except for very high LET particles, the nonlethal damage produced by a charged particle is proportional to its LET. A consequence of this assumption is that equal doses of all radiations produce the same amount of such damage. If this is taken to be true for the present model, then when the dose D_1 has been delivered, the cells contain exactly the same amount of damage as they would if they had been irradiated with the second radiation to that dose. Since this damage is the only "memory" the cells have of what went before, they respond to the second irradaiation just as though the first radiation had been of the same type as the second. In other words, if they had been the same type, S would be $S_2(D_1 + D_2)$; but, at the end of the first irradiation, the fraction was $S_1(D_1)$ rather than $S_2(D_1)$. Correcting by the ratio of these numbers gives

$$S = S_2(D_1 + D_2) + S_1(D_1)/S_2(D_1) \quad (15)$$

for the fraction surviving the two-dose experiment.

Applying this same reasoning to a number of steps, first one radiation then the other, and making the length of the steps approach zero, gives a differential equation for a simultaneous mixture of two radiations. Its solution is

$$S = S1(D)^{F}\ S2(D)^{(1 - F)} \qquad (16)$$

for a total dose D, F + D of which is due to the first radiation and (1 - F) + D due to the second.

No experiments have been done specifically to test Equations (15) or (16). A number of experiments with mixed radiations have been reported in the literature, however. Figure 30 shows the data from one of them compared with Equation (15). Raju and Jett (1974) irradiated aerated T-1 cell cultures, first with ^{239}Pu alpha particles (to 0, 11, 45, 64, or 100% of the dose), then with 250-kVP X-rays. S1 and S2 were determined from their 100% and 0% data and then calculated the curves shown in the figure for the other data. The fit is fairly good, considering the experiment was not done to test the theory. Other instances in the literature fit the theory about as well.

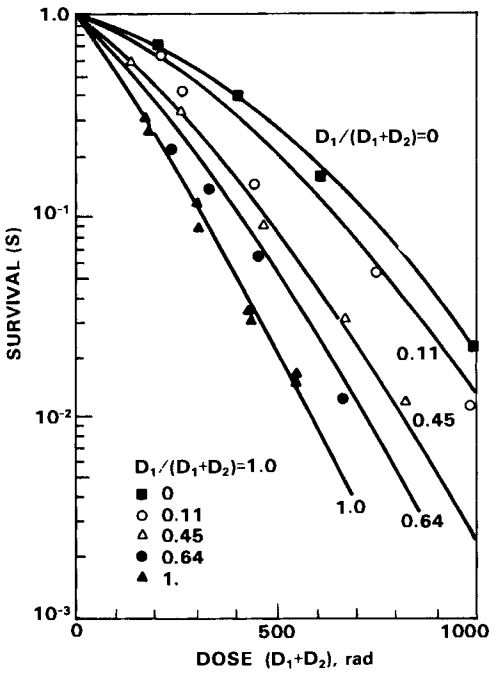

FIGURE 30. Experimental (Points) and Theoretical (Lines) Survival of Aerated T-1 Cells to a Dose D_1 of Alpha Particles Followed by D_2 of X-rays

Equations (15) and (16) follow from the very simple assumption that equal doses of all radiations produce the same kind and amount of sublethal damage. Several alternative assumptions come to mind. In particular, Tobias (1971) and Kellerer and Rossi (1972) had to introduce nonlinearity to account for saturation in the LET effect. Also, very fast recovery processes might have time to take effect if the interval between the two doses for Equation (15) is not short enough.

Microdosimetric Single-Event Densities

W. C. Roesch and L. A. Braby

Changes in response with changes in radiation quality pose problems in the application of and in the protection from radiation. Theories aimed at understanding these changes by relating the characteristics of charged particles to the cellular effects they produce currently often use the concepts and data of microdosimetry. Some of the earlier discussions in this report make clear our own immediate needs for such data for fast electrons. Electron data tend to be relatively inaccurate because electronic noise interferes with measurement of the small pulses electrons produce in the Rossi proportional counters used for microdosimetry. Last year (Braby and Roesch 1978; Braby and Roesch 1979), we reported a method for estimating mean values of some microdosimetric quantities from measurements made with a pulsed beam from an electron van de Graaff accelerator. We continued work on the method, trying to obtain more than just mean values from it. Although the work is not finished, we think we can obtain reasonable estimates of the single-event densities in specific energy for fast electrons.

To obtain these densities, we employ the relation (Kellerer 1970) between the Fourier transforms (denoted by F) of the multievent density f(z) and the single-event density $f_1(z)$.

$$F(f) = \exp(-M[1 - F(f_1)]) \qquad (17)$$

Actually, two sources contribute to the observed density: the fast electrons and the system electronic noise. Their contributions are convoluted; hence, their transforms are multiplied together. Thus, we have (also taking logarithms)

$$\ln F(f) = -M_n\left[1 - F(f_n)\right] - M\left[1 - F(f_1)\right] \quad (18)$$

where subscript n denotes the noise contribution. Here, f and, thus, ln F(f), and a quantity Q that is proportional to M are known from our measurements. For calculations, we approximate Fourier transforms with discrete Fourier transforms. Then for each element of the discrete transform, Equation (18) constitutes two equations (because transforms are complex numbers) in which the left sides are known and in which the right sides consist of one constant term, $-M_n[1 - F(f_n)]$, and a term that is a constant, $-(M/Q)[1 - F(f_1)]$, times Q. Each of these equations is solved by least squares using data for different values of Q. The transform of f_1 is obtained from the last constant and a value for M/Q. It is inverted to obtain f_1.

Figure 31 shows an example of the result of this process for 1.0 MeV electrons in a 1.89 μm rectangular cylinder site in tissue. The single-event density in the energy, E, deposited in the site is plotted rather than the density in Z. The mean values determined from this curve agree with those we determined last year by our original method. The electronic noise seems to have been eliminated. The density at E=0 is not zero, however, and this may be due to some residual noise. But it may also be due to stochastics originating in the statistics of the pulse counting, producing random variations in the phase of the Fourier transform. Such phase changes could make significant density shifts where the curve is steep. Work is continuing on dealing objectively with the stochastic variations.

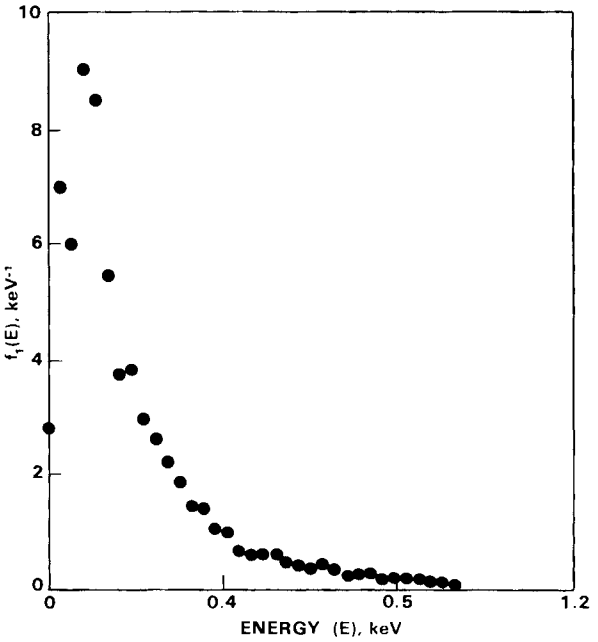

FIGURE 31. An Example of a Single-Event Density Obtained from a Multi-Event Density by the Fourier-Transform Method — 1.0-MeV Electrons in a 1.89-μm Rectangular Cylinder in Tissue

Calculation of Distributions for Energy Deposition and Ionization in Submicron Sites

W. E. Wilson and H. G. Paretzke

The spatial dependence and correlation of the energy depositions and the number of interactions or ionizations produced by a radiation field in macromolecular volumes are of continuing interest in radiation biology. This interest indicates that knowledge of the energy concentration is needed on a nanometer scale; and, ultimately, the spatial correlations among neighboring activations are needed for the relative efficiency of production of primary lesions in vital biomolecules.

Experimental methods for measuring the distributions in energy imparted for energetic heavy ions have concentrated on the use of proportional counters to magnify the microscopic site to experimentally realizable dimensions by lowering the molecule density (Glass and Gross 1972). Owing to experimental limitations, this approach is generally restricted to volumes greater than about 0.1 μm diameter. At present, the only tractable method for calculating particle transport in charged particle track structure that retains the inherent stochastics is the Monte Carlo method.

In this section, we report further calculations made with our positive-ion track structure code MOCA13. A description of

the primary interaction model and initial tests of the code for ion track structure calculations, including comparisons with experimentally measured ionization frequency distributions (Glass and Roesch 1972), were reported previously (Wilson et al. 1978; Wilson 1977).

Representative ionization distributions are shown in Figures 32a and 32b for 1.0-MeV protons passing through spherical sites of diameters ranging from 100 to 1 nm. These distributions are for frequency of "event size," where event size is measured by the number of ion pairs produced within the site boundary by individual protons passing along a diameter of the site (diametric track). The distributions for the smallest sites are represented by delta functions at the integer values of the number of ionizations. For the larger sites, the distributions exhibit the familiar skewed Gaussian shape similar to energy loss straggling distributions. Distributions for energy imparted are calculated in MOCA13 independently and simultaneously with ionization distributions.

The shapes of the energy distributions are found to be, for the most part, the same as the shapes of the ionization distributions. An example is presented here only to illustrate a necessary difference between energy and ionization distributions. Graphs of the frequency for energy imparted by 1-MeV protons in sites of 5, 2, and 1 nm diameter are presented in Figure 33. For the same ion energy and site size, the frequency of zero energy deposition will, in general, be smaller than the frequency of zero ionization (compare Figure 33 with Figure 32b). This follows from the simple fact that the cross section for energy deposition (total interaction cross section) includes the cross section for ionization. Some events may deposit energy without producing ionization. Stated differently, if an event imparts "zero" energy, then it certainly creates "zero" ionization; however, the converse is not necessarily true.

The spatial variation of the distributions around the ion track is investigated by calculating the distributions for tracks that pass through the site but off-center. These distributions are found to be very similar to those for diametric tracks, except for ion paths near the edge of the site. The distributions for nearly tangential tracks are significantly different, especially for larger sites. Figure 34 shows ionization distributions for 1-MeV protons tangential to 100, 50, and 20 nm sites. Note that the frequency of zeros is high because the actual proton path length within the site is zero. Also, the relative widths of the distributions are significantly larger than for diametric tracks, a behavior which was first observed experimentally and explained by Glass and Roesch (1972).

The calculated frequency of zero ionization for diametric tracks produced by 1.0-MeV protons is shown in Figure 35. Straight lines join successive points merely to aid the eye. The dependence on site size is very nearly exponential; this is readily understood because the frequency of zero ionization for very small absorbers is essentially given by the probability that the ion will travel a distance x greater than the site diameter between successive primary ionizations. This latter probability is given by

$$p_x = \exp(n \cdot \sigma \cdot x) - \exp(-x/\bar{\lambda}) \quad (19)$$

where n is the number of molecules per unit volume, σ is the ionization cross section, and λ is the mean free path for ionization. For $x = \bar{\lambda}$, $p = 1/e$, the value of $\bar{\lambda}$ is indicated by the arrow in Figure 35. The calculated frequency of zeros is slightly smaller than would be predicted from just the cross sections for primary ionization alone because secondary electrons will occasionally produce ionization in the volume when there is no primary ionization, thus reducing the frequency of zero ionization.

These results indicate that with sophisticated algorithms describing the basic physical interactions, the Monte Carlo method can be employed effectively to obtain quantitative energy and ionization distributions about positive ion tracks of a few MeV for absorber sites which are too small to be amenable to direct experimental measurements.

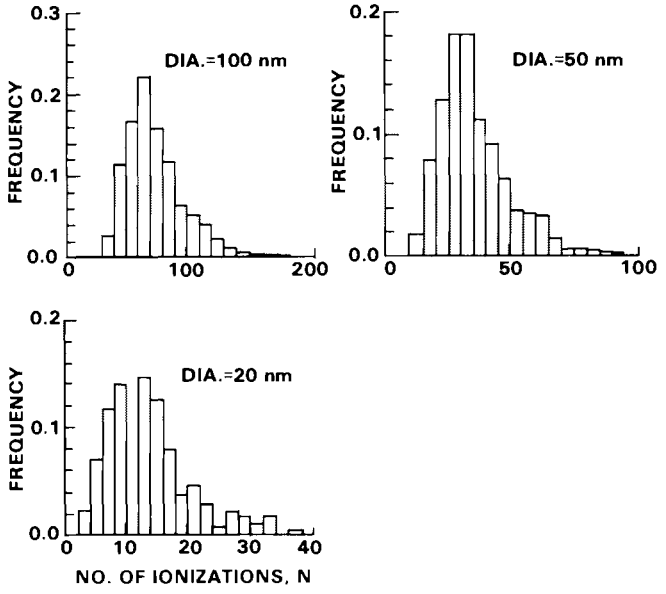

FIGURE 32a. Ionization Frequency Distributions for 1-MeV Protons Passing Diametrically Through 100-, 50-, and 20-nm-Diameter Spherical Sites in Unit-Density Water

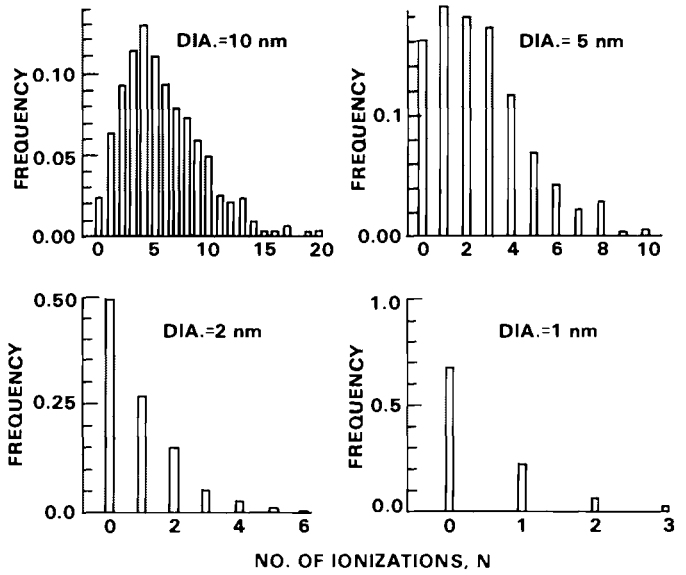

FIGURE 32b. Ionization Frequency Distributions for 1-MeV Protons Passing Diametrically Through 10-, 5-, 2-, and 1-nm-Diameter Spherical Sites in Unit-Density Water

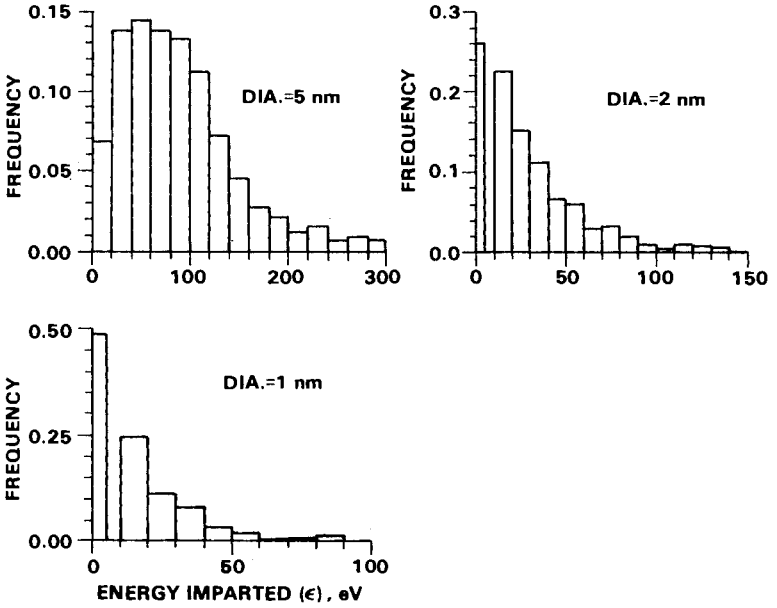

FIGURE 33. Frequency Distributions in Energy Imparted for 1-MeV Protons Passing Diametrically Through Spherical Sites of 5-, 2-, and 1-nm-Diameter

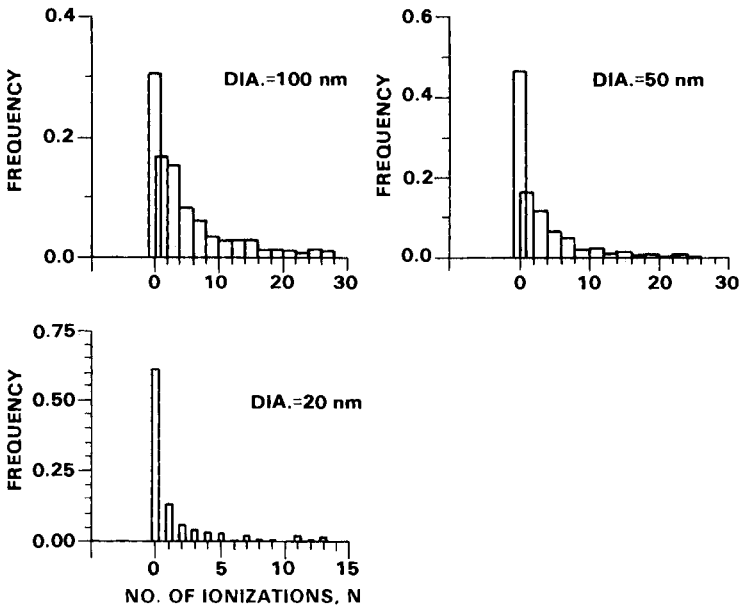

FIGURE 34. Ionization Frequency Distributions for 1-MeV Proton Tracks Tangential to 100-, 50-, and 20-nm-Diameter Spherical Sites

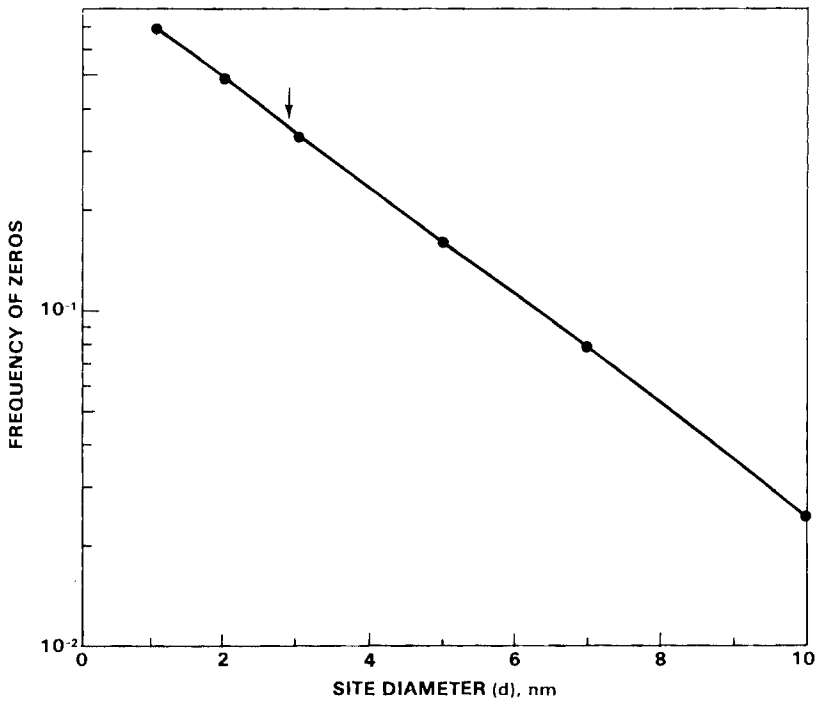

FIGURE 35. Frequency of Zero Ionization as a Function of Site Size for 1.0-MeV Protons Passing Diametrically Through Spherical Sites. Inverted arrow indicates mean free path for primary ionization

• Microdosimetry of Internal Sources

The purpose of this study is to develop practical methods for calculating microdosimetric distributions of plutonium or other alpha-emitting elements that are deposited especially as particulates in soft tissue and lung tissue. This study will aid the correlation and extrapolation of radiation effects measured at different levels of exposure and in different species. Computational methods will be developed and tested in the Radiological Physics Section. Concurrently, the Dosimetry Technology Section will develop cell and tissue models in which those methods will be applied.

Lung Tissue Modeling for Microdosimetry Application

D. R. Fisher, J. L. Daniel, and G. F. Piepel

Computational methods for determining the microdosimetry of internally deposited alpha-emitting radionuclides were developed by W. C. Roesch to deal with the random nature of energy deposition in small tissue volumes (Roesch 1977). These complicated mathematical methods require the use of a large computer. Initially, the microdosimetry calculations were limited to those involving dose distributions within a homogeneous unit-density medium.

Of current interest is the microdosimetry of plutonium and other alpha emitters in the lung, which is an inhomogeneous tissue. In recent years, a controversy developed over whether a nonuniform concentration of radioactivity would inflict greater biological harm to the lung than the same amount of radioactive material distributed uniformly throughout the organ. Although experimentation with animals indicates that nonuniform "hot spot" distributions of plutonium in the lung are likely to be less harmful than uniformly distributed material, the physical explanation and confirmation of these results are missing. Conventional dose averaging techniques overlook two very essential keys to understanding the carcinogenic response from internally deposited alpha emitters: (1) the fundamental processes involved in energy deposition events, which are by nature highly stochastic and limited to a small region surrounding the particle track; and (2) the fact that the biologically sensitive "target" is not the entire mass of the organ, or a particular type of cell, but rather a region within and smaller than the particular cell. Microdosimetry, on the other hand, takes each of these factors into account.

From the start, our research program in microdosimetry has had as its primary objective the capability to correlate the late biological effects of plutonium and other internal emitters in the lung with the microscopic distribution of charged-particle energy. The lung modeling task was initiated to provide a statistical characterization of the microstructure of mammalian lung tissue to which microdosimetry calculations could be directly applied.

We developed and tested methods to measure the statistical distributions of tissue, air space, and cell nuclei in pulmonary lung tissue. These distributions are needed to model the energy dissipation of an alpha particle as it traverses a straight-line path through lung tissue. To accomplish this task, we employed an automated image analysis system consisting of a light transmission microscope coupled to a quantitative image contrast analyzer (Quantimet®) and a programmable calculator. The system was programmed to scan lung tissue specimens and compile air and tissue chord length data, including relative locations of epithelial cell nuclei within tissue components. For more flexible operation, the system was set to allow operator input of tissue type information and verification of the automated analysis.

® Registered trademark of Cambridge Instrument Co.

We obtained lung tissue specimens from three healthy adult male beagle dogs. Whole lungs were extracted and fixed with 1.5% buffered gluteraldehyde at 30-cm water pressure. A randomized scheme was used to select tissue specimens from each of five different lobes. Microscope slides were prepared in triplicate from each tissue block and handstained with either trichrome or hematoxylin, or left unstained.

Image analysis was performed on the tissue specimens at orientations of 0^{o} and 90^{o} to the horizontal position of each slide. For each random field of view, ten evenly spaced horizontal line scans or "tracks" were analyzed. Twenty fields were chosen at random from each slide. Chord length and nuclear distribution data were recorded for approximately 10,000 tracks. To check the system, a smaller data set was obtained from hand measurements of enlarged photomicrographs.

Early study of these data indicates that there is no correlation between adjacent air chamber and alveolar wall thicknesses (Figure 36). In other words, the length of one chord is not dependent upon successive others. This implies mathematically that Monte Carlo microdosimetry studies in pulmonary tissues can be performed with statistical validity. These statistical tests are continuing. From the data we will also be able to investigate the heterogeneity that may exist between dogs, lobes within with a lung, and sections within a lobe.

In a preliminary experiment, we used the track data to simulate an initial plutonium aerosol deposition in the deep lung. Alpha particle tracks were assumed to originate from randomly selected loci on air exchange surfaces of peripheral lung tissue, conductive airways, and transitional regions. Figure 37 shows a frequency distribution of nuclei transected per line scan for dog No. 1172. On the average, each simulated track intersected 1.7 nuclei prior to passing through 40 μm of cumulative tissue space, the approximate range of a ^{239}Pu alpha particle (we assumed no energy loss in air space). Nuclei were intersected by 74% of the tracks, and four or more nuclei were traversed by 14% of the tracks. From this, we may be able to conclude that isotropic

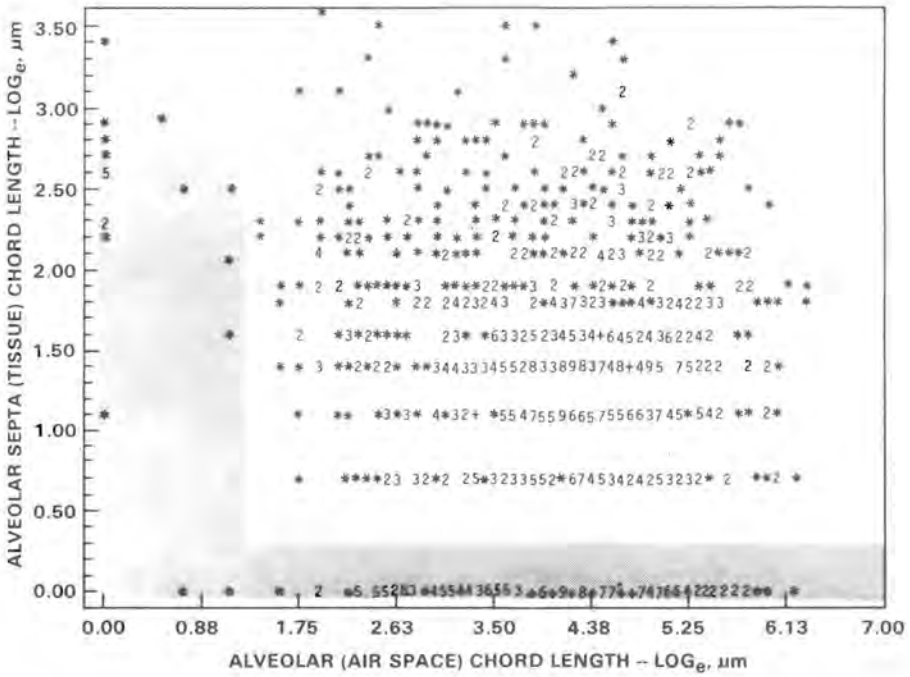

FIGURE 36. A Measure of the Joint Distribution of Adjacent Alveolar Chord Lengths (Air Space Chord Versus Tissue Chord Lengths). No correlation is shown. The data represent results from one lobe of dog 1172. Complete analysis of all data is continuing.

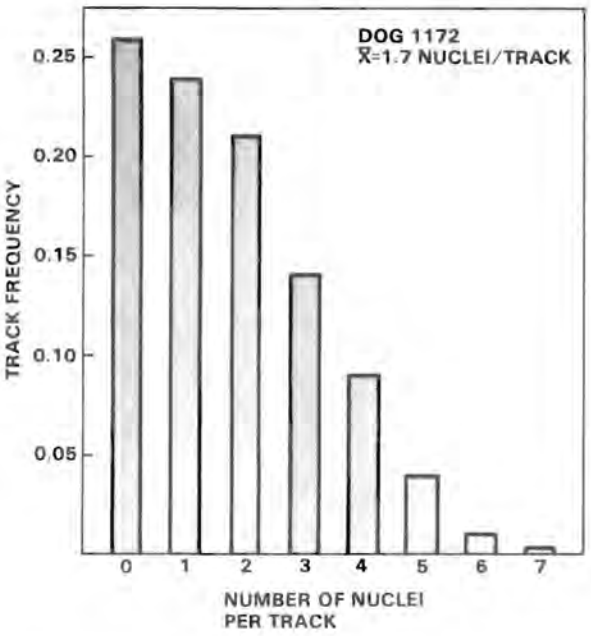

FIGURE 37. Frequency Distribution of Nuclei Transected per Line Scan for Dog 1172

point sources effectively irradiate nuclei within alpha particle range, and the efficiency of cellular inactivation may therefore increase as the activity is more uniformly distributed throughout the tissue.

Often in conventional lung dosimetry, the maximum plutonium alpha-particle path length through pulmonary tissue is assumed to be 180 μm. Our data show many simulated tracks traversing up to 600 μm of pulmonary tissue and air space, with a considerable fraction having paths 200 μm or more in length.

Preliminary observations of line scan data also indicate that the probability of an alpha particle intersection with a cell nucleus is approximately constant with respect to distance from particle origin.

Following the necessary refinements, line scan data from all three dogs will be combined mathematically to form the lung tissue model for computerized microdosimetry.

Computer Programs for Microdosimetry of Alpha Particles in the Lung

W. C. Roesch

Last year, we reported (Roesch 1979a) a simplified version of the mathematical theory of the microdosimetry of particulate sources aimed at those who are interested in the theory but who do not wish to become specialists in it. As a consequence, we were invited to prepare a similar paper (Roesch 1979b) for presentation at the Sixth International Congress of Radiation Research at Tokyo. This provided a chance to refine and illustrate further the concepts of internal microdosimetry.

Work is in progress on adapting the present computer programs to microdosimetry in the lung. For this purpose, the inhomogeneous structure of the lung is being modeled as consisting of materials of just two densities: normal tissue and vacuum. Negligible error results from treating the air spaces as vacua for the short distances the alpha particles travel in the lung. Little that is conceptually new has to be added to the present programs to adapt them for the lung, but wholesale changes are needed in the order in which quantities are computed. For the present calculations for homogeneous tissue, all input quantities that may be needed are calculated in an initial step that economizes computer time but requires much computer memory. For the lung, this step would require too much memory; therefore, input quantities have to be generated as needed.

Advantage is being taken of the need for these alterations to improve a particular part of the performance of the system. In a few circumstances, the system calculates more than 99% of the density in specific energy correctly, but errs in the absorbed dose by as much as 25% because it neglects very rare, but very large, energy depositions. This error is of no practical consequence in biophysics applications because so few events are involved; but it has been annoying because it has recurrently required reassurance and special education of users of the system.

• Dosimetry of Internal Emitters

The Dosimetry of Internal Emitters Program develops dosimetric techniques and radiological methods for the assessment of internally deposited nuclides. The program endeavors to refine the correlation radiation dose and observed biological effects. The principal investigators work closely with the staff of Pacific Northwest Laboratory's Biology Department and investigators working on the Microdosimetry of Internal Sources Program.

Dosimetric and Radiobiological Analysis of Internally Deposited Nuclides

D. W. Murphy, G. W. R. Endres, and
D. L. Haggard

Since the Internal Emitters Program does not perform any actual radiobiology studies, data for analysis are obtained from the Biology Department at PNL. The program reviews the radiobiology studies that have been and are being conducted at PNL and performs dosimetric analyses using refined techniques. In conjunction with the Microdosimetry of Internal Sources Program, microdosimetric theory is being applied to studies involving radiation dose from alpha-emitting radionuclides. During the past year, the development of dosimetric techniques and modeling was performed for

1) an in vitro suspension of rabbit lung macrophages and $^{241}AmO_2$ particles

2) the organ dose assessment of ^{232}U and its daughters in rats

3) absorbed ^{238}Pu in the fetal pig gut

4) rats exposed to an "infinite" cloud of ^{85}Kr.

A brief description of each task follows.

In Vitro Suspension of Rabbit Lung Macrophages and $^{241}AmO_2$ Particles

To demonstrate the usefulness of microdosimetry techniques, efforts were recently begun to calculate the alpha particle dose to rabbit lung macrophages from $^{241}AmO_2$. The first evaluation was the calculation of the specific energy imparted to an in vitro suspension of rabbit lung macrophages and $^{241}AmO_2$ particulates. For this evaluation the cells and cell nuclei were assumed to be spherical, with diameters of 8.0 μm and 4.5 μm, respectively. The activity of the solution was 3.1 μCi ^{241}Am/ml, comprised of 0.1 μm particulate sources containing 1.85×10^{-14} Ci. The solution also contained 5×10^6 macrophage cells/ml, which were assumed to be randomly mixed with the $^{241}AmO_2$ particulates. Using computational methods developed at this laboratory (Roesch 1977), the frequency distribution of specific energies (the average of which is the average absorbed dose) was calculated. Following the completion of this study, the effect of different concentrations of ^{241}Am upon the specific energy distribution to the cells will be evaluated. Also, microdosimetry calculations for macrophages that have phagocytized single particulate sources will be performed.

Organ Dose Assessment of ^{232}U and Its Daughters in Rats

Radiation dose assessment is being developed for the Toxicity of Thorium Cycle Nuclides Program. The determination of the radiation dose from ^{232}U and its respective daughters in various organs was initiated. Since the ^{232}U daughters will translocate at different rates in the living animal, the concentration of each daughter will differ from organ to organ. The individual nuclide contribution to organ dose is difficult to assess if progenitive nuclides are present. The problem arises in attempting to determine the initial nuclide concentration in the presence of radioactive build-in from the progenitors. This difficulty is magnified by the short radiological half-lives of the daughters past ^{224}Ra. Counting

times and counting sequences for the analyses of the initial organ levels of the ^{232}U daughter nuclides by gamma spectroscopy were optimized. A blood sample and the right femur of a rat were analyzed. The blood from a rat sacrificed 24 hr after a 4 μCi injection of ^{232}U contained only ^{212}Pb. The ^{212}Pb activity was determined to be 16.1 ±2.8 nCi/ml. The bone analysis has not been completed. Refinements in the spectroscopy techniques and the determination of radiation dose due to individual daughter nuclides to the organ dose will continue in FY80.

Absorbed ^{238}Pu in the Fetal Pig Gut

Dosimetric techniques are being developed to analyze the alpha dose to the intestine from absorbed ^{238}Pu based on the information and tissue supplied by the Gut-Related Studies of Radionuclide Toxicity. The intestinal absorption of ^{238}Pu by neonatal swine has been shown to be greater than by neonatal rats, guinea pigs, dog or adult swine (Sullivan 1978). Since the undifferentiated cells of the gut proliferate by mitotic division to continually renew the epithelial covering of the villi, the alpha radiation dose to these cells from the absorbed ^{238}Pu in the neonatal intestine must be determined. The development of a model for the distribution of the activity and the geometry of the particulates in relationship with these cells was initiated. The model, which is being developed for the neonatal swine gut only, will be used to determine the radiation dose by conventional and microdosimetric techniques.

"Infinite" Cloud of ^{85}Kr Effects on Rats

Dosimetric analyses for the Toxicology of the Krypton-85 Program was continued from last year. Rats are continuously exposed to three concentrations of ^{85}Kr (3×10^{-3}, 3×10^{-4}, 3×10^{-5} μCi/ml air) to determine the long-term biological effect. The experiment is designed to give a skin dose of 2000 rad/yr for the highest exposure group. Determination of the true radiation dose is difficult since the exposure chambers do not meet "infinite" cloud criteria due to the chamber design and the shielding effect of the cages and the animals. The radiation dose is being measured by bare, unshielded thermoluminescent dosimeters (^{7}LiF known as TLD-700s) which are suspended between the animal cages. As cages become available upon the deaths of the animals, TLD measurements will be made inside the individual cages to determine the correlation between the between-cage and within-cage measurements. External radiation doses based on the TLD measurements to date are estimated at 2746 rad/yr, 375 rad/yr, and 39 rad/yr for the highest to lowest ^{85}Kr concentrations, respectively. The purpose of this task is to correlate the external exposures to internal organ doses and biological effects.

In addition to these tasks, input was provided to the lung model development for the Microdosimetry of Internal Sources. The lung modeling has been described elsewhere in this report.

• Real-Time Measurement of Pu in Air at Below-MPC Levels

A direct-inlet mass spectrometer (DIMS) is being developed for monitoring low-level airborne plutonium on a real-time basis. The instrument will be capable of measuring plutonium concentrations below the maximum permissible concentration (MPC) level. The final major hurdle to satisfactory operation of the instrument has been its low measurement sensitivity due to bounce of incident particles off the ionizing filament. Solution of the bounce problem has been demonstrated by use of an oven ionizer in which the particles are trapped. Development of the plutonium DIMS can now be completed by optimizing the oven design and calibrating the instrument's performance.

Direct-Inlet Mass Spectrometer Development

J. J. Stoffels

Existing techniques for monitoring airborne plutonium are limited by the rate of radioactive decay which, for ^{239}Pu, amounts to only one disintegration per second for every 10^{12} atoms present. A new technique using direct-inlet surface ionization mass spectrometry is being developed. It will measure one ion count for approximately every 10^3 atoms of ^{239}Pu present and will do this on an individual particle basis. The direct-inlet mass spectrometer (DIMS) we have developed and the direct-inlet mass spectrometric technique are described in previous PNL Annual Reports. Current work has used uranium dioxide as an analog for plutonium dioxide.

Particle bouncing on impact with the ionizing filament of the mass spectrometer was reported last year. Particle bouncing was found to reduce measurement sensitivity (ions detected/atoms in the particle) for nominal 10 μm uranium dioxide particles entering via the capillary inlet by five to six orders of magnitude compared with the sensitivity for particles preloaded directly on the flat rhenium filament. To investigate the effect of particle melting point on the particle bounce problem, sensitivity measurements were made on nominal 10 μm particles of uranyl nitrate (m.p. 60°C) and cesium nitrate (m.p. 414°C) as well as on uranium dioxide (m.p. 2880°C).

Measurement sensitivity was first determined for particles preloaded on the ionizing filament of the mass spectrometer. Particles were then introduced into the mass spectrometer via the direct inlet and impinged on the filament at nearly sonic velocity. Uranyl nitrate and cesium nitrate both exhibited the loss of sensitivity attributed to particle bounce that was previously observed with uranium dioxide.

An oven ionizer has been designed and constructed for the purpose of trapping the high-speed particles which enter via the direct inlet. The oven is shown schematically in Figure 38. A particle entering the oven through a 1-mm diameter aperture may undergo many collisions with the interior surfaces before it comes to rest and is ionized. Ions emerge from the same aperture and are focused by the electrostatic lens of the mass spectrometer. The probability of a particle bouncing back out through the aperture has not been determined but should be small.

Figure 39 is a photograph of the oven assembly. The oven itself is fabricated of 0.0005-in. thick rhenium foil.

Sensitivity measurements have been made with 10-μm particles of uranium dioxide and uranyl nitrate preloaded in the rhenium oven. The measured sensitivities were the same for both compounds and were identical to those obtained with particles preloaded on a flat rhenium filament.

Individual 10-μm particles of uranium dioxide and uranyl nitrate have also been introduced into the mass spectrometer via the direct inlet. Since the area of the oven aperture is only about one-sixth the area of the particle beam, most of the

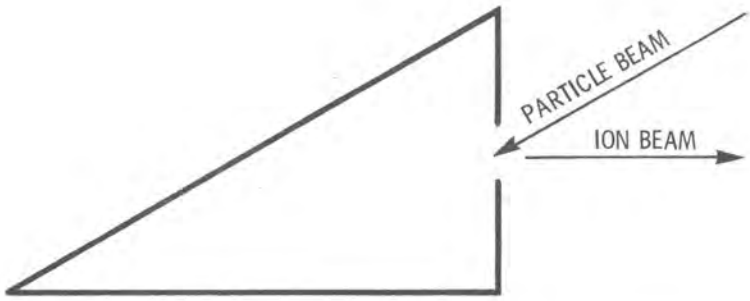

FIGURE 38. Schematic Cross Section of an Oven for Trapping and Ionizing High-Speed Particles in a Direct-Inlet Mass Spectrometer

FIGURE 39. Oven Ionizer Assembly

particles impinged upon the front face of the oven and bounced off. The resulting ion intensities were low and persisted for only a few seconds to a few minutes. However, some of the particles were trapped inside the oven as evidenced by the fact that the corresponding ion intensity and duration equaled those obtained with preloaded particles. Ion emission from individual 10-μm particles persisted for 40 min to 2 hr at temperatures up to 1800°C, yielding a measurement sensitivity comparable to that for preloaded particles.

These initial experiments have demonstrated the feasibility of using an oven ionizer to trap high-speed particles, thereby eliminating the loss of measurement sensitivity that results when particles bounce from a flat ionizing filament. Further work is needed to optimize the oven geometry for greater acceptance of the particle beam while maintaining particle trapping.

Our total experience to date in measurement sensitivity for uranium dioxide particles under different conditions in the direct-inlet mass spectrometer is summarized in Table 4. Our standard for comparison is the sensitivity obtained for a nominal 1-μm particle preloaded on a carburized rhenium

filament and run with the inlet closed. Under these conditions, emission of the uranium metal ion occurs, and one ion is detected for every 100 atoms in the particle. This 1% sensitivity matches many years' experience with our analytical mass spectrometers.

When the same size particle is preloaded on an uncarburized rhenium filament and run with the inlet open, the high partial pressure of oxygen causes emission of the uranium dioxide ion. Under these conditions, the measurement sensitivity is reduced by an order of magnitude.

When the nominal particle size is increased to 10 μm, another order of magnitude reduction in measurement sensitivity is experienced. This particle size effect is also in general agreement with the experience of our analytical mass spectrometers.

Introducing the 10-μm particle via the direct inlet onto a flat filament results in a sensitivity loss of at least four more orders of magnitude because the high-speed particle bounces from the filament, leaving only a small residue to be ionized.

Use of the rhenium oven ionizer obtains the same measurement sensitivity as the flat filament for particles that are preloaded. The oven ionizer can also obtain the same sensitivity for high-speed particles entering via the direct inlet as for particles that are preloaded. For 10-μm particles, this sensitivity is 0.01%. By extrapolation of the data, the sensitivity for 1-μm particles that are trapped in the oven should be 0.1%.

The measurement sensitivities stated above are order of magnitude figures. Measurement sensitivity exhibits some variability because of factors that are not unequivocally defined. Sensitivities up to an order of magnitude lower than those stated are obtained in some instances.

Prior to the above sensitivity measurements, the decay times of ion signals from particles of uranium dioxide, uranyl nitrate, and cesium nitrate were measured in order to determine appropriate filament operating temperatures for these materials. The ion signal from a particle impinging on the ionizing filament of the mass spectrometer exhibits a rapid rise followed by an approximately exponential decay. The decay time is the time during which the ion signal decays from the maximum value to 1/e of the maximum value.

The ion signals from uranium dioxide and uranyl nitrate have been found to exhibit a two-component decay--an approximately exponential decay component associated with the short duration ion burst and a decay component of very long duration. The mechanisms responsible for the two different decay components are not known. The decay times for the uranium compounds were determined from the short duration component only.

The variation of decay time with filament temperature is shown in Figure 40. The most remarkable result of these measurements is the difference in decay times for uranium dioxide and uranyl nitrate. Although both compounds of uranium emit the same ionic species, namely UO_2^+, the decay time for uranium dioxide is thirty times longer than the decay time for uranyl nitrate. This suggests that the short decay component may be related to melting of the particle.

TABLE 4. Order-of-Magnitude Sensitivity for Measurement of UO_2 Particles by Direct-Inlet Mass Spectrometry

Direct Inlet	Type of Re Ionizer	Species of Ions	Particle Size	Loading Method	Measurement Sensitivity, Ions Detected/Atom
Closed	Flat ribbon, carburized	U+	1 μm	Preload	$1/10^2$
Open	Flat ribbon, uncarburized	UO_2^+	1 μm	Preload	$1/10^3$
Open	Flat ribbon, uncarburized	UO_2^+	10 μm	Preload	$1/10^4$
Open	Flat ribbon, uncarburized	UO_2^+	10 μm	Direct inlet	$1/10^8$
Open	Oven, uncarburized	UO_2^+	10 μm	Preload	$1/10^4$
Open	Oven, uncarburized	UO_2^+	10 μm	Direct inlet	$1/10^4$

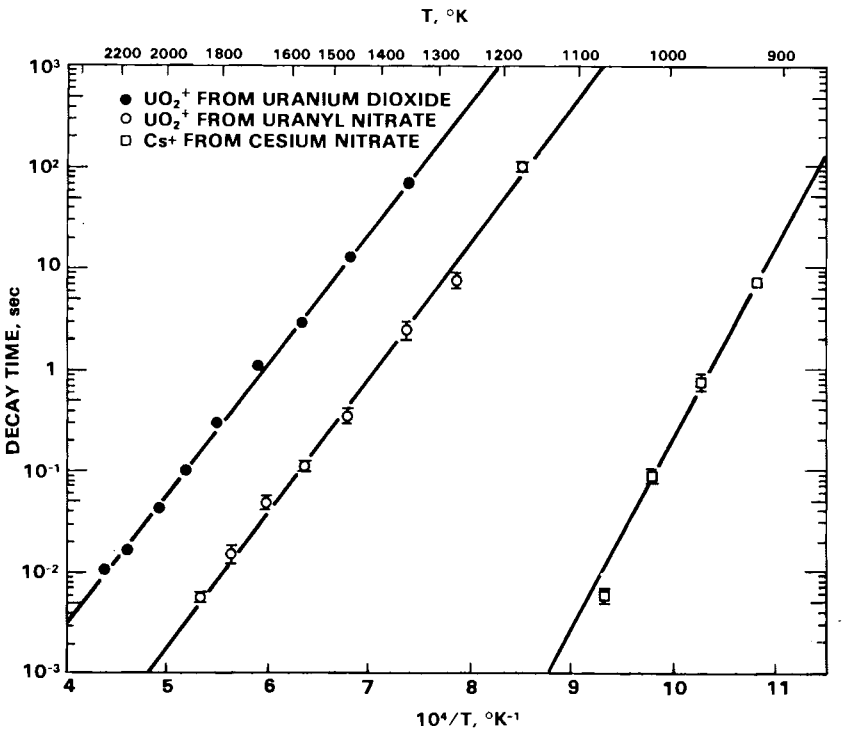

FIGURE 40. Decay Time Versus Temperature for the Ion Current from Particles of Different Materials Impinging on a Rhenium Filament in 10^{-5} Torr of Air. Error bars are the standard deviation of the mean. No error bars have been assigned to the uranium dioxide data.

A brief investigation of the effect of static charge on focusing of the particle beam from the inlet capillary has also been conducted. A polydisperse iron-oxide aerosol with a count medium diameter of about 0.1 μm was generated for this purpose. The aerosol generation technique is known to produce particles with a static charge. Focusing of the aerosol beam was monitored by collecting the particles on the adhesive side of transparent tape placed at the position of the ionizing filament.

The focusing of a beam of charged aerosol particles was compared with the focusing of aerosol particles that were passed through a ^{85}Kr charge neutralizer. The neutralizer reduces the charge on the particles to a Boltzmann equilibrium distribution. No difference between the charged and neutralized aerosol beam was observed.

Since the particle beam passes through part of the electrostatic ion lens which operates at 4,000 V, the possible effect of this voltage on focusing of a charged particle beam was also investigated. Again, no difference in particle beam focusing was observed with the lens high voltage on or off for either the charged or neutralized aerosol particles.

• Analytical Techniques for Measurement of ^{99}Tc In Environmental Samples

Three highly sensitive methods for ^{99}Tc measurements are described. The first involves electrothermal atomic absorption, requires minimal chemical separation steps, and allows detection of about 60 pg. The second method involves counting of beta particles from ^{99}Tc and internal conversion electrons from ^{97m}Tc, allows detection of as little as 25 pg of ^{99}Tc, and also allows determination of the chemical recovery. The third method involves isotope dilution mass spectrometry employing ^{97}Tc as a tracer and is capable of detecting sub-picogram quantities of ^{99}Tc. Procedures developed during the past year for analysis of soil and water samples are described, and the results of an evaluation of a resin bead technique for mass spectrometric analysis of ^{99}Tc are presented.

Ultrasensitive Measurement Methods for ^{99}Tc

J. H. Kaye

From an environmental and hazard viewpoint, ^{99}Tc is one of the most troublesome radionuclides produced through nuclear fission. This is due to the long half-life (2.13×10^5 yr), the volatile nature of the heptoxide, the mobility of the pertechnetate ion in aqueous solution, the high fission yield (over 6%), and the affinity of several organs of the human body for this element. Furthermore, technetium is almost impossible to detect at very low levels by direct counting methods since its half-life is long and it emits only low-energy beta radiation.

Since this is a final report on this research project, the overall accomplishments of this study will be reviewed in addition to covering what has been achieved during the past year. The goal of this project has been to develop more sensitive methods for the detection of ^{99}Tc than are currently available. This goal has been achieved. Three different methods have been developed and evaluated: 1) graphite furnace atomic absorption spectrometry, 2) beta counting with ^{97m}Tc as an isotopic tracer, and 3) isotope dilution mass spectrometry.

The first of these methods, graphite furnace atomic absorption spectrometry, requires only a minimal amount of chemical separation. For some applications, it may only be necessary that the technetium be in solution form and in some cases even milligram quantities of solid samples could be analyzed directly. A special hollow cathode lamp is required, since no technetium lamp is commercially available as yet. However, a demountable lamp such as the one used for this study can be purchased for just over $800. Approximately 5 mg of ^{99}Tc must then be emplaced in it. With use of this lamp and neon fill gas, a detection limit of about 60 pg (1.0 pCi) was obtained at a wavelength of 261.5 nm (Kaye and Ballou 1978). Time and funding did not allow investigation of interference levels, which should be studied in order to develop the technique into a routine measurement method.

The second measurement method involves beta counting. It was found during this study that sufficient ^{97m}Tc is produced in the decay of ^{97}Ru to provide a useable tracer for technetium. (Production of ^{97}Ru by neutron irradiation of ^{96}Ru has been for the purpose of manufacturing ^{97}Tc for use as a tracer in mass spectrometric analyses for ^{99}Tc.) Technetium-97m decays with an 89-day half life by emission of a 96-keV photon, which is highly internally converted, giving rise to very low energy electrons. The fact that these electrons may be easily stopped by a thin amount of aluminum absorber allowed us to develop a counting technique by which both the chemical yield and the amount of ^{99}Tc in the sample may be determined. A small amount of ^{97m}Tc tracer is added to the sample before chemical separation.

After purification and electrodeposition, the sample is counted with and without a 14 mg/cm^2 aluminum absorber. The detection limit of this method is about 25 pg (0.42 pCi).

The counting technique can be used as a screening method to decide if the more sensitive, but also more costly, mass spectrometric analysis method is required. The same chemical separation and purification procedure is used for both methods. If the counting method does not give a positive result, the electrodeposited sample may be dissolved and further separations performed on a micro-scale to remove molybdenum contamination that is introduced during the plating step. These micro-scale steps involve solvent extractions of the tetraphenylarsonium complex into chloroform. The final solution containing the technetium is loaded onto a rhenium filament for mass spectrometric analysis (Kaye, Rapids, and Ballou 1977). Measurement of ^{99}Tc at the 1-pg level (0.02 pCi) can be accomplished by the mass spectrometric method. Measurements at lower levels should be possible with further development of the method.

During the past year, ^{99}Tc was determined in a set of vegetation samples by the beta-counting method. These samples were then dissolved, repurified using the micro-scale solvent extraction procedure, replated and recounted in order to verify the quantitativity of the counting method. The amount of ^{99}Tc in the samples before and after recycling was found to be the same within experimental errors. This work has been submitted for publication (Kaye, Rapids and Ballou 1979).

An evaluation was made of a resin-bead technique, which has been reported to give a ten-fold increase in signal compared to a sample directly loaded onto a mass spectrometer filament from aqueous solution (R. L. Walker 1978). We did not, however, observe this increase for the case of technetium. In fact, the mass 99 signal was only 64% of that obtained for the aqueous solution case. Further investigation is needed here. We were, however, able to nearly quantitatively transfer the activity from ^{95m}Tc tracer to a single 22-μm bead of anion exchange resin.

Chemical separation procedures have been developed for analysis of soil and water samples in addition to vegetation. The soil procedure involves fusion with Na_2O_2 in a ratio of five parts Na_2O_2 to one part soil. The water procedure involves making the sample basic with NH_4OH or NaOH and passing it through an anion exchange resin. Samples of all three types are currently being analyzed for the Ecological Sciences Department at Pacific Northwest Laboratory and for other laboratories.

• Radiation Instrumentation — Radiological Chemistry

During the past year, major efforts in this program have concentrated on lowering the background for the measurement of small amounts of radioactivity by beta and gamma counting, on the design of specialized systems, on specific procedures for the measurement of certain radionuclides, on improved computer programs for the analysis of gamma-ray spectral data, on the development of magnetic field dosimeters, and on the development of X-ray fluorescence techniques that permit concentrations to be measured without the weight of the sample being known.

Subcritical Neutron Multiplier Facility

H. G. Rieck

Hardware components for a modified pneumatic sample transfer system were installed in the subcritical neutron multiplier at Pacific Northwest Laboratory and testing is in progress. Modified Flextran programs have been written for TN-11 computer control of the cyclic operation of the pneumatic transfer system. A new sample transfer mechanism at the counting station was designed and fabricated. This transfer device permits simultaneous sample irradiation and counting of a previously irradiated sample.

Computer control of the simultaneous mode has been demonstrated; however, a commercial four-way diverter valve in the system has not performed reliably and is being modified. During the first 6 mo of CY 1979, the multiplier was used to analyze 560 samples for their elemental constituents using short (5 min) and long (60 hr) irradiations.

A Low-Background, Ge(Li) Gamma-Ray Spectrometer Shielded with a Multidimensional NaI(Tl) Crystal System

N. A. Wogman

Past research at Pacific Northwest Laboratory has developed a variety of low background, multidimensional gamma-ray spectrometer systems (Wogman, Perkins and Kaye 1969). From their conception, these systems were designed to provide the lowest possible achievable background at their construction time. Thus, it seemed natural to utilize their low-background character in conjunction with an intrinsic germanium detector to provide a large NaI(Tl)-shielded intrinsic germanium gamma-ray spectrometer system. Such a system is shown assembled in Figure 41. The area between the two large NaI(Tl) crystals is occupied by the Ge(Li) detector and by square extruded NaI(Tl) crystals, which are operated in a summing mode with the two large NaI(Tl) crystals from the original multidimensional gamma-ray spectrometer system.

The efficiency of the Ge(Li) detector used in this study was 25% of that of 3 by 3-in. NaI(Tl) detector and had a resolution of 2.13 keV at the 1332-keV photopeak of ^{60}Co. The peak-to-Compton ratio for the Ge(Li) detector was 48.4 to 1. With the NaI(Tl) crystals serving as a coincidence photon detection system for the diode, two spectra are recorded. The first is the "single events" from the diode only; the second is the events in the diode which are in coincidence with events in the NaI(Tl) system. Cobalt-60, which emits two photons per disintegration, has many of its photon events stored in the coincidence spectrum. However, some coincidence photons are not detected by the NaI(Tl) crystal and thus ^{60}Co photopeaks are present in the singles spectrum. The ratio of the 1332-keV photopeak in the coincidence-to-singles spectrum for ^{60}Co in this sytem is 5.4 to 1. The overall peak-to-Compton ratio achieved with a 1-cm thick soil sample in the system is >100.

Where large NaI(Tl) crystals are used, a ringing effect may occur in the output signal due to deposition of large amounts of energy from cosmic-ray penetration of the system. A blocking circuit (discussed by Brown later in this report) using a 1416

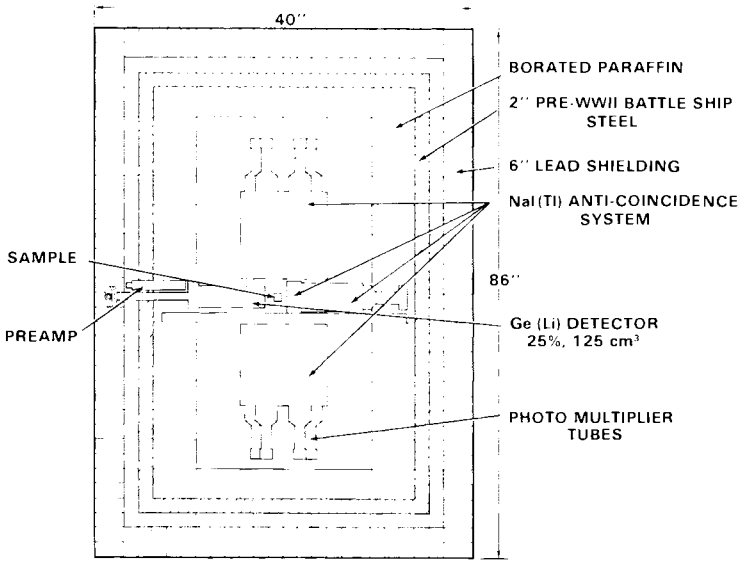

FIGURE 41. A Ge(Li) Gamma-Ray Spectrometer Using a Large-Volume, NaI(Tl) Multidimensional Gamma-Ray System for Detection of Coincident Photons

pile-up ejector was applied to eliminate the ringing problem. The circuit applied a block of 550 msec duration to the diode output whenever the NaI(Tl) detectors received greater than 8 MeV of energy. In this manner, the ringing problem was removed and the diode background reduced. The background of the germanium detector surrounded by the crystal and lead/iron mass is shown in Figure 42. For these measurements, the detector system was operating without the anticoincidence output from the NaI(Tl) crystals. The spectra compare the operation of the system with and without the 550-msec, cosmic-ray block. The blocking circuit reduces the overall background continuum about two-fold. As presently operating, the circuit does cause a peak at 10 keV; however, the system is normally not operated below 30 keV so this proves to be no problem.

In Figure 43, the singles and coincidence spectra taken with and without cosmic-ray blocking are shown. The upper spectral pair shows the background obtained with the germanium diode operating normally in the coincidence mode with the NaI(Tl) spectrometer. No blocking for cosmic rays has been applied. In this case, the singles background in the spectrum varies from 1 to 100 counts/min over the various energy ranges. The singles spectrum beyond 511 keV has only a few counts/keV/1000 min, whereas the coincidence spectrum has primarily four peaks due to ^{226}Ra, ^{232}Th, and the 511 peak. The coincidence spectrum varies from approximately 5 to 100 counts/keV/1000 min over the energy range 0 to 2 MeV.

Shown in the same figure is the identical system operating with the cosmic-ray blocking circuit. The background is reduced two-fold by operation of the cosmic-ray block system.

By use of the multidimensional spectrometer system, a background has been obtained which is lower than that achieved by other low-background systems presently in operation in the United States. Interference from cosmic-ray events has also been reduced.

A Low-Background, Ge(Li) Gamma-Ray Spectrometer Shielded with a Low-Background, NaI(Tl) Anticoincidence Well Crystal

N. A. Wogman

An anticoincidence-shielded gamma-ray spectrometer has been constructed using a 24.4% Ge(Li) diode housed in ultra-pure aluminum cladding. The anticoincidence NaI(Tl) well crystal is also constructed of material proven to be free of potassium, thorium, and uranium at the parts-per-billion level. Calcium carbonate was used

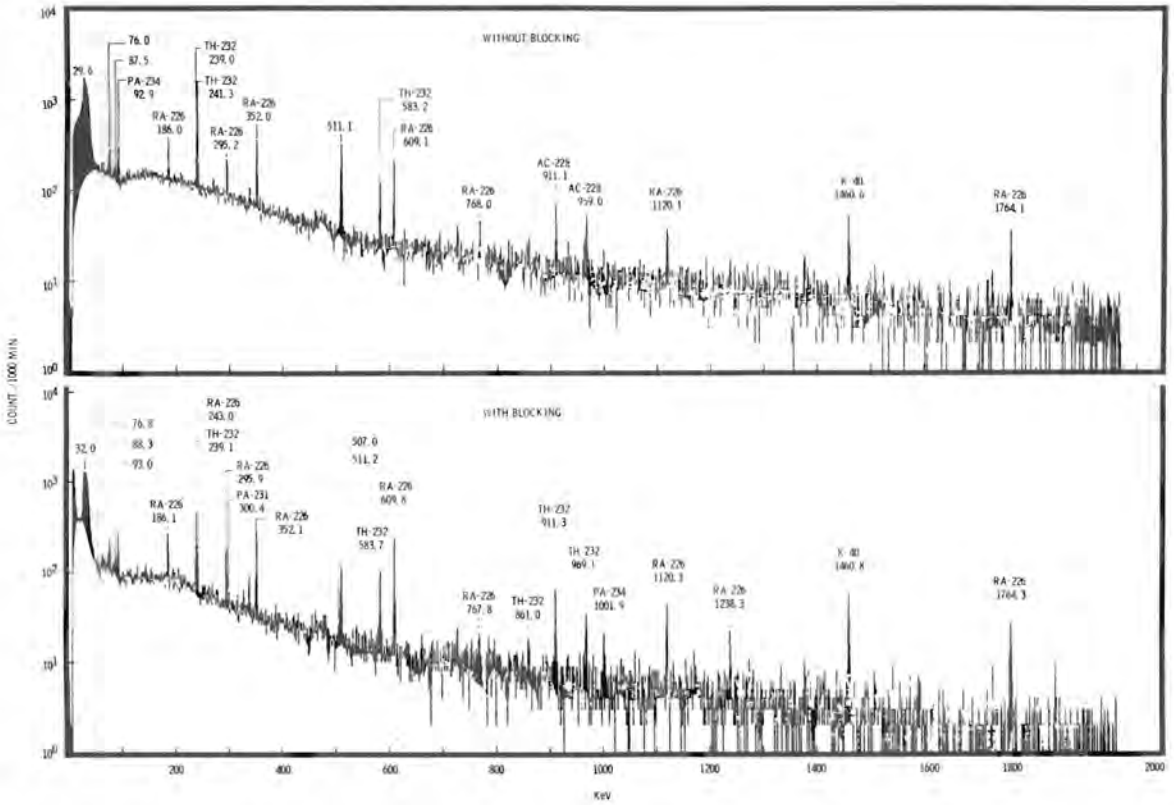

FIGURE 42. A Comparison of Germanium Diode Gamma-Ray Spectra as a Function of Cosmic-Ray Blocking

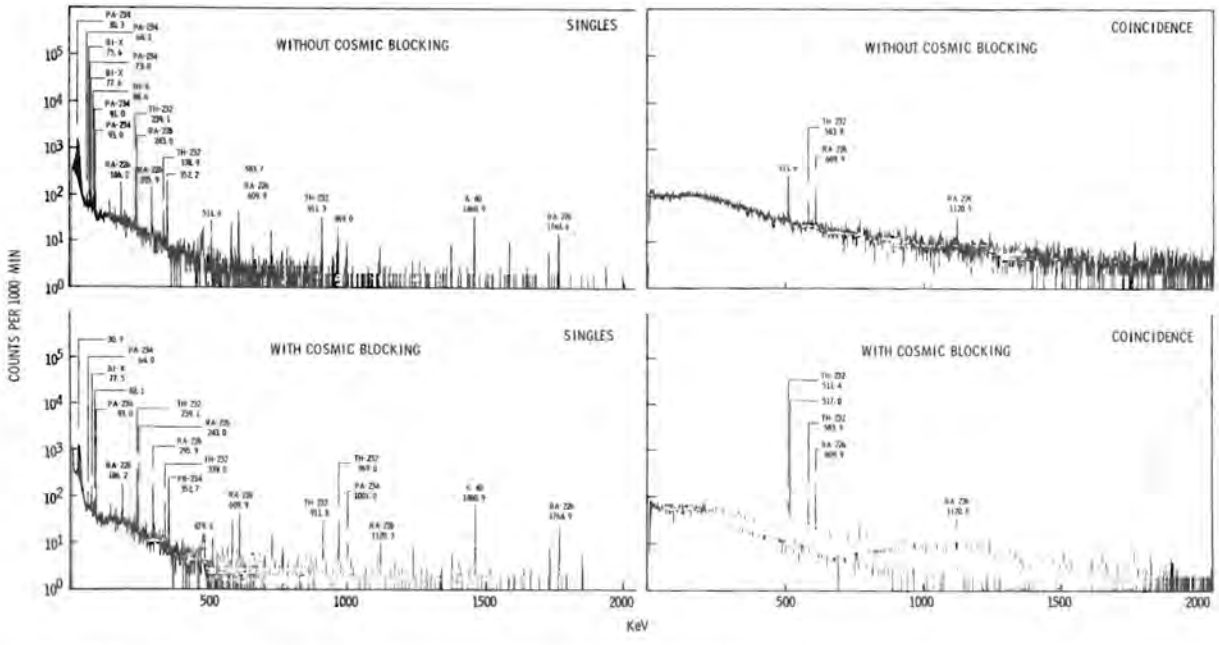

FIGURE 43. A Comparison of Coincidence and Single Gamma-Ray Backgrounds for an All-NaI(Tl)-Shielded Germanium Spectrometer as a Function of Cosmic-Ray Blocking

as the packing and reflecting material for the NaI(Tl) crystal. The iron that was used to encase the crystal was from pre-World War II oil tanks and contained only parts-per-billion levels of uranium and thorium and less than 1 dpm ^{60}Co/kg iron. The Ge(Li) gamma-ray spectrometer system was assembled as shown in Figure 44 in a cave composed of 10-cm lead shielding inside of which is 10-cm borated paraffin. The borated paraffin (5% by weight boron) served to reduce the cosmic-ray neutron flux generated in the lead shielding. This procedure eliminated background events created from the cosmic-ray neutrons interacting in the NaI(Tl) or Ge(Li) spectrometers.

The resolution of the Ge(Li) system was 1.74 keV at ^{60}Co, with a peak-to-Compton ratio of 55 to 1.

The coincidence and singles spectra of ^{241}Am, ^{137}Cs, and ^{60}Co taken with this system are shown in Figure 45. The ^{137}Cs is in the singles spectrum. The singles-to-coincidence spectrum ratio of 8.6 to 1 defines the selectivity of the spectrometer. The system thus provides an excellent discrimination for coincidence and single photon events. The peak-to-Compton ratio for the system is greater than 100 in its anticoincidence operating mode. Figure 46 shows the background of the system with the various ^{238}U, ^{232}Th, and their daughter photo-peaks. Even though a superpure-NaI(Tl) anticoincidence crystal was used, a large quantity of natural radioactivity remained. A copper shadow shield was used in the Ge(Li) crystal to eliminate line-of-sight between the molecular-sieve, vacuum-pumping material and the detector ingot. Figure 46 illustrates the background in the coincidence and singles spectra showing the elimination of background in the coincidence section. Since this crystal system is designed to be used for coincidence photons in low-background measurements of biota, the system should have an excellent detection sensitivity. To minimize the interference from ^{40}K photons arising at the phototube, lead-shot shielding will be used around the phototube assembly to absorb the radiation from the glass phototubes prior to their entrance into the NaI(Tl) crystal.

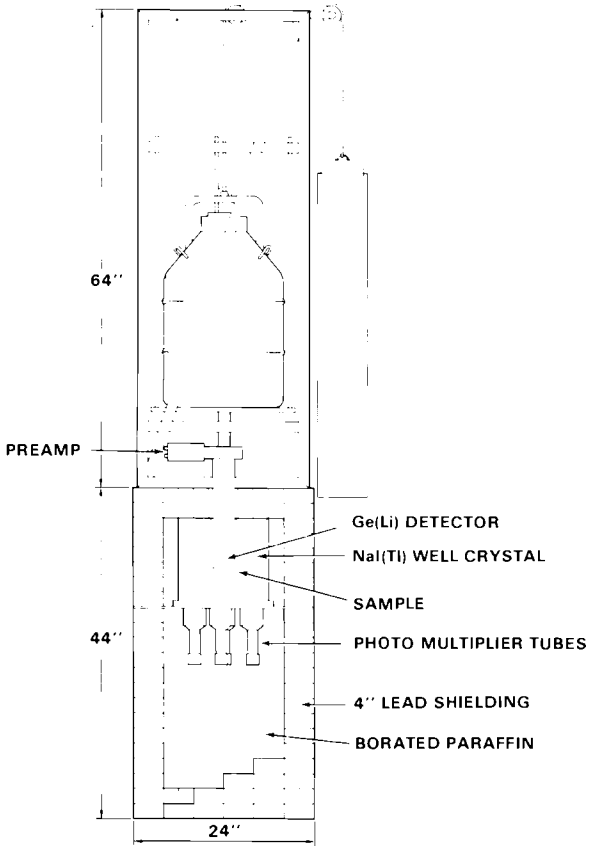

FIGURE 44. A Ge(Li) Gamma-Ray Spectrometer Using a Large Volume NaI(Tl) Well Crystal for Detection of Coincident Photons

Design of an Intrinsic Germanium-Diode, Plastic-Phosphor, Anticoincidence-Shielded, Gamma-Ray Spectrometer Using Charcoal Vacuum Pumping

N. A. Wogman

In the analysis of gamma-ray emitters in environmental samples, counting systems are required which have backgrounds below those presently available. The primary source of background in gamma-ray spectrometer systems results from natural radioactive species in the construction materials and cosmic-ray interactions in the system. Figure 47 shows an intrinsic germanium, gamma-ray spectrometer that uses a plastic-phosphor, anticoincidence detector to surround a specially designed intrinsic germanium diode that has been vacuum pumped with charcoal rather than the usual molecular sieve. The efficiency of the detector is 28.0% with a resolution of 2.20 keV full width half maximum at 1332 keV. The peak-to-Compton ratio is 48.9 to 1.

Various molecular sieve materials were analyzed by multidimensional gamma-ray spectrometry (Wogman, Perkins and Kaye 1969) and found to contain from 1 to 5 disintegrations per minute per gram (dpm/g) of uranium, thorium, and potassium. Various charcoal samples were evaluated using the same

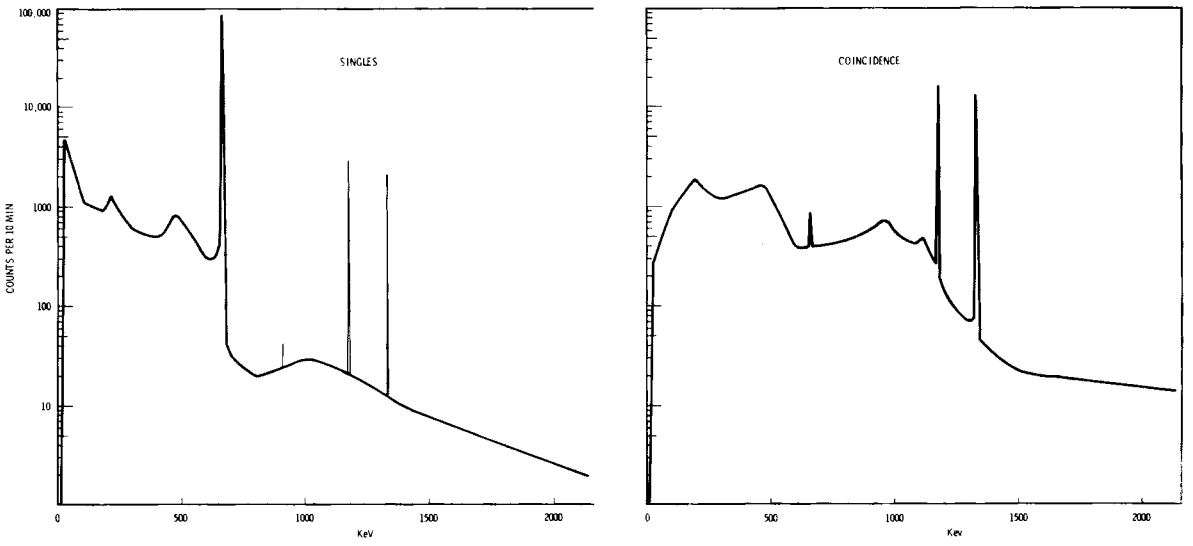

FIGURE 45. The Coincidence and Single Gamma-Ray Spectra of ^{241}Am, ^{137}Cs, and ^{60}Co from an Au-Nal (Tl)-Shielded Ge(Li) Spectrometer

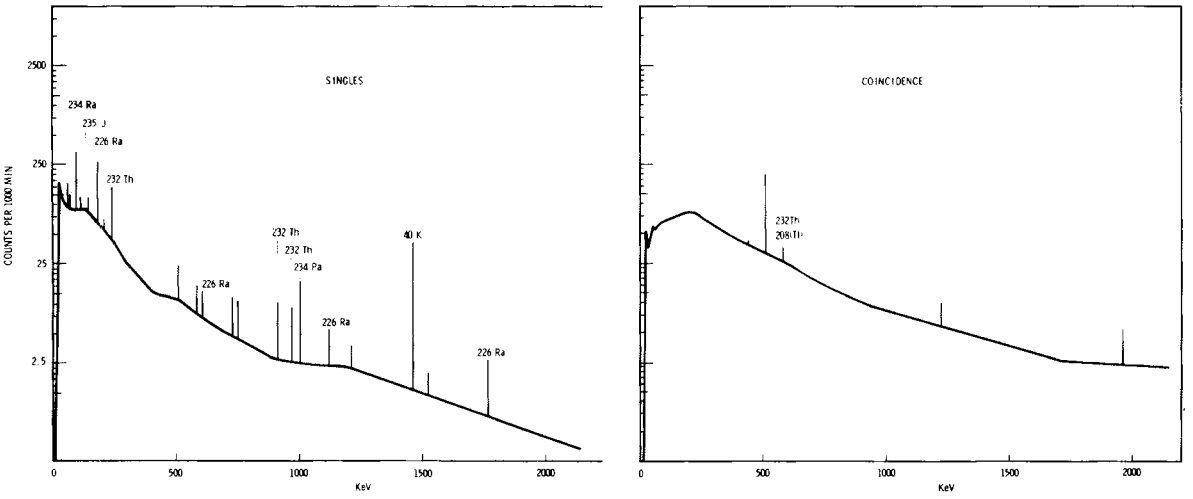

FIGURE 46. The Coincidence and Single Gamma-Ray Spectra Background from an Au-Nal (Tl)-Shielded Ge(Li) Gamma-Ray Spectrometer

system and found to be free of these materials at the 0.001 dpm/g level. A detector described above was therefore assembled using low-background charcoal as its vacuum-enhancing medium and is presently being evaluated.

Lead has been used as the primary shielding material and studies to determine the effect of borated-paraffin and cadmium-sheet shielding materials are being initiated. The boron and cadmium capture the neutrons produced in the lead shield by cosmic rays so they do not strike the anti-coincidence plastic phosphor.

Computer Programs in Support of Gamma-Ray Spectrometry

J. W. Brothers

Computer programs have been developed for a PDP-11/35 to provide quantitative and qualitative data reduction in the analysis

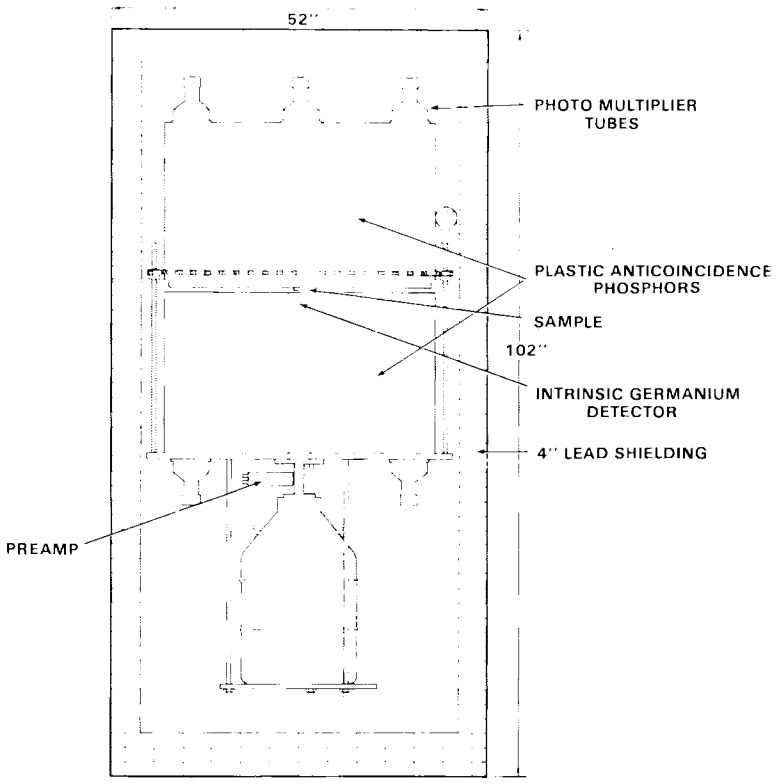

FIGURE 47. An Intrinsic Germanium Gamma-Ray Spectrometer Using a 90-cm-Diameter N.E. 102 Plastic Phosphor for Detection of Coincident Photons

of gamma-emitting samples by Ge(Li), intrinsic germanium, and NaI(Tl) systems. The programs written in FORTRAN IV are for the current computer environment, which consists of an 88-K PDP-11/35 with three 1.25-megaword disk cartridges, dual floppy diskette, electrostatic printer/plotter, four alphanumeric display terminals, and CAMAC multichannel-analyzer interface equipment. At the present time, there are seven Si(Li), Ge(Li), or Ge(Li) anticoincidence analyzers directly connected to the system and four multidimensional NaI(Tl) spectrometers connected through magnetic tape transfer.

Data transfers are performed automatically for two of the Si(Li) analyzers with automatic sample changers, while data transfers for the remainder are controlled by the user through one of the computer terminals. A typical transfer time is less than 8 sec per 4096 channels of 6-digit BCD data, including BCD-to-binary conversion and writing to disk file. All data acquisition takes place asynchronously with other data acquisition and data reduction activity on the system. The operating system used is RSX-11M, Version 3.1. In addition to the transfer of data by direct connection, spectra have been read from different types of magnetic tape cassettes, punched paper tapes, and floppy diskettes generated by other systems.

All spectra acquired are stored on floppy diskettes for archival purposes. Utility programs have been prepared to add user-determined parameters, print, plot, and move the spectral data from one disk to another.

There are currently three data reduction programs for Ge(Li) spectra in use (Table 5). The primary use of CANGAS is for activation analysis. SUM is used for single sample analysis such as standards and environmental samples, while SLAVE is used for unknown samples. CANGAS and SUM programs are used primarily for quantitative analysis, while SLAVE is primarily used as a qualitative tool.

Pulse Pile-Up Rejector/Live-Time Corrector Modifications for Use as an Anticoincidence Circuit

D. P. Brown

Many multichannel analyzer-based, gamma-ray spectrometer systems use a pulse pile-up rejector/live-time corrector, such as the Canberra Model 1468A, to eliminate pulse-height error due to the arrival of two or more signal pulses within the pulse decay time of the amplifier. The logic circuits of the unit will reject pulses in which pile up occurs. However, when leading-edge pile up occurs and the circuits reject the pulse, the busy output comes true and remains until the next noncontaminated event. At reasonably high count rates, the additional busy time does not unduly increase the total counting time, but when the counting rate is low, such as when counting background, long busy periods can result from a single leading-edge, contaminated event. As much as 20 sec of busy time per single event have been observed. Because of this increased counting time and because the pile-up rejector is not necessary at low count rates, an operating procedure was established whereby the unit was turned off for low count-rate operation (less than 5% dead time). Subsequently, the 1468A was found to generate certain output signals useful to activate logic circuits in developing anticoincidence-shielded, solid-state, detector systems. The long busy signals that occurred occasionally at low count rates became unacceptable.

When a noncontaminated or a falling-edge contaminated event occurs, the 1468A amplifier discriminator returning to its nonactive state at the conclusion of the event or the ADC dead-time signal (whichever occurs last) will reset busy. This does not occur for lead-edge pile up as noted previously. To overcome this difficulty, the circuit shown in Figure 48 was designed and installed within the 1468A. The figure shows the signals used to generate the "block busy" signal. When the amplifier discriminator and the inhibit signal are both active simultaneously, a 500-msec, monostable flip-flop is activated. At the end of the 500-msec delay, the falling edge of the signal and the pulse-shaping circuits generate a short pulse that will reset the busy signal if it has not yet been reset by other means. The 500-msec delay time was found by experiment to be the minimum delay time required by the 1468A to properly correct for the dead time over all count rates. This circuit will reset the busy signal within 500 msec, thereby eliminating the long periods of system busy encountered at very low count rates, and will permit using the 1468A for any count rate without the need for special operating procedures, as well as permitting its use in special anticoincidence-shielded detector systems. The new circuit has been incorporated in a new low-background, anticoincidence-shielded, intrinsic

TABLE 5. Capabilities and Requirements of Data Reduction Programs for Ge(Li) Spectra

Data Reduction Capabilities	CANGAS	SUM	SLAVE
Integrated areas	Yes	Yes	Yes
Energy determination	No	No	Yes
Overlapping peak corrections	No	Yes	No
Labeled plots	Yes	No	Yes
Activity from standards	Yes	No	No
Activity from efficiency	Yes	Yes	No
Nuclide identification	No	No	Yes
Speed	15 sec/sample	15 sec/sample	>4 min/sample
Data Reduction Requirements			
Resolution	No	No	No
Gain	No	No	Yes
Efficiency	No	Yes	No
Peak channels	Yes	Yes	No
Integration limits	Yes	Yes	No
Background limits	Yes	Yes	No

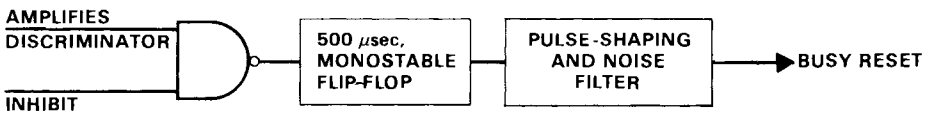

FIGURE 48. Busy Killer Block Diagram

germanium, gamma-ray spectrometer designed to measure ^{232}U and its daughters at the 1 pCi/g level.

Evaluation of a Phoswich Detector for Laboratory and In-Situ Analysis of ^{90}Sr

N. A. Wogman, R. L. Brodzinski, and D. P. Brown

Strontium-90 produced in the nuclear-weapons testing and commercial nuclear reactor programs must be measured in a variety of environmental samples from nuclear-waste storage areas and reactor sites. Strontium-90, a pure beta emitter, can be measured without chemical separation by direct analysis of its beta emissions, by the analysis of bremsstrahlung produced from the interaction of its beta particles in surrounding media, and by neutron activation analysis. Bremsstrahlung and activation analysis technologies can be utilized for only relatively high levels of ^{90}Sr. This study shows that a phoswich detector can be used for the measurement of ^{90}Sr in the presence of other fission product species, ^{106}Ru, ^{137}Cs, ^{238}Pu, ^{239}Pu, ^{241}Am, and ^{244}Cm, normally found in waste areas. The phoswich system (Figure 49) is composed of a 3.45-mm-thick by 12.5-cm-diameter $CaF_2(Eu)$ crystal coupled to a 6.35-cm-thick NaI(Tl) crystal. A 3.2-mm quartz absorber light pipe is placed between the two crystals. A 0.006-mm aluminized mylar coating protects the $CaF_2(Eu)$ crystal. The electronics consist of a high-voltage power supply for the photomultiplier tube, a preamplifier, a pulse-shape amplifier/analyzer, and two scaler/timers. One scaler records the pulses from the $CaF_2(Eu)$ activated crystal and the other the photons detected in the NaI(Tl) crystal.

The system is calibrated using sources of ^{90}Sr, ^{137}Cs, ^{106}Ru, ^{238}Pu, ^{239}Pu, ^{241}Am, and ^{244}Cm in matrices typical of those found in waste areas--sands, soils, thin plates, etc. In calibration of the system, the time output connector of the pulse-shape amplifier system is connected to a multichannel analyzer and a time spectrum is made of the radioactive sources. Two time distributions are detected, one characteristic of the beta particles being absorbed in the $CaF_2(Eu)$ crystal and the second time distribution for pulses recorded by the NaI(Tl) crystal. By removing first the beta source (^{90}Sr), then the other standards (e.g., ^{137}Cs), the time distribution peak areas were identified. A time output oscilloscope was used to observe the amplitude and general width of the pulse-height distribution. This observed amplitude served as a guide in setting the time controls of the pulse-shape amplifier. In this way, calibration optimization was made for specific isotope interferences to ^{90}Sr.

In normal phoswich detector operation, the secondary crystal, NaI(Tl), serves as an anticoincidence shield for the primary crystal, $CaF_2(Eu)$. However, in this evaluation, both crystal outputs were recorded such that a measure of the beta and gamma events coming from a variety of pure isotopic sources could be studied. Using the aforementioned procedure, the effect of various absorber materials on the response of each crystal to a specific radionuclide photon or beta energy was studied. Wood, aluminum, sand, calcium sulfate, nickel-calcium sulfate, and polyvinylchloride absorbers were used varying from 10 to 10^4 mg/cm^2 thickness.

The isotopes ^{238}Pu, ^{239}Pu, ^{241}Am, and ^{244}Cm do not contribute a significant interference to the detection of ^{90}Sr; however, ^{137}Cs and ^{106}Ru do interfere with its analysis. An efficiency evaluation indicated that the phoswich system was 4.5% efficient for the $^{90}Sr(^{90}Y)$ beta and 0.2% efficient for bremsstrahlung produced by the interaction of the $^{90}Sr(^{90}Y)$ beta particle in its environment. Similarly, ^{137}Cs disintegrations were detected with a 0.2% efficiency in $CaF_2(Eu)$ and a 6.5% efficiency in NaI(Tl). A 600-mg/cm^2 absorber decreased the beta efficiency 25-fold for $^{90}Sr(^{90}Y)$. $CaF_2(Eu)$ detection efficiency for ^{137}Cs decreased 11-fold when the same 600-mg/cm^2 absorber was used. The ^{137}Cs photon efficiency was not changed with the 600-mg/cm^2 absorber. The quantity of ^{90}Sr in the presence of ^{137}Cs was defined using a simultaneous equation for the two species, with constants generated from an analysis of those isotopes using absorbers. In sandy

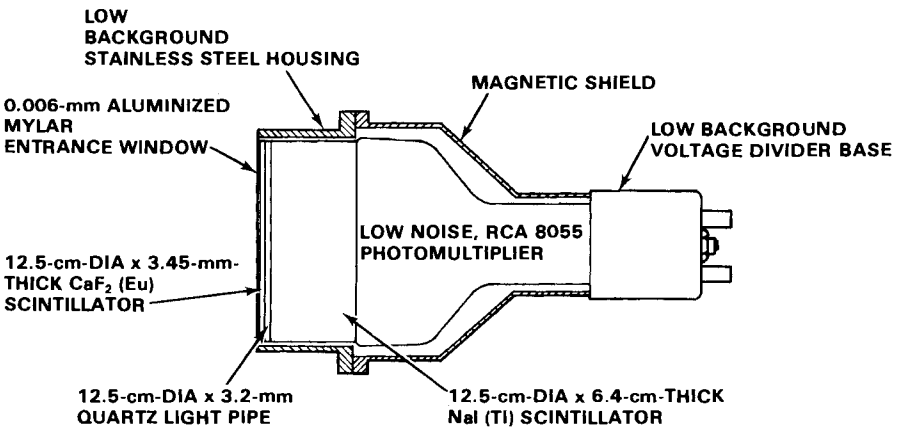

FIGURE 49. Schematic Model of a Low Background Phoswich Detector Designed to Measure ^{90}Sr in the Presence of Gamma-Ray Emitting Radionuclides

soil typical of Hanford, Washington, nuclear waste areas, 2000 d/m ^{90}Sr can be measured where contaminating radionuclides such as ^{137}Cs and ^{106}Ru are <2000 d/m. When the system was operated with the NaI(Tl) crystal in anticoincidence without trying to selectively resolve the photon pulse, the system could be adjusted to achieve a 45% efficiency for $^{90}Sr(^{90}Y)$ beta particles from a 12-cm-diameter source. This could be used only when the photon interferences were 10-fold lower than the ^{90}Sr disintegration rate.

A Procedure to Determine ^{228}Th and ^{232}U in Tissue Samples

C. W. Thomas

An analytical procedure to rapidly measure ^{228}Th and ^{232}U in tissue samples has been developed so that these radionuclides can be analyzed in organ tissues of small laboratory exposure animals. The procedure uses 1-g sample sizes and traces the radiochemical yield with ^{234}Th and ^{236}U. The sample is first frozen in liquid nitrogen to help break the tissue structures, then digested in 50 ml of concentrated HNO_3, diluted to 8N, and passed through an anion exchange column previously equilibrated with 8N HNO_3 at flow rates of 2 ml/min. The effluent is collected and evaporated to dryness and saved for uranium analysis. The column is then washed with 8M HNO_3, the thorium eluted with 100 ml of concentrated HCl and the thorium solution taken to dryness, redissolved in H_2SO_4, and electroplated. Thorium-234 is used to determine the chemical yield. The residue containing the uranium fraction is digested in 50 ml of concentrated HCl, the solution is diluted to 10M HCl, and loaded on an anion exchange column previously equilibriated with 10M HCl, at flow rates of 2 ml/min. The column is then washed with 10M HCl. The uranium is removed from the column with 8N HNO_3, taken to dryness, and electroplated from a H_2SO_4 media. The uranium recovery is determined by measuring the ^{236}U tracer.

Radiochemical yields are about 50%-70% for thorium and uranium. Approximately 15-20 samples per day can be chemically analyzed with measurements made on an alpha energy spectrometer yielding detection limits of 0.08 dpm ^{232}U and 0.08 dpm ^{228}Th.

Multielement X-Ray Fluorescence Samples of Unweighed Geological and Biological Samples Using the SAP3 Program

K. K. Nielson and R. W. Sanders

An optional feature to the SAP3 program (Nielson 1977) has been developed and evaluated for X-ray fluorescence analysis of geological and biological samples of unknown thickness and nonstandard configuration. The feature consists of the accurate measurement of sample mass from backscatter intensities. This obviates the need for weighing or extensive preparation of samples and thereby reduces cost and potential contamination and extends the application of X-ray fluorescence to a greater variety of samples. As reported previously (Nielson

1977), the SAP3 program also avoids the need for standards of similar matrix to the sample being analyzed.

Various geological and biological standard reference materials have been analyzed, both as pelletized wafers and as loose powders supported by thin plastic films. The quantitative analyses are based on a single-thin-film calibration of the spectrometer and subsequent matrix corrections for self-absorption and enhancement. An energy-dispersive detector was used with second-source (Zr) excitation to provide adequate separation of coherent and incoherent backscatter peaks. A Colorado oil shale analysis summarized in Table 6 for aliquots covering a twenty-fold range of sample thickness illustrates the versatility and accuracy of the method.

Table 6 compares the element concentrations per unit weight generated by the program for a series of unknown sample weights to the element concentrations determined from known sample weights using X-ray fluorescence, instrumental neutron activation, and atomic absorption techniques on weighed samples. Except for chromium, the average of the concentration data generated for unweighed samples agrees for all elements to within ±5% of that for weighed samples analyzed by the three different techniques. Chromium concentrations agree to within ±10% of the average value.

The SAP3 method is inherently a multielement technique and entails solving for all major sample constituents. The coherent and incoherent scatter intensities are used to estimate the light element components (Z<13) of the sample. Numerical matrix corrections are then made from fundamental constants and the constituent concentrations in an iterative manner. A unique set of correction factors is thus generated for each sample. The method provides accurate self-absorption corrections even for light elements such as silicon, for which the factor often exceeds 100 in geological samples. The calculations, including peak analysis, typically require 10 to 30 sec for analysis of 24 elements in a 1024-channel spectrum using a 64-K, PDP-11/34 minicomputer operating under RSX-11M, Version 3.1.

TABLE 6. Major and Trace Elements in Colorado Oil Shale as Determined by X-Ray Fluorescence Analysis

	%							μg/g														
Sample Mass[a] mg/cm²	Si %	P %	S %	Cl %	K %	Ca %	Ti %	Fe %	Y	Cr	Mn	Co	Ni	Cu	Zn	Ga	Hg	Se	Pb	As	Br	Rb	Sr
12.6	12.9	1.04	.77	<.05	1.58	9.8	.19	2.00	86	26	314	<39	30	37	66	10.8	<5.2	2.4	25	43	<1.7	75	740
25.3	13.4	.82	.77	<.05	1.67	10.1	.20	2.04	61	21	322	<35	24	40	68	9.6	<4.5	2.2	25	42	<.2	75	708
37.9	13.9	.64	.74	<.06	1.69	10.6	.20	2.12	81	36	354	<34	24	41	70	8.8	<3.9	2.5	26	42	<.0	75	680
50.5	13.8	.68	.71	<.06	1.74	10.4	.20	2.07	<46	51	309	<33	21	41	70	11.7	<3.6	2.2	24	41	<.9	75	682
63.2	13.1	<.50	.68	<.06	1.63	10.2	.20	2.02	72	26	326	<32	26	41	67	11.2	<3.5	2.2	26	41	<.9	74	688
75.8	12.9	.71	.81	<.06	1.61	10.0	.19	1.98	66	39	311	<32	24	41	68	9.8	<3.4	1.7	27	40	<.9	75	698
101.0	13.5	.73	.75	<.06	1.61	10.2	.20	2.05	83	21	337	<34	23	39	68	9.8	<3.7	2.6	25	43	<.9	75	703
126.3	12.9	.78	.66	<.07	1.61	10.2	.19	2.01	66	29	330	<32	25	40	69	9.8	<3.5	2.6	25	43	<.8	77	712
252.6	13.5	.71	.71	<.07	1.63	10.2	.19	2.03	75	24	320	<32	25	42	68	11.1	<3.8	2.4	26	42	<.9	76	736
$\bar{X}$[b] ± Std. Dev.	13.3	.73	.73		1.64	10.2	.19	2.04	71	30	325		25	40	68	10.3		2.3	25	42		75	705
	.4	.7	.05		.05	.2	.01	.04	13	10	14		2	1	1	.9		.3	1	1		1	22
$\bar{Y}$[c] ± Std. Dev.	13.8		.68		1.69	10.2	.18	2.02	80	36	330	9	26	39	67	9		2.2	25	46		74	698
	.3		.02		.07	.5	.02	.03	9	1	20	.2	3	5	4	1		.2		1		4	14

[a] Sample area = 7.92 cm² for all masses; the computer must estimate the mass to percent concentration per unit weight.

[b] Average for all element concentrations as determined from masses of 12.6 to 252.6 mg/cm².

[c] Average for all element concentrations as determined from accurately weighed sampled (data given to computer) as well as data developed from atomic absorption and instrumental neutron activator analysis procedures.

• Magnetic Field Dosimetry Development

A magnetic field dosimeter is being developed to measure the exposure of personnel who work in magnetic field environments. It will aid researchers in establishing the effect of long-term magnetic field exposure on humans. The battery-powered device uses Hall-effect sensors and a microprocessor controller. The total dose above four threshold levels, as well as maximum field strength, is recorded for subsequent read-out analysis.

Magnetic Field Dosimeter Development

D. K. Lemon, J. R. Skorpik, and D. L. Lessor

A magnetic field dosimeter is being developed for use in monitoring the exposure of personnel who work in the magnetic fields of fusion test facilities. The data obtained by such dosimeters would be useful in establishing if there are any biological hazards related to magnetic field exposure. Two approaches were taken in the dosimeter design: 1) a Hall-effect device that would be recharged each day, and 2) passive, long-term dosimeters for several weeks' use. No feasible long-term dosimeter concepts were identified so research in that area was terminated. All effort has been placed on developing a working model of a Hall-effect dosimeter. A breadboard model of a microprocessor-controlled device is nearly complete. It is undergoing initial tests and refinements.

Hall Effect Dosimeter

The Hall-effect dosimeter is designed to measure accumulated dose and peak field exposure. Sensing of the three components (x, y, and z) of the magnetic field is performed by inexpensive, miniature, linear Hall-effect sensors. As a Hall device is brought into the presence of a magnetic field, a voltage change across the device is developed that is proportional to the magnetic field. The prototype dosimeter utilizes three Hall-effect sensors, respectively, for the three magnetic field components. Each Hall device is monitored on a time basis by separately switching from one output to another. Each Hall device is sampled several times per second with each sample being digitized and temporarily stored in the internal memory of a single-chip microprocessor for real-time data computations.

The microprocessor, aside from being the system controller, performs key computations on the collected data. Real-time computations provide for data reduction and, in turn, minimize data storage. For each sample interval, the total field will be calculated by performing the sum-of-the-squares calculation. This total instantaneous field will be stored into one of four possible ranges according to programmable present threshold levels. Each range category will have associated with it a running summation in addition to the number of entries entered. Each computed total instantaneous field will be compared to the previous computed value and the larger value retained giving a continuously updated peak value. The microprocessor retains these computed and categorized values in its own internal memory for readout to a console package for additional analysis and data listing. The prototype package is presently being evaluated in the presence of magnetic fields. Present sensitivity of the prototype is approximately 1-2 gauss. Items yet to be completed for the prototypes are a low battery monitor, a low battery alarm, and readout console.

Long-Term Dosimeter Concepts

A number of alternate concepts to the Hall probe device were considered. Three which merit mention are outlined below.

Faraday Rotation Dosimeter. The concept has a light path from a source through a polarizer, a magneto-optically active medium, an analyzer oriented with light polarization pass direction perpendicular to

that of the polarizer, and a light detector. Achieving adequate discrimination of polarizer and analyzer might make the Faraday rotation dosimeter more expensive and troublesome.

Ferromagnetic Suspension Drift Dosimeter. This concept features a liquid with suspended ferromagnetic particles saturating a porous medium like a sponge surrounding a larger magnetizable object like a ball bearing or piece of steel shot. Calculations showed that the magnetic field-induced drift velocities were too slow to make a useful device.

Ferromagnetic Liquid Agglomerative Device. The change in agglomeration rate of ferromagnetic particles in the presence of a magnetic field was considered. This was not judged to be a practical means of measuring dose since many other factors (temperature, etc.) also could affect the agglomeration.

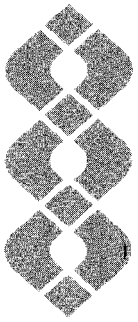

Geothermal

• Heavy-Metal and Noxious-Gas Emission from Geothermal Resource Development

Although geothermal energy is generally considered a relatively clean source of power, the high-temperature processes that create the hydrothermal provinces mobilize some undesirable constituents. In this section, we report on current efforts underway to characterize and compare effluents from a number of different geothermal sites and to determine deposition of constituents from these sites.

Accumulation of Trace Elements in Soils in the Vicinity of Geothermal Power Plants at The Geysers

D. E. Robertson and C. L. Wilkerson

Geothermal steam used for power generation at The Geysers geothermal power plants contains relatively high concentrations of a number of toxic trace elements, including boron, mercury, and arsenic. These contaminants can be released to the environment via several routes, including condensate spills, cooling-tower water spills, cooling-tower drift, and gaseous emissions. Boron emissions in cooling-tower drift have been responsible for damage to some vegetation growing in the immediate vicinity of the power plants. However, little is known concerning the areal and depth distribution of geothermal contaminants that have accumulated in soils around the generating units.

In August 1979, soil sampling was conducted at The Geysers to determine the extent of soil contamination around the generating units. Soil cores to a depth of 3 in. were collected in 8 compass directions at Units 3, 4, and 11 at distances of 10, 100, 200, and 400 yd from each unit. In addition, four cores were collected at Unit 12 and four "background" cores were collected between Unit 15 and Healdsburg. The soils were sieved through standard 32-mesh screens and were analyzed for the following constituents:

Constituent	Method
Total mercury	Volatilize onto gold trap; flameless AA
Leachable mercury	Leach with 0.1N HNO_3 -HCl; flameless AA
Leachable boron	Leach with 0.1N HNO_3 -HCl; plasma emission spectrometry
Total arsenic, iron, sulfur, others	Direct X-ray fluorescence

Figures 1 and 2 present the concentrations of leachable boron in surface (top 1 in.) soils around Unit 11 and Units 3 and 4. It is obvious that soils within a 200-yd radius have been contaminated with boron and mercury. Leachable boron concentrations within 10 to 20 yd of the Unit 11 perimeter fence to the north, south, and west ranged from 116 to 200 ppm. These concentrations are about 27 times higher than the average ambient boron concentrations (4.4 ppm) in soils sampled between 200 and 400 yd from Unit 11. The accumulation of leachable boron in soils within a 200-yd radius of Unit 11 is probably due to fallout of cooling-tower drift. Cooling-tower water at Unit 11 contains boron concentrations ranging from 55 to 150 ppm. The four "background" soil samples collected between Unit 15 and Healdsburg contained leachable boron concentrations ranging from 0.16 to 0.71 ppm and averaged 0.46 ppm. It is apparent that the soils within the Known Geothermal Resource Area (KGRA) at The Geysers naturally contain elevated boron concentrations about an order of magnitude higher than in nongeothermal areas.

A similar boron deposition pattern was observed in soils collected around Units 3 and 4 (Figure 2). However, the intense boron accumulation occurred mainly west of the units, with 127 ppm observed near the west perimeter fence line. Boron accumulation amounting to 2 to 3 times higher than ambient concentrations in soils around Units 3 and 4 also extended at least 400 yd to the east and northeast of the units. Undoubtedly, these soils also receive cooling-tower drift from Units 5 and 6, which is only about 600 to 700 yd east of Units 3 and 4.

Studies are currently underway to determine the depth distribution of leachable boron in soils at The Geysers KGRA and the chemical forms that are present.

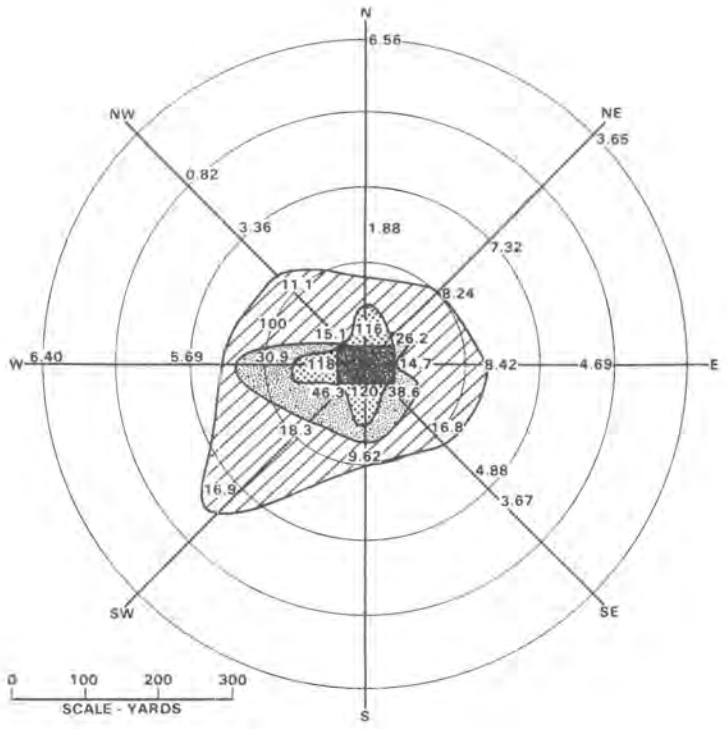

FIGURE 1. Unit 11 - The Geysers Leachable Boron (ppm) in Top Inch of Soil

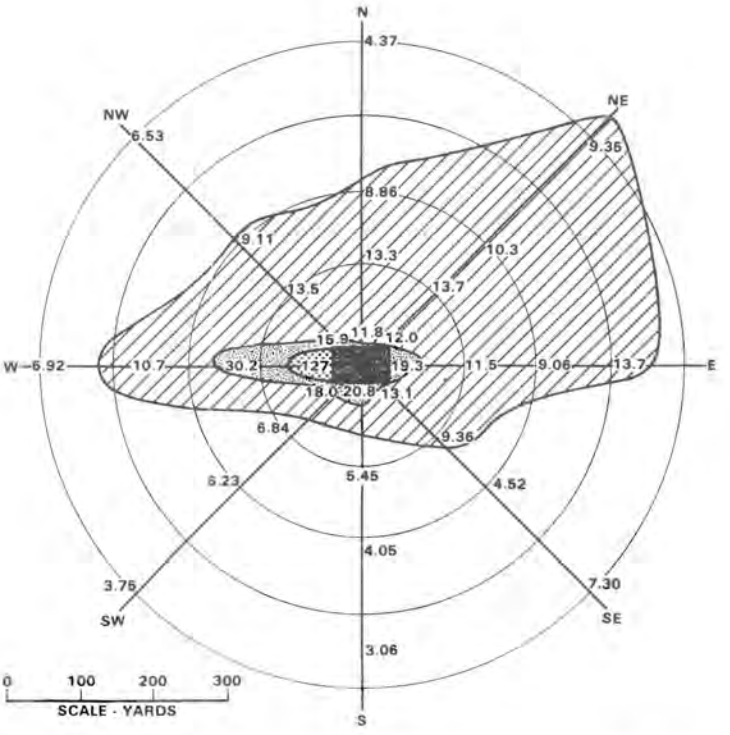

FIGURE 2. Units 3 and 4 - The Geysers Leachable Boron (ppm) in Top Inch of Soil

Figures 3 and 4 present the distribution of "total" mercury in surface (top 1 in.) soils surrounding Unit 11 and Units 3 and 4. At Unit 11, a mercury deposition pattern similar to that observed for leachable boron was observed in the soils. Mercury accumulation obviously elevated over ambient concentrations extended over a radius of about 200 yd from the unit. The highest contamination was observed to the west, where soils within 10 to 20 yd of the perimeter fence contained 2890 ppb of mercury. The mercury concentrations in the obviously contaminated soils at Unit 11 decreased systematically with depth, indicating the accumulation probably resulted from fallout of cooling-tower drift. Unfiltered cooling-tower water at Unit 11 contains 10 to 60 µg/ℓ of mercury, which is about 10^3 to 10^4 times higher than uncontaminated natural surface waters. At Units 3 and 4, no systematic mercury accumulations attributable to power plant emissions could be detected. Units 3 and 4 are located in the Sulfur Bank area of The Geysers KGRA, an area characterized by natural fumaroles and geothermal activity. The soils in this immediate area are all high in mercury, apparently due to naturally-occurring mercury mineralization resulting from the near-surface natural geothermal activity. No significant variations in mercury concentrations as a function of soil depth were observed at Units 3 and 4, indicating that fallout deposition could not be identified above the high ambient concentrations naturally present in the soils. The mercury in the "background" soils decreased systematically from 1290 ppb at Mercuryville (0.7 miles from Unit 15) to 60 ppb near Healdsburg.

The mercury in contaminated soils at The Geysers appears to be highly insoluble and unavailable for biological assimilation. The "leachable" (0.1N HNO_3-HCl) mercury fractions averaged only about 0.1% of the total mercury. The mercury is probably present in the soils as the sulfide or in combination with sulfur compounds. Studies are presently under way to identify the actual chemical forms that are present in the soils.

The arsenic, iron, sulfur, and other elements present in the soils are presently being measured by X-ray fluorescence spectroscopy.

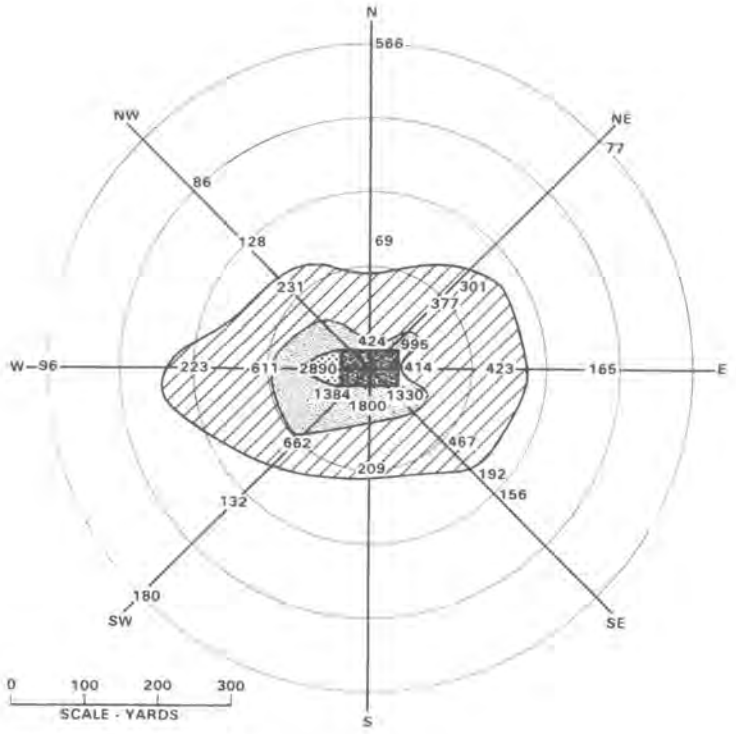

FIGURE 3. Unit 11 - The Geysers Total Mercury (ppb) in Top Inch of Soil

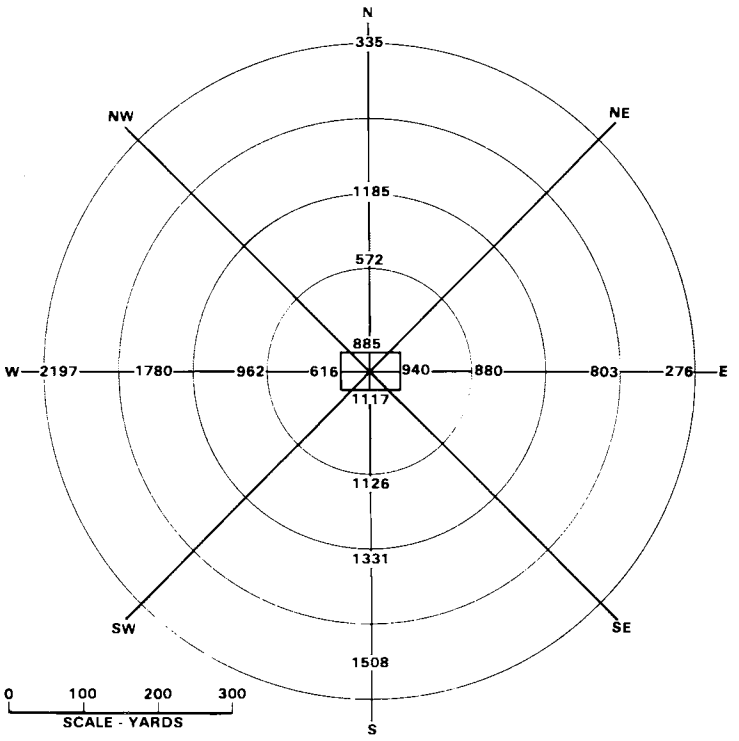

FIGURE 4. Units 3 and 4 - The Geysers Total Mercury (ppb) in Top Inch of Soil

Quantifying Gaseous Emissions from Geothermal Power Plant Cooling Towers

D. E. Robertson, J. D. Ludwick,
C. L. Wilkerson, and J. C. Evans

The greatest uncertainties in conducting mass balances of steam constituents through geothermal power plants lie in the quantification of gaseous and drift emissions from the cooling towers. Each of the stacks on the cooling towers behave differently with respect to air flow, water flow, and temperature distributions. In addition, the cross-sectional distribution of gases, drift particles, updraft air velocity, and temperature within individual stacks is very nonuniform. It is therefore difficult to accurately measure the emission rates of materials from the cooling towers.

To make reliable estimates of emission rates of gaseous constituents, it is necessary to make detailed measurements of the updraft air velocity and temperature and cross-sectional distributions of the gases of interest in a number of individual stacks (preferably all) on each cooling tower. To illustrate the nonuniform distribution of these constituents in cooling-tower stacks, Figures 5 and 6 show the variations observed in temperature, updraft air velocity, and H_2S concentrations as a function of position inside two separate stacks on The Geysers Unit 11 cooling tower. These parameters were measured on a real-time basis by inserting instrumentation and sampling lines into various positions inside the stacks. Temperature was measured by a digital-readout, calibrated thermistor; the updraft air velocity was determined by positioning a direct-reading Gill anemometer inside the stack; and H_2S was measured by pumping air through Teflon® tubing into an Interscan® H_2S analyzer capable of making real-time analyses. These stacks have a 6-in.-diameter viewing port and six 1-in.-diameter holes equally spaced around the stacks for inserting sampling and measurement probes.

Temperatures can vary up to 11°C, and in the winter this variation could even be

---

® Teflon - Registered trademark of E. I. duPont deNemours and Co.
® Interscan - Registered trademark of Interscan Corporation.

greater. Thus, volume corrections as a function of temperature for the air must be made. The updraft air velocity typically shows low values near the outside edge of the stacks and reaches maximum flow (13 to 15 m/sec) between 0.5 and 2.5 m from the outside edge. The air velocity actually becomes negative at the center of the stacks with downdrafts (or recirculating eddies) as much as -2 m/sec. The H_2S distribution within a stack is governed by water flow rates around the stack, the points of entry of noncondensable gases into the stack, and the dynamics of air flow through the stack. As shown in Figures 5 and 6, the H_2S concentrations within individual stacks can vary by over twenty fold.

To make reliable calculations of the emissions of gases from the cooling towers, the variable parameters can be integrated by dividing the stacks into segmented cross sections and then summing the sections. As shown in Figures 5 and 6, the cross section of each stack has been divided into six wedges and four concentric zones. The average H_2S emission rate in each area can be calculated and summed to give an estimate of each stack's total emission rate. The H_2S emissions from Stacks 11-8 and 11-2 were estimated to be 14.3 and 27.9 kg/day, respectively. Only by making these detailed measurements can cooling-tower stack emissions be accurately estimated. This detailed characterization also permits more accurate grab sampling for other constituents, such as mercury vapor and ammonia, that are not possible to measure on a real-time basis.

Characterization of Gases and Trace Elements at The Geysers Geothermal Power Plants

D. E. Robertson, J. D. Ludwick,
J. C. Evans, and C. L. Wilkerson

In June 1979, field studies were conducted at The Geysers geothermal power plants to characterize the gases and trace elements entering and leaving the generating units. Of particular interest were the two new units, Unit 15 and Unit 12, which both came on line in the spring of 1979. Unit 15 is unique among the power plants at The

UNIT 11
STACK 11-2
@ OBSERVATION PORT

TEMP (°C)	FLOW m/sec	H_2S (ppm)	DISTANCE FROM EDGE (m)
35.6	5.5	0.4	0.15
33.9	11	0.25	0.30
32.3	14.5	0.1	0.61
31.3	14	0.1	0.91
31.7	14.5	0.1	1.2
32.2	13.5	0.1	1.5
31.7	14	0.1	1.8
32.3	15	0.25	2.1
33.3	12	0.5	2.4
32.78	3	1.2	2.7
28.3	1.5	1.55	3.0
28.9	2	1.8	3.4
29.4	-1	1.9	3.7
29.4	-1	1.8	4.0
30.0	0 → -2	1.8	4.3

ESTIMATED INTEGRATED H_2S STACK EMISSION RATE
27.9 kg/day

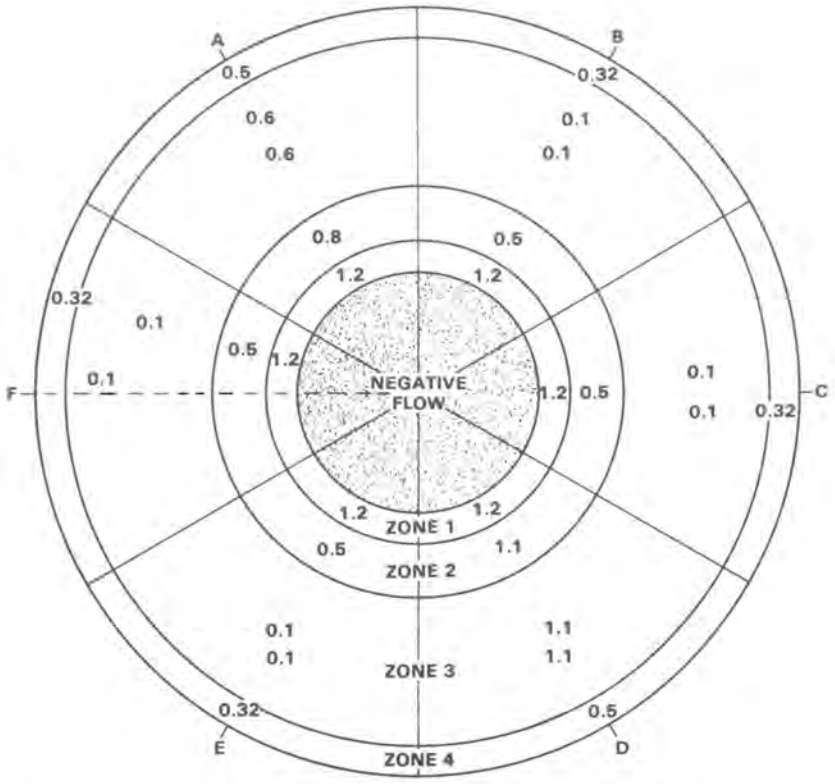

FIGURE 5. Hydrogen Sulfide Cross-Sectional Distribution (ppm) Inside Cooling-Tower Stack 11-2 at Unit 11, The Geysers, June 1979

UNIT 11
STACK 11-8
F PORT PROFILE

TEMP (°C)	FLOW (m/sec)	H_2S (ppm)	DISTANCE FROM EDGE (m)
36.7	6.5	0.45	0.15
35.0	13.5	0.2	0.30
31.1	15	0.1	0.61
27.8	14.5	0.08	0.91
32.8	14.5	0.1	1.2
31.1	14.5	0.1	1.5
33.9	14.0	0.1	1.8
24.4	15.0	0.1	2.1
24.4	13.5	0.15	2.4
23.9	5	0.3	2.7
25.6	-1	1.0	3.0
26.1	-1.5	1.4	3.4
26.1	-1.5	1.0	3.7
25.6	-1.5	2.7	4.0
26.7	-0.5	2.3	4.3

ESTIMATED INTEGRATED H_2S
STACK EMISSION RATE
14.3 kg/day

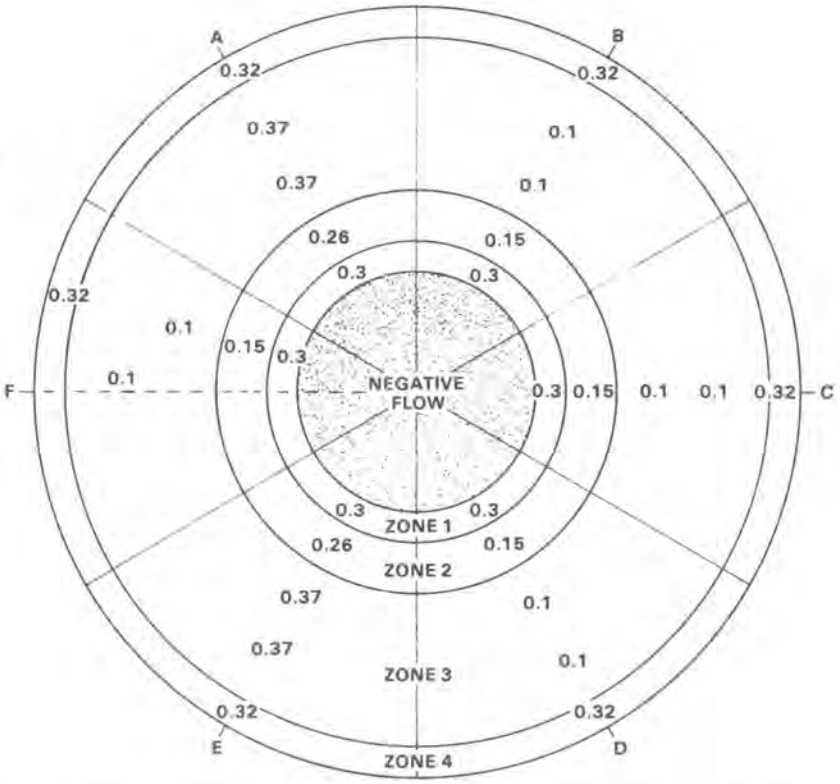

FIGURE 6. Hydrogen Sulfide Cross-Sectional Distribution (ppm) Inside Cooling-Tower Stack 11-8 at Unit 11, The Geysers, June 1979

Geysers because of its H_2S abatement system, which uses a surface condenser and Stretford plant for removing the H_2S and converting it into usable sulfur. Unit 15 is also located in an area of past mercury mining and therefore has the potential for higher than normal mercury vapor in its steam.

The flow diagram and selected sampling points at Unit 15 for the indicated constituents are shown in Figure 7. The noncondensable gas, containing most of the H_2S, is piped from the surface condenser to the Stretford plant for conversion of H_2S to sulfur. The Stretford process uses a vanadium-catalyzed oxidation reaction for this conversion. The exhaust gases from the Stretford plant are then piped to the cooling tower. At the time of this field study, it was not possible to conduct sampling on the cooling tower, so the tower work has been rescheduled for January 1980.

Unit 12 is fairly typical of the newer generating units at The Geysers, but the gas content of the steam is 5 to 10 times lower than other units and therefore does not require H_2S abatement.

Unit 11 has been operational since 1974 and was the first unit to use the iron-catalyzed H_2S abatement technology. Since soil sampling was to be conducted around this unit, we wanted to have additional information regarding its chemical emissions.

Table 1 presents the H_2S concentrations in noncondensable gases at Units 15, 12, and 11, and Table 2 gives the total composition of the noncondensable gases at Unit 15. At Unit 15, a twofold difference in H_2S concentrations in the noncondensable gas was observed when using a PNL glass condenser compared to the Unit 15 surface condenser, which gave concentrations of 4.97% and 2.49%, respectively. This could be due to differences in condenser designs, or to the fact that the samplings were made one day apart. The gases leaving the Stretford plant contained only 10.5 ppm H_2S. This represents a removal of 99.96% of the H_2S in the noncondensable gases by the Stretford process, which is obviously working very successfully.

Noncondensable gases from Unit 12 steam contained 2.35% H_2S, but the total amounts

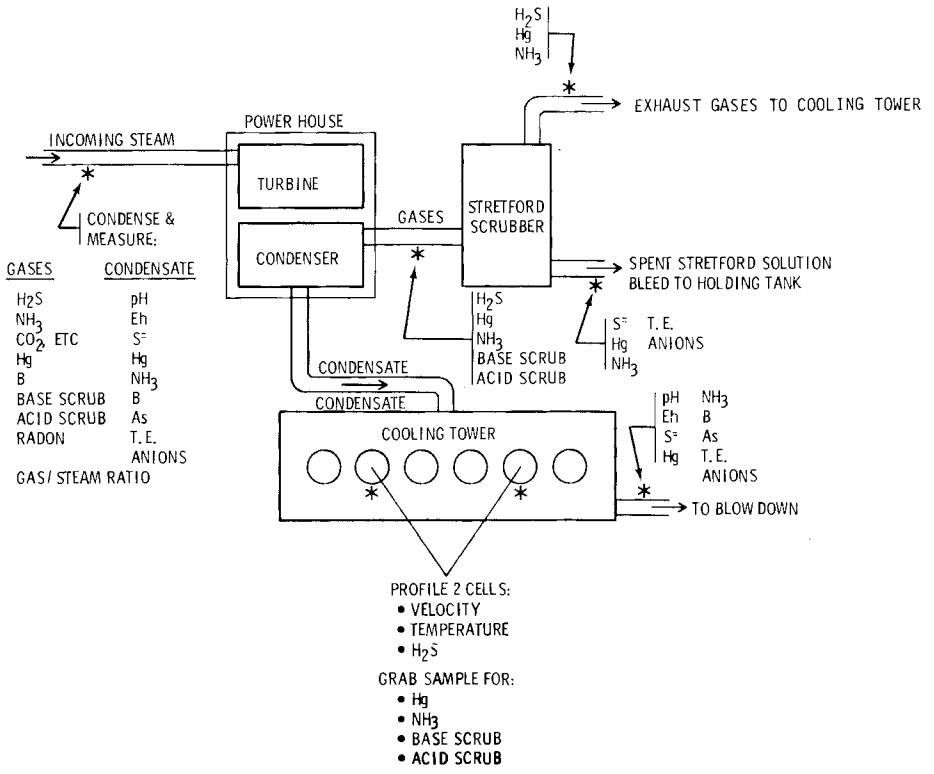

FIGURE 7. Sampling Scheme at Unit 15 at The Geysers

entering Unit 12 are 5 to 10 times lower than other units because of the relatively small amount of noncondensable gas in the steam (0.42 ℓ/kg for Unit 12, compared to 2.58 ℓ/kg and 5.00 ℓ/kg for Units 15 and 11, respectively).

The mercury concentrations in liquid samples are shown in Table 3. Mercury concentrations in steam condensates at Unit 15 are the highest ever observed in our studies. The Stretford scrubber solution contained 2 ppm mercury. This high concentration is the result of either efficient removal of mercury from the noncondensable gases by the Stretford scrubber solution or high mercury impurities in the chemicals used in preparing this solution. Mercury concentrations in Unit 12 liquids were relatively low. At Unit 11, moderately high mercury concentrations were observed in the steam condensate and very high amounts were present in unfiltered cooling-tower water. This cooling-tower water contains suspensions of hydrous iron oxide and sulfur compounds, which are good scavengers of mercury. Table 4 presents mercury concentrations observed in gases at The Geysers generating units. Again, Unit 15 noncondensable gas contained the highest mercury concentrations, which averaged about 2 μg/ℓ, or about 2 million times higher than the ambient air in the region. Unit 11 contained intermediate levels of mercury in the gases, whereas at Unit 12 relatively low concentrations were observed. The chemical forms of mercury present in the noncondensate gases are partitioned between 78% as elemental Hg^0 vapor and 22% Hg^{++} forms.

Table 5 presents measured values for pH, Eh, dissolved $S^=$ ion, F^- ion, As, B, and NH_3. These constituents, in addition to H_2S and mercury, are considered to be the most potentially serious contaminants in geothermal steam. The concentrations of these constituents in the new Units 12 and 15 are fairly typical of those observed in the older generating units. An obvious exception is the high concentrations of As and F^-

TABLE 1. Hydrogen Sulfide Concentrations in Noncondensable Gases at The Geysers—June 1979

Sample	Sampling Date and Time	H_2S Concentration, ppm_v
	Unit 15	
Noncondensable gas—incoming steam(a)	6/25/79 @ 1320	49,700
Noncondensable gas—after PG&E unit condenser(b)	6/26/79 @ 1400	24,900
Noncondensable gas—exit gas from Stretford process(c)	6/26/79 @ 1500	10.5
	Unit 12	
Noncondensable gas—incoming steam(d)	6/27/79 @ 1200	23,500
	Unit 11	
Noncondensable gas—incoming steam(e)	6/28/79 @ 1000	34,000

(a) Sampled from main steam header to Unit 15 with the PNL glass condenser
(b) Sampled from gas line going to the Stretford plant
(c) Sampled at the #1 manifold to the Unit 15 cooling tower—an unknown interference gave high readings on two Interscan H_2S analyzers and this concentration was measured with a Delmar colorimetric analyzer
(d) Sampled from main steam header with the PG&E stainless steel sampling condenser
(e) Sampled from main steam header to Unit 11 with the PNL glass condenser

Note: Unit 15 tripped off-line on 6/26/79 @ 0930 for 90 min—back on-line @ 1100.

present in steam condensate at Unit 12. The pH of this condensate (5.5) is one of the lowest yet observed in our work, and Unit 12 appears to have some unique chemistry associated with its steam.

Cooling-tower waters contain higher concentrations of the nonvolatile constituents B, As, and F^- relative to steam condensates, whereas the volatile constituents $S^=$, Hg, and NH_3 are lower in the cooling-tower water. This is due to much of the $S^=$, Hg, and NH_3 escaping to the atmosphere in the cooling tower; whereas the B, As, and F^- are concentrated in the cooling-tower water, since about 80% to 90% of the steam condensate is lost as water vapor in the cooling towers.

Chemical Characterization of Gases and Trace Elements in Natural Hot Springs and Fumaroles in the Mono-Long Valley, California KGRA

D. E. Robertson, J. D. Ludwick, J. C. Evans, and C. L. Wilkerson

The Mono-Long Valley Known Geothermal Resource Area (KGRA), located on the eastern slope of the Sierra-Nevada mountains in central California, is characterized by many surface manifestations of geothermal activity, including hot springs, fumaroles and relatively recent volcanic edifices. This area is being considered for development of its geothermal resources and much interest has been manifested in the natural emissions

TABLE 2. Gas Chromatographic and Mass Spectrometric Analysis of Noncondensable Gas Separated from Incoming Steam at Unit 15, June 1979

Constituent	Concentration (in mole % or ppm)
Hydrogen	25.301
Water	0.403
Nitrogen	0.187
Oxygen	0.000
Argon	0.011
Carbon dioxide	61.216
Carbon monoxide	0.000
Benzene	0.004
Toluene	0.001
Acetone	0.000
Hydrogen sulfide	4.238
Isopropanol	0.000
Sulfur dioxide	0.000
Methane (ppm)	86227
Ethane (ppm)	117
Propane (ppm)	28
Isobutane (ppm)	1
n-butane (ppm)	6
Isopentane (ppm)	1
n-pentane (ppm)	1
Hexane (ppm)	4
Heptane (ppm)	2
Octane (ppm)	ND<1

of geothermal gases and waters, both from an environmental and an exploratory standpoint. In June 1978, a field study was conducted at Mono-Long Valley to chemically characterize the gases and waters associated with a number of hot springs and fumaroles. Figure 8 shows the sampling location in the Mono-Long Valley area. Sampling for gases and waters was conducted at the Casa Diablo Hot Springs and fumarole area, at Hot Creek Gorge, at Travertine Hot Springs, at Fales Hot Springs, and at Paoha Island in Mono Lake.

Table 6 presents the gas composition of noncondensable gases associated with the hot springs as determined by gas chromatographic/mass spectrometric measurements, and Table 7 gives the concentrations of hydrogen sulfide and radon gas. Carbon dioxide is the major gas constituent, except at the Paoha Island hot spring, which contained 71 mole % methane and lesser amounts of heavier hydrocarbons. Hydrogen sulfide concentrations were highly variable, with the highest levels (0.566%) in the gases separated from the steam emitted at the Casa Diablo fumaroles. No H_2S could be detected in Fales Hot Springs gases, but 0.6 ppm of SO_2 was present. Radon gas concentrations were likewise highly variable, with the highest level (32,665 pCi/ℓ) associated with gases at the Paoha Island hot spring. This is the highest radon concentration we have ever observed in any kind of geothermal gases.

Mercury concentrations in gases are presented in Table 8 and show highly elevated levels compared to the ambient air in the region. Gases from Hot Creek Gorge contained the highest mercury concentrations (79,000 ng/m^3), followed by those from the Paoha Island hot spring (15,700 ng/m^3). Mercury concentrations in the water samples are also given in Table 8. The highest mercury concentrations were observed in the Paoha Island hot spring water (4085 ng/ℓ avg.) and in steam condensate from a large fumarole at Casa Diablo (3945 ng/ℓ avg.). These concentrations are about 1000 times higher than mercury levels in uncontaminated surface waters. The mercury concentrations in gases from the Hot Creek Gorge hot springs were relatively low, even though the gases from these springs contained the highest mercury levels. It is apparent that the high temperatures and vigorous boiling of the Hot Creek Springs volatilize most of the mercury from solution.

Other trace constituents measured in the hot spring waters are presented in Table 9. The steam condensate from the Casa Diablo fumarole, apart from traces of $S^=$ and NH_3, is extremely pure water. The Paoha Island hot spring water is very reducing and contains relatively high concentrations of $S^=$, NH_3, F^-, As, B, and alkali metals. Its high silicon content indicates that this water comes from the hottest reservoir of any of the hot springs studied (assuming no significant mixing with nonreservoir water occurs).

These data are presently being compiled and analyzed for preparation of a journal publication.

TABLE 3. Mercury Concentrations at The Geysers — June 1979

Sample	Sampling Date and Time	Hg Concentration, ng/ℓ
	Unit 15	
Incoming steam condensate	6/25/79 @ 1230	18,000; 18,500[a]
	6/25/79 @ 1650	11,700; 13,000[a]
	6/26/79 @ 1350	13,000; 14,000[b]
Steam condensate after turbine	6/26/79 @ 1350	3,500; 4,250
	6/27/79 @ 1700	2,750; 2,000
Cooling-tower water - inlet (unfiltered)	6/26/79 @ 1600	13,200; 12,400
Cooling-tower water - blowdown (unfiltered)	6/25/79	4,100; 4,100
Stretford scrubber solution (unfiltered)	6/26/79 @ 1350	2,000,000; 1,800,000
	Unit 12	
Incoming steam condensate	6/27/79 @ 1230	3,000; 3,100[b]
Cooling-tower water - inlet (unfiltered)	6/27/79 @ 1300	1,000; 1,100
Cooling-tower water - blowdown (unfiltered)	6/27/79 @ 1300	600; 600
Cooling-tower water - blowdown (filtered)	6/27/79 @ 1300	20; 25
	Unit 11	
Incoming steam condensate	6/28/79 @ 1130	9,250; 9,250[a]
Cooling-tower water - inlet (unfiltered)	6/28/79 @ 1130	55,000; 61,250
Cooling-tower water - blowdown (unfiltered)	6/28/79 @ 1130	5,750; 5,750

[a] PNL glass condenser used
[b] PG&E stainless steel incoming steam sampling condenser

Note: Unit 15 tripped off-line on 6/26/79 @ 0930 for 90 minutes - back online @ 1100.

TABLE 4. Mercury Concentrations in Noncondensable Gases at The Geysers — June 1979

Sample	Sampling Date and Time	Hg Concentration, ug/ℓ
	Unit 15	
Noncondensable gas— incoming steam[a]	6/25/79 @ 1000	1.58; 0.68; 0.50
	6/25/79 @ 1400	2.06; 2.30
	Best estimate— mean of #1, #4, #5 =	1.98 ± 0.37
Noncondensable gas— going into Stretford plant[b]	6/26/79 @ 1000	<0.01; <0.01
	6/26/79 @ 1300	<0.01; <0.01
	Best estimate =	<0.01
Noncondensable gas— exit gas from Stretford plant[c]	6/26/79 @ 1700	0.015; 0.013
	Best estimate =	0.014 ± 0.001
	Unit 12	
Noncondensable gas— incoming steam[d]	6/27/79 @ 1230	0.58; 0.50; 0.51
	Best estimate =	0.053 ± 0.003
	Unit 11	
Noncondensable gas— incoming steam[e]	6/28/79 @ 1100	0.76
	6/28/79 @ 1400	1.60; 0.92
	Best estimate =	1.09 ± 0.44
Chemical forms present:	22% Hg^{++} forms 78% elemental Hg^{o} <4% $(Me)_2$ Hg	
Cooling tower exhaust[f]		
Stack 11-8	6/28/79 @ 1750	0.00015
Stack 11-2	6/28/79 @ 1815	0.00173

[a] Sampled from main steam header to Unit 15 with the PNL glass condenser
[b] Sampled from gas line going to the Stretford plant
[c] Sampled at the #1 manifold to the Unit 15 cooling tower
[d] Sampled from main steam header with the PG&E sampling condenser
[e] Sampled from main steam header to Unit 11 with the PNL glass condenser
[f] Sampled at 4 ft in from the edge of the stack in the flat region of highest vertical air velocity

TABLE 5. Elemental Constituents in Geothermal Liquids at The Geysers Generating Units

Unit 15	Sampling Date and Time (June 1979)	pH	Eh, mV	$S^{=}$, ppm	F^{-}, ppm	As, ppm	B, ppm	NH_3, ppm
Incoming steam condensate[a]	6/25/79 @ 1230	7.2	-285	48.5	<0.03	0.079	32	115
Incoming steam condensate[a]	6/25/79 @ 1700	7.1	-180	55.3	<0.03	0.059	35	118
Steam condensate[b]	6/26/79 @ 1350	8.6	-235	49.5	<0.03	0.065	30	118
Cooling-tower water[c]	6/25/79	8.0	+140	0.13	0.06	0.530	124	37.8
Stretford solution[d]	6/26/79 @ 1350	8.3	+ 10	<2	0.10	3.20	307	5.9
Unit 12								
Steam condensate[e]	6/27/79 @ 1230	5.5	-145	73	1.1	2.80	27	41
Cooling-tower water[f]	6/27/79 @ 1300	7.0	0	7.2	0.13		88	
Cooling-tower water[c]	6/27/79 @ 1300	6.6	+180	0.17	0.11		88	122
Unit 11								
Steam condensate[a]	6/28/79 @ 1130	6.4	-200	113	<0.03	0.011	26	248
Cooling-tower water[f]	6/28/79 @ 1130	8.1	+ 90	13.9	0.16		149	108
Cooling-tower water[c]	6/28/79 @ 1130	8.2	+100	0.32	0.16		155	113

[a] Collected from PNL glass condenser
[b] Collected from Unit 15 SS surface condenser
[c] Blowdown collected at bottom of cooling tower
[d] Sampled at recirculation pump
[e] Collected from PG&E SS sampling condenser
[f] Water entering at top of cooling tower

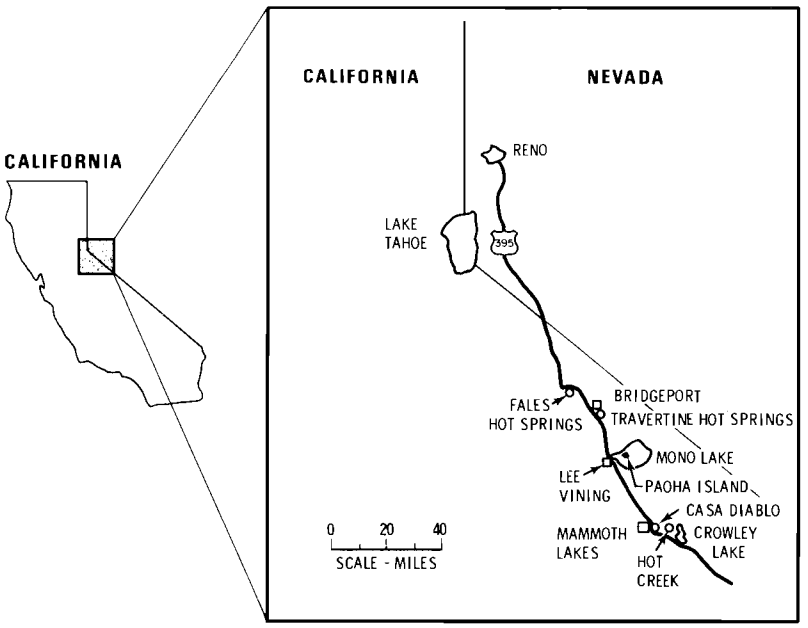

FIGURE 8. Sampling Locations in Long Valley, California

TABLE 6. Gas Chromatographic and Mass Spectrometric Analysis of Gases from Mono-Long Valley Hot Springs and Fumaroles, June 1978

Gas Constituent	Concentrations, mole % or ppm_v				
	Paoha Island Hot Spring	Hot Creek Gorge Hot Springs	Casa Diablo Fumarole	Travertine Hot Springs	Fales Hot Springs
Hydrogen	0.04	0.04	0.02	0.39	0.01
Water	0.40	0.13	0.13	0*	0.56
Nitrogen	20.69	35.00	22.90	5.1	4.40
Oxygen	0.00	8.57	5.27	0.37	0.22
Argon	0.31	0.44	0.28	0.07	0.07
Carbon dioxide	3.15	55.82	71.37	94.0	94.74
Carbon monoxide	0.00	0.00	0.00	0.00	0.00
Methane	71.00	0.00	0.02	0.02	0.00
Ethane	2.81	—	—	—	—
Propane	0.91	—	—	—	—
Iso-butane	0.12	—	—	—	—
n-butane	0.20	—	—	—	—
Iso-pentane	0.09	—	—	—	—
n-pentane	0.04	—	—	—	—
C_6hydrocarbons	0.12	—	—	—	—
C_7hydrocarbons	0.06	—	—	—	—
Benzene	0.04	0.00	0.01	0.00	0.00
Toluene	0.01	—	—	—	—
Xylene	0.01	—	—	—	—

*The water fraction was subtracted out; it appeared that some water contamination had occurred.

TABLE 7. Hydrogen Sulfide and Radon Concentrations in Gases from Mono-Long Valley Hot Springs and Fumaroles, June 1979

	Paoha Island Hot Spring	Hot Creek Gorge Hot Springs	Casa Diablo Fumarole	Travertine Hot Springs	Fales Hot Springs
H_2S, ppm_v	110-135	450	5660	0.25 (0.05 SO_2)	0.0 (0.6 SO_2)
Radon, pCi/ℓ	32,665	3980	6540	410	10,030

TABLE 8. Mercury Concentrations in Ambient Air, Noncondensable Gases and Waters from Hot Springs of Long Valley, California, June 1978

Date	Location	Sample Type	Total Hg, ng/m³
		Gases	
6/6/78	Casa Diablo Hot Springs	Ambient air	9
		Noncondensable gases from fumarole	2,700
6/7/78	Hot Creek Gorge	Ambient air	<3
		Noncondensable gases from hot spring (93°C)	79,000
6/8/78	Travertine Hot Springs	Ambient air	<3
		Noncondensable gases from hot spring (70°C)	1,600
6/8/78	Fales Hot Springs	Ambient air	<3
		Noncondensable gases from hot spring (63°C)	1,400
6/22/78	S. E. Quadrant Paoha Island, Mono Lake	Noncondensable gases from hot spring (80°C)	15,700
		Waters	
6/6/78	Casa Diablo	Steam condensate from Fumarole #1	1450; 1580
6/6/78	Casa Diablo	Steam condensate from Fumarole #2	3680; 4210
6/7/78	Hot Creek Gorge	Water from small boiling pool	491
6/7/78	Hot Creek Gorge	Water from large boiling pool	371
6/8/78	Travertine Hot Springs	Water from hot springs	57; 58
6/8/78	Fales Hot Springs	Water from hot springs	69; 77
6/21/78	Paoha Island	Water from small boiling spring	4010; 4160

TABLE 9. Trace Element Composition of Hot Spring Waters in the Mono-Long Valley Area, June 1978
(All Concentrations in mg/ℓ [ppm])

Parameter	Casa Diablo Steam Condensate	Hot Creek Gorge Small Boiling Spring	Hot Creek Gorge Large Boiling Spring	Travertine Hot Springs	Fales Hot Springs	Paoha Island Hot Spring
Temperature (°C)	94	93	93	70	63	85
pH	4.1	8.1	8.5	6.8	6.8	8.9
Eh	+315	-52	-85	+132	+150	-290
S=	9.6	0.83	0.91	0.06	<0.1	43.4
F^-	<0.02	9.4	10.4	5.6	5.6	27.1
NH_3	1.7	0.29	0.47	0.25	0.23	37
B	0.02	10.1	9.90	9.00	6.97	132
As	<0.002	0.92	1.0	1.1	1.3	6.2
Na	<1	342	339	1037	497	7980
Si	<0.1	63.5	62.4	37.5	43.8	90.0
K	<5	22.9	23.5	53.0	35.5	214
Mg	<0.05	0.10	0.08	13.1	9.0	0.055
Ca	<0.2	1.8	1.2	17.2	23.9	0.32
Sr	<0.01	0.17	0.17	3.8	1.15	0.05
Ba	<0.01	0.04	0.1	0.03	<0.1	0.02
Li	<0.05	3.0	2.6	3.0	0.3	2.9
P	<0.1	<0.1	0.1	0.1	<0.1	3.2
Ag	<0.01	<0.01	<0.01	<0.01	<0.01	<0.01
Cd	<0.01	<0.01	<0.01	<0.01	<0.01	<0.01
Co	<0.02	0.01	0.01	0.02	<0.01	<0.01
Cr	<0.05	<0.05	<0.05	<0.05	<0.05	<0.05
Cu	<0.01	<0.01	<0.01	<0.01	<0.01	<0.01
Fe	<0.1	0.40	<0.1	0.50	0.1	<0.1
Mn	<0.01	<0.01	0.01	0.01	0.03	<0.01
Mo	<0.5	<0.5	<0.5	<0.5	0.5	<0.5
Ni	<0.01	<0.01	<0.01	<0.01	<0.01	<0.01
Pb	<0.1	<0.1	<0.1	<0.1	<0.1	<0.1
Sb	<0.05	<0.1	<0.1	<0.05	<0.05	<0.05
Se	<0.1	<0.1	<0.1	<0.1	<0.1	<0.1
Sn	<0.1	<0.1	<0.1	<0.1	<0.1	<0.1
Th	<0.1	<0.1	<0.1	<0.1	<0.1	<0.1
Ti	<0.05	<0.05	<0.05	<0.05	<0.05	<0.05
Tl	<0.1	<0.1	<0.1	<0.1	<0.1	<0.1
U	<0.05	<0.05	<0.05	<0.05	<0.05	<0.05
Zn	<0.05	<0.05	<0.05	<0.05	<0.05	<0.05
Zr	<0.05	<0.05	<0.05	<0.05	<0.05	<0.05

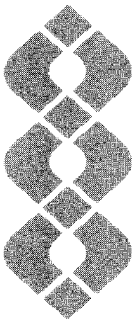

Oil Shale

• Oil Shale and Tar Sand Research

Oil shale and tar sand in the United States represent a potential supply of nearly one trillion barrels of crude oil for the country's future use. The renewed commercial interest in developing these reserves has increased the need for studies that would help developers assure that conversion processes are carried out in an environmentally acceptable manner. A vital part of this environmental research program is the physical and chemical characterization of the effluents from the various proposed conversion schemes. Characterization studies are important and should begin at an early stage of development, preferably at the pilot plant or semiworks stage. Because of the complex nature of the effluents, new sampling, analysis, and chemical separation procedures have had to be developed. In this section, new and improved techniques for organic, inorganic, and speciation analysis are presented with applications for oil shale research. Also reported is the progress of a program to provide representative and well-characterized fossil-fuel samples for environmental and health effects studies and for interlaboratory comparisons to ensure accuracy of the data.

Analysis of Shale Oil from an In-Situ Process

C. L. Wilkerson, R. W. Sanders, and J. S. Fruchter

The elemental abundance of sulfur and eight trace metals (arsenic, cobalt, iron, molybdenum, nickel, selenium, vanadium, and zinc) was measured in shale oils produced by in-situ and aboveground retorting. The abundances of these elements were then compared to abundances for the average of 88 North American crude oils. The data on the North American crudes are those of Hitchon, Filby and Shah (1975). All of the PNL elemental analyses were obtained by a combination of instrumental neutron activation analysis and X-ray fluorescence analysis. The data are compared in Table 1. The concentrations of sulfur in both of the shale oils are essentially the same as the average value determined for the 88 natural crude oils, namely 0.8%. Relative to the average value reported for petroleum, both of the shale oils are about two orders of magnitude more abundant in arsenic. Compared to the aboveground shale oil, the in-situ shale oil is somewhat lower in arsenic and selenium, but is somewhat higher in transition metals. Both shale oils are almost two orders of magnitude lower than the natural crudes in nickel and vanadium. The high level of arsenic and selenium in shale oil may be of concern and may require control technology for removal in an actual process since they are undesirable environmental contaminants and may act as catalyst poisons in subsequent refining.

TABLE 1. Comparison of Two Shale Oils with 88 North American Crude Oils - Preliminary Data (ppm Except as Noted)

			88 North American Crudes	
	Oxy-Rm6	Aboveground Retort	Ave.	Max.
As	16	27	0.1	1.9
Co	3.6	1.5	.053	2.0
Fe	80	60	10.8	254
Mo	2.0	<0.3	—	—
Ni	8.7	2.7	9.4	74
S (%)	0.75	0.75	0.8	3.8
Se	0.54	0.96	.05	0.4
V	0.41	0.24	13.6	177
Zn	3.0	0.43	0.4	5.9

Note: Oxy crude lower in As and Se, higher in transition metals than shale oil from an aboveground retort.

Analysis of Retort and Associated Water Samples from an In-Situ Oil Shale Retort

J. S. Fruchter, R. W. Sanders, and C. L. Wilkerson

Samples of retort water, boiler blowdown, and groundwater were obtained from Occidental's Retort 6. These waters were analyzed for a number of elements of environmental interest, including arsenic, boron, bromine, calcium, chlorine, fluorine, lithium, molybdenum, sodium, and total sulfur. The analyses for the retort water are shown in Table 2 and are compared to retort waters from other in-situ and aboveground retorts. The numbers in parentheses in the table indicate the amount of each element in milligrams emitted per barrel of shale oil produced. These numbers show that although in-situ product waters have lower concentrations in some cases than aboveground retort product waters, total release rates are higher for in-situ processes because of the much larger amounts of water produced per barrel of oil.

Table 3 shows the analysis of two bedrock groundwater wells taken near Occidental's in-situ retorts at Logan Wash, Colorado. Well LW-108 is approximately 500 m from Retort 6. Well LW-106 is located approximately 1500 m from the retort. It can be seen that the closer well was considerably enriched in a number of constituents over the water from the further well. Interestingly, many of the elements in Well LW-108 are not found in the same ratios as they are present in the retort water. Thus, factors other than contamination by retort waters may be responsible for the enrichment of elements in this water well.

TABLE 3. Analyses of Oxy Groundwater Wells - Preliminary Data (ppm)

	LW 106 (Bedrock)	LW 108[a] (Bedrock)
B	0.062	9.8
Br	0.02	0.35
Ca	42	38
Cl	6.5	44
F	0.35	5.2
Fe	0.71	0.28
Li	0.03	0.45
Mg	52	52
Na	136	500
S	50	150

[a]Considerably higher values of several elements detected in LW-108 than in LW-106

Shale Oil Paraffins

D. S. Sklarew, S. P. Downey, M. D. Walker, and J. S. Fruchter

The n-alkane distribution in four shale oils and two petroleums has been determined. A silica gel column with hexane as the eluant was used to separate aliphatic hydrocarbons from more polar materials. The

TABLE 2. Comparison of Three Retort Waters - Preliminary Data (ppm)

	Oxy-Rm6[a]	Other In Situ[a]	Aboveground[a]	Oxy Boiler Blowdown
As	1.3 (206)	2.5 (397)	4.9 (49)	2.8
B	13 (2100)	150 (24,000)	12 (119)	
Ca	<2	4 (630)	33 (330)	
F	35 (5600)	26 (4100)	10 (100)	
Li	1.8 (286)	0.4 (64)	0.1 (1.01)	
Mo	0.25 (40)	2.5 (400)	0.07 (0.7)	7.3
Na	2800 (446,000)	——	93 (930)	14,500
S	2700 (1.1 x 10^6)	3100 (490,000)	17,000 (170,000)	

[a]Values in parentheses are calculated in mg/barrel of oil produced

Note: Although in-situ product waters have lower concentrations of many elements than aboveground product waters, total emission rates for many elements are higher for in-situ processes.

hydrocarbons were then analyzed by glass capillary gas chromatography. N-alkanes predominate in the chromatograms of these samples; however, in one petroleum (Gato Ridge), n-alkanes were overwhelmed by other constituents, presumably cyclic or branched alkanes. N-alkenes are minor or absent in the samples studied with the exception of Paraho and, to a lesser extent, Livermore. The n-alkane distributions from Paraho, Occidental, Vernal, Utah and Livermore shale oils, Occidental sludge oil, Occidental light oil, and Prudhoe Bay and Wilmington crude oils are shown in Figure 1. Most of the samples also have decreasing amounts of n-alkanes up to at least C_{36}. It can readily be seen that Paraho, Vernal, Utah, Occidental product, and Occidental sludge are similar with respect to n-aklanes. The Livermore product is also similar to the other shale oils except for the large peak at nC_{14}. The petroleums differ from the shale oils and from each other; the odd carbon predominance seen in the shale oils is less pronounced in the petroleums studied.

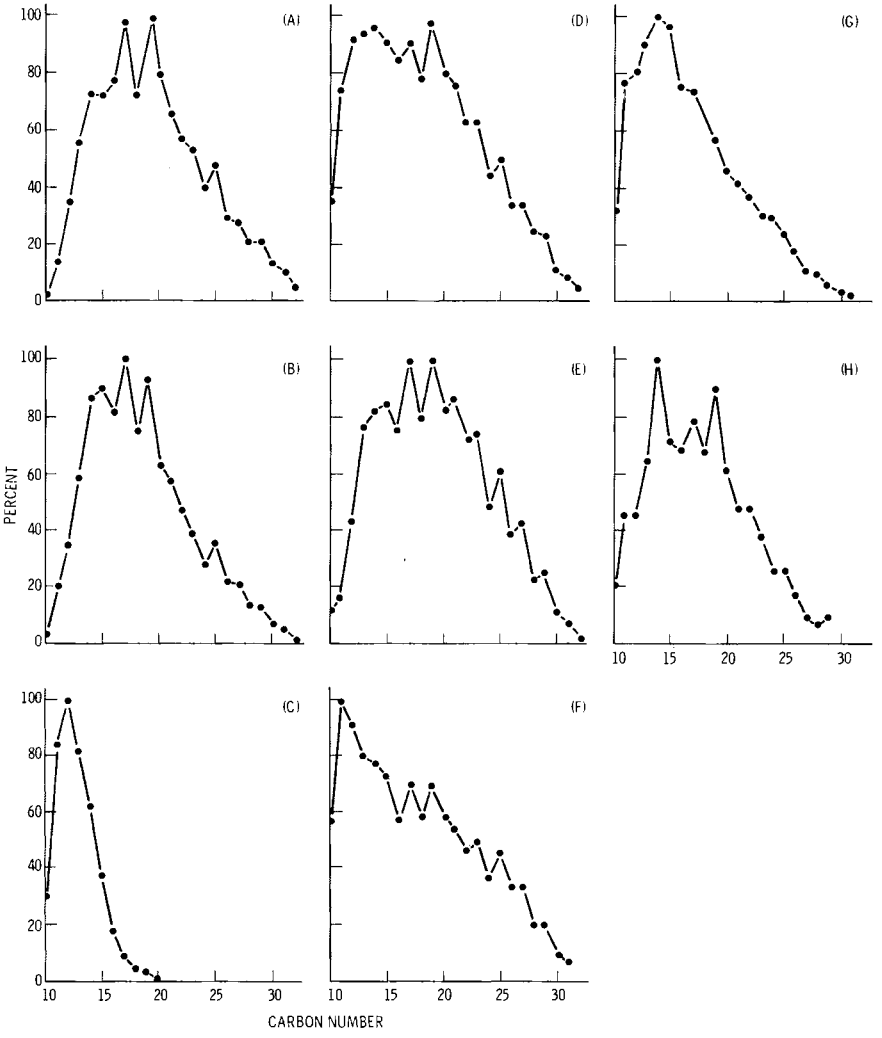

FIGURE 1. Distribution of n-alkane in (a) Occidental Product Oil, (b) Occidental Sludge Oil, (c) Occidental Light Oil, (d) Vernal, Utah Shale Oil, (e) Paraho Shale Oil, (f) Livermore Shale Oil, (g) Prudhoe Bay Crude Oil, and (h) Wilmington Crude Oil

Arsenic Speciation Analyses in Oil Shale Retort Offgases

J. S. Fruchter, E. A. Crecelius, and R. W. Sanders

An improved sample train (Figure 2) was developed and tested using ^{76}As tracer for determination of particulate arsenic, arsine, and arsenic trioxide vapor in air and process gas streams. A demister was used for oil-water mist removal. Particulates were removed by a filter. Vapor arsenic trioxide was collected in an impinger solution, and arsine gas was collected on silvered glass beads. A four-stage charcoal trap was used as a backup in case the silvered trap should saturate. All glassware was quartz with ground fittings. Teflon® was used for inlet and outlet tubing. The demister-filter section was temperature controlled at the temperature of the process gases to be sampled, while the impinger transport lines and silver and charcoal traps were held at 90°C. An integrating flowmeter and an absolute volume displacement unit were used for sample volume measurements.

Laboratory results showed that the silvered beads were an effective trap for arsine, but had a saturation limit. It was also found that 0.5M NaOH, H_2O, 0.5M HNO_3, as well as 0.5M HN_4OH solution traps were efficient and had high loading capacities for arsenic trioxide vapor. Field use verified the effectiveness of the demister assembly.

Using the above design system, samples of offgas from an in-situ oil shale retort were measured for arsenic speciation on three occasions. The results are shown in Table 4 and indicate that very little arsenic was emitted in the gas phase from this retort, since most of the reported numbers are near blank levels.

® Registered trademark of E. I. duPont deNemours and Co.

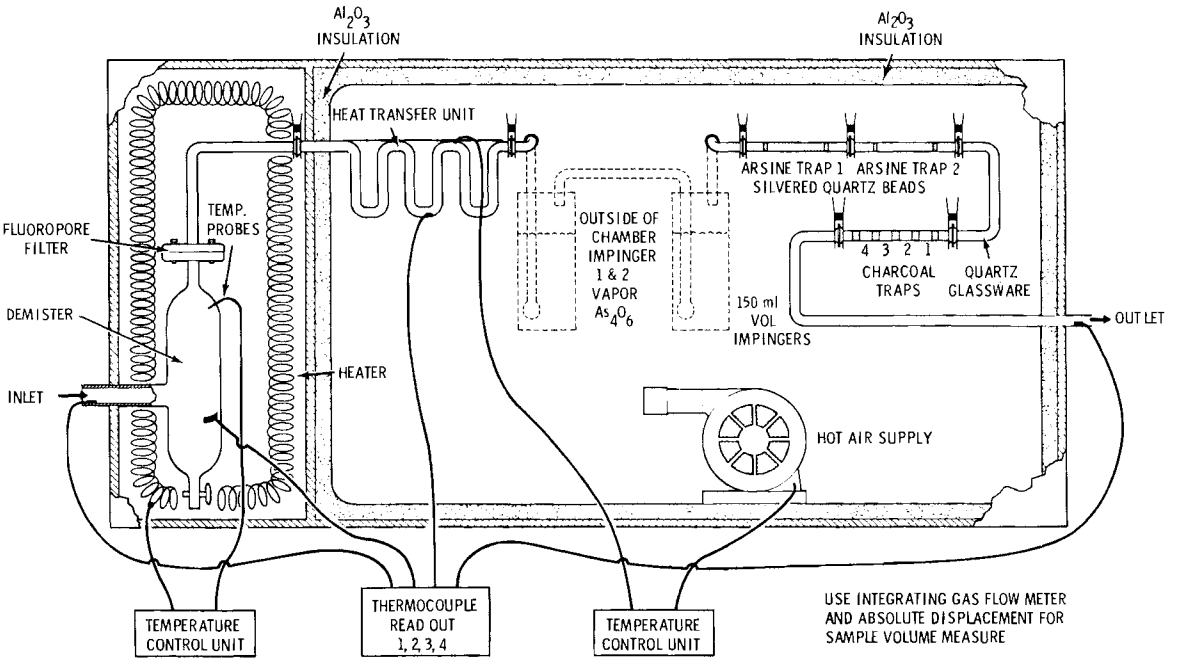

FIGURE 2. Sample Train Using ^{76}As Tracer for Determination of Particulate Arsenic, Arsine, and Arsenic Trioxide Vapor in Air and Process Gas Streams

TABLE 4. Arsenic Speciation in Offgas from an In-Situ Oil Shale Retort - Preliminary Data ($\mu g/m^3$)

	As_4O_6	AsH_3	Organic Forms
3/6/79	1.8 ± 0.8	3.5 ± 1.0	<0.4
3/7/79	<0.8	1.8 ± 0.8	<0.9
3/28/79	<0.8	0.85 ± 0.35	<0.9

Vapor Mercury Levels in the Offgas of Occidental's Modified In-Situ Retort 6

C. L. Wilkerson

Recent elemental mass balance studies of oil shale retorting processes have shown that the retorting phase of shale oil production will volatilize a significant fraction of the mercury from the raw shale matrix. The released mercury is then redistributed primarily into the product shale oil and the effluent gas stream. To date, the measured elemental abundances of mercury in oil shale reserves of the Green River Formation have been in the range of 50 to 500 ppb, or approximately equal to those of U.S. coals. However, extensive studies of trace element variation as a function of location and depth have not been completed for these principal oil shale reserves. Because of the large volumes of raw shale that will be processed in future proposed commercial shale oil plants and because of the many design options and operational parameters for each major technology, it is important to determine the volatilization yield and total vapor mercury concentration in the offgas stream of each retorting process. This information is essential to environmental impact and control technology assessments, especially if important oil shale reserves are identified which contain relatively high levels of mercury.

During the past year the total vapor mercury in the offgas of Occidental's modified in-situ retort Room 6 was measured as a function of time during the retort burn. This retort used a steam-air mixture to support and control combustion. Aliquots of the offgas were sampled over a few minutes' period during selected days from March to July 1979. Total vapor mercury in the offgas was collected by absorption tubes containing 80-100 mesh gold-coated beads. The absorption tubes were then analyzed for collected mercury by cold-vapor atomic absorption spectrometry. The resulting time sequence data are shown in Figure 3, along with reported mercury concentration levels in the flared product gas of the Paraho surface retorting process and mercury levels in the stack gases from a western coal-fired power plant.

The data in Figure 3 show that the observed mercury concentrations in the effluent gases of Occidental's Retort 6 ranged from 10 to 26 $\mu g/m^3$, with the maximum concentration occurring May 10, 1979. These values are greater than reported mercury concentration levels in the flared product gas of the Paraho process (direct mode) but lower than those of the unflared Paraho product offgas. They are also greater than concentrations found in stack gases from a typical western coal-fired power plant.

Neutron Activation Analysis of Oil Shale Retort Waters and Crude Shale Oils

C. L. Wilkerson

Instrumental neutron activation analysis (INAA) is a highly sensitive, multielement analytical technique that may be used to great advantage in developing a basis for understanding the process chemistry of oil shale retorting technologies. During the past year this technique was applied to determine trace element abundances in retort water and crude shale oil from three different oil shale retorting processes. The PNL-developed ^{252}Cf-^{235}U fueled subcritical multiplier facility was used for neutron activation of 10 ml samples, and INAA provided quantitative measurement of the elements Al, As, Br, Ca, Cl, Co, Cr, Cu, Fe, K, Mg, Mn, Mo, Na, Ni, S, Sb, Se, U, V, and Zn.

The resulting analyses, given in Table 5, show representative elemental abundances in the retort water and crude shale oil of the following oil shale retorting processes: (1) the Paraho surface process at Anvil Points, Colorado (semiworks retort--direct mode); (2) the Occidental modified in-situ process at Logan Wash, Colorado (Retort 6--steam injection); and (3) the horizontal true in-situ process being developed near Vernal, Utah.

The data in Table 5 indicate that Paraho retort water is characterized by a high total-sulfur concentration (~4%) and a moderately high magnesium concentration (~800 ppm). Relative to the two in-situ processes, the Paraho retort water also has

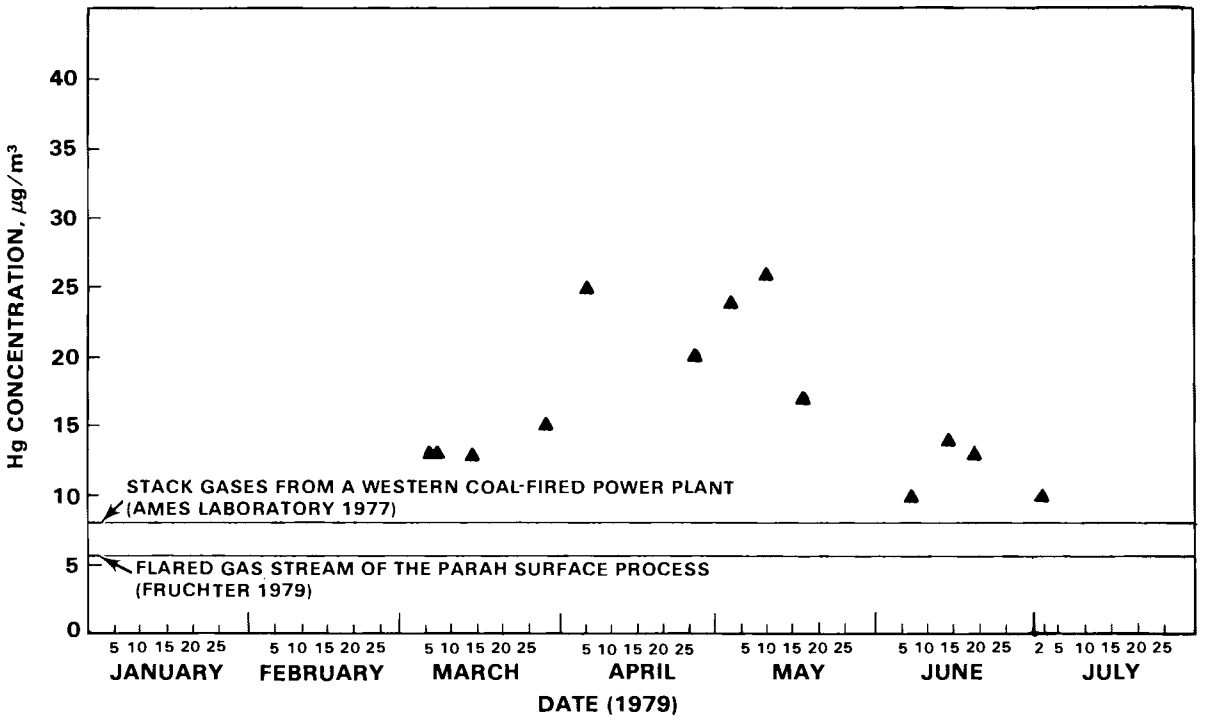

FIGURE 3. Total Vapor Mercury in Effluent Gases from Occidental's Retort 6

TABLE 5. Elemental Abundances in Retort Water and Crude Shale Oil from Three Retorting Technologies (ppm)

	Crude Shale Oils			Retort Waters		
	Surface	Modified In-Situ	True In-Situ	Surface	Modified In-Situ	True In-Situ
Al	33	0.2	<0.1	<1	<1	<1
As	31	16	10	11	1.4	9.1
Br	<0.03	<0.05	<0.03	<0.3	0.5	0.7
Ca	113	<30	<30	30	<40	<40
Cl	4	1	<0.5	64	232	117
Co	1.5	3.6	2.0	<0.4	<0.02	<0.3
Cr	<0.1	<0.1	<0.1	<0.1	<0.4	<0.1
Fe	80	40	70	<4	<4	<5
K	<50	<10	<10	<90	<100	<200
Mg	60	<10	<3	740	<30	<30
Mn	0.40	0.02	<0.03	0.2	<0.1	<0.1
Mo	<0.3	2.7	3.4	0.3	0.4	1.5
Na	21	12	0.5	285	2950	6050
Ni	4.1	9.9	5.9	0.4	<0.3	<1
S	8200	7500	7200	42,000	<4000	4000
Sb	0.07	<0.05	<0.02	<0.02	0.02	0.32
Se	1.72	0.71	0.76	6.2	0.04	0.23
U	0.02	<0.01	<0.01	<0.1	<0.1	0.2
V	0.29	0.41	0.39	0.07	<0.04	<0.05
Zn	0.6	2.1	4.1	0.4	<0.2	<0.5

a significantly high concentration of the trace element selenium. The latter observation is consistent with the high sulfur level and the known chemical similarities between sulfur and its analog selenium. The two in-situ retort waters are characterized by sodium concentrations of 3000 to 6000 ppm, a range that is 10 to 20 times that of the aboveground retort water. These relatively high sodium levels may suggest intrusion and contamination by local groundwater. The Vernal, Utah, true in-situ retort water was observed to contain a relatively high concentration of the element antimony. At present, the explanation for this anomaly is unknown.

The analyses show the aboveground shale oil to have a significantly higher concentration of the elements aluminum, magnesium, manganese, and sodium. The presence of these elements indicates that small quantities of raw and/or retorted shale fines have been entrained in the offgas oil mist which is subsequently condensed to form the Paraho product oil. Relative to the data presented in Table 5 for the in-situ processes, the Paraho shale oil will thus have a significantly higher "ash" content. Conversely, the elements molybdenum and zinc are more concentrated in the two in-situ produced shale oils. The reason for these relative enrichments is unknown at present; however, it is reasonable to conclude that they probably reflect major differences in the retorting methods rather than differences due to variations in the local raw oil shale. This statement is supported by the abundance comparisons in Table 5 between the important volatile trace elements arsenic, iron, and selenium, which agree within a factor of two to three. The differences noted above for zinc, and especially for molybdenum, exceed this margin of agreement.

Analysis of a Spent Shale Core from a Modified In-Situ Oil Shale Retort

J. S. Fruchter, C. L. Wilkerson, K. B. Olsen, and R. W. Sanders

Samples of the spent shale core from Occidental Oil Shale Retort 3E at Logan Wash, Colorado, were obtained and analyzed for a number of elements of environmental interest. The data are presented in Table 6. The core samples show considerably higher compositional variation than found in shale samples from aboveground and simulated in-situ retorts.

Boron, aluminum, arsenic, sulfur, and molybdenum were found to generally increase with depth, whereas other elements fluctuated more or less randomly. All core samples measured showed residual mercury concentrations as opposed to simulated in-situ shales, which showed no detectable mercury. The Occidental core spent shales were found to be generally higher in boron and calcium and lower in sodium and molybdenum than other shales that had been carefully studied to date.

Shale Oil Fractionation and Mutagenicity

D. S. Sklarew, R. A. Pelroy, S. P. Downey, and J. T. Cresto

Analysis of organic components in various shale oil materials is an integral part of the shale oil program with the major consideration being the identification of organic compounds that are biologically/environmentally hazardous. Two shale oil fractionation schemes are currently being compared. PNL Physical Sciences and Biology Departments are coordinating on this project. Fractions prepared by Physical Sciences personnel are provided to Biology personnel for microbiological assays. Those fractions determined to be potentially hazardous are further characterized by Physical Sciences personnel.

The first fractionation scheme considered is the acid-base extraction described in previous annual reports (Fruchter, Petersen, and Laul 1979). The second method involves partition chromatography on Sephadex LH-20 and was a modification of a scheme described by Klimisch and Stadler (1972) and further developed by Jones, Guerin, and Clark (1977). The Sephadex LH-20 is swelled in methanol:water (85:15); the sample is eluted with hexane, toluene:hexane (95:5), and finally with methanol. An alternate elution sequence was tried in which the toluene:hexane step was eliminated. These elution schemes give a gross separation according to polarity of the components. For example, corresponding work with standards indicates that aliphatic hydrocarbons and polycyclic aromatic hydrocarbons should elute in the hexane phase; aromatic amines and phenolics elute in the methanol phase. The hexane fraction has been subdivided into aliphatics and aromatics by an adsorption mechanism in which the Sephadex LH-20 is swelled in isopropanol and eluted with isopropanol followed by tetrahydrofuran.

Shale oils (product oils) from Paraho, Occidental, Livermore, and Vernal, Utah, plus a sludge oil from Occidental, were fractionated by both the Sephadex and acid-

TABLE 6. Spent Shale from Oxy Retort 3E - Preliminary Data (ppm except as noted)

Sample No.	Element and Method of Analysis																
	Al,%(N)	As(N)	B(P)	Ba(N)	Ca,%(X)	Cs(N)	Fe,%(N,X)	Hg,ppb(F)	K,%(N,X)	Mg,%(N,A)	Mo(X)	Na,%(N)	Ni(X)	P,%(X)	S,%(X)	Si,%(X)	Ti(X)
1	4.5	6.2	228.1	800	28	3.5	2.51	34	2.7	8.2	4.8	1.19	17	2.0	0.45	20	1400
2	2.5	21	98.3	550	23	2.2	1.29	38	0.92	4.9	4.0	1.28	16	1.4	1.3	13	1200
3	3.3	26	154.5	670	18	3.0	1.72	39	1.2	5.4	5.2	1.12	16	1.1	0.40	18	1100
4	5.6	25	154.2	720	10	5.3	1.74	51	0.81	2.5	9.8	3.31	18	< .5	0.40	27	590
5	4.3	21	184.0	750	18	3.6	2.42	20	2.6	5.9	2.9	0.53	26	1.2	0.38	16	1100
6	4.3	19	330.2	520	17	4.6	2.51	34	2.8	6.6	4.1	0.79	23	0.86	0.37	17	980
7	4.2	23	227.8	740	20	6.4	2.06	43	2.7	6.3	4.5	1.31	26	1.03	0.46	19	1200
8	4.2	23	239.5	530	18	5.2	2.24	38	3.1	6.9	4.5	0.96	27	0.83	0.33	19	1100
9	4.2	12	145.8	730	21	4.8	2.18	24	2.9	6.4	5.3	1.22	35	1.4	0.35	17	1400
10	4.4	17	195.2	670	22	6.2	2.14	42	2.5	5.7	5.9	1.43	41	1.6	0.52	17	1500
11	4.2	29	208.1	710	24	4.6	2.49	67	2.8	6.1	7.9	1.05	30	2.0	0.47	16	1400
12	4.5	24	192.5	700	23	4.7	2.54	38	3.3	5.9	8.2	1.01	36	1.3	0.38	16	1300
13	5.3	17	244.6	580	19	6.2	3.06	43	4.0	5.9	15	0.98	32	1.4	0.36	20	1100
14	5.6	15	310.2	640	20	6.0	3.02	77	3.6	5.4	23	1.15	34	0.91	0.40	21	1200
15	4.9	76	216.7	700	24	5.8	2.76	44	2.5	7.3	15	1.43	34	2.1	0.67	18	1400
16	4.8	29	217.6	760	22	8.8	2.64	44	2.7	6.1	23	1.50	30	1.6	0.65	21	1300
17	6.7	40	553.3	610	12	4.4	3.16	24	6.3	3.6	19	0.87	36	< .5	0.72	24	730
18	7.1	39	641.0	500	8.2	6.3	3.33	35	6.4	4.9	18	1.14	36	< .5	0.78	25	560

(N) Instrumental neutron activation
(P) DC plasma emission spectroscopy
(X) X-Ray fluorescence
(A) Atomic absorption spectroscopy
(F) Flameless atomic absorption spectroscopy

base methods. A crude petroleum from Prudhoe Bay and a solvent-refined coal (SRC-II heavy distillate) were run for comparison. Tables 7 and 8 show the relative amount of each fraction for the seven samples studied.

Each fraction has been analyzed for mutagenicity in the Ames assay using Salmonella typhimurium TA98 as the target cell. The data are presented in Figures 4 and 5. The fractions give a linear response over at least a factor of 10 range in concentration.

TABLE 7. Recovery of Material from the Sephadex Method (%)

	Hexane	Toluene/Hexane	Methanol	Recovery
Paraho	83.4	1.9	3.2	88.5
Oxy Product	82.4	2.4	1.2	86.0
Oxy Sludge	78.2	1.7	1.0	80.9
Livermore	74.0	2.0	3.9	79.9
Vernal, Utah	79.0	1.9	4.7	85.6
Prudhoe Bay	77.8	0.5	0.1	78.4
SRC II	72.2	6	9.9	88.1

TABLE 8. Recovery of Material from the Acid-Base Method

	Acid	Base	Neutral	PAH	"Acid Tar"	"Basic Tar"	"Neutral Tar"	Recovery
Paraho	3.9	4.2	53.9	4.0	1.1	15.3	7.0	89.4
Oxy Product	.6	3.5	40.5	5.6	2.6	5.5	24.4	82.7
Oxy Sludge	33.9	4.8	38.2	2.8	.5	7.3	14.6	102.1
Livermore	5.7	5.8	42.6	4.5	1.8	15.2	3.6	79.2
Vernal, Utah	1.0	5.5	40.5	9.9	9.7	7.7	25.7	100
Prudhoe Bay	—	14.6	55	1.5	.7	.6	11.5	83.9

In contrast, the unfractionated shale oils gave a nonlinear response. Therefore, fractionation is necessary for quantitative estimates of mutagenicity.

For each sample, mutagenicity was concentrated in the methanol fraction from the Sephadex scheme; the hexane and toluene/hexane fractions showed essentially no activity above background (SRC-II is a minor exception). Further fractionation of the Paraho hexane fraction resulted in no activity. When the toluene/hexane step was elminated, the mutagenic activity in the methanol phase decreased significantly. In the acid-base extraction technique, mutagenicity was concentrated in the basic, "basic" tar, and "neutral" tar fractions.

Of the shale oils, only Paraho, Livermore, and Vernal, Utah samples (unfractionated crudes or fractions) were genetically

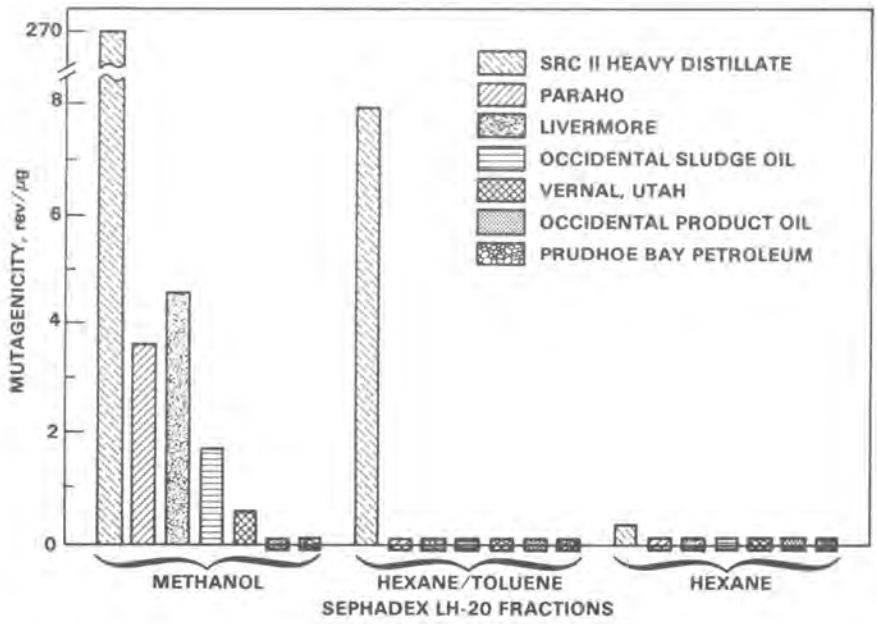

FIGURE 4. Mutagenicities of Sephadex LH-20 Column Fractions of Paraho, Livermore, Occidental, and Vernal, Utah Shale Oils, Occidental Sludge Oil, SRC II Heavy Distillate, and Prudhoe Bay Petroleum

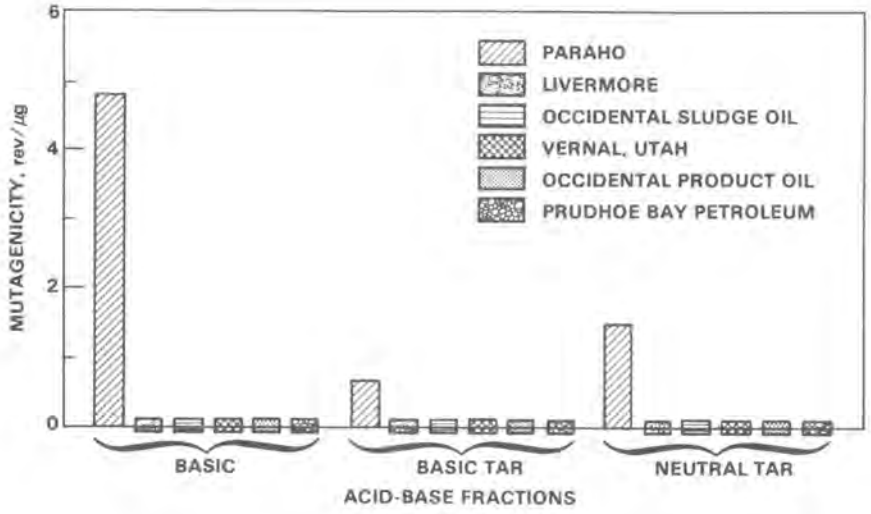

FIGURE 5. Mutagenicities of Acid/Base Extracts of Paraho, Livermore, Occidental, and Vernal, Utah Shale Oils, Occidental Sludge Oil, SRC II Heavy Distillate, and Prudhoe Bay Petroleum

active in the Ames assay. Occidental sludge also showed activity. Occidental product oil, as well as Prudhoe Bay petroleum, was inactive or extremely weak, both as the crude and fractionationed materials. SRC-II heavy distillate yielded a much higher degree of mutagenic activity in the methanol fraction from Sephadex than did the shale oils. The acid-base data from SRC-II have been previously presented (Pelroy, Cresto, and Petersen 1979). Recovery of mutagenic activity was comparable by the two methods for Paraho and SRC-II. However, the Sephadex fractionation procedure appeared to be superior to acid-base extraction for recovery of mutagenicity in Livermore and Vernal, Utah shale oil and Occidental sludge oil samples.

Fossil-Fuel Research Materials

J. S. Fruchter

The purpose of the fossil-fuel research materials program is to obtain, store, prepare, and distribute homogeneous and chemically analyzed synthetic fossil-fuel samples for characterization, environmental, and health effects studies. A number of samples from oil shale retorts and coal conversion processes that were available in our refrigerated repository were listed in last year's annual report. These, plus those added in this year's work, are listed in Table 9. The major activities during the past year have involved collection of samples from Occidental Oil's Logan Wash, Colorado, research site for our own use and for distribution to members of the Assistant Secretary for Environment's Modified In-Situ Task Force.

Samples collected at Logan Wash included crude shale oil, light shale oil, product water, steam plant water, boiler blowdown, and mine sump water from Occidental's Retort 6. In addition, groundwater samples were obtained from both bedrock and alluvial water wells, and leachate water was obtained from Retorts 1-5. Finally, samples of spent shale were obtained from Retort 3E. A core of raw shale was obtained nearby at the location of water well LW108. The points at which the retort was sampled are shown in Figure 6. These samples were returned to PNL where they were processed, homogenized, and distributed to other members of the task force. Unused portions of the samples were retained in the PNL refrigerated repository for future use. Studies conducted on these samples included inorganic chemical analysis and interlaboratory comparison studies, organic analysis and separation of spent shale leaching studies, Ames mutagenicity assays, mammalian cell assays, and skin painting tests.

Additional samples obtained for the program included products from Standard Oil of Ohio's Toledo, Ohio refinery run of 90,000 barrels of Paraho shale oil. Products obtained included raw shale oil, hydrotreated

TABLE 9. Currently Available Fossil Fuel Reference Materials

1. Solvent-Refined Coal Process-I
   a. Solvent-refined coal
   b. Mineral residue
   c. Light oil (naphtha)
   d. Recycle solvent
   e. Wash solvent
2. Lawrence Livermore 125-kg Retort
   a. Mahogany Zone raw shale (24 gal/ton)
   b. Spent shale (Run S-11)
3. Lawrence Livermore 7-T Retort
   a. Spent shale (Run L-1)
   b. Crude shale oil (Run L-1)
   c. Process water (Run L-1)
4. Vernal, Utah In Situ
   a. Process water
   b. Crude shale oil
5. Crude Petroleums
   a. Wilmington (high N)
   b. Gato Ridge (high metals, high N, high S)
   c. Prudhoe Bay
6. Paraho Semiworks Retort[a]
   a. Raw shale
   b. Retorted shale
   c. Crude shale
   d. Product water
   e. Raw shale crushing fines from filter baghouse
   f. Retorted shale fines from filter baghouse
7. CO_2 Acceptor
   a. Ash
   b. Spent acceptor
8. Solvent-Refined Coal Process II
   a. Light distillate
   b. Middle distillate
   c. Heavy distillate (product)
   d. Vacuum bottoms
9. Paraho Refined Fuels
   a. Hydrotreated shale oil
   b. JP-5 (jet)
   c. JP-8 (jet)
   d. DFM (diesel)
   e. Acid sludge
10. Conventional Petroleum Fuels
    a. JP-5 (jet)
    b. JP-8 (jet)
    c. DFM (diesel)
11. Occidental In-Situ Retort[b]
    a. Crude shale oil
    b. Retort water (Room 6)
    c. Boiler blowdown
    d. Leach water from old retorts (Rooms 1-5)

[a]Use of any materials from Paraho requires approval from Development Engineering, Inc. (operators of Paraho retort) on a case-by-case basis.

[b]Use of any materials from Occidental requires coordination through the DOE-ASEV Modified In Situ Task Force - W. Chappell, University of Colorado, Chairman.

shale oil, JP-5, JP-8, diesel fuel marine, hydrotreating residue, and acid sludge. In addition, samples of JP-5, JP-8, and diesel fuel marine refined from conventional petroleum were obtained from the Navy for comparative studies. Characterization and toxicity studies of these fuels have begun.

Health Effects Related to Chemical Composition of Several Shale Oil Products

B. W. Wilson and R. A. Pelroy

Among the shale oil products tested thus far, there are significant variations in the degree of activity exhibited in the Ames test. Mutagenic activity, when found in acid-base fractionations of the crude product, is most often associated with the basic fraction of the shale oil; however, it is also present to a lesser extent in basic and neutral tars.

This report concerns the results of efforts to chemically characterize the basic fraction with the objective of identifying the compound or compounds that may be responsible for the observed mutagenicity.

Analysis was accomplished by first subjecting aliquots of the basic fractions to

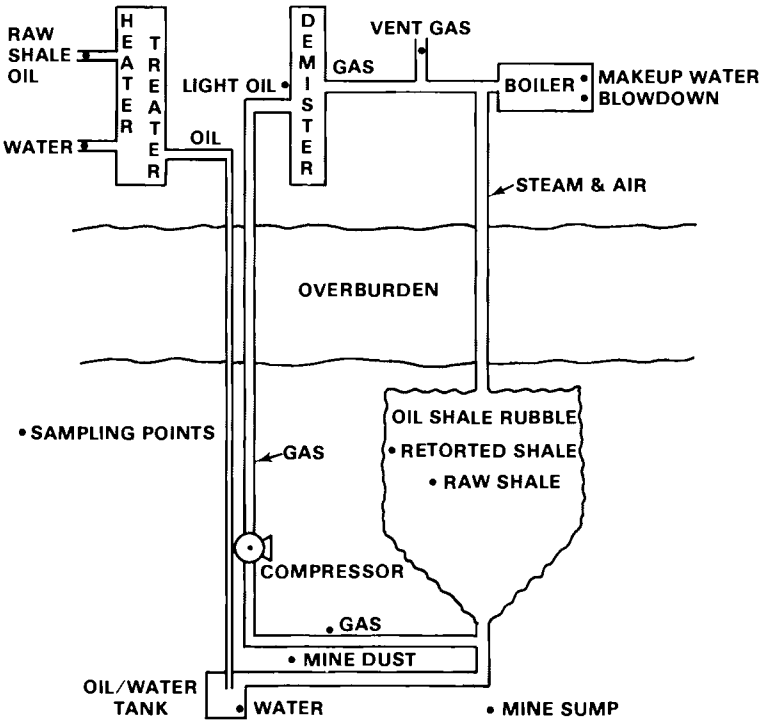

FIGURE 6. Simplified Flow Diagram and Sampling Points for Oxy Retort 6

thin layer chromatography (TLC) using a solvent system in which the most polar compounds remain near the origin. Based on visualization that was possible under ultraviolet light, the chromatograms were then cut into five or six regions, each having one or more bands. The regions were eluted, and the resulting solutions analyzed for mutagenicity by Ames testing and for chemical composition by gas chromatographic/mass spectrometry (GC/MS) analysis. Compound identifications were based on the relative mobility, GC retention time, selected ion chromatographic data, and high resolution probe mass spectral data.

In similar studies with coal-derived materials, which in general are more potent mutagens than the shale oil products, it was found that there existed good correlation between the observed activity of the TLC fractions and the concentrations of primary aromatic amines present (Table 10). A number of primary aromatic amines, such as 9-amino phenanthrene, are known to be mutagenic in the Ames test, and at least four, including 2-amino naphthalene, are known or suspected human carcinogens.

Analysis of the shale oil basic fractions by GC/MS showed primary aromatic amines (PAAs) to be present in exceedingly low concentrations relative to comparable coal liquid products. The mutagenic activity of the TLC fractions correlated roughly to the concentration of PAAs.

While the coal materials contained detectable concentrations of PAAs having up to five rings, the shale products contained no detectable PAAs having more than two rings, with the exception of trace amounts of amino phenanthrene in Paraho shale.

Although the shale oil products are extremely complex in their organic compositions, evidence from this and other work on related products indicates that PAAs may be the constituents in shale oil products that are principally responsible for their mutagenic activity in the Ames test.

TABLE 10. Concentrations of Primary Aromatic Amines Related to the Observed Mutagenic Activity

		Total Content[a] of all isomers found in the basic, basic tar and neutral tar fractions in ppm of the crude product			Relative Mutagenicity by Ames Test (TA 98 Salmonella)
		Total Amino Naphthalenes	Total Amino Anthrane Phenanthrene	Total Amino Pyrene + Higher Holologs	
Coal Derived	SRC II Heavy Distillate Cut	50	60	20	100
	SRC I Process Solvent	20	30	10	25
Oil shale Derived	Paraho Crude Product	4	Trace	ND	5
	Vernal, Utah Crude Product	1	Trace	ND	1
	Oxy Crude Product	0.5	ND	ND	ND
Petroleum Product	Prudhoe Bay	ND	ND	ND	ND
	Petroleum Crude	ND	ND	ND	ND

[a]Concentrations were measured by ratio with m/e 188 ion of d_{10} anthracene internal standard using selected ion monitoring GC/MS. Values are rounded and not adjusted for recoveries during preparation of samples.

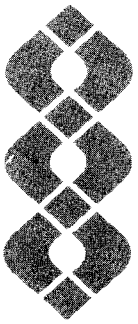

Multitechnology

• Environmental Pollutant Characterization by Direct-Inlet Mass Spectrometry

The utility of direct-inlet mass spectrometry (DIMS) for the detection, characterization, and monitoring of important particulate airborne pollutants which arise as by-products of energy production and other industrial activities is being experimentally determined. Studies of the response of the entire DIMS system to artificially generated aerosols of $CsNO_3$ have been continued.

Characterizing Environmental Pollutants by DIMS

C. R. Lagergren and R. L. Gordon

The purpose of this program is to experimentally determine the utility of direct-inlet mass spectrometry (DIMS) as an analytical technique for the detection, characterization, and monitoring of important particulate airborne pollutants that enter the environment as by-products of energy generation (or other industrial) activities.

In the DIMS technique, airborne particles are introduced as a jet directly into the ion source of a surface ionization mass spectrometer. Particles striking the hot filament form bursts of ions that are then mass analyzed and measured. Burst rates are related to particle concentration in sampled air, while the total charge per burst is a measure of particle size. Ionization efficiencies by surface ionization for a wide range of elements are sufficiently high so that submicrometer size particles of compounds of these elements can be detected.

To determine the utility of DIMS as a sensitive, species-selective, and real-time analytical technique for measuring airborne pollutants, the nature of the ionization produced by surface ionization of specific pollutant materials of interest must be established. The ionization efficiency, cracking pattern (ion spectrum), and time characteristics of the signals that are produced are not only functions of the molecular and physical form of the pollutant material, but are also functions of the nature and temperature of the filament surface. These quantities and relationships are unknown and need to be determined for successful application of the technique.

An essential step in this study is the determination of the response of the entire system to a population of particles of known sizes and composition. For this purpose, $CsNO_3$ was selected as a test material and aerosols of it were produced in a jet-mill-type particle generator. In an initial experiment, previously reported, it was found that the distribution of total charge measured per particle resembled a distribution of areas rather than volumes of a set of particles subsequently collected on the surface ionization filament. This interpretation of preliminary data depended on the assumption that the size distribution of particles that were ionized to produce the total charge data could be properly determined from the set of particles collected on the surface ionization filament at another time. Subsequent studies of the DIMS system response to particles of $CsNO_3$ have been performed to characterize more fully the relationships between particle sizes and ion signals.

Variations in consecutive sets of charge data collected over a short interval of time indicated that the output size distribution of the jet-mill particle generator changes with time. This means that it is necessary to collect particles for size measurement and to accumulate integrated current data simultaneously. To do this, a narrow surface ionization filament was used which intercepted less than one-half of the beam of particles and allowed the remaining portion to be collected beyond it for particle-size measurements. The particle collections were made on gold-coated glass and photographs were taken of the scanning electron microscope (SEM) views of the particles. The distribution of particle sizes from the SEM photographs was found to be constant over the pattern of collected particles. A comparison of the measured number density of

collected particles to the integrated particle-beam flux density, as determined from the total number of particles detected by ion bursts, indicates that less than 23% of the incident particles stuck to the glass. The low collection efficiency, which is a consequence of the high velocity (~350 m/s) that the inlet system imparts to all of the particles, may be a function of particle size. Therefore, particle-size distributions will have to be measured ahead of the inlet system.

Another way of defining the sizes of particles striking the surface ionization filament is to use mono-disperse aerosols. For this purpose, an Electrostatic Classifier® has been procured and will be used as a variable particle-size filter for the selection of nearly mono-disperse portions of the poly-disperse sample distributions.

An improved ion-current integration system was developed which is more nearly linear in response and is capable of distinguishing between the integration of a pulse of current and the integration of an uncompensated level of background current.

® Registered trademark of Thermo-System, Inc.

• Trace Analysis by Laser Excitation

Laser excitation techniques offer the potential of being the most sensitive of any analytical methods, often giving orders-of-magnitude higher sensitivities than currently used trace analysis procedures. Under certain conditions, these methods may provide the ultimate sensitivity: the detection of a single atom. Low-level detection, along with the capability for real-time measurement, makes laser-based techniques attractive for the assessment of low-level environmental pollutants associated with energy production cycles where the systems of interest may be complex and dynamic.

Work in this laboratory is currently directed toward the development of methods that use medium-power (10-100 kW) pulsed, tunable dye lasers to induce selective photoionization. Of the wide variety of laser analysis schemes available, ionization processes are the most attractive for ultra-trace analysis since single quantum events may be detected with unit efficiency. These methods are applicable to a wide variety of airborne materials ranging from atomic species to complex organic compounds. This is illustrated by the systems reported here: atomic rubidium and several polynuclear aromatic hydrocarbons.

Multiphoton Ionization Spectroscopy of Gas-Phase Polynuclear Aromatic Hydrocarbons

B. A. Bushaw and T. J. Whitaker

Polynuclear aromatic hydrocarbons (PAHs) are released into the environment by several processes associated with fossil-fuel energy production. Since many of these PAHs are considered carcinogenic, it is necessary to identify those being produced and to quantify the amounts being released. Multiphoton ionization (MPI) spectroscopy may be a very sensitive tool for detection of atoms and molecules when resonant intermediate states are available. We have investigated the practicability of using MPI on some representative PAHs.

Naphthalene and anthracene have been chosen as model compounds for the development of MPI spectroscopic analysis of PAHs. The high symmetry (D_{2h}) and reasonably well-defined spectroscopic parameters of these compounds allow theoretical confirmation of experimental results. Three photon ionization spectra have been recorded and a number of spectral features observed can be attributed to the following excitation pathways:

$$(1)\quad S_0 \xrightarrow{2h\nu} S_n \xrightarrow{h\nu} \text{Ionization}$$

$$(2)\quad S_0 \xrightarrow{h\nu} T_1 \xrightarrow{h\nu} T_n \xrightarrow{h\nu} \text{Ionization}$$

In the first pathway, the singlet ground state (S_0) simultaneously absorbs two photons to produce a high excited singlet state (S_n), which then absorbs a third photon bringing the molecule above the ionization limit. The initial two-photon absorption in this pathway is important to fundamental energy level measurements since the states excited are of "even" symmetry and are forbidden in normal absorption and fluorescence techniques.

The second pathway involves the sequential absorption of three photons. The first populates the lowest triplet state (T_1), the second raises T_1 to a higher triplet (T_n) which is ionized by the third photon. The resonances observed by this process are identical to those that have been seen previously in triplet-triplet absorption spectroscopy.

Figure 1 shows the three-photon ionization spectra of naphthalene. The trace in the low portion of the figure is the ratio of the ionization signal for circularly polarized light relative to that when linear polarization is used. This ratio is useful in the assignment of the symmetry of the

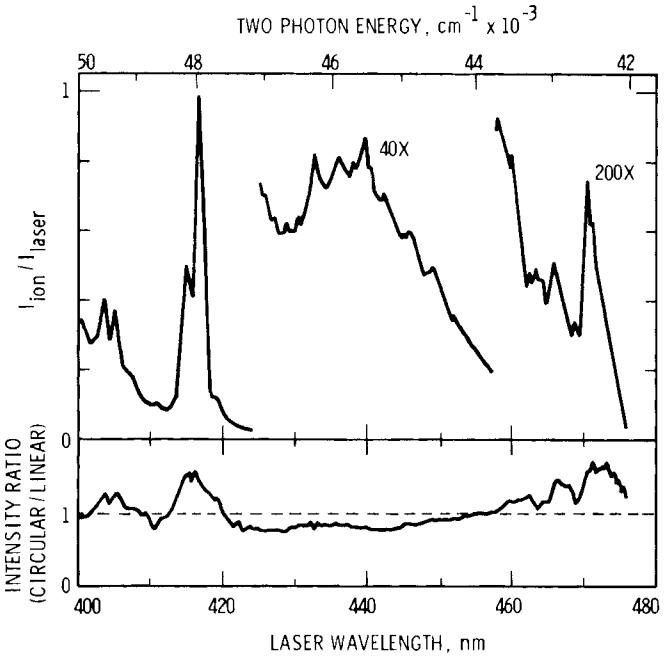

FIGURE 1. Three Photon Ionization Spectra of Gas-Phase Napthalene Using Circularly Polarized Light

observed states. The intense peak at 417 nm is attributed to the triplet-triplet absorption pathway, while all other peaks are due to two-photon resonances in the singlet manifold. The bands in the 460-480 nm region are due to vibrationally-induced levels of the one photon allowed $^1Bu_{3u}$ state. The series of bands from 434-450 nm are attributed to a two-photon allowed $^1B_{1g}^+$ state and the bands near 405 nm to another two-photon allowed state, $^1B_{1g}^-$.

Similar spectra have been obtained for anthracene with a strong triplet type band near 427 nm. The assignment of other features has not yet been completed due to the higher density of electronic states.

The results thus far indicate that MPI spectroscopy may be useful as an analytic technique for PAHs. The method exhibits low detection limits, allowing measurement of quantities in the part-per-trillion range. Also, the sharp structure of the triplet bands indicates that a reasonable degree of selectivity may be achieved, permitting identification and measurement of a particular PAH in the presence of chemically similar molecules.

Two Photon Resonant Ionization of Rubidium

T. J. Whitaker and B. A. Bushaw

A photoionization method for the detection of single rubidium atoms is currently being developed. The interest is not in rubidium itself, but rather in the fact that ^{85}Rb is the decay product of ^{85}Kr, an environmentally important by-product of the nuclear fuel cycle. Conventional β^- decay analysis of low levels of ^{85}Kr is greatly hampered by background events. Coincident detection of the decay product, ^{85}Rb, would confirm that a detected β^- was due to ^{85}Kr decay and effectively eliminates any signal due to background.

The laser-induced ionization is similar to the single cesium atom detection scheme, which has been successfully demonstrated at Oak Ridge National Laboratory.

It is a sequential two-photon ionization:

$$Rb \xrightarrow{h\nu} Rb^* \qquad (1)$$

$$Rb^* \xrightarrow{h\nu} Rb^+ + e^- \qquad (2)$$

The laser is tuned to a single photon resonance to produce the intermediate excited rubidium atom and then a second photon ionizes the excited atom. We have investigated the resonances with the $6^2P_{1/2}$ and $6^2P_{3/2}$ states using a laser wavelength near 420 nm. Figure 2 shows the spectra of these two states under conditions where the resonance step is saturated (trace A, focused laser beam) and where it is not (trace B, 1-cm-diameter unfocused beam).

Saturation of both steps is required for single atom detection. For a sample volume of 1 cm^3, the laser system used easily saturates the first step, but the second is only about 0.1% efficient when the second photon is of the same frequency as the first. Thus, detection limits are currently on the order of 10^3 atoms. This may be remedied by using a second laser frequency for the second step, exciting the atom to a high Rydberg or autoionization level where the absorption cross sections are much larger than in the ionization continuum.

Pacific Northwest Laboratory-Oak Ridge National Laboratory Interaction

T. J. Whitaker and B. A. Bushaw

Cooperative efforts between this group and G. S. Hurst's group at Oak Ridge National Laboratory (ORNL) have continued. T. J. Whitaker assisted the ORNL group in an experiment to detect satellites in the photoionization spectrum of cesium in P-10 counting gas. These satellites are caused by cesium-argon molecular interactions. Several ideas and equipment designs used in the cesium experiments at ORNL have been or soon will be incorporated into the rubidium experiments at PNL.

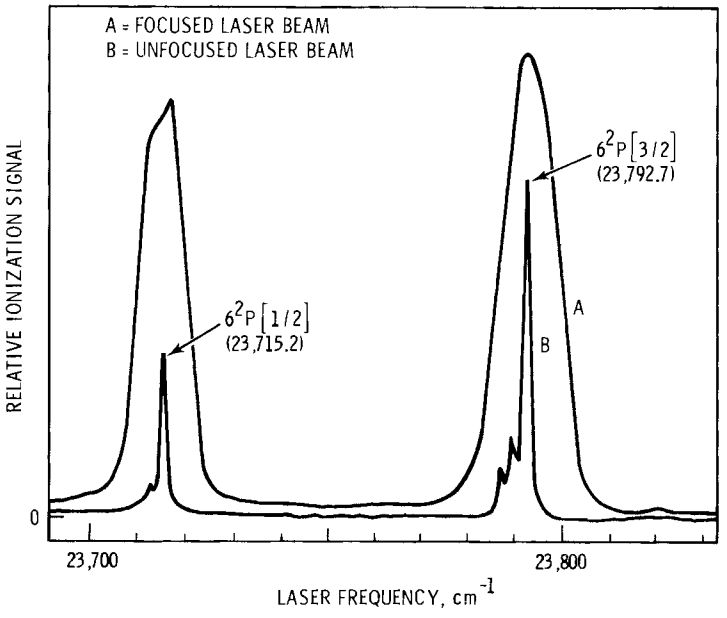

FIGURE 2. Two Photon Resonant Ionization Spectra of the 6P Levels of Rubidium Vapor at 25°C

• Direct-Coupled Plasma Emission Spectroscopy

Direct-coupled (DC) plasma emission spectroscopy is being investigated for its applicability to environmental sample. Analyses have been successfully obtained for about 35 elements including boron. Many of the elements cannot be determined by other methods. It has proved useful for both aqueous and solid sample analyses. At present, the spectrometer is being upgraded so that it will determine 20 elements simultaneously.

DC Plasma Emission Spectroscopy Analysis

J. C. Evans and K. B. Olsen

A DC plasma emission spectroscopy analysis system has been in use in our laboratory for the past two years. In its present form the system is used in sequential mode only. About 35 elements can be analyzed in this manner. During the past year, the system was used successfully on a wide variety of sample types. These included oil shale process waters, geothermal waters, leachates and environmental samples from uranium mining, leachates from gold extraction systems, and fusion samples from oil shale. A multielement intercomparison was carried out on sodium carbonate fusions of oil shale referenced against nondestructive instrumental neutron activation and X-ray fluorescence analysis. The results are shown in Table 1. In general, plasma emission spectroscopy compared favorably with the other two techniques for the 15 elements on which

TABLE 1. Oil Shale Analytical Intercomparison

Element	PES[a]	INAA[b]	XRF[c]
Al (%)	3.78 ± .08	3.67 ± .07	—
B (ppm)	94 ± 2	—	—
Ba (ppm)	515 ± 8	483 ± 23	—
Ca (%)	9.9 ± .1	10.0 ± .4	10.3 ± .2
Cr (ppm)	33.8 ± .6	33.9 ± 1.0	29 ± 5
Cu (ppm)	40 ± 5	—	41.1 ± 1.9
Fe (%)	2.01 ± .04	2.02 ± .03	2.03 ± .04
K (%)	1.79 ± .03	1.72 ± .07	1.62 ± .03
Mg (%)	3.42 ± .05	3.4 ± .1	—
Mn (ppm)	322 ± 11	297 ± 16	314 ± 22
Ni (ppm)	27.6 ± .6	26.0 ± 3.3	22.8 ± .7
Mo (ppm)	20.9 ± 1.9	22.3 ± 2.8	—
Sr (ppm)	712 ± 14	698 ± 14	665 ± 13
V (ppm)	96 ± 3	83 ± 3	79 ± 9
Zn (ppm)	73 ± 4	68 ± 3	67.6 ± 1.5
Zr (ppm)	36.2 ± 1.3	—	37.6 ± 2.2

[a]Plasma emission spectroscopy
[b]Instrumental neutron activation analysis
[c]X-ray fluorescence analysis

Note: Six replicates were run by each technique. Errors quoted are replication errors.

comparison was possible. The procedure was somewhat laborious, however, due to the necessity for sequential analysis.

A study was carried out during the past two months to assess the desirability of upgrading the system to full simultaneous 20-element capability. It was concluded that this would be very useful when combined with a modest level of computerization to handle curvature correction, background correction, line overlaps, and ionization interferences.

Spectral lines have been chosen for inclusion in a multielement cassette based on compatability with the sample matrices in common use in our related programs. Of particular importance in line selection is our intention to develop the capability for direct multielement analysis of shale oil. A program has already been initiated and will be continued in the next year to systematically identify the curvature and matrix parameters for each line to be used. This information will then be incorporated into an off-line software package suitable for either sequential or multielement use. A program of hardware upgrading will be carried out simultaneously.

This technique has already proven its capabilities for highly sensitive, selective, precise and accurate inorganic analysis. With appropriate upgrading, it should prove to be an extremely powerful analytical tool for use on a wide variety of problems.

• Applications of Holography

Hardware and data analysis procedures for applying holography to the detection and characterization of airborne particulate pollutants are being developed. The data collection portion of the system consisting of a laser head, control electronics and camera is sufficiently small and self-contained to be applied to the characterization of underwater particulates and organisms as well. The system provides the capability for characterizing particulates and organisms in terms of size, location in three-dimensional space and speed of movement, and it does this with no disturbance of the matter contained within the volume being examined.

Applications of Holography to Environmental Studies

B. B. Brendon

Holography is a technique that records a scene in three dimensions. Most holographic systems require complete stability, i.e., the system will fail to record the scene if there is motion within the scene exceeding more than 0.1 μm during the time the film is being exposed. The limitation is least restrictive when exposure times are very short. Exposure times in the range of 30 - 100 nsec are not uncommon using Q-switched ruby lasers, but the use of commercially available Q-switched ruby lasers for particulate studies has been retarded because of the cost, size, and power requirements associated with these systems. It has, therefore, been the objective of this program to develop a small, battery-operated, double-pulsed, Q-switched ruby laser and to incorporate this laser in a photographic system capable of recording the position, size, shape, velocity, and velocity distribution of particles within a volume approximately 2.5-cm diameter and 10-cm deep.

A unique Q-switching mechanism has been developed which produces two to three pulses of light per laser firing. The Q-switching action is produced by pumping a ruby rod while it is vibrating. A 2-mm diameter, 50-cm long ruby rod is clamped at its output end and held in cantilever fashion. The free end is pulled down and released to excite vibration at the natural frequency (1000 Hz) of the rod. Optical pumping, initiated by the release of the rod, is provided by a small xenon lamp. Laser output occurs only when the rod passes through its rest position. Initially, pulse durations of 20 μsec were observed; the timing of the xenon flash relative to the release of the rod varied by several tenths of a millisecond and the period between pulses was inexplicably erratic. Mechanical and electronic improvements have resulted in pulse durations of 1 - 10 μsec, xenon flash timing to an accuracy of 2 μsec, and a pulse separation period of 0.510 msec accurate to ±0.008 msec.

Holograms of test targets indicate that the current resolving capability lies in the 5 - 15 μm range. Further refinements are expected to reduce the pulse duration to 1 μsec and improve the resolving capability to about 1 μm. Operating with a system of these characteristics we can expect to characterize 1 μm or greater sized particles at velocities of up to 150 cm/sec and 20 μm or greater sized particles at velocities of up to 3000 cm/sec.

References

REFERENCES

Coal

Campbell, J. A., et al. 1979. "Characterization of Micron-Size Flyash Particles by X-Ray Photoelectron Spectroscopy (ESCA)." Science of the Total Environment 12:75.

Jones, A. R., M. R. Guerin and B. R. Clark. 1977. "Preparative-Scale Liquid Chromatographic Fractionation of Crude Oils Derived from Coal and Shale." Anal. Chem. 49:1766-71.

Klimisch, H. J., and L. Stadler. 1972. "Trennung Komplexer Stoffgemische Lipophiler und Hydrophiler Substanzen Druck Gel-Verteilungschromgto-Graphie on Sephadex LH-20." J. Chromatog. 67:291-7.

Petersen, M. R., J. C. Laul and P. W. Ryan. 1977. "Characterization of Substances in Products, Effluents, and Wastes from a Solvent Refined Coal Pilot Plant." In Part 3 Pacific Northwest Laboratory Annual Report for 1976 to the ERDA Assistant Secretary for the Environment, PNL-2100, pp. 13-17, Pacific Northwest Laboratory, Richland, Washington.

Ryan, P. W., and M. R. Petersen. 1977. Direct Analysis for Polynuclear Aromatic Hydrocarbons at the ppb Levels by GC/MS. BNWL-SA-6496. Pacific Northwest Laboratory, Richland, Washington.

Smith, R. D., J. A. Campbell and K. K. Nielson. 1979a. Atmos. Environ. 13:607-617.

Smith, R. D., J. A. Campbell and K. K. Nielson. 1979b. Environ. Sci. Technol. 13:553-558.

Wise, S. A., et al. 1977. "Chemically-Bonded Aminosilane Stationary Phase for the High-Performance Liquid Chromatographic Separation of Polynuclear Aromatic Compounds." Anal. Chem. 49:2306-10.

Fission

Braby, L. A., and J. M. Nelson. 1979. "Use of High Dose-Rate Electron Beams to Study Cellular Repair Mechanisms." IEEE Transaction Nuclear Science NS-26:1758-1762.

Braby, L. A., and W. C. Roesch. 1978a. "Direct Measurement of f(z) for Fast Electrons." In Proceedings of the Sixth Symposium on Microdosimetry, ed. J. Booz and H. G. Ebert, pp. 251-260. Harwood Academic Publishers, London.

Braby, L. A., and W. C. Roesch. 1978b. "Testing of Dose-Rate Models with Chlamydomonas reinhardi." Radiat. Res. 76:259-270.

Braby, L. A., and W. C. Roesch. 1979. "A Noise-Free Determination of $\bar{z}_1$." In Part 4 of Pacific Northwest Laboratory Annual Report for 1978 to the DOE Assistant Secretary for Environment, PNL-2850, pp. 2.32-2.34, Pacific Northwest Laboratory, Richland, Washington.

Brandt, D., M. Prost and N. Stolterfoht. 1979. "Decay of Collisonally Excited Autoionization States of Helium in the Field of the Slow Li^+ Projectile." In Abstracts of Papers, IX ICPEAC, pp. 660-661. The Society for Atomic Collision Research, Japan.

Christophorous, L. G. 1976. "Electron Attachment to Molecules in Dense Gases ("Quasi-liquids")." Chem. Rev. 76:409-423.

Criswell, T. L., L. H. Toburen and M. E. Rudd. 1977. "Energy and Angular Distribution of Electrons Ejected from Argon by 5 keV to 1.5 MeV Protons." Phys. Rev. 16:508-517.

Dillon, M. A., and M. Burton. 1965. "Excitation Transfer and Decay Processes in Multi-Component Systems: Cyclohexane + benzene + p-Terphenyl." In Pulse Radiolysis, ed. M. Ebert, J. P. Keen, and A. J. Swallow, pp. 259. Academic Press, New York.

Elkind, M. M., and G. F. Whitmore. 1967. The Radiobiology of Cultured Cells, pp. 237-302. Gordon and Breach, New York.

Fuchs, C., and F. Heisel. 1978. "Temporal Analysis of the Delayed Fluorescence in Isotropic and Anisotropic Aromatic Media Under Electron Excitation." Radiat. Phys. Chem. 12:95-105.

Ganguly, A. K., and J. Magee. 1956. "Theory of Radiation Chemistry. III. Radical Reaction Mechanism in Tracks of Ionizing Radiation." J. Chem. Phys. 25:129-134.

Glass, W. A., and W. E. Gross. 1972. Radiation Dosimetry, Suppl. 1. Academic Press, New York.

Glass, W. A., and W. C. Roesch. 1972. "Measurements of Ionization Distributions in Tissue-Equivalent Gas." Radiat. Res. 49:477-494.

Gregory, T. A., and W. P. Helman. 1972. "Temperature Dependence of Specific Rates of Benzene Monomer and Excimer Fluorescence." J. Chem. Phys. 56:377-385.

Hahn, G. M., and J. B. Little. 1972. "Plateau Phase Cultures of Mammalian Cells: An in vitro Model for Human Cancer." Curr. Topics in Radiat. Res. Q. 9:39-83.

Johnson, C. H. 1975. "A Ring Lens for Focusing Ion Beams to Uniform Densities." Nucl. Instr. & Meth. 127:163-171.

Kaye, J. H., and N. E. Ballou. 1978. "Determination of Technetium by Graphite Furnace Atomic Absorption Spectrometry." Anal. Chem. 50:2076.

Kaye, J. H., M. S. Rapids and N. E. Ballou. 1977. "Determination of Picogram Levels of Technetium-99 by Isotope Dilution Mass Spectrometry." Proceedings of Third International Conference on Nuclear Methods in Environmental and Energy Research, U.S. Department of Energy publication CONF-771072, p. 210. Columbia, Missouri.

Kaye, J. H., M. S. Rapids and N. E. Ballou. 1979. "A Quantitative Radiochemical Method for Determination of ^{99}Tc." PNL-SA-7026, Pacific Northwest Laboratory, Richland, Washington.

Kellerer, A. M. 1970. "Analysis of Patterns of Energy Deposition." In Proceedings of the Second Symposium on Microdosimetry, ed. H. G. Ebert, p. 107-134. Euratom, Brussels.

Kellerer, A. M., and H. H. Rossi. 1972. "The Theory of Dual Radiation Action." Curr. Topics in Radiat. Res. Q. 8:85-158.

Kupperman, A. 1974. "Diffusion Kinetics in Radiation Chemistry: An Assessment." In Physical Mechanisms in Radiation Biology, pp. 155-197. U.S. Atomic Energy Commission.

Little, J. B., and J. R. Williams. 1976. "Enhancement of Survival of Irradiated Plateau Phase Cells by Dinitrophenol: Effect of Dose Rate and Cell Strain." Radiat. Res. 66:90-99.

Malcolm, A. W., and J. B. Little. 1978. "Rapid Split-Dose Recovery in Irradiated Human Diploid Cells." Radiat. Res.

Manson, S. T., and L. H. Toburen. 1977. "Energy and Angular Distribution of Electrons Ejected from Kr by 1 MeV Proton Impact Ionization: Theory and Experiment." In Abstracts of Papers, X ICPEAC, pp. 990-991. Commissariat A L'Energie Atomic, Paris.

Manson, S. T., et al. 1975. "Energy and Angular Distribution of Electrons Ejected from Helium by Fast Protons and Electrons: Theory and Experiment." Phys. Rev. A. 12:60-79.

Miller, J. H., and A. E. S. Green. 1973. "Proton Energy Degradation in Water Vapor." Radiat. Res. 54:343-363.

Miller, J. H., and M. L. West. 1977. "Quenching of Benzene Fluorescence in Pulsed Proton Irradiation: Dependence on Proton Energy." J. Chem. Phys. 67:2793-2797.

Miller, J. H., and M. L. West. 1978. "Nonhomogeneous Chemical Kinetics in Pulsed Proton Irradiation." Biophys. J. 24:376-379.

Miller, J. H., and M. L. West. 1979. "Track Structure Effects in the Quenching of Proton and Alpha Particle Induced Luminescence." In VI International Congress of Radiation Research, pp. 202. Japanese Association for Radiation Research, Tokyo.

Nelson, J. M. 1979. "Noncycling Plateau Phase Mammalian Cells." In Part 4 of Pacific Northwest Laboratory Annual Report for 1978 to the DOE Assistant Secretary for Environment, PNL-2850, pp. 2.29-2.31, Pacific Northwest Laboratory, Richland, Washington.

Nelson, J. M., L. A. Braby and W. C. Roesch. 1979a. "Rapid Repair Processes in Irradiated Chlamydomonas reinhardi." In Part 4 of Pacific Northwest Laboratory Annual Report for 1978 to the DOE Assistant Secretary for Environment, PNL-2850, pp. 2.26-2.27, Pacific Northwest Laboratory, Richland, Washington.

Nelson, J. M., L. A. Braby and W. C. Roesch. 1979 (In Press). "Characterization of Rapid Recovery in Chlamydomonas reinhardi." Radiat. Res. PNL-6751A, Pacific Northwest Laboratory, Richland, Washington.

Nielson, K. K. 1977. "Matrix Correction for Energy Dispersive X-Ray Fluorescence Analysis of Environmental Samples with Coherent/Incoherent Scattered X-Rays." Anal. Chem. 49:641-648.

Olivero, J. J., R. W. Staget and A. E. S. Green. 1972. "Electron Deposition in Water Vapor with Atmospheric Applications." J. Geophys. Res. 72:3933-3941.

Paretzke, H. 1973. In Proceedings of the Fourth Symposium on Microdosimetry, September 24-28, 1973. Verbania, Pallanza, Italy.

Payne, M. G., and W. R. Garrett. 1975. "Models for Cell Survival with Low LET Radiation." Radiat. Res. 62:169-179.

Raju, M. R., and J. H. Jett. 1974. "RBE and OER Variations in Mixtures of Plutonium Alpha Particles and X-Rays for Damage to Human Kidney Cells (T-1)." Radiat. Res. 60:473-481.

Roesch, W. C. 1975. "Theory of LET Effects." In Part 4 of Pacific Northwest Laboratory Annual Report to the DOE Assistant Secretary for Environment, PNL-2850, pp. 69-71, Pacific Northwest Laboratory, Richland, Washington.

Roesch, W. C. 1977. "Microdosimetry of Internal Sources." Radiat. Res. 70:494-510.

Roesch, W. C. 1978a. "Models of the Radiation Sensitivity of Mammalian Cells." In Third Symposium on Neutron Dosimetry in Biology and Medicine, pp. 1-27. Commission of the European Communities, Luxembourg.

Roesch, W. C. 1978b. "Dose-Rate and Fractionation Theory for Multiple Recovery Processes." In Part 4 of Pacific Northwest Laboratory Annual Report to the DOE Assistant Secretary for Environment, PNL-2850, pp. 2.15-2.17, Pacific Northwest Laboratory, Richland, Washington.

Roesch, W. C. 1979a. "Calculations for Microdosimetry of Internal Sources." In Part 4 of Pacific Northwest Laboratory Annual Report for 1978 to the DOE Assistant Secretary for Environment, PNL-2850, p. 2.37, Pacific Northwest Laboratory, Richland, Washington.

Roesch, W. C. 1979b (In Press). "Microdosimetry for Radiation Non-Equilibrium." In Proceedings of the Sixth International Congress of Radiation Research. Japanese Association for Radiation Research, Tokyo.

Rudd, M. E., and J. H. Macek. 1972. "Electron Production in Ion-Atom Collisions." Case Studies in Atomic Physics 3:47-136.

Rudd, M. E., and J. Macek. 1979. "A New Description of Electron Ejection by Low Energy Protons." In Abstracts of Papers, IX ICPEAC, pp. 626-627. Society for Atomic Collisions Research, Japan.

Rudd, M. E., L. H. Toburen and N. Stolterfoht. 1979 (In Press). "Differential Cross Sections for Ejection of Electrons from Argon by Protons." Atomic Data and Nuclear Data Tables. PNL-SA-7908, Pacific Northwest Laboratory, Richland, Washington.

Samuel, A. H., and J. Magee. 1953. "Theory of Radiation Chemistry: II. Track Effects in Radiolysis of Water." J. Chem. Phys. 21:1080-1087.

Schwarz, H. A. 1968. "Application of the Spur Diffusion Model to the Radiation Chemistry of Aqueous Solutions." J. Phys. Chem. 78:1928-1937.

Stolterfoht, N. 1978. "Excitation in Energetic Ion-Atom Collisions Accompanied by Electron Emission." In Topics in Current Physics, Vol. 5, ed. I. A. Sellin, pp. 152-199. Springer-Verlag, Berlin.

Stolterfoht, N. 1979. "Angular Distributions of Autoionization Electrons from Post-Collision Mixed States." In Abstracts of Papers XI ICPEAC, pp. 656-657. The Society for Atomic Collisions Research, Japan.

Sullivan, M. F. 1978. "Absorption of Actinide Elements from the Gastrointestinal Tract of Neonatal Animals." PNL-SA-7104, Pacific Northwest Laboratory, Richland, Washington.

Tobias, C. A. 1971. "Physical Energy Transfer and Biological Effect." In Advances in Medical Physics, ed. J. S. Laughlin and E. W. Webster, pp. 28-50. Second International Conference on Medical Physics, Boston, Massachusetts.

Toburen, L. H. 1979. "Differential Cross Sections for Electron Emission in Heavy-Ion Collisions." In Proceedings of the 1978 Conference on the Application of Small Accelerators in Research and Industry, ed. J. L. Duggan and J. L. Morgan. IEEE Transactions on Nuclear Science NS-26:1056-1061.

Toburen, L. H., S. T. Manson and Y.-Ki. Kim. 1978. "Energy Distributions of Secondary Electrons. III. Projectile Energy Dependence for Ionization of He, Ne, and Ar by Protons." Phys. Rev. A. 17:148-159.

Toburen, L. H., and W. E. Wilson. 1977. "Energy and Angular Distribution of Electrons Ejected from Water Vapor by 0.3-1.5 MeV Protons." J. Chem. Phys. 66:5202-5213.

Toburen, L. H., and W. E. Wilson. 1979a (In Press). "Secondary Electron Emission in Ion-Atom Collisions." In Proceedings of the VI International Congress on Radiation Research. Japanese Association for Radiation Research, Tokyo.

Toburen, L. H., and W. E. Wilson. 1979b. "Differential Cross Sections for Ionization of Argon by 0.3-2.0 MeV He^{2+} and He^{+} Ions." Phys. Rev. 19:2214-2224.

Toburen, L. H., W. E. Wilson and R. J. Popowich. 1979 (In Press). "Secondary Electron Emission from Ionization of Water Vapor by 0.3-2.0 MeV He^{+} and He^{2+} Ions." Radiat. Res. PNL-SA-7124, Pacific Northwest Laboratory, Richland, Washington.

Todd, P., et al. 1968. "Pulsed High-Intensity Roentgen Rays." Acta Radiol. 7:22-26.

Walker, R. L. 1978. Report at 22nd Conference on Analytical Chemistry in Energy Technology, October 10-12, Gatlinburg, Tennessee.

Weitkamp, W. G., and F. H. Schmidt. 1974. "The University of Washington Three-Stage Tandem Van de Graaff Accelerator." Nuc. Instr. & Meth. 122:65-69.

West, M. L., and J. H. Miller. 1978. "Experimental Studies of Fluorescence Quenching in Pulsed Proton Irradiation." In Part 2 of Pacific Northwest Laboratory Annual Report for 1978 to the DOE Assistant Secretary for Environment, PNL-2850, p. 2.19, Pacific Northwest Laboratory, Richland, Washington.

West, M. L., and J. H. Miller. 1979. "Quenching of Benzene Fluorescence in Pulsed Proton Irradiation: Temperature Dependence." J. Phys. Chem. 83:1205-1207.

West, M. L., and J. H. Miller. 1979. "Quenching of Fluorescence for Proton and Alpha Particle Irradiation." In University of Washington Nuclear Physics Laboratory Annual Report, p. 127. University of Washington Press, Seattle, Washington.

Wilson, W. E. 1978. "Analytical Expression for Cross Section Data." In Part 4 of Pacific Northwest Laboratory Annual Report for 1977 to the DOE Assistant Secretary for Environment, PNL-2850, pp. 2.7-2.9, Pacific Northwest Laboratory, Richland, Washington.

Wilson, W. E., and L. H. Toburen. 1975. "Electron Emission from Proton-Hydrocarbon-Molecule Collisions at 0.3-2.0 MeV." Phys. Rev. A. 11:1303-1308.

Wilson, W. E., L. H. Toburen and H. G. Paretzke. 1978. "Calculation of Energy Deposition Spectra in Small Gaseous Sites and Its Applicability to Condensed Phase." In Proceedings of Sixth Symposium on Microdosimetry, ed. J. Booz and H. G. Ebert, pp. 239-250. Harwood Academic Publishers, London.

Wilson, W. E., L. H. Toburen and H. G. Paretzke. 1979. "Ionization Distributions in Condensed Phase." In Part 4 of Pacific Northwest Laboratory Annual Report for 1978 to the DOE Assistant Secretary for Environment, PNL-2850, pp. 2.11-2.12, Pacific Northwest Laboratory, Richland, Washington.

Woerlee, P. H., et al. 1979. "Continuous Electron Spectra Produced in Ne^{n+}-Ne Collisions." In Abstracts of Papers, XI ICPEAC, pp. 748-749. Society for Atomic Collision Research, Japan.

Wogman, N. A., R. W. Perkins and J. H. Kaye. 1969. "An All Sodium Iodide Anticoincidence Shielded Multidimensional Gamma-Ray Spectrometer for Low-Activity Samples." N.I.M. 74:197-212.

Oil Shale

Ames Laboratory. 1977. Quarterly Report to the Energy Research and Development Administration. Activity RX-02-03. Iowa State University, Ames, Iowa.

Fruchter, J. S., M. R. Petersen and J. C. Laul. 1979. "Characterization of Products, Effluents and Wastes from Oil Shale Retort Pilot Plants." In Part 4 of Pacific Northwest Laboratory Annual Report for 1976 to the ERDA Assistant Secretary for Environment, PNL-2100, Pacific Northwest Laboratory, Richland, Washington.

Fruchter, J. S., et al. 1979. Source Characterization Studies PARAHO SEMI Works Retort. PNL-2945, Pacific Northwest Laboratory, Richland, Washington.

Hitchon, B., R. H. Filby and K. R. Shah. 1975. "Geochemistry of Trace Elements in Crude Oils, Alberta, Canada." In The Role of Trace Metals in Petroleum, ed. T. F. Yen. Ann Arbor Science Publishers, Inc., Ann Arbor, Michigan.

Jones, A. R., M. R. Guerin and B. R. Clark. 1977. "Preparative-Scale Liquid Chromatographic Fractionation of Crude Oils Derived from Coal and Shale." Anal. Chem. 49:1766-71.

Klimisch, H. J., and L. Stadler. 1972. "Trennung Komplexer Stoffgemische Lipophiler und Hydrophiler Substanzen Druck Gel-Verteilungschromgto-Graphie on Sephadex LH-20." J. Chromatog. 67:291-7.

Pelroy,. R. A., J. T. Cresto and M. R. Petersen. 1979. "Mutagenicity of Shale Oil and Solvent Refined Coal Products." In Part 1 of Pacific Northwest Laboratory Annual Report to DOE Assistant Secretary for Environment, PNL-2880, pp. 5.5-5.9, Pacific Northwest Laboratory, Richland, Washington.

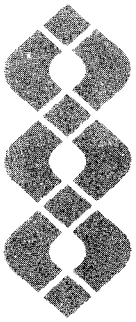

Publications and Presentations

PUBLICATIONS

Bean, R. M., et al. 1979. "Organohalogen Production from Chlorination of Natural Waters Under Simulated Biofouling Control Conditions." In Proceedings of the Third Conference on Water Chlorination: Environmental Impact and Health Effects, October 28-November 2, Colorado Springs, Colorado.

Braby, L. A., and J. M. Nelson. 1979. "Use of High Dose-Rate Electron Beams to Study Cellular Repair Mechanisms." In Proceedings of the 1978 Conference on the Applications of Small Accelerators in Research and Industry, eds. J. L. Duggan and J. L. Morgan. IEEE Transactions on Nuclear Science NS-26:1758-1762.

Braby, L. A., and W. C. Roesch. 1978. "Direct Measurement of f(z) for Fast Electrons." In Proceedings of Sixth Symposium on Microdosimetry, eds. J. Booz and H. G. Ebert, pp. 251-260. Harwood Academic Publishers, London.

Brauer, F. P., and R. S. Strebin, Jr. 1979. "Standard Materials for Iodine Activation Analysis." In Proceedings of the Nuclear Activation Techniques in the Life Sciences, pp. 27-35, IAEA-SM-227/65. International Atomic Energy Agency, Vienna, Austria.

Brauer, F. P., W. A. Mitzlaff and J. E. Fager. 1978. "Uranium and Plutonium Analyses with Well-Type Ge(Li) Detectors." In ACS Symposium Series 79, Nuclear Safeguards Analysis, pp. 144-157.

Brodzinski, R. L. 1979. "In Situ Radiation Measurements and Instrumentation for Monitoring Nuclear Waste Storage Facilities." To be published in Proceedings of the IEEE Short Course: An Introduction to Nuclear Waste Management and Storage, San Francisco, California.

Brodzinski, R. L. 1979. "A Technique for the In Situ Determination of Transuranium Elements in Relatively Inaccessible Locations." Submitted for publication to Nucl. Instrum. & Methods. PNL-SA-7260, Pacific Northwest Laboratory, Richland, Washington.

Brodzinski, R. L. 1979. "A Technique for In Situ Moisture Level Determinations in Relatively Inaccessible Matrices." Submitted for publication to Nucl. Instrum. & Methods. PNL-SA-7259, Pacific Northwest Laboratory, Richland, Washington.

Brodzinski, R. L., and H. L. Nielson. 1979. "A Well Logging Technique for the In Situ Determination of ^{90}Sr." Submitted for publication to Nucl. Instrum. & Methods. PNL-SA-7246, Pacific Northwest Laboratory, Richland, Washington.

Brodzinski, R. L., et al. 1979. "An Instrument for Determining the Transuranic Element Content of Chopped Leached Fuel Hulls and Other Materials." In Proceedings of the 20th Annual Meeting of the Institute of Nuclear Materials Management, p. 438, Albuquerque, New Mexico.

Campbell, J. A., et al. 1979. "Characterization of Micron-Size Flyash Particles by X-Ray Photoelectron Spectroscopy (ESCA)." Sci. Total Environ. 12:75.

Christensen, D. C., and W. C. Weimer. 1979 (In Press). "Enhanced Photodegradation of Persistent Halogenated Organic Wastes." In Proceedings of the 34th Annual Purdue Industrial Waste Conference. Lafayette, Indiana.

Evans, J. C., and C. L. Wilkerson. 1979. "Arsenic Analysis in Oil Shale Process Water." In Proceedings of Committee D-19 on Water, American Society for Testing Materials (ASTM), Pittsburgh, Pennsylvania.

Fox, J. P., et al. 1979. "Inter-comparison Study of Elemental Abundances in Raw and Spent Oil Shales." In Proceedings of the EPA Symposium on Sampling Analysis and Quality Assurance of Oil Shale Materials, Denver, Colorado.

Fruchter, J. S., et al. 1978. "High Precision Trace Element and Organic Constituent Analysis of Oil Shale and Solvent-Refined Coal Particles." In Analysis of Oil Shale and Tar Sand (Comparison with Coal and Petroleum). Advances in Chemistry Series 170, pp. 255-281.

Fruchter, J. S., C. L. Wilkerson and J. C. Evans. 1979. "Redistribution of Elements and Species During Retorting at an Above-Ground Oil Shale Pilot Plant." In Proceedings of the 12th Oil Shale Symposium, April 18-20, Golden, Colorado.

Fruchter, J. S., et al. 1979. "Analysis of Paraho Oil Shale Products and Effluents: An Example of the Multitechnique Approach." In Proceedings of the EPA Symposium on Sampling Analysis and Quality Assurance of Oil Shale Materials, Denver, Colorado.

Garcia, S. R., K. B. Olsen and D. R. Kalkwarf. 1979. "Trace Element Concentrations in Colstrip's Coal-Fired Power Plant Plume." Submitted to Env. Science and Technology. PNL-SA-7805, Pacific Northwest Laboratory, Richland, Washington.

Kaye, J. H. 1979. "Tellerium Interference of ^{129}I Activation Analysis." In Proceedings of the 23rd ORNL Conference on Analytical Chemistry and Energy Technology, Gatlinburg, Tennessee.

Kaye, J. H., and N. E. Ballou. 1978. "Determination of Technetium by Graphite Furnace Atomic Absorption Spectrometry." Anal. Chem. 50:2076-2078.

Laul, J. C., W. C. Weimer and L. A. Rancitelli. 1979. Biogeochemical Distribution of Rare Earths and Other Trace Elements in Plants and Soils, ed. G. Protas, pp. 819-827, Pergammon Press, New York.

Lessor, D. L., J. S. Hartman and R. L. Gordon. 1979. "Quantitative Surface Topography Determination by Normarski Reflection Microscopy. 1. Theory." J. of Optical Soc. of America 69(2):357-366.

Miller, J. H., and M. L. West. 1979. "Pulsed Proton Radioluminescence in Binary Liquid Scintillators." In Proceedings of the 1978 Conference on the Application of Small Accelerators in Research and Industry, eds. J. L. Duggan and J. L. Morgan. IEEE Transactions on Nuclear Science NS-26:1765-68.

Miller, J. H., and M. L. West. 1979. "Track Structure Effects in the Quenching of Proton and Alpha Particle Induced Luminescence" (abstract). In Proceedings of the Sixth International Congress of Radiation Research, p. 202, Japanese Association for Radiation Research, Tokyo.

Nelson, J. M., L. A. Braby and W. C. Roesch. 1979 (In Press). "Characterization of Rapid Recovery in Chlamydomonas reinhardi." Radiation Res. PNL-6751A, Pacific Northwest Laboratory, Richland, Washington.

Roesch, W. C. 1979. "Microdosimetry f[illegible] Radiation Nonequilibrium." In Proceed[illegible] of the Sixth International Congress of [illegible] diation Research. Japanese Association f[illegible] Radiation Research, Tokyo.

Roesch, W. C., J. M. Nelson and L. A. Braby. 1979. "Repair in Mitotic CHO Cells" (abstract). In Proceedings of Sixth International Congress of Radiation Research, p. 220, Japanese Association for Radiation Research, Tokyo.

Rudd, M. E., L. H. Toburen and N. Stolterfoht. 1979 (In Press). "Differential Cross Sections for Ejection of Electrons from Argon by Protons." Atomic Data and Nuclear Data Tables. PNL-SA-7908, Pacific Northwest Laboratory, Richland, Washington.

Smith, R. D. 1979. "A Direct Mass Spectrometric Study of the Mechanism of Toluene Pyrolysis at High Temperatures." J. Phys. Chem. 83:1553.

Smith, R. D. 1979. "Formation of Radicals and Complex Organic Compounds by High Temperature Pyrolysis: The Pyrolysis of Toluene." Combustion and Flame 35:179.

Smith, R. D. 1979. "Mass Spectrometric Study of the Thermal Pyrolysis of S_4N_4 over Quartz Wool and Silver Wool." Chem. Soc., Dalton Trans., p. 478.

Smith, R. D. 1979. "The Trace Element Chemistry of Coal During Combustion and the Emissions from Coal-Fired Plants." Accepted for publication in Progress in Energy and Combustion Science. PNL-SA-7552, Pacific Northwest Laboratory, Richland, Washington.

Smith, R. D., J. A. Campbell and K. K. Nielson. 1979. "Characterization and Formation of Submicron Particles in Coal-Fired Plants." Atmos. Environ. 13:607.

Smith, R. D., J. A. Campbell and K. K. Nielson. 1979. "Concentration Dependence upon Particle Size of Volatilized Elements in Fly Ash." Environ. Sci. Technol. 13:553.

Smith, R. D., J. A. Campbell and K. K. Nielson. 1979. "Volatility of Fly Ash and Coal." Accepted for publication in Fuel. PNL-SA-7306, Pacific Northwest Laboratory, Richland, Washington.

Stoffels, J. J., and D. R. Ells. 1979. "Electropolishing the Bore of Metal Capillary Tubes: A Technique for Adjusting the Critical Flow." Review of Science Instruments, Vol. 50.

Styris, D. L., et al. 1979. "Plasma-Wall Interaction and the Tokamak Fusion Reactor." In Proceedings of First International Conference on Alternative Energy Sources, 5:2477-2497.

Toburen, L. H. 1978. "Secondary Electron Emission Resulting from Ionization of Argon by Carbon Ions." Bull. Am. Phys. Soc. 23:1087.

Toburen, L. H. 1979. "Differential Cross Sections for Electron Emission in Heavy Ion-Atom Collisions." In Proceedings of the 1978 Conference on the Application of Small Accelerators in Research and Industry, eds. J. L. Duggan and J. L. Morgan. IEEE Trans. on Nuclear Science NS-26:1056-1061.

Toburen, L. H., and W. E. Wilson. 1979. "Differential Cross Sections for Ionization of Argon by 0.3-2.0 MeV He^{2+} and He^{+} Ions." Phys. Rev. 19:2214-2224.

Toburen, L. H., and W. E. Wilson. 1979. "Secondary Electron Emission in Collisions of Heavy Ions with Atoms and Molecules" (abstract). In Proceedings of Sixth International Congress of Radiation Research, p. 87, Japanese Association for Radiation Research, Tokyo.

Toburen, L. H., W. E. Wilson and R. J. Popowich. 1979 (In Press). "Secondary Electron Emission from Ionization of Water Vapor by 0.3-2.0 MeV He^{+} and He^{2+} Ions." Radiat. Res. PNL-SA-7124, Pacific Northwest Laboratory, Richland, Washington.

Weimer, W. C., and D. E. Armstrong. 1979. "Naturally Occurring Organic Phosphorus Compounds in Rooted and Free-Floating Aquatic Plants." Environ. Sci. Tech. 13:826-829.

Weimer, W. C., J. C. Laul and J. C. Kutt. 1979 (In Press). "Prediction of the Ultimate Biological Availability of Transuranium Elements in the Environment." In Contaminants and Sediments, ed. R. A. Baker, Ann Arbor Science, Ann Arbor, Michigan.

West, M. L., and J. H. Miller. 1979. "Quenching of Benzene Fluorescence in Pulsed Proton Irradiation. Temperature Dependence." J. Phys. Chem. 83:1205-07.

West, M. L., and J. H. Miller. 1979. "Quenching of Fluorescence for Proton and Alpha Particle Irradiation." In University of Washington Nuclear Physics Laboratory Annual Report, p. 127, University of Washington Press, Seattle, Washington.

Wilson, W. E., and H. G. Paretzke. 1978. "Calculation of Proton Ejection of Electrons from Foils." Bull. Am. Phys. Soc. 23:1106.

Wilson, B. W., and R. W. Pelroy. 1979. "Mass Spectral Analysis of Mutagenically Active Subfractions from Coal Liquids." In Proceedings of the 27th Conference of the American Society of Mass Spectrometry, Seattle, Washington.

Wilson, B. W., R. A. Pelroy and J. T. Cresto. 1979. "Gas Chromatography - Mass Spectrometry and Mutagenic Analyses of Several Coal Liquefaction Materials." Submitted for publication to Mutation Research. PNL-SA-8146, Pacific Northwest Laboratory, Richland, Washington.

Wilson, W. E., L. H. Toburen and H. G. Paretzke. 1979. "Calculation of Energy Deposition Spectra in Small Gaseous Sites and Its Applicability to Condensed Phase." In Proceedings of the Sixth Symposium on Microdosimetry, eds. J. Booz and H. G. Ebert, pp. 239-250. Harwood Academic Publishers, London.

Wogman, N. A., R. L. Brodzinski and D. P. Brown. 1979. "Evaluation of a Phoswich Detector for the In Situ Analysis of ^{90}Sr." In Proceedings of the IEEE Nuclear Science Symposium, San Francisco, California.

PRESENTATIONS

Bean, R. M., et al. 1979. "Aqueous Suspensions of Solvent Refined Coal Liquids: Effects of Preparation Procedure on Chemical Composition and Toxicity." Presented at the Fourth ASTM Symposium on Aquatic Toxicology, October 16-17, 1978, Chicago, Illinois.

Braby, L. A., W. C. Roesch and J. M. Nelson. 1979. "Repair of Radiation Damage: Effects on RBE." PNL-SA-7510. Presented at the Health Physics Society Meeting, July 8-13, 1979, Philadelphia, Pennsylvania.

Brodzinski, R. L. 1979. "In Situ Radiation Instruments and Instrumentation for Monitoring Nuclear Waste Storage Facilities." Presented at the IEEE Short Course, An Introduction to Nuclear Waste Management and Storage, October 20, 1979, San Francisco, California.

Brodzinski, R. L. 1979. "Small Package Counting at PNL." Presented at the LASL/DOE Radioactive Waste Assay Instrumentation Workshop, October 23-25, 1979, Los Alamos, New Mexico.

Brodzinski, R. L. 1979. "A Technique for the In Situ Determination of Transuranic Elements in Relatively Inaccessible Locations." PNL-SA-7260. Presented at the ACS-CSJ Chemical Congress, April 1-6, 1979, Honolulu, Hawaii.

Brodzinski, R. L. 1979. "A Technique for In Situ Moisture Level Determinations in Relatively Inaccessible Matrices." PNL-SA-7259. Presented at the ACS-CSJ Chemical Congress, April 1-6, 1979, Honolulu Hawaii.

Brodzinski, R. L., et al. 1979. "Waste Assay Matrix, Accuracy, Sensitivity, Interference, and Container Size Considerations." Panel presentation at the LASL/DOE Radioactive Waste Assay Instrumentation Workshop, October 23-25, 1979, Los Alamos, New Mexico.

Brodzinski, R. L., and H. L. Nielson. 1979. "A Well Logging Technique for the In Situ Determination of ^{90}Sr." PNL-SA-7246. Presented at the ACS-CSJ Chemical Congress, April 1-6, 1979, Honolulu, Hawaii.

Brodzinski, R. L., et al. 1979. "An Instrument for Determining the Transuranic Element Content of Chopped Leached Fuel Hulls and Other Materials." PNL-SA-8548. Presented at the ACS-CSJ Chemical Congress, April 1-6, 1979, Honolulu, Hawaii.

Brodzinski, R. L., et al. 1979. "An Instrument for Determining the Transuranic Element Content of Chopped Leached Fuel Hulls and Other Materials." Presented at the Symposium on Recent Advances in Analytical Technology for Nuclear Waste, 34th Northwest Regional Meeting, American Chemical Society, June 13-15, 1979, Richland, Washington.

Brodzinski, R. L., et al. 1979. "An Instrument for Determining the Transuranic Element Content of Chopped Leached Fuel Hulls and Other Materials." Presented at the Institute of Nuclear Materials Management 20th Annual Meeting, July 16-18, 1979, Albuquerque, New Mexico.

Campbell, J. A., and R. D. Smith. 1979. "The Association of Trace Elements in Coal." PNL-SA-7598. Presented at the Symposium on Recent Advances in Analytical Technology for Nuclear Waste, 34th Northwest Regional Meeting, American Chemical Society, June 13-15, 1979, Richland, Washington.

Christensen, D. C., and W. C. Weimer. 1979. "Enhanced Photodegradation of Persistent Halogenated Organic Materials." Presented at the 34th Annual Purdue Industrial Waste Conference, May 7-10, 1979, West Lafayette, Indiana.

Crecelius, E. A. 1979. "Atmospheric Input of Particulate Elements Along the Washington Coast." PNL-SA-7686A. Presented at the DOE Workshop on Radionuclides and Metals in the Continental Shelf Environments, March 7-9, 1979, Washington, D.C.

Crecelius, E. A., et al. 1979. "Background Air Particulate Chemistry Near Colstrip, Montana." PNL-SA-7397. Presented at the American Chemical Society Northwest Regional Meeting, June 13-15, 1979, Richland, Washington.

Evans, J. C., and C. L. Wilkerson. 1979. "Arsenic Analysis in Oil Shale Process Water." PNL-SA-7532A. Presented at the Meeting of Committee D-19 on Water, American Society for Testing Materials, June 4-8, 1979, Pittsburgh, Pennsylvania.

Fager, J. E., and F. P. Brauer. 1979. "Analysis of Fissile Materials in Heterogeneous Matrices." PNL-SA-7219A. Presented at the Symposium on Recent Advances in Nuclear Analytical Techniques Sponsored by the American Chemical Society, Division of Nuclear Chemistry and Technology, April 1-6, 1979.

Felix, W. D., M. R. Petersen and W. C. Weimer. 1979. "The Solvent Refining of Coal: Progress of Technology and Chemical Characterization." Presented at the American Chemical Society Northwest Regional Meeting, June 13-15, 1979, Richland, Washington.

Fruchter, J. S. 1979. "Some Potential Environmental Aspects of Using Oil Shale as an Energy Source." PNL-SA-7504. Presented at the Health Physics Society Meeting, July 8-13, 1979, Philadelphia, Pennsylvania.

Fruchter, J. S., C. L. Wilkerson and J. C. Evans. 1979. "Redistribution of Elements and Species During Retorting at an Above-Ground Oil Shale Pilot Plant." PNL-SA-7435A. Presented at the 12th Oil Shale Symposium, Sponsored by the Colorado School of Mines, April 18-20, 1979, Golden, Colorado.

Fruchter, J. S., et al. 1979. "Analysis of Paraho Oil Shale Products and Effluents: An Example of the Multitechnique Approach." PNL-SA-7579. Presented at the EPA Symposium on Sampling, Analysis, and Quality Assurance of Oil Shale Materials, March 1979, Denver, Colorado.

Garcia, S. R., K. B. Olsen and D. R. Kalkwarf. 1979. "Trace Element Concentrations in Colstrip's Coal-Fired Power Plant Plume." PNL-SA-7805A. Presented at the 34th American Chemical Society Northwest Regional Meeting, June 13-15, 1979, Richland, Washington.

Kalkwarf, D. R. 1979. "Permeability of Phospholipid Bilayer Membranes to SO_3/HSO_3^-." Presented at the 178th National Meeting of the American Chemical Society, September 9-14, 1979, Washington, D.C.

Kelley, J. M., and D. M. Robertson. 1979. "Processes Affecting Plutonium Desorption from Carburized and Metallic Rhenium." PNL-SA-7222A. Presented at the ACS/CSJ Chemical Congress, April 1-6, 1979, Honolulu, Hawaii.

Kutt, J. C., J. A. Campbell and W. C. Weimer. 1979. "Characterization of Electro-Chemically Active Species in Oil Shale Process Water." Presented at the American Chemical Society Regional Meeting, June 13-15, 1979, Richland, Washington.

Kutt, J. C., and W. C. Weimer. 1979. "The Electroanalytical Determination of Se(IV) in Environmental Matrices Using a Static Mercury Drop Electrode." Presented at the American Chemical Society Northwest Regional Meeting, June 13-15, 1979, Richland, Washington.

Lepel, E. A., et al. 1979. "Background Air Particulate Chemistry near Colstrip, Montana." PNL-SA-7806A. Presented at the 34th American Chemical Society Regional Meeting, June 13-15, 1979, Richland, Washington.

Ludwick, J. D., et al. 1979. "Air Quality Measurements in the Coal-Fired Power Plant Environment of Colstrip, Montana. PNL-SA-7753. Presented at the 34th American Chemical Society Northwest Regional Meeting, June 13-15, 1979, Richland, Washington.

Miller, J. H., and M. L. West. 1979. "Track Structure Effects in the Quenching of Proton and Alpha Particle Induced Luminescence." PNL-SA-7363. Presented at the Sixth International Congress on Radiation Research, May 13-19, 1979, Tokyo, Japan.

Nielson, H. L., and R. L. Brodzinski. 1979. "Gamma-Ray Spectrometry for Process Control in Nuclear Waste Vitrification." Presented at the Symposium on Recent Advances in Analytical Technology for Nuclear Waste, 34th Northwest Regional Meeting, American Chemical Society, June 13-15, 1979, Richland, Washington.

Reeder, P. L., and R. A. Warner. 1979. "Energy Spectra and Average Energies of Delayed Neutron Precursors." PNL-SA-1790A. Presented at the ACS/CSJ Chemical Congress, April 1-6, 1979, Honolulu, Hawaii.

Reeder, P. L., and R. A. Warner. 1979. "Measurement of Average Neutron Energies by a Counting Rate Ratio Technique." PNL-SA-7536. Presented at the IAEA Consultants Meeting on Delayed Neutron Properties, March 26-30, 1979, Vienna, Austria.

Robertson, D. E., K. H. Abel and E. A. Crecelius. 1979. "Neutron Activation and Cold Vapor Atomic Absorption Techniques Applied to Seawater Analysis." PNL-SA-7298A. Presented at the ACS/CSJ Chemical Congress, April 1-6, 1979, Honolulu, Hawaii.

Roesch, W. C. 1979. "Microdosimetry for Radiation Nonequilibrium." PNL-SA-7417. Presented at the Sixth International Congress on Radiation Research, May 13-19, 1979, Tokyo, Japan.

Roesch, W. C., J. M. Nelson and L. A. Braby. 1979. "Repair in Mitotic CHO Cells." PNL-SA-7374. Presented at the Sixth International Congress on Radiation Research, May 13-19, 1979, Tokyo, Japan.

Schoengold, D. M. 1979. "Selective Chemical Ionization Reagent Gases for Carcinogens in Fuels." PNL-SA-7787A. Presented at the 27th Conference of the American Society of Mass Spectrometry, June 3-8, 1979, Seattle, Washington.

Smith, R. C. 1979. "The High Temperature Pyrolysis of Aromatic Hydrocarbons." PNL-SA-7373A. Presented at the 27th Conference of the American Society of Mass Spectrometry, June 3-8, 1979, Seattle, Washington.

Smith, R. D. 1979. "High Temperature Pyrolysis of Toluene." PNL-SA-7125A. Presented at the 177th National Meeting of the American Chemical Society, April 1-7, 1979, Honolulu, Hawaii.

Smith, R. D. 1979. "Modulated Molecular Beam Mass Spectrometric Studies of the High Temperature Pyrolysis of Hydrocarbons." Presented at the Eighth International Mass Spectrometry Conference, August 12-18, 1979, Oslo, Norway.

Smith, R. D., J. A. Campbell and K. K. Nielson. 1979. "Determination of the Organic Affinities of Trace Elements in Coal." PNL-SA-7212A. Presented at the 177th National Meeting of the American Chemical Society, April 1-6, 1979, Honolulu, Hawaii.

Smith, R. D., et al.. 1979. "Mechanisms of Trace Element Transformation During Coal Combustion." Presented at the American Institute of Chemical Engineers 87th National Meeting, August 19-22, 1979, Boston, Massachusetts.

Smith, R. D., and W. D. Felix. 1979. "Atmospheric Trace Element Pollutants from Coal Combustion." PNL-SA-7547. Presented at the AIME Annual Meeting, February 18-22, 1979, New Orleans, Louisanna.

Toburen, L. H. 1979. "Secondary Electron Emission in Collisions of 1.2 MeV C^+ Ions with He, Ne, Ar, and CH_4." Presented at the Eleventh ICPEAC Meeting, September 3-7, 1979, Kyoto, Japan.

Toburen, L. H., and S. T. Manson. 1979. "Differential Cross Sections for Ionization of Krypton by Fast Protons: Theory and Experiment." PNL-SA-7682. Presented at the Eleventh ICPEAC Meeting, September 3-7, 1979, Kyoto, Japan.

Toburen, L. H., and W. E. Wilson. 1979. "Secondary Electron Emission in Collisions of Heavy Ions with Atoms and Molecules." PNL-SA-7372. Presented at the Sixth International Congress on Radiation Research, May 13-19, 1979, Tokyo, Japan.

Toburen, L. H., and W. E. Wilson. 1979. "Secondary Electron Emission in Ion-Atom Collisions." PNL-SA-7412. Presented at the Sixth International Congress on Radiation Research, May 13-19, 1979, Tokyo, Japan.

Warner, R. A., and P. L. Reeder. 1979. "Fission Fragment Isomer Yield Ratios by an On-Line Technique." PNL-SA-7192A. Presented at the ACS/CSJ Chemical Congress, April 1-6, 1979, Honolulu, Hawaii.

Warner, R. A., et al. 1979. "Delayed Neutron Branches by Gamma Spectroscopy." PNL-SA-7761A. Presented at the Workshop on Nuclear Spectroscopy of Fission Products at the Institute Laue-Langevin, May 22-23, 1979, Grenoble, France.

Warner, R. A., et al. 1979. "Delayed Neutron Emission Probabilities Determined by Gamma-Spectroscopy." PNL-SA-7404A. Presented at the Workshop on Nuclear Spectroscopy of Fission Products, Institute Laue-Langevin, May 22-23, 1979, Grenoble, France.

Weimer, W. C., J. C. Laul and J. C. Kutt. 1979. "Prediction of the Ultimate Biological Availability of Transuranium Elements in the Environment." PNL-SA-7305. Presented at the ACS/CSJ Chemical Congress, April 1-6, 1979, Honolulu, Hawaii.

Wilkerson, C. L., et al. 1979. "Comparison and Contrast of Trace Elements in Crude Shale Oils and Petroleum." PNL-SA-8082A. Presented at the Symposium on Environmental Control in Synfuels Processes, American Chemical Society, March 1979, Houston, Texas.

Wogman, N. A., R. L. Brodzinski and D. P. Brown. 1979. "Evaluation of a Phoswich Detector for the In Situ Analysis of ^{90}Sr." Presented at the IEEE Nuclear Science Symposium, October 17-19, 1979, San Francisco, California.

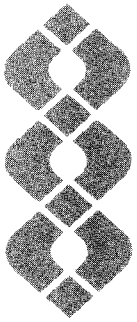

Author Index

AUTHOR INDEX

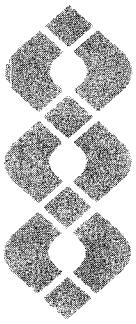

Organization Charts Distribution

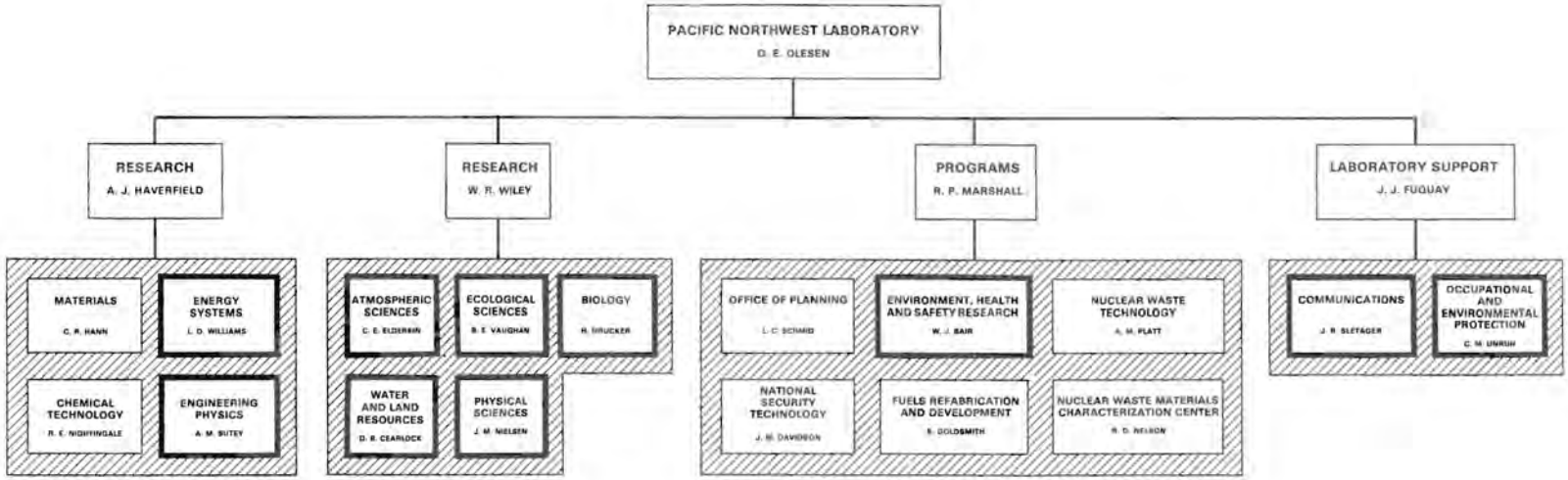

NOTE:
HEAVY BLACK LINES DENOTE ORGANIZATIONAL COMPONENTS IN WHICH ENVIRONMENT, HEALTH AND SAFETY RESEARCH IS BEING CONDUCTED AS OF DECEMBER 1, 1979

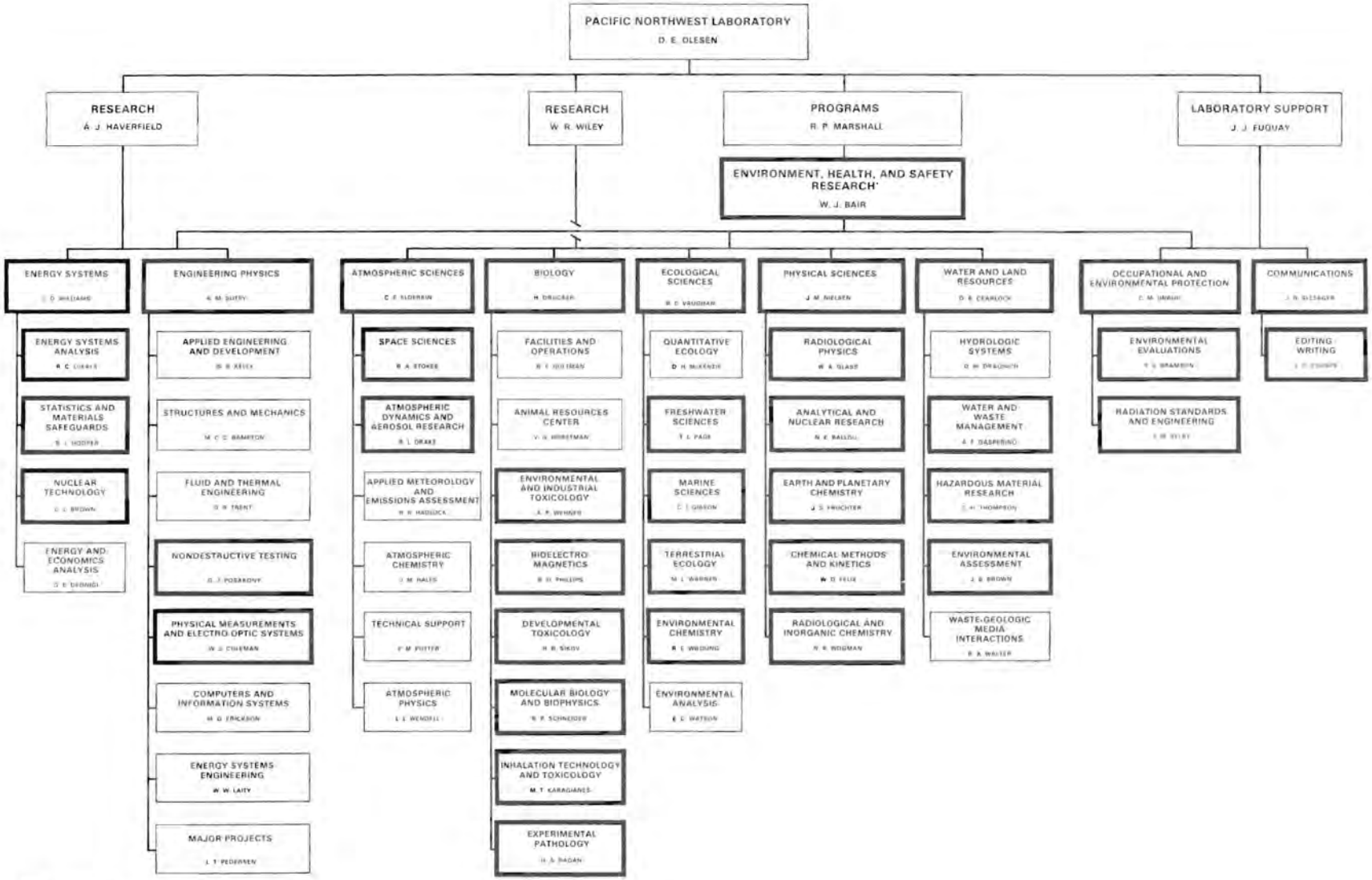

NOTE
HEAVY BLACK LINES DENOTE ORGANIZATIONAL COMPONENTS IN WHICH ENVIRONMENT, HEALTH AND SAFETY RESEARCH IS BEING CONDUCTED AS OF DECEMBER 1, 1979

December 1, 1979

PHYSICAL SCIENCES DEPARTMENT
(7HA0)

JM (Julian) Nielsen, Manager
FL (Louise) Barton, Secretary

RW (Dick) Perkins, Assoc. Manager
RM (Rose) Garcia, Secretary

#JD (Jim) Wasson, Contract Administrator (1831)

#HA (Herman) Jackson, Financial Specialist
#*EM (Elaine) Maxwell, Financial Clerk

#BE (Boyd) Smith, Quality Engineer

Coordinator for Inter-departmental Research
°°°NA (Ned) Wogman

Laboratory Program Coordination - EPRI
H (Harold) Harty
NL (Naomi) Brimhall, Secretary

EI (Earl) Wandling, Specialist
NG (Nancy) Robertson, Clerk

Radiological Physics
(7HA3)

WA (Bill) Glass, Manager
JA (Judy) Ewing, Secretary

Radiological Research Group

WC (Bill) Roesch, Technical Leader, Radiation Biophysics

LH (Larry) Toburen, Technical Leader, Radiation Physics

LA (Les) Braby
JH (John) Miller
JM (John) Nelson
CN (Chick) Newman
LL (Lowell) Nichols
CA (Charlie) Ratcliffe
ML (Martin) West
WE (Walt) Wilson

MS (Mike) Creek
MK (Marvin) Lein
R (Rudy) Rodriquez
°DD (Daniel) Sanders

Accelerator Facility
(7HA4)

Analytical and Nuclear Research
(7HA5)

NE (Nate) Ballou, Manager
GJ (Jean) Clark, Secretary
KM (Kathy) Blackwell, Secretary

FP (Fred) Brauer
JE (Jon) Fager
RC (Robert) Fukuda
RW (Ron) Goles
RL (Dick) Gordon
JH (Jim) Kaye
JM (Jim) Kelley
CR (Bob) Lagergren
WA (Bill) Mitzlaff
PL (Paul) Reeder
DM (Dean) Robertson
JJ (Jim) Stoffels
RS (Bob) Strebin
DL (Dave) Styris
H (Harvey) Tenney
RA (Ray) Warner

NL (Lois) Abbey
LA (Lee) Bond
DR (Don) Ells
RM (Rose Ann) Graves
RA (Robert) Kiddy
***LA (Laurie) McVey
RB (Roberta) Myers
MS (Mike) Rapids
DE (Donald) Rinehart
LW (Lena) Schock
CJ (Carol) Seaman
CA (Christie) Shields
SC (Shirley) Simpson

Earth and Planetary Chemistry
(7HA7)

JS (Jon) Fruchter, Manager
CM (Carole) Smyser, Secretary

KH (Keith) Abel
+EA (Eric) Crecelius
JC (John) Evans
JC (JC) Lau
JH (Jim) Reeves
HG (George) Rieck, Jr.
DE (Dave) Robertson
WB (Wyatt) Silker
DS (Debbie) Sklarew
CL (Connie) Wilkerson
JA (Jim) Young

LL (Lavern) Baker
EF (Ermel) Briggs
DA (Dave) Cochran
SP (Sylvia) Downey
CL (Chuck) Nelson
°CW (Clay) Philbrick
WC (Wayne) Richey

Chemical Methods and Kinetics
(7HA8)

WD (Dale) Felix, Manager
CH (Cozette) Connally, Secretary

JE (Jim) Burger
BA (Bruce) Bushaw
DR (Don) Kalkwarf
JC (John) Kutt
JC (Jim) Langford
JR (John) Morrey
***MR (Mike) Petersen
DM (Don) Schoengold
RD (Dick) Smith
BA (Barbara) Vieux
WC (Wally) Weimer
TJ (Tom) Whitaker
BW (Bary) Wilson

DR (Don) Edwards
°KA (Kris) Loss
C (Chuck) Veverka, Jr.
MD (Mike) Walker

Radiological and Inorganic Chemistry
(7HA9)

°°°NA (Ned) Wogman, Manager
JA (Judy) Buckenberger, Secretary

LJ ("Rip") Kirby, Project Manager

AC (Art) Case
RL (Ron) Brodzinski
DP (Don) Brown
PO (Pete) Jackson
EA (Elwood) Lepel
ML (Mary Lou) Mauch
HL (Howard) Nielson
KB (Khris) Olsen
RW (Ron) Sanders
CW (Chuck) Thomas
VW (Bill) Thomas, Jr.

VC (Velma) Beard
GG (Gwen) Brodaczynski
RM (Rush) Campbell
BG (Chris) Christensen
JD (Jerry) Forsythe
DT (Dottie) Harless
°BK (Barry) Hayden
JG (Grant) Pratt

LEGEND:
°°°Dual Assignment, included in total.
***Hourly employee included in total.
#Assigned from another organization, not included in total.
+Offsite, Marine Research Lab., Sequim, Washington.
°IIS Program - included in total.

Total Number of Exempt = 71
Total Number of Non-exempt = 46
117

DISTRIBUTION

No. of Copies

A. A. Churm, Director
Patent Division
DOE - Chicago Operations Office
9800 South Cass Ave.
Argonne, IL 60439

27 DOE Technical Information Center

3 Ruth C. Clusen
Assistant Secretary
Department of Energy
Office of the Assistant Secretary for Environment
Washington, DC 20545

W. R. Albers
Department of Energy
Office of the Assistant Secretary for Environment
Washington, DC 20545

D. S. Ballantine
Department of Energy
Office of the Assistant Secretary for Environment
Washington, DC 20545

R. W. Barber
Department of Energy
Office of the Assistant Secretary for Environment
Washington, DC 20545

N. F. Barr
Department of Energy
Office of the Assistant Secretary for Environment
Washington, DC 20545

R. W. Beadle
Department of Energy
Office of the Assistant Secretary for Environment
Washington, DC 20545

No. of Copies

J. W. Benson
Department of Energy
Office of the Assistant Secretary for Environment
Washington, DC 20545

J. R. Blair
Department of Energy
Office of the Assistant Secretary for Environment
Washington, DC 20545

R. P. Blaunstein
Department of Energy
Office of the Assistant Secretary for Environment
Washington, DC 20545

L. C. Brazley
Department of Energy
Office of the Assistant Secretary for Environment
Washington, DC 20545

W. A. Brobst
Department of Energy
Office of the Assistant Secretary for Environment
Washington, DC 20545

L. Brothers
Department of Energy
Office of the Assistant Secretary for Environment
Washington, DC 20545

W. W. Burr, Jr.
Department of Energy
Office of the Assistant Secretary for Environment
Washington, DC 20545

R. J. Catlin
Department of Energy
Office of the Assistant Secretary for Environment
Washington, DC 20545

No. of Copies

J. A. Coleman
Department of Energy
Office of the Assistant Secretary for Environment
Washington, DC 20545

R. A. Conaway
Department of Energy
Office of the Assistant Secretary for Environment
Washington, DC 20545

D. K. Craig
Department of Energy
Office of the Assistant Secretary for Environment
Washington, DC 20545

L. J. Deal
Department of Energy
Office of the Assistant Secretary for Environment
Washington, DC 20545

R. De Lorenzo
Department of Energy
Office of the Assistant Secretary for Environment
Washington, DC 20545

G. P. Dix
Department of Energy
Office of the Assistant Secretary for Environment
Washington, DC 20545

A. P. Duhamel
Department of Energy
Office of the Assistant Secretary for Environment
Washington, DC 20545

C. W. Edington
Department of Energy
Office of the Assistant
Secretary for
Environment
Washington, DC 20545

C. Eifert
Department of Energy
Office of the Assistant
Secretary for Environment
Washington, DC 20545

T. G. Frangos
Department of Energy
Office of the Assistant
Secretary for Environment
Washington, DC 20545

R. E. Franklin
Department of Energy
Office of the Assistant
Secretary for Environment
Washington, DC 20545

P. M. Gerhardt
Department of Energy
Office of the Assistant
Secretary for Environment
Washington, DC 20545

G. Goldstein
Department of Energy
Office of the Assistant
Secretary for Environment
Washington, DC 20545

R. E. Grossman
Department of Energy
Office of the Assistant
Secretary for Environment
Washington, DC 20545

J. H. Harley
Environmental Measurements
Laboratory
376 Hudson St.
New York, NY 10014

N. P. Hart
Department of Energy
Office of the Assistant
Secretary for Environment
Washington, DC 20545

E. B. Harvey
Department of Energy
Office of the Assistant
Secretary for Environment
Washington, DC 20545

J. C. Hock
Department of Energy
Office of the Assistant
Secretary for Environment
Washington, DC 20545

H. L. Hollister
Department of Energy
Office of the Assistant
Secretary for Environment
Washington, DC 20545

P. W. House
Secretary for Environment
Office of Technology
Impacts
Washington, DC 20545

F. P. Hudson
Department of Energy
Office of the Assistant
Secretary for Environment
Washington, DC 20545

C. A. Jolly
Department of Energy
Office of the Assistant
Secretary for Environment
Washington, DC 20545

R. L. Leith
Department of Energy
Office of the Assistant
Secretary for Environment
Washington, DC 20545

F. A. Leone
Department of Energy
Office of the Assistant
Secretary for Environment
Washington, DC 20545

R. A. Lewis
Department of Energy
Office of the Assistant
Secretary for Environment
Washington, DC 20545

W. J. Little, Jr.
Department of Energy
Office of the Assistant
Secretary for Environment
Washington, DC 20545

K. E. Lockridge
Department of Energy
Office of the Assistant
Secretary for Environment
Washington, DC 20545

J. N. Maddox
Department of Energy
Office of the Assistant
Secretary for Environment
Washington, DC 20545

J. R. Maher
Department of Energy
Office of the Assistant
Secretary for
Environment
Washington, DC 20545

D. Mayhew
Department of Energy
Office of the Assistant
Secretary for
Environment
Washington, DC 20545

H. M. McCammon
Department of Energy
Office of the Assistant
Secretary for
Environment
Washington, DC 20545

W. J. McCool
Department of Energy
Office of the Assistant
Secretary for
Environment
Washington, DC 20545

T. McCraw
Department of Energy
Office of the Assistant
Secretary for
Environment
Washington, DC 20545

B. F. McCully
Department of Energy
Office of the Assistant
Secretary for
Environment
Washington, DC 20545

C. E. Miller, Jr.
Department of Energy
Office of the Assistant
Secretary for
Environment
Washington, DC 20545

M. L. Minthorn, Jr.
Department of Energy
Office of the Assistant
Secretary for
Environment
Washington, DC 20545

D. R. Monti
Department of Energy
Office of the Assistant
Secretary for
Environment
Washington, DC 20545

W. E. Mott
Department of Energy
Office of the Assistant
Secretary for
Environment
Washington, DC 20545

W. H. Pennington
Department of Energy
Office of the Assistant
Secretary for
Environment
Washington, DC 20545

A. F. Perge
Department of Energy
Office of the Assistant
Secretary for Environment
Washington, DC 20545

R. W. Ramsey, Jr.
Department of Energy
Office of the Assistant
Secretary for Environment
Washington, DC 20545

S. L. Rose
Department of Energy
Office of the Assistant
Secretary for Environment
Washington, DC 20545

D. M. Ross
Department of Energy
Office of the Assistant
Secretary for Environment
Washington, DC 20545

M. Schulman
Department of Energy
Office of the Assistant
Secretary for Environment
Washington, DC 20545

D. E. Shaw
Department of Energy
Office of the Assistant
Secretary for Environment
Washington, DC 20545

G. R. Shepherd
Department of Energy
Office of the Assistant
Secretary for Environment
Washington, DC 20545

R. D. Shull
Department of Energy
Office of the Assistant
Secretary for Environment
Washington, DC 20545

M. Shulman
Department of Energy
Office of the Assistant
Secretary for Environment
Washington, DC 20545

N. F. Simpson
Department of Energy
Office of the Assistant
Secretary for Environment
Washington, DC 20545

D. H. Slade
Department of Energy
Office of the Assistant
Secretary for Environment
Washington, DC 20545

D. A. Smith
Department of Energy
Office of the Assistant
Secretary for Environment
Washington, DC 20545

J. Snyder
Department of Energy
Office of the Assistant
Secretary for Environment
Washington, DC 20545

R. J. Stern
Department of Energy
Office of the Assistant
Secretary for Environment
Washington, DC 20545

A. R. Vincent
Department of Energy
Office of the Assistant
Secretary for Environment
Washington, DC 20545

B. W. Wachholz
Department of Energy
Office of the Assistant
Secretary for Environment
Washington, DC 20545

R. L. Watters
Department of Energy
Office of the Assistant
Secretary for Environment
Washington, DC 20545

S. Weinstein
Department of Energy
Office of the Assistant
Secretary for Environment
Washington, DC 20545

J. C. Whitnah
Department of Energy
Office of the Assistant
Secretary for Environment
Washington, DC 20545

T. Williams
Department of Energy
Office of the Assistant
Secretary for
Environment
Washington, DC 20545

R. W. Wood
Department of Energy
Office of the Assistant
Secretary for
Environment
Washington, DC 20545

C. W. Fischer
Department of Energy
Office of Assistant
Secretary
for Energy Research
Washington, DC 20545

J. S. Kane
Department of Energy
Office of Assistant
Secretary
for Energy Research
Washington, DC 20545

G. C. Facer
Department of Energy
Office of the Assistant
Secretary for Defense
Programs
Washington, DC 20545

G. B. Pleat
Department of Energy
Office of the Assistant
Secretary for Defense
Programs
Washington, DC 20545

C. B. Curtis
Department of Energy
Office of the Assistant
Secretary for Federal
Energy Regulatory
Commission
Wasington, DC 20545

J. M. Deutch
Undersecretary
Department of Energy
Washington, DC 20585

T. J. Dobry
Departnent of Energy
Office of the Assistant
Secretary for Energy
Technology
Washington, DC 20545

F. A. Koomanoff
Department of Energy
Office of the Assistant
Secretary for Energy
Technology
Washington, DC 20545

C. Kuhlman
Department of Energy
Office of the Assistant
Secretary for Energy
Technology
Washington, DC 20545

G. Ortel
Department of Energy
Office of the Assistant
Secretary for Energy
Technology
Washington, DC 20545

H. F. Soule
Department of Energy
Office of the Assistant
Secretary for Energy
Technology
Washington, DC 20545

H. E. Thomas
Department of Energy
Office of the Assistant
Secretary for Energy
Technology
Washington, DC 20545

R. L. Butenhoff
Department of Energy
Office of Health and
Environmental Research
Washington, DC 20545

R. P. Blaunstein
Department of Energy
Office of Health and
Environmental Research
Washington, DC 20545

D. W. Cole, Jr.
Department of Energy
Office of Health and
Environmental Research
Washington, DC 20545

A. N. Heller
Department of Energy
Office of the Assistant
Admin. for Conservation
Washington, DC 20545

J. R. Maher
Deparment of Energy
Office of Technology
Overview
Washington, DC 20545

G. Hagey
Department of Energy
Office of Technology
Overview
Washington, DC 20545

E. J. Vallario
Department of Energy
Office of Safety, Standards
and Compliance
Washington, DC 20545

A. A. Schoen
Department of Energy
Office of Safety, Standards
and Compliance
Washington, DC 20545

F. R. Zintz
Department of Energy
Office of Safety, Standards
and Compliance
Washington, DC 20545

C. I. York
Department of Energy
Office of Safety, Standards
and Compliance
Washington, DC 20545

D. E. Patterson
Department of Energy
Office of Safety, Standards
and Compliance
Washington, DC 20545

E. K. Loop
Department of Energy
Office of Safety, Standards
and Compliance
Washington, DC 20545

M. A. Bell
Department of Energy
Office of Safety, Standards
and Compliance
Washington, DC 20545

J. D. Griffith
Department of Energy
Development and
Demonstration Branch
Washington, DC 20555

E. E. Held
Office of Standards
Development
U.S. Nuclear Regulatory
Commission
Washington, DC 20555

W. E. Lotz
EPRI
1800 Massachusetts
Avenue NW
Suite 7000
Washington, DC 20036

J. O'Toole
Ames Laboratory
Iowa State University
Ames, IA 50010

P. F. Gustafson
Argonne National
Laboratory
9700 South Cass Ave.
Argonne, IL 60439

J. Sedlet
Argonne National
Laboratory
9700 Cass Ave.
Argonne, IL 60439

C. Jackson
Department of Energy
San Francisco Operations
Office
133 Broadway
Wells Fargo Building
Oakland, CA 94616

J. H. Spickard
Department of Energy
Idaho Operations
Commission
550 Second Street
Idaho Falls, ID 83401

M. M. Williamson
Department of Energy
Idaho Operations
Office
550 Second Street
Idaho Falls, ID 83401

D. M. Gardiner
Department of Energy
Chicago Operations
Office
9800 South Cass Ave.
Argonne, IL 60439

J. Robertson, Director
Department of Energy
Region X Office
1992 Federal Building
915 Second Avenue
Seattle, WA 98174

M. E. Gates
Department of Energy
Nevada Operations Office
P. O. Box 14100
Las Vegas, NV 89114

R. Ray
Department of Energy
Nevada Operations Office
P. O. Box 14100
Las Vegas, NV 89114

P. B. Dunnaway
Department of Energy
Nevada Operations Office
P. O. Box 14100
Las Vegas, NV 89114

J. R. Roeder
Department of Energy
Albuquerque Operations Office
P. O. Box 5400
Albuquerque, NM 87115

E. W. Bean
Rocky Flats Area Office
Department of Energy
Albuquerque Operations Office
P. O. Box 928
Golden, CO 80401

J. F. Stevens
Dayton Area Office
Department of Energy
Albuquerque Operations Office
P. O. Box 66
Miamisburg, OH 45342

B. Morgan
Department of Energy
Savannah River Operations Office
P. O. Box A
Aiken, SC 29801

W. Reese
Department of Energy
Savannah River Operations Office
P. O. Box A
Aiken, SC 29801

J. A. Lenhard
Department of Energy
Oak Ridge Operations Office
P. O. Box E
Oak Ridge, TN 37830

J. S. Ball
Bartlesville Energy Technology Center
Department of Energy
P. O. Box 1398
Bartlesville, OK 74003

G. H. Gronhovd
Grand Forks Energy Technology Center
Department of Energy
Box 8213, University Station
Grand Forks, ND 58202

A. W. Decora
Laramie Energy Technology Center
Department of Energy
P. O. Box 3395
University Station
Laramie, WY 82071

D. Farrier
Laramie Energy Technology Center
Department of Energy
P. O. Box 3395
University Station
Laramie, WY 82071

H. Jensen
Laramie Energy Research Center
Department of Energy
P. O. Box 3395
University Station
Laramie, WY 82701

A. A. Pitrolo
Morgantown Energy Technology Center
Department of Energy
P. O. Box 880
Morgantown, WV 26505

I. Wender
Pittsburgh Energy Technology Center
Department of Energy
4800 Forbes Avenue
Pittsburgh, PA 15213

B. M. Erickson
Department of Energy
Schenectady Naval Reactors Office
P. O. Box 1069
Schenectady, NY 12301

T. M. Schoenberg
Department of Energy
Schenectady Naval Reactors Office
P. O. Box 1069
Schenectady, NY 12301

NRC Advisory Committee on Reactor Safeguards
Washington, DC 20555

W. Cool
Nuclear Regulatory Commission
Washington, DC 20545

R. Alexander
Nuclear Regulatory Commission
Washington, DC 20545

F. Swanberg
Nuclear Regulatory Commission
Washington, DC 20545

2 J. J. Davis
Assistant Director of Research
Nuclear Regulatory Commission
Washington, DC 20545

R. A. Scarano
Nuclear Regulatory Commission
Mill Licensing Section
Washington, DC 20545

D. D. Dominick
Office of Categorical Programs
Environmental Protection Agency
Washington, DC 20460

M. Gottlieb
Environmental Protection Agency
Office of Radiation Programs
Washington, DC 20545

D. Smith
Environmental Protection Agency
Washington, DC 20460

W. A. Mills
Director
Division of Criteria and Standards
Office of Radiation Program
Environmental Protection Agency
Rickville, MD 20852

J. H. Harley
Environmental Monitoring Laboratory
376 Hudson St.
New York, NY 10014

W. R. Ney
Executive Director
National Council on
Radiation Protection
and Measurement
7910 Woodmont Avenue
Suite 1061
Washington, DC 20014

M. K. Hubbert
Department of the
Interior
U.S. Geological Survey
Water Resources Division
Washington, DC 20242

D. N. Breiter
National Bureau of
Standards
A121, Building 222
Washington, DC 20234

J. R. DeVoe
National Bureau of
Standards
A121, Building 222
Washington, DC 20234

J. W. McCaslin
INEL, Aerojet Nuclear
550 Second Street
Idaho Falls, ID 83401

R. C. Yoder
Rockwell International
P. O. Box 888
Golden, CO 80401

A. R. Boulogne
E. I. duPont deNemours and
Company, Aiken
Savannah River Laboratory
Technical Information
Service
Room 773A
Aiken, SC 29801

K. MacMurdo
E. I. duPont deNemours and
Company, Aiken
Savannah River Laboratory
Technical Information
Service
Room 773A
Aiken, SC 29801

C. M. Patterson
E. I. duPont deNemours
and Company
Savannah River Plant
Aiken, SC 29801

B. C. Rusche
E. I. duPont deNemours
and Company, Aiken
Savannah River Laboratory
Technical Information
Service
Room 773A
Aiken, SC 29801

Technical Information
Service
Room 773A
Savannah River Laboratory
E. I. duPont deNemours
and Company
Aiken, SC 29801

R. J. Beyers
Savannah River Ecology
Laboratory
University of Georgia
Savannah River Plant
P. O. Box A
Aiken, SC 29801

C. L. Karl
National Lead Company
of Ohio
P. O. Box 39158
Cincinnati, OH 45239

V. P. Bond
Brookhaven National
Laboratory
Upton,
Long Island, NY 11973

L. P. Hatch
Brookhaven National
Laboratory
Research Library
Reference Section
Information Division
Upton,
Long Island, NY 11973

C. B. Meinhold
Brookhaven National
Laboratory
Upton,
Long Island, NY 11973

Librarian
Research Library,
Reference
Brookhaven National
Laboratory
Upton,
Long Island, NY 11973

B. Manowitz
Radiation Division
Brookhaven National
Laboratory
Upton,
Long Island, NY 11973

G. M. Woodwell
Brookhaven National
Laboratory
Research Library
Reference Section
Information Division
Upton, Long Island, NY 11973

C. R. Richmond
Oak Ridge National
Laboratory
P. O. Box X
Oak Ridge, TN 37830

S. I. Auerbach
Oak Ridge National
Laboratory
Oak Ridge Operations
Office
P. O. Box X
Oak Ridge, TN 37830

J. A. Auxier
Oak Ridge National
Laboratory
P. O. Box X
Oak Ridge, TN 37830

G. D. O'Kelley
Oak Ridge National
Laboratory
Oak Ridge Operations
Office
P. O. Box X
Oak Ridge, TN 37830

E. G. Struxness
Oak Ridge National
Laboratory
Oak Ridge Operations
Office
P. O. Box X
Oak Ridge, TN 37830

J. E. Turner
Oak Ridge National
Laboratory
Oak Ridge Operations
Office
P. O. Box X
Oak Ridge, TN 37830

W. K. Sinclair
Argonne National
Laboratory
9700 South Cass Ave.,
Argonne, IL 60439

J. W. McCaslin
INEL, Aerojet Nuclear
550 Second Street
Idaho Falls, ID 83401

E. L. Alpen
Lawrence Berkeley
Laboratory
University of California
Building 90, Room 2056
No. 1 Cyclotron Road
Berkeley, CA 94720

R. E. Heft
Lawrence Radiation
Laboratory
University of California
Lawrence Livermore
Laboratory
Technical Information
Department, L-3
P. O. Box 808
Livermore, CA 94550

G. H. Higgins
Lawrence Radiation
Laboratory
University of California
Lawrence Livermore
Laboratory
Technical Information
Department, L-3
P. O. Box 808
Livermore, CA 94550

J. B. Knox
Lawrence Radiation
Laboratory
University of California
Lawrence Livermore
Laboratory
Technical Information
Department, L-3
P. O. Box 808
Livermore, CA 94550

M. L. Mendelsohn
University of California
Lawrence Livermore
Laboratory
P. O. Box 808
Livermore, CA 94550

P. Phelps
Lawrence Radiation
Laboratory
University of California
Lawrence Livermore
Laboratory
Technical Information
Department, L-3
P. O. Box 808
Livermore, CA 94550

Librarian
Lawrence Radiation
Laboratory
University of California
Technical Information
Department, L-3
P. O. Box 808
Livermore, CA 94550

G. L. Voelz
University of California
Los Alamos Scientific
Laboratory
P. O. Box 1663
Los Alamos, NM 87545

Librarian
Los Alamos Scientific
Laboratory
P. O. Box 1663
Los Alamos, NM 87545

J. W. Healy
Los Alamos Scientific
Laboratory
University of California
P. O. Box 1663
Los Alamos, NM 87545

S. D. Nielsen
Los Alamos Scientific
Laboratory
University of California
P. O. Box 1663
Los Alamos, NM 87545

D. F. Petersen
Los Alamos Scientific
Laboratory
University of California
P.O. Box 1663
Los Alamos, NM 87545

R. O. McClellan
Inhalation Toxicology
Research Institute
Lovelace Foundation for
Medical Education and
Research
P.O. Box 5890
Albuquerque, NM 87115

R. M. Jefferson
Sandia Laboratories
P. O. Box 5800
Albuquerque, NM 87115

K. A. Smith
Sandia Laboratories
P. O. Box 5800
Albuquerque, NM 87115

T. W. Ambrose
Battelle Memorial
Institute
Columbus Laboratories
505 King Avenue
Columbus, OH 43201

Librarian
Battelle Memorial
Institute
Columbus Laboratories
505 King Avenue
Columbus, OH 43201

R. S. Paul
Vice President
Battelle Memorial
Institute
Columbus Laboratories
505 King Avenue
Columbus, OH 43201

L. A. Rancitelli
Battelle Memorial
Institute
Room 291
505 King Avenue
Columbus, OH 43201

E. W. Ungar
Director, Columbus
Laboratories
Battelle Memorial
Institute
505 King Avenue
Columbus, OH 43201

Director
Joint Center for
Graduate Study
100 Sprout Road
Richland, WA 99352

Librarian
Joint Center for
Graduate Study
100 Sprout Road
Richland, WA 99352

David Rall, Director
NIEHS
P. O. Box 12233
Research Triangle
Park, NC 27709

D. Beirman
Chief, Document Service
Branch
Central Intelligence
Agency
Attn: CRS/DPSD/DSB/IAS/
409779/DB
Washington, DC 20505

Council on Environmental Quality
72 Jackson Place, N.W.
Washington, DC 20006

B. B. Hicks
Atmospheric Physics Section
Radiological and Environmental Research Division
Argonne National Laboratory
9700 South Cass Avenue
Argonne, IL 60439

W. R. Ney
Executive Director
National Council on Radiation Protection and Measurements
7910 Woodmont Ave.
Suite 1061
Washington, DC 20014

L. Bustad, Dean
College of Veterinary Medicine
Washington State University
Pullman, WA 99163

R. H. Filby
Director
Nuclear Radiation Center
Washington State University
Pullman, WA 99163

V. R. Thayer
E. I. duPont deNemours and Company
Polymer Intermediate Department
Department of Energy
Wilmington, DE 19898

M. Haworth
Montana Power
(Colstrip)
P.O. Box 419
Colstrip, MT 59323

A. G. Sharkey
Pittsburgh Energy Research Center
4800 Forbes Ave.
Pittsburgh, PA 15213

E. D. Goldberg
Scripps Institute of Oceanography
University of California
La Jolla, CA 92093

D. Lal
Scripps Institute of Oceanography
University of California
La Jolla, CA 92093

J. R. Arnold
Chemistry Department
University of California
San Diego
La Jolla, CA 92037

W. Broecker
Lamont Geological Observatory
Columbia University
Palisades, NY 10964

Education and Information Section
Health Physics Division
Oak Ridge National Laboratory
Oak Ridge, TN 37830

M. C. Gaske
Assistant to Executive Secretary
Advisory Committee on Reactor Safeguards
U.S. Nuclear Regulatory Commission
Washington, DC 20555

C. Gordon
Department of Botany
University of Montana
Missoula, MT 59801

N. Harley
New York University Medical Center
550 First Ave.
New York, NY 10016

D. P. Kharkar
LFE Corporation
Environmental Analysis Laboratories
2030 Wright Ave.
Richmond, CA 94804

H. W. Kirby
Monsanto Research Corporation
Mound Laboratory
Miamisburg, OH 45342

P. K. Kuroda
Department of Chemistry
University of Arkansas
Fayetteville, AR 72701

P. LaFluer
Nuclear Reactor Laboratory
National Bureau of Standards
Gaithersburg, MD 20760

C. Menninga
Physics Department
Calvin College
1331 Franklin St. S.E.
Grand Rapids, MI 49506

D. Montgomery
Environmental Protection Agency
26 W. St. Clair St.
Cincinnati, OH 45219

A. Seymour
Laboratory of Radiation Ecology
University of Washington
College of Fisheries
Seattle, WA 98105

W. Singlevich
Air Force Technical Applications Center/TD-4
Patrick AFB, FL 32925

C. V. Theis
U.S. Geological Survey
P. O. Box 436
Albuquerque, NM 87106

D. Uhl
Nuclear Engineering and Operations Department
Electric Power Research Institute
3412 Hillview Ave.
P. O. Box 10412
Palo Alto, CA 94303

FOREIGN

D. J. Benison
Comision Nacional de Energia Atomica
Buenos Aires
ARGENTINA

E. Vander Elst
Comision Nacional de Energia Atomica
Buenos Aires
ARGENTINA

Chief
Commonwealth Scientific and Industrial Research Organization, DAP
Aspendal, Victoria 3195
AUSTRALIA

Librarian
Commonwealth Scientific
and Industrial Research
Organization
314 Albert Street
P.O. Box 89
East Melbourne, Victoria
AUSTRALIA

Librarian
CS/RO
Riverina Laboratory
P. O. Box 226
Deniliquin
New South Wales
AUSTRALIA 2710

A. W. R. Wilson
Australian AEC
Post Office Coogee
New South Wales
AUSTRALIA

H. Daw
Director, Division of
Health, Safety and Waste
Management
International Atomic Energy
Agency
Kartner Ring 11
P. O. Box 590
A 1011 VIENNA, AUSTRIA

Director, Office of Nuclear
Safety and Environmental
Protection
International Atomic Energy
Agency
Kartner Ring 11
P. O. Box 590
A 1011 VIENNA, AUSTRIA

J. Z. Minczewski
International Atomic Energy
Agency
Kartner Ring 11
P. O. Box 590
A 1011 VIENNA, AUSTRIA

Librarian
Eurochemic Library
B 2400
MOL
BELGIUM
Library
Ontario Hydro
620 University Ave.
Toronto, Ontario
CANADA

A. M. Marko
Director
Atomic Energy of
Canada Ltd.
Biology and Health
Physics Division
Chalk River Nuclear
Laboratories
Chalk River, Ontario
KOJ IJO
CANADA

D. P. Meyerhoff
Environmental Radioactivity
Section
Nuclear Safety Division
Radiation Protection Bureau
Brookfield Road
Ottawa, Ontario
KIAICI
CANADA

I. Ophel
Atomic Energy of
Canada Ltd.
Chalk River, Ontario
CANADA

R. V. Osborne
Atomic Energy of
Canada, Ltd.
Chalk River, Ontario
CANADA

J. C. Dalton
U.K. Atomic Energy
Authority
Windscale Works, P.G.
Sellafield, Seascale,
Cumberland
ENGLAND

Librarian, Building 465
Atomic Energy Research
Establishment
Harwell, Didcot
OXON OXII ORD, ENGLAND

5 Librarian
Ministry of Agriculture
Fisheries and Food
Laboratory
Lowestoft, Suffolk
ENGLAND

Librarian
National Radiation
Protection Board
Harwell, Didcot
Oxfordshire OXII ORQ
ENGLAND

Andrew McLean
National Radiological
Protection Board
Harwell, Didcot
Oxfordshire OXII ORQ
ENGLAND

D. H. Peirson
AERE (Atomic Energy
Research Establishment)
Health Physics and
Medical Division
B. 364
Harwell, Didcot, Berkshire
ENGLAND

F. D. Sowby
International Commission on
Radiological Protection
Clifton Avenue
Sutton, Surrey
ENGLAND

A. R. Gopal-Ayengar
Inst. für Biophysik
Herrenhauser Str. 2
3000 Hannover, 21
FEDERAL REPUBLIC OF GERMANY

J. K. Miettinen
University of Helsinki
Department of
Radiochemistry
Unionkatu 35, Helsinki
FINLAND

A. Barbreau
Centre d'Etudes
Nucléaires de Saclay
P. O. Box 2, Saclay
Gif-sur-Yvette
(S & O)
FRANCE

Director
Commissariat a l'Energie
Atomique
Center d'Etudes
Nucléaires de Fontenay-aux-
Roses (Seine)
FRANCE

F. Duhamel
Centre d'Etudes
Nucléaires de Saclay
P.O. Box 2, Saclay
Gif-sur-Yvette
(S & O)
FRANCE

Librarian
Centre d'Etudes
Nucléaires de Saclay
P.O. Box 2, Saclay
Fig-sur-Yvette
(S & O)
FRANCE

A. M. Menoux
Commissariat a l'Energie
Atomique
Centre d'Etudes
Nucléaires Fontenay-aux-
Roses,
BP n°, 6-9226
Fontenay-aux-
Roses,
FRANCE

M. Rzekiecki
Commissariat a l'Energie
Atomique
Centre d'Etudes
Nucléaires de Cadarache
BP n°, 3-St. Paul
Les Durance
FRANCE

P. Slizewicz
Centre d'Etudes
Nucléaires de Saclay
P. O. Box 2, Saclay
Gif-sur-Yvette
(S & O)
FRANCE

E. Wallauschek
ENEA (OECD) Health and
Safety Office
38, Blvd. Suchet
Paris IVI,
FRANCE

A. K. Ganguly
Atomic Energy
Establishment
Trombay, Bombay 73
INDIA

F. Girardi
C.C.R. EURATOM-ISPRA
(VERESE)
ITALY

A. Malvicini
Chief, Protection
Service
C.C.R. EURATOM-ISPRA
(VERESE)
ITALY

T. Kumatori,
Director
National Institute of
Radiological Sciences
4-9-1, Anagawa
Chiba-shi
JAPAN

M. Saiki
National Institute of
Radiological Sciences
Environmental Hygiene
Division
4-9-1, Anagawa
Chiba-shi
JAPAN

M. Suzuki
National Institute of
Radiological Sciences
Environmental Hygiene
Division
4-9-1, Anagawa
Chiba-shi
JAPAN

K. Edvarson
Forsvarets Forskningsanstalt
Res. Institute of National
Defence
Avdelning 4,
Stockholm 80
SWEDEN

E. Komarov
HCS/EHE
World Health Organization
Geneva,
SWITZERLAND

Librarian
World Meteorological
Organization
Geneva
SWITZERLAND

H. Krause
Gelleschaft für Kernforschung
mbH
Postfach 3640
D-7500 Kärlsruhe
WEST GERMANY

ONSITE

10 DOE Richland Operations Office

R. E. Austin
T. E. Austin
P. F. Dunigan
J. L. Landon
H. E. Ransom
P. R. Rhodes
F. R. Standerfer
M. W. Tiernan
J. D. White
M. G. White

5 Hanford Environmental Health Foundation

Medical Library (2)
B. D. Breitenstein
P. A. Fuqua
D. G. Quilici

142 Pacific Northwest Laboratory

W. J. Bair (20)
N. E. Ballou (5)
D. B. Cearlock
J. R. Corley
J. M. Davidson
H. Drucker
C. E. Elderkin
S. J. Farmer
W. D. Felix (10)
J. W. Finnigan
J. C. Fox (5)
J. S. Fruchter (10)
J. J. Fuquay
C. I. Gibson
W. A. Glass (10)
A. J. Haverfield (5)
D. L. Hessel
J. L. Hooper
R. L. Hooper
V. G. Horstman
L. J. Kirby
H. V. Larson
R. C. Liikala
S. Marks
R. P. Marshall
I. C. Nelson (5)
J. M. Nielsen (10)
R. E. Nightingale
D. E. Olesen
J. F. Park
R. W. Perkins (5)
W. D. Richmond
C. L. Simpson
W. H. Swift
W. L. Templeton
C. M. Unruh
B. E. Vaughan
W. R. Wiley
N. A. Wogman (15)
Biology Library (2)
Technical Information (5)
Publishing Coordination (2)

5 Battelle Seattle

G. W. Duncan
J. Hebert
S. Nealey
J. O'Toole
J. E. Rasmussen